

EBF1 AS A NUCLEAR MATRIX PROTEIN

Thesis submitted for the degree of

Doctor of Philosophy

at the University of Leicester

by

Inara Liepina MRes

Department of Molecular and Cell Biology

University of Leicester

September 2019

Abstract

Ebf1 as a nuclear matrix protein

Inara Liepina

EBF1 is a highly conserved transcription factor that plays pivotal roles in the development of normal and malignant B cells. In mice, homozygous loss of *Ebf1* completely suppresses normal B-cell development, while heterozygosity results in decreased pro-B cell numbers and increased DNA damage accumulation upon UV light exposure. In man, *EBF1* deletions are typically heterozygous and frequently occur in B-cell precursor acute lymphoblastic leukaemia. In contrast to *EBF1* deletions, *EBF1* mutations are found in mature B cell malignancies. Both mutations and deletions are thought to function via loss of *EBF1*'s transcriptional activities.

Here, I show that *Ebf1* depletion in Abelson transformed murine pro-B cells resulted in rapid cell cycle arrest associated with nuclear collapse and heterochromatin accumulation at the periphery of the nuclei. Using *in situ* fractionation, I was able to show that a fraction of *EBF1* was detected in the isolated nuclear matrix fraction, suggesting that *EBF1* might be involved in nuclear matrix regulation of pro-B cells. Preliminary proteomics data suggested that *EBF1* might interact with nuclear structural proteins including SRSF2, RPL14, LGALS9 and MTDH; loss of function of these proteins might play a role in the nuclear collapse upon *EBF1* depletion.

EBF1 depletion also resulted in pro-B cell arrest at the G1 phase and rapid *CCND3* protein degradation. *CCND3* was previously shown to localize on the nuclear structural matrix in pro-B cells. Therefore, it was hypothesized that *CCND3* might interact with *EBF1* at the nuclear matrix. Here I show that *EBF1* does not interact with *CCND3*, and they do not have a potential common structural binding partners.

Conclusion: My data suggest that *EBF1* may have functions within the nuclear matrix independent of its transcriptional activities.

Acknowledgements

This work would not be possible without the financial support of MIBTP and BBSRC or the University of Leicester throughout my PhD and maternity leave. I want to express my very great appreciation to Dr Ildiko Gyory for her guidance, useful critiques and suggestion during planning and development of this research and to Prof Martin Dyer for his valuable and constructive suggestions during final stages of my PhD in planning and organizing my thesis and final experiments. Their willingness to give their time so generously has been very much appreciated.

Each of the members of my Dissertation Committee has provided me with extensive professional guidance. I would like to especially thank Prof Shaun Cowley for his useful critiques and suggestions ant my final stages of PhD.

I would also like to thank my MPIBTP tutors Dr Ezio Rosato and Dr Jonathan McDearmid, for their valuable guidance.

I am grateful to all of those with whom I had the pleasure to work during this project. My thanks are also extended to Dr Kees Straatman for his support in confocal imaging, Dr Aude Echali er for assistance in bacterial protein purification, Dr Oksana Gonchar for teaching cellular fractionation method, to Dr Olga Makarova for help in troubleshooting co-immunoprecipitation protocol and Mrs Jennifer Hincks for advice and assistance in Flow cytometry.

I thank my fellow labmates, especially Dan Bowden, for the stimulating discussions and for all the fun we had in the last two years.

I would also like to thank the staff of PROTEX facility for provided service in sequencing and Mass spec, and a technician Anna Straatman-Iwanowska in Electron Microscopy Facility for sample preparation and imaging.

Also, I would like to thank Mr Martin Coffey for the opportunity to participate and support throughout preparation for Biotechnology Yes, as well as my thanks goes to team

members Dr Akang Ekpeyong-Akiba, Dr Razif Abas and Dr Meetal Solanki and the Biotechnology Yes organizations and all speakers for their guidance and support.

With a special mention to Dr Jonathan Barratt and colleagues who provided me an opportunity to join their team and for the guidance and support through my internship in Renal Research Unit, Leicester General Hospital and Prof Tatjana Stankovic and Dr Nichola Davies in School of Cancer Science, University of Birmingham, who provided me an opportunity to join their team and who gave access to the laboratory and research facilities.

I would like to acknowledge the support provided by my family and foremost to my partner, Kamil Trykowski and my daughter Sophie Trykowska, during the preparation of my final year. Many thanks for your patience and support.

Table of Contents

Chapter 1	Introduction.....	30
1.1	B-cell development and functions	30
1.2	EBF1 maintains and regulates B-cell development.....	36
1.2.1	EBF1 is an important transcriptional factor	37
1.2.2	EBF1 poises chromatin prior transcription	38
1.2.3	EBF1 restricts lineage potential	39
1.2.4	EBF1 structure.....	40
1.3	Cell cycle regulating proteins and their functions in B-cell development.....	43
1.3.1	Structure of Cyclins	46
1.3.2	CCND3 is indispensable in B-cell development.....	52
1.3.3	CCND transcription activity	54
1.3.4	CCND3 localisation and degradation	55
1.4	Nuclear matrix	57
1.4.1	Nuclear matrix history	58
1.4.2	Nuclear matrix is a non-chromatin structure in the nuclei not an artefact	59
Chapter 2	The aims of the project	63
Chapter 3	Materials and Methods	64
3.1	Cell lines used and cell culture conditions.....	64
3.1.1	Conditional <i>Ebf1</i> depleted mouse pro-B cell lines	64
3.1.2	MPI-2 GM-CSF dependent macrophages.....	65
3.1.3	293T cells	65
3.1.4	DH5 and BL21 pLysS alpha Competent bacteria preparation	65
3.2	Drug preparation.....	66
3.3	Plasmids.....	66
3.4	Cloning.....	75
3.4.1	PCR amplification of Δ H Δ T <i>Ebf1</i> and Δ D <i>Ebf1</i>	75
3.4.2	PCR product purification.....	75
3.4.3	PCR product recombination into pCR II TOPO vector	76
3.4.4	PCR product recombination from pCR II TOPO vector into retroviral expression vector pMYs IRES GFP	79

3.5	<i>Ebf1</i> depletion in transformed murine <i>Ebf1^{fl/fl}RERT^{Cre}::A-MuLV</i> pro-B cell lines	81
3.6	Subcellular fractionation	81
3.7	NM isolation via <i>in situ</i> fractionation	83
3.8	Testing the effect of different concentration of HDAC inhibitors alone and in combination with OHT	84
3.8.1	Pro-B cell treatment with HDAC inhibitors and OHT	85
3.9	Protein expression and affinity purification	85
3.9.1	His-tagged CCNA2 expression in BL21 pLysS	85
3.9.2	FLAG EBF1 protein expression in 293T cells	86
3.9.3	Co-purification of mammalian and bacterial proteins	86
3.10	Protein immunoprecipitation	87
3.10.1	Co-IP protocol 1	87
3.10.2	Co-IP protocol 2	88
3.10.3	Protein immunoprecipitation for the MS analysis using Pierce Co-IP Kit	88
3.11	Flow cytometry and confocal microscopy	92
3.11.1	Reagent preparation	92
3.11.2	Sample preparation	92
3.11.3	Flow cytometry	95
3.11.4	Confocal microscopy	95
3.11.5	Calculation of cell nuclear blebbing	95
3.12	Sample preparation for Electron microscopy (EM)	96
3.13	Genomic DNA PCR	97
3.14	RT-qPCR	98
3.15	Western blot analysis	99
3.15.1	Bradford assay	99
3.15.2	Coomassie Blue staining of acrylamide gel	99
3.15.3	Silver staining of acrylamide gel	100
3.15.4	Protein transfer from acrylamide gel to nitrocellulose membrane	100
3.15.5	Membrane staining and protein analysis	101
3.16	P-value calculation	103
Chapter 4	<i>Effect of acute EBF1 depletion on Abelson transformed mouse pro-B cells</i>	104

4.1	Acute EBF1 depletion in Abelson transformed mouse pro-B cells results in cell cycle arrest and cell death	104
4.2	EBF1 depletion in pro-B cells results in rapid CCND3 degradation	109
4.3	EBF1 is a potential NM structural protein in pro-B cells	117
4.4	HDAC3 inhibitors does not reverse the phenotype of EBF1 depleted pro-B cells	127
Chapter 5	<i>EBF1 does not interact with CCNA2 and CCND3.....</i>	140
5.1	DBD of EBF1 might be required for CCNA2 binding	142
5.2	EBF1 does not interact with CCND3 and CCNA2 in <i>Ebf1^{fl/fl}RERT^{Cre}::A-MuLV</i> pro-B cells	146
Chapter 6	<i>Investigating whether the unique NM function of EBF1 and CCND3 is mediated by B-cell specific CCND3 and/or EBF1 association partners</i>	151
6.1	Possible B-cell specific EBF1 association partners identified by immunoprecipitation and MS	151
6.2	Possible B-cell specific CCND3 association partners identified by immunoprecipitation and MS	154
6.3	EBF1 and CCND3 common binding partners.....	167
Chapter 7	<i>Discussion.....</i>	171
7.1	EBF1 depletion causes nuclear blebbing of <i>Ebf1^{fl/fl}RERT^{Cre}::A-MuLV</i> pro-B cells and an increase in the levels of the heterochromatin at the periphery of the nuclei.....	172
7.2	HDAC3 inhibitors does not rescue EBF1 depleted <i>Ebf1^{fl/fl}RERT^{Cre}::A-MuLV</i> pro-B cells from nuclear blebbing.....	173
7.3	Cells that are at G1 phase during OHT induced EBF1 depletion might not display nuclear blebbing upon EBF1 depletion.....	174
7.4	EBF1 is a potential nuclear matrix proteins.....	174
7.5	Potential structural binding partners of EBF1	176
7.6	Exploring EBF1 and CCND3 relationship in <i>Ebf1^{fl/fl}RERT^{Cre}::A-MuLV</i> pro-B and possible cause of decrease in CCND3 levels upon EBF1 depletion	177
Chapter 8	<i>Summary and Further studies</i>	180

Chapter 9	<i>Bibliography</i>	182
Chapter 10	<i>Appendix</i>	199

List of Figures

- Figure 1-1 Early stages of antibody production and the BCR repertoire via genetic recombination in B-cell development**, where V_H – immunoglobulin heavy chain variable, J_H – immunoglobulin heavy chain joining, D_H – immunoglobulin heavy chain diversity gene segment, C_H – immunoglobulin heavy chain constant gene segment, V_L – immunoglobulin light chain variable, J_L – immunoglobulin light chain joining, C_L – immunoglobulin light chain constant gene segment, Ig_H – immunoglobulin heavy chain, Ig_L – immunoglobulin light chain, SL – surrogate light chain, Image adapted from (Parkhouse 1990, Fuentes-Panana, Bannish et al. 2004, Winkler and Martensson 2018).32
- Figure 1-2 Transcription factor network that regulates B-cell specification, commitment and development.** (A) The schematic depicts major TFs regulating B-cell specification and commitment, direct positive regulation between two factors at the transcriptional level is indicated by the corresponding arrows, while repression is represented by thin, barred lines that end with a perpendicular line. Image adapted from (Boller and Grosschedl 2014) (B) A schematic view of B-cell lymphopoiesis and developmental arrest upon loss of TFs, where HSC - hematopoietic stem cell, LMPP - lymphoid-primed multipotent progenitor, CLP - common lymphoid progenitor, with lines that end with a perpendicular line depicts the approximate points of the developmental arrest in mice that have defective TFs - SP1, Ikaros, IL-7R, TCF3, EBF1, PAX5 and RUNX1. Image adapted from (Fuxa and Skok 2007, Spooner, Cheng et al. 2009, Zarnegar and Rothenberg 2012, Boller and Grosschedl 2014).35
- Figure 1-3 Sequence and structural representation of EBF1** (A) EBF1 protein sequence, where DBD - DNA binding domain is represented in yellow, IPT – immunoglobulin in green, plexins, transcription factors-like domain in blue, HLH - a helix-loop-helix dimerization domain and TAD - transactivation domain in grey (B) The structure of DNA bound EBF1, where DBD - DNA binding domain, IPT - immunoglobulin, plexins, transcription factors-like domain, HLH - a helix-loop-helix dimerization domain and TAD - transactivation domain. Images taken from (Boller and Grosschedl 2014).42
- Figure 1-4 Cell cycle regulation via CCN and CDK interaction and cell cycle checkpoint regulation** (A) Cell cycle phases and checkpoints (B) Cyclin expression throughout cell cycle. Image taken from (Yang 2018).45

Figure 1-5 CCN sequence alignment. The first line shows the amino acid conservation index (> 5). The sequences were automatically aligned against CCND2 (the eleventh line). Representative sequences of CCNA1 (the sixth line), CCNA2 (the fifth line), CCNB1 (the eighth line), CCNB2 (the seventh line), CCNB3 (the fourth line), CCND1 (the tenth line), CCND2 (the eleventh line), CCND3 (the ninth line), CCNE1 (the second line) and CCNE2 (the third line) coloured according to predicted secondary structures (red: alpha-helix, blue: beta-strand). Consensus_aa -Consensus amino acids: identical amino acids are presented in bold and uppercase letters, l-aliphatic residues, @- aromatic residues, h- hydrophobic residues, o - alcohol residues, p - polar residues, t - tiny residues, s - small residues, b - bulky residues, "+" - positively charged residues, "-" -negatively charged residues, c - charged). Consensus_ss -Consensus secondary structures, where h – alpha-helix, e- beta-strand (Pei, Kim et al. 2008).47

Figure 1-6 CCND expression in different tissues and during B cell maturation phases (A) CCND expression in different tissues (Uhlen, Fagerberg et al. 2015) (B) CCND expression in different B cell maturation phases, where HSC – hematopoietic stem cell, MPP – multipotent progenitor, LMPP - lymphoid-primed multipotent progenitor, CLP – common lymphoid progenitor (Cooper, Sawai et al. 2006, Fuxa and Skok 2007, Lukin, Fields et al. 2008, Perez-Vera, Reyes-Leon et al. 2011, Boller and Grosschedl 2014, Choukrallah and Matthias 2014).53

Figure 1-7 Nuclear matrix schematic representation, where IF – intermediate filaments. (Figure taken from Frey and Penman, 1988).57

Figure 3-1 WT and mutant FLAG EBF1 schematic representation. DNA binding domain (D) is necessary for EBF1 binding to DNA, helix-loop-helix (H) dimerization domain aids in EBF1 binding to DNA, an “immunoglobulin, plexins, transcription factors-like” (I) domain, whose function is not yet known, and a transactivation domain (T), which participates in the gene transcriptional activation in the absence of other TFs. FLAG and streptavidin (ST) - protein tags67

Figure 3-2 Verification of pCR II TOPO ΔHΔT *Ebf1* and pCR II TOPO ΔD *Ebf1* cloning. ΔHΔT *Ebf1* and ΔD *Ebf1* were PCR amplified and ligated into pCR II TOPO vector. PCR product ligation into pCR II TOPO vector was confirmed by enzymatic digest of pCR II TOPO FLAG ΔHΔT *Ebf1* and pCR II TOPO FLAG ΔD *Ebf1* using EcoRI. (A) Agarose gel image, where ΔHΔT *Ebf1* and

$\Delta D Ebf1$ fragments are 1094 and 1053bp large. (B) Schematic representation of pCR II TOPO $\Delta H\Delta T Ebf1$ and pCR II TOPO $\Delta D Ebf1$, where EcoRI digestion sites are shown in red.78

Figure 3-3 Verification of pMYs FLAG $\Delta H\Delta T Ebf1$ and pMYs FLAG $\Delta D Ebf1$ cloning. pCR II TOPO FLAG $\Delta H\Delta T Ebf1$ and pCR II TOPO FLAG $\Delta D Ebf1$ and pMys FLAG $Ebf1$ vectors were digested with EcoRI and XhoI. $\Delta H\Delta T Ebf1$ and $\Delta D Ebf1$ fragments were reinserted into pMYs vector. Ligation was confirmed by enzymatic digest of pMYs FLAG $\Delta H\Delta T Ebf1$ and pMYs FLAG $\Delta D Ebf1$ using EcoRI and XhoI. (A) Agarose gel image, where $\Delta H\Delta T Ebf1$ and $\Delta D Ebf1$ fragments are 1088 and 1047bp large. (B) Schematic representation of pCR II TOPO $\Delta H\Delta T Ebf1$ and pCR II TOPO $\Delta D Ebf1$, where EcoRI and XhoI digestion sites are shown in red.80

Figure 3-4 Flow chart of the MS data analysis identifying potential B-cell unique and structural binding partners of EBF1 and CCND3. Analysis of the EBF1 or CCND3 binding partners is color-coded, respectively, in green and orange, while analysis of potential binding partners of EBF1 and CCND3 is shown in blue.91

Figure 4-1 Verifying OHT induced EBF1 depletion via PCR amplification and Western Blot analysis. $1_3 Ebf1^{fl/fl}RERT^{Cre}::A$ -MuLV pro-B cells were treated with 2 μ M OHT, EtOH was used as a control. Samples were collected every day for four days (A) Genomic DNA was purified from the collected samples. $Ebf1$ gene cleavage was verified via PCR amplification of floxed and cleaved alleles. (B) Cells were lysed and proteins were separated via acrylamide gel electrophoresis, then proteins were transferred to nitrocellulose membrane and stained for EBF1 and GAPDH. Representative Western blot image of the change in EBF1 protein levels upon OHT treatment over time using GAPDH as a loading control. (C) Relative change in EBF1 protein levels upon EBF1 depletion over time. EBF1 protein levels were normalized to GAPDH protein levels, where *** - $p < 0.001$, **** - $p < 0.0001$ (n = 4 experiments). 105

Figure 4-2 EBF1 depletion causes $1_3 Ebf1^{fl/fl}RERT^{Cre}::A$ -MuLV pro-B cells arrest in the G1 phase. Representative flow cytometry images of $1_3 Ebf1^{fl/fl}RERT^{Cre}::A$ -MuLV pro-B cells upon EBF1 depletion over time, where collected events are gated for single cells (gate A), viable and healthy cells (gate B) and all events (gate C). The percentage of cells in the S and G1 phase for B gated and C gated cells is, respectively, shown in blue and red. Cells were treated with 2 μ M OHT; and collected every day for four consecutive days. 0.5 μ M EdU was added 3 hours prior sample collection in order to allow for its incorporation into newly synthesized DNA. After sample collection, harvested cells were washed in PBS and fixed in 4% PFA, then cells were permeabilized using Perm buffer. Incorporated EdU was stained with Click-iT EdU

Alexa Fluor 488. In order to separate cells by their DNA contain cells were stained with PI and samples were analysed using flow cytometer. Alexa Fluor 488 is detected in FITC channel (EdU FITC), while PI in PE channel (PI PE). 107

Figure 4-3 The change in cell viability and percentage of 1_3 *Ebf1^{fl/fl}RERT^{Cre}::A-MuLV* pro-B cells in G1 and S phase upon OHT treatment over time. Cells were treated with 2µM OHT; and collected every day for four consecutive days. 0.5µM EdU was added 3hours prior sample collection in order to allow for its incorporation into newly synthesized DNA. After sample collection, harvested cells were washed in PBS and fixed in 4% PFA, then cells were permeabilized using Perm buffer. Incorporated EdU was stained with Click-iT EdU Alexa Fluor 488. In order to separate cells by their DNA contain cells were stained with PI and samples were analysed using flow cytometer. Alexa Fluor 488 is detected in FITC channel (EdU FITC), while PI in PE channel (PI PE). G1 and S distribution in (A) all detected events and (B) healthy and viable cells, where percentage of cell in S phase is shown in red and in G1 phase in green. ns – not significant, * - p<0.05, ** - p<0.01 (n = 4 experiments)..... 108

Figure 4-4 Subcellular localization of CCND3 and EBF1 in 1_3 *Ebf1^{fl/fl}RERT^{Cre}::A-MuLV* pro-B cells. Cells were harvested and washed with PBS. Total lysate sample was collected prior subcellular fractionation (Total). Then cells were resuspended in hypotonic buffer A and cell walls were disrupted mechanically. The mixture was spun down and supernatant was collected into a new microcentrifuge tube and resuspended in Buffer B (Cytosol). The nuclei fraction was resuspended in Buffer C (Nuclei) and were disrupted mechanically. The homogenized nuclei were spun down and the supernatant (Nuclear extract) and the pellet (Chromatin) were collected. The “Total”, “Nuclei” and “Chromatin” samples were lysed in RIPA buffer and proteins in all collected samples were separated via acrylamide gel electrophoresis. Then proteins were transferred to nitrocellulose membrane and stained for EBF1 and CCND3. GAPDH was used as a cytoplasmic control, H4ac and LAP2β were used as chromatin fraction control, and THOC1 and RUNX1 were used as NM controls. (A) Representative Western blot image of the subcellular fractionation of 1_3 *Ebf1^{fl/fl}RERT^{Cre}::A-MuLV* pro-B cells. (B) Fluorescence intensity of the bands was measured and average intensity was calculated for each of the protein in each fraction, where protein levels in the Nuclear Extract is represented in red, in the Chromatin in Blue and in the Cytosol in Green, Protein levels in the Nuclei is the combination of the protein levels in the Nuclear extract and Chromatin, while Total levels are combination of the protein levels in the all three presented fractions (n=3 experiments). 110

Figure 4-5 CCND3 and EBF1 localization in 1_3 *Ebf1^{fl/fl}RERT^{Cre}*::A-MuLV pro-B cells via confocal imaging. Cells were collected, washed with PBS, fixed in 4% PFA, then permeabilized using Perm buffer. Cells were incubated with primary EBF1 and CCND3 antibodies, followed by incubation with secondary Alexa Fluor 488 or Alexa Fluor 647 antibodies. Stained cells were cytospun onto slides, air-dried and DNA was stained with 300nM DAPI. (A) Confocal images of 1_3 *Ebf1^{fl/fl}RERT^{Cre}*::A-MuLV pro-B cells stained for EBF1 (red), CCND3 (green) and DAPI (blue). (B) Fluorescence intensity of the CCND3 and EBF1 in the nuclei and whole cell was measured. Average total intensity of the EBF1 and CCND3 in the nuclei and Cytoplasm represents their protein level distribution between these two compartments. (from 50 cells; n = 3 experiments, ×10 magnification)..... 112

Figure 4-6 EBF1 depletion causes a substantial decrease in CCND3 protein levels, but not in *Ccnd3* RNA levels. 1_3 *Ebf1^{fl/fl}RERT^{Cre}*::A-MuLV pro-B cells were treated with 2µM OHT, EtOH was used as a control. Samples were collected every day for four days (A) Cells were lysed and proteins were separated via acrylamide gel electrophoresis, then proteins were transferred to nitrocellulose membrane and stained for EBF1, CCND3 and GAPDH. Representative Western blot image of the change in CCND3 protein levels upon OHT treatment over time using GAPDH as a loading control. (B) Relative change in CCND3 protein levels upon EBF1 depletion over time. CCND3 protein levels were normalized to GAPDH protein levels, where ns – not significant, * - p<0.05. (C) The change in Ct value of *Ccnd3* upon EBF1 depletion over time. *Ccnd3* Ct values were normalized to *Hrtp* Ct value (n = 4 experiments). 114

Figure 4-7 EBF1 Depletion causes a decrease in CCND3 protein levels. 1_1 and 1_3 *Ebf1^{fl/fl}RERT^{Cre}*::A-MuLV pro-B cells were treated with 2µM OHT and samples were collected on the third day, washed with PBS, fixed in 4% PFA, then permeabilized using Perm buffer. Cells were incubated with primary CCND3 antibodies, followed by incubation with secondary Alexa Fluor 488. Stained cells were cytospun onto slides, air-dried and DNA was stained with DAPI. (A) Representative confocal images of 1_1 and 1_3 *Ebf1^{fl/fl}RERT^{Cre}*::A-MuLV pro-B cells stained for CCND3 (green) and DNA (blue)..... 115

Figure 4-8 Depletion causes a decrease in CCND3 protein levels. 1_1 and 1_3 *Ebf1^{fl/fl}RERT^{Cre}*::A-MuLV pro-B cells were treated with 2µM OHT and samples were collected on the third day, washed with PBS, fixed in 4% PFA, then permeabilized using Perm buffer. Cells were incubated with primary CCND3 antibodies, followed by incubation with secondary Alexa Fluor 488. Stained cells were cytospun onto slides, air-dried and DNA was stained with DAPI. Fluorescence intensity of the CCND3 in the nuclei and whole cell was measured. Average

total intensity of CCND3 in the nuclei and cytoplasm represents CCND3 protein level distribution between these two compartments before and after EBF1 depletion (from 25 cells; n = 4 experiments, ×10 magnification)..... 116

Figure 4-9 EBF1 depletion in *Ebf1^{fl/fl}RERT^{Cre}::A-MuLV* pro-B cells causes nuclear blebbing. 1_1 and 1_3 *Ebf1^{fl/fl}RERT^{Cre}::A-MuLV* pro-B cells were treated with 2μM OHT, EtOH was used as a control. Samples were collected on the third day, washed with PBS, fixed in 4% PFA, then permeabilized using Perm buffer. Cells were incubated with primary Lap2β antibodies, followed by incubation with secondary Alexa Fluor 488. Stained cells were cytospun onto slides, air-dried and DNA was stained with DAPI. Representative confocal images of 1_1 and 1_3 *Ebf1^{fl/fl}RERT^{Cre}::A-MuLV* pro-B cells stained for Lap2β (green) and DNA (blue). Representative cells with the nuclear blebbing severity: full flower shape - 4, two fissures - 3, one fissure or another cell deformation - 2, normal – 1, are shown with the red arrows and corresponding number. 119

Figure 4-10 Assessment of nuclear blebbing upon OHT-induced EBF1 depletion. 1_1 and 1_3 *Ebf1^{fl/fl}RERT^{Cre}::A-MuLV* pro-B cells were treated with 2μM OHT, EtOH was used as a control. Samples were collected on the third day, washed with PBS, fixed in 4% PFA, then permeabilized using Perm buffer. Cells were incubated with primary Lap2β antibodies, followed by incubation with secondary Alexa Fluor 488. Stained cells were cytospun onto slides, air-dried and DNA was stained with DAPI. Nuclear blebbing of 1_1 and 1_3 *Ebf1^{fl/fl}RERT^{Cre}::A-MuLV* pro-B cells was assessed from 3D confocal images using a scoring system of nuclear blebbing severity: full flower shape - 4, two fissures -3, one fissure or another cell deformation - 2, normal – 1. (>50 cells per each sample)..... 120

Figure 4-11 EBF1 depletion in *Ebf1^{fl/fl}RERT^{Cre}::A-MuLV* pro-B cells causes heterochromatin localization at the nuclear membrane. 1_4 *Ebf1^{fl/fl}RERT^{Cre}::A-MuLV* (*Ebf1^{fl/fl}*) and c3_4 *Ebf1^{+/+}RERT^{Cre}::A-MuLV* (*Ebf1^{+/+}*) pro-B cells were treated with 2μM OHT for two days prior cell fixation. (A) Transmission electron images of 1_4 *Ebf1^{fl/fl}RERT^{Cre}::A-MuLV* pro-B cells and c3_4 *Ebf1^{+/+}RERT^{Cre}::A-MuLV* pro-B cells Heterochromatin accumulation at the periphery of the nuclei in the OHT depleted 1_4 *Ebf1^{fl/fl}RERT^{Cre}::A-MuLV* pro-B cells is show via white arrows. (B) The area euchromatin and heterochromatic occupied within the nuclei was calculated. Euchromatin and heterochromatin distribution in the nuclei before and after EBF1 depletion, where euchromatin, heterochromatin localized in the nuclear body (internal heterochromatin) and at the periphery of the nuclei (membrane bound

heterochromatin) are show, respectively, via green, blue and red (from 10 cells; n = 1 experiments). 122

Figure 4-12 EBF1 is a potential NM protein in *Ebf1^{fl/fl}RERT^{Cre}::A-MuLV* pro-B cells. 1_3
Ebf1^{fl/fl}RERT^{Cre}::A-MuLV pro-B cells were seeded on poly-L lysine coated coverslips day before in situ fractionation. Briefly, cells were treated with CSK buffer supplemented with 0.1% (v/v) Triton X-100, followed by treatment with CSK buffer supplemented with 0.5% (v/v) Triton X-100 and with CSK buffer supplemented with 100µg/ml of DNase I. Then cells were fixed in 4% PFA and permeabilized using Perm buffer. Cells were incubated with primary Lap2β, RUNX1 and EBF1 antibodies, followed by incubation with secondary Alexa Fluor 488 or Alexa Fluor 647 and DNA staining with DAPI. Mean intensity of the EBF1 and RUNX1 in the nuclei (from whole cell images) and in the NM (the parts that are free from DNA) were calculated Representative confocal images of 1_3 *Ebf1^{fl/fl}RERT^{Cre}::A-MuLV* pro-B cells before (Whole cell) and after *in situ* fractionation (Nuclear matrix) stained for (A) Lap2β (green), EBF1 (red) and DNA (blue) and for (B) RUNX1 (green), EBF1 (red) and DNA (blue). (C) Relative mean intensity of the EBF1 and RUNX1 per pixel in the whole nuclei and in the NM (from 25 cells; n = 3 experiments, x10 magnification). 125

Figure 4-13 Combined treatment of Droxinostat and OHT causes an increase in the cell death compared to a cell death in single treated cells with Droxinostat or OHT . 1_1 and 1_3
Ebf1^{fl/fl}RERT^{Cre}::A-MuLV pro-B cells were treated with and without 2µM OHT on day zero after 8h of Droxinostat was added at different concentrations, combination of EtOH and DMSO was used as a control. Cells were collected three days after OHT treatment and stained with PI. (A) Representative flow cytometry images of untreated, single or double treated pro-B cells with 2µM OHT and 2.5µM Droxinostat. Collected events are gated for all events (gate A), single cells (gate B), PI unstained cells (gate C) and PI stained cells (Gate D). (B) The change in nuclear PI staining in OHT untreated and treated pro-B cells upon an increase in Droxinostat dose. (n = 4 experiments)..... 129

Figure 4-14 Combined treatment of RGFP966 and OHT causes an increase in the cell death compared to a cell death in single treated cells with RGFP966 or OHT. 1_1 and 1_3
Ebf1^{fl/fl}RERT^{Cre}::A-MuLV pro-B cells were treated with and without 2µM OHT on day zero, after 8h of RGFP966 was added at different concentrations, combination of EtOH and DMSO was used as a control. Cells were collected three days after OHT treatment and stained with PI. (A) Representative flow cytometry images of untreated, single or double treated pro-B cells with 2µM OHT and 2.5µM RGFP966. Collected events are gated for all events (gate A),

single cells (gate B), PI unstained cells (gate C) and PI stained cells (Gate D). (B) The change in nuclear PI staining at in OHT untreated and treated pro-B cells upon an increase in RGFP966 dose. (n = 4 experiments)..... 130

Figure 4-15 Verification of EBF1 depletion in *Ebf1^{fl/fl}RERT^{Cre}::A-MuLV* pro-B cells after OHT and/or HDAC3 inhibitor treatment. 1_1 and 1_3 *Ebf1^{fl/fl}RERT^{Cre}::A-MuLV* pro-B cells were treated with and without 2µM OHT on Day zero, 2.5µM RGFP966 was added 8h after OHT addition, combination of EtOH and DMSO was used as a control. Cells were collected three days after OHT treatment, lysed and proteins were separated via acrylamide gel electrophoresis, then proteins were transferred to nitrocellulose membrane and stained for EBF1 and GAPDH. 131

Figure 4-16 HDAC3 inhibitors do not rescue 1_1 *Ebf1^{fl/fl}RERT^{Cre}::A-MuLV* pro-B cells from OHT induced nuclear blebbing collapse. 1_1 *Ebf1^{fl/fl}RERT^{Cre}::A-MuLV* pro-B cells were treated with and without 2µM OHT on Day zero, 2.5µM RGFP966 or 2.5µM Droxinostat was added 8h after OHT addition, combination of EtOH and DMSO was used as a control. Cells were collected three days after OHT treatment, washed with PBS, fixed in 4% PFA, then permeabilized using Perm buffer. Cells were incubated with primary Lap2β antibodies, followed by incubation with secondary Alexa Fluor 488. Stained cells were cytopun onto slides, air-dried and DNA was stained with DAPI. Representative confocal images of 1_1 and *Ebf1^{fl/fl}RERT^{Cre}::A-MuLV* pro-B cells stained for Lap2β (green) and DNA (blue)..... 133

Figure 4-17 HDAC3 inhibitors does not rescue 1_3 *Ebf1^{fl/fl}RERT^{Cre}::A-MuLV* pro-B cells from OHT induced nuclear blebbing collapse. 1_3 *Ebf1^{fl/fl}RERT^{Cre}::A-MuLV* pro-B cells were treated with and without 2µM OHT on Day zero, 2.5µM RGFP966 or 2.5µM Droxinostat was added 8h after OHT addition, combination of EtOH and DMSO was used as a control. Cells were collected three days after OHT treatment, washed with PBS, fixed in 4% PFA, then permeabilized using Perm buffer. Cells were incubated with primary Lap2β antibodies, followed by incubation with secondary Alexa Fluor 488. Stained cells were cytopun onto slides, air-dried and DNA was stained with DAPI. Representative confocal images of 1_3 and *Ebf1^{fl/fl}RERT^{Cre}::A-MuLV* pro-B cells stained for Lap2β (green) and DNA (blue)..... 134

Figure 4-18 Assessment of nuclear blebbing upon pro-B cell treatment with OHT, Droxinostat or RGFP966 alone or their combination. 1_1 and 1_3 *Ebf1^{fl/fl}RERT^{Cre}::A-MuLV* pro-B cells were treated with and without 2µM OHT on Day zero, 2.5µM RGFP966 or 2.5µM Droxinostat was added 8h after OHT addition, combination of EtOH and DMSO was used as a control. Cells

were collected three days after OHT treatment, washed with PBS, fixed in 4% PFA, then permeabilized using Perm buffer. Cells were incubated with primary Lap2 β antibodies, followed by incubation with secondary Alexa Fluor 488. Stained cells were cytopun onto slides, air-dried and DNA was stained with DAPI. Nuclear blebbing of 1_1 and 1_3 *Ebf1^{fl/fl}RERT^{Cre}*::A-MuLV pro-B cells was assessed from 3D confocal images using a scoring system of nuclear blebbing severity: full flower shape - 4, two fissures -3, one fissure or another cell deformation - 2, normal - 1. (>100 cells per each sample)..... 135

Figure 4-19 EBF1 depletion in 1_1 *Ebf1^{fl/fl}RERT^{Cre}*::A-MuLV pro-B cells does not a cause change in Runx1 nuclear localisation. 1_1 *Ebf1^{fl/fl}RERT^{Cre}*::A-MuLV pro-B cells were treated with and without 2 μ M OHT on Day zero, 2.5 μ M RGFP966 or 2.5 μ M Droxinostat was added 8h after OHT addition, combination of EtOH and DMSO was used as a control. Cells were collected three days after OHT treatment, washed with PBS, fixed in 4% PFA, then permeabilized using Perm buffer. Cells were incubated with primary RUNX1 antibodies, followed by incubation with secondary Alexa Fluor 488. Stained cells were cytopun onto slides, air-dried and DNA was stained with DAPI. Representative confocal images of 1_1 and *Ebf1^{fl/fl}RERT^{Cre}*::A-MuLV pro-B cells stained for RUNX1 (green) and DNA (blue). 137

Figure 4-20 EBF1 depletion in 1_3 *Ebf1^{fl/fl}RERT^{Cre}*::A-MuLV pro-B cells does not a cause change in Runx1 nuclear localisation. 1_3 *Ebf1^{fl/fl}RERT^{Cre}*::A-MuLV pro-B cells were treated with and without 2 μ M OHT on Day zero, 2.5 μ M RGFP966 or 2.5 μ M Droxinostat was added 8h after OHT addition. Cells were collected three days after OHT treatment, washed with PBS, fixed in 4% PFA, then permeabilized using Perm buffer. Cells were incubated with primary RUNX1 antibodies, followed by incubation with secondary Alexa Fluor 488. Stained cells were cytopun onto slides, air-dried and DNA was stained with DAPI. Representative confocal images of 1_3 and *Ebf1^{fl/fl}RERT^{Cre}*::A-MuLV pro-B cells stained for RUNX1 (green) and DNA (blue)..... 138

Figure 4-21 RUNX1 protein levels increase upon EBF1 depletion in *Ebf1^{fl/fl}RERT^{Cre}*::A-MuLV pro-B cells. 1_1 and 1_3 *Ebf1^{fl/fl}RERT^{Cre}*::A-MuLV pro-B cells were treated with and without 2 μ M OHT on Day zero, 2.5 μ M RGFP966 or 2.5 μ M Droxinostat was added 8h after OHT addition, combination of EtOH and DMSO was used as a control. Cells were collected three days after OHT treatment, washed with PBS, fixed in 4% PFA, then permeabilized using Perm buffer. Cells were incubated with primary RUNX1 antibodies, followed by incubation with secondary Alexa Fluor 488. Stained cells were cytopun onto slides, air-dried and DNA was stained with DAPI. Fluorescence intensity of the RUNX1 was measured in each RUNX1

stained cell. The change in relative intensity of RUNX1 upon different treatments of (A) 1_1 and (B) 1_3 *Ebf1^{fl/fl}RERT^{Cre}*::A-MuLV pro-B cells (from 50 cells; n = 2 experiments). 139

Figure 5-1 CCNA2 and CCND3 are highly similar by structure. Comparison of CCNA2 (in green) (PBD ID: 3DOG) (Bettayeb, Oumata et al. 2008) and CCND3 (in red) (PBD ID: 3G33) (Takaki, Echaliier et al. 2009) protein structure. Protein sequences were downloaded from RCSB PBD database and aligned via PyMOL. 140

Figure 5-2 CCNA2 and CCND3 hold low sequence identity. CCNA2 and CCND3 sequence alignment, the first line shows the amino acid conservation index (> 5). Representative sequences of CCNA2 (the third line) and CCND3 (the second line) coloured according to predicted secondary structures (red: alpha-helix, blue: beta-strand). Consensus_aa - Consensus amino acids: identical amino acids are presented in bold and uppercase letters, l-aliphatic residues, @- aromatic residues, h- hydrophobic residues, o - alcohol residues, p - polar residues, t - tiny residues, s - small residues, b - bulky residues, "+" - positively charged residues, "-" -negatively charged residues, c - charged). Consensus_ss -Consensus secondary structures, where h – alpha-helix, e- beta-strand (Pei, Kim et al. 2008). 141

Figure 5-3 Recombinant FLAG WT EBF1 and FLAG ΔT EBF1 affinity purification together with recombinant CCNA2 His using Ni-NTA resin. CCNA2 His was expressed in bacteria, while FLAG WT EBF1 and FLAG ΔT EBF1 were expressed in 293T cells. Bacterial lysate containing CCNA2 His was incubated together with the equilibrated Ni-NTA resin, flow through was collected and column was washed twice. Mammalian lysate containing FLAG-EBF1 was add to the CCNA2 His bound NI-NTA resin. After incubation, flow through was collected and column was washed twice. FLAG EBF1 was purified together with CCNA2 His using Ni-NTA elution buffer. (A) FLAG WT EBF1 and (B) FLAG ΔT EBF1 affinity purification was verified via Western blot analysis, CCNA2 His affinity purification via Coomassie staining, where L BL21– bacterial lysate containing recombinant CCNA2 His, L 293T – mammalian lysate containing FLAG WT EBF1 or FLAG ΔT EBF1 protein, FT BL21– flow through after addition of bacterial lysate containing recombinant CCNA2 His, FT 293T – flow-through after addition of mammalian lysate containing FLAG WT EBF1 or FLAG ΔT EBF1 protein..... 143

Figure 5-4 Recombinant FLAG WT and mutant EBF1 affinity purification together with recombinant CCNA2 His using Ni-NTA resin. CCNA2 His was expressed in bacteria, while FLAG WT EBF1 and FLAG ΔT EBF1 were expressed in 293T cells. Bacterial lysate containing CCNA2 His was incubated together with the equilibrated Ni-NTA resin, flow through was

collected and column was washed twice. Mammalian lysate containing FLAG-EBF1 was added to the CCNA2 His bound Ni-NTA resin. After incubation, flow through was collected and column was washed twice. FLAG EBF1 was purified together with CCNA2 His using Ni-NTA elution buffer. Protein expression and affinity purification were verified via Western blot analysis. (A) FLAG WT and mutant EBF1 affinity purification together with CCNA2 His, where UB – unspecific binding. (B) FLAG WT EBF1 affinity purification with and without CCNA2 His, where N1 and N2 are two separate experiments. FLAG WT (+) EBF1 – FLAG WT EBF1 affinity purification together with CCNA2 His (n=5 experiments), FLAG WT (-) EBF1 – FLAG WT EBF1 affinity purification with bacterial lysate (n=3), FLAG ΔT EBF1 (n=6), FLAG ΔI EBF1 (n=7), FLAG ΔIΔT EBF1 (n=7), FLAG ΔD EBF1 (n=5) FLAG ΔDΔIΔT EBF1 (n=4), FLAG HES1 (n=4).
 145

Figure 5-5 Optimizing Co-IP protocol for (A) EBF1 Co-IP together with CCND3 and (B) CCNA2 and CCND3 Co-IP together with EBF1. 1_4 *Ebf1^{fl/fl}RERT^{Cre}*::A-MuLV pro-B cells were harvested, washed with PBS, lysed and sonicated and proteins were Co-IP using Protocol 1 (Pr1) and Protocol 2 (Pr2). For CCND3 pulldown CCND3 mouse monoclonal antibodies were coupled to A/G PLUS-agarose, normal mouse IgG antibodies coupled to A/G PLUS agarose were used as isotype control (IC). For EBF1 pulldown EBF1 rabbit polyclonal antibodies were coupled to A/G PLUS-agarose, normal rabbit IgG antibodies coupled to A/G PLUS agarose were used as isotype control (IC). Protein elution was verified via Western blot analysis, FT- flow through..... 147

Figure 5-6 Optimizing EBF1 elution together with CCND3. 1_4 *Ebf1^{fl/fl}RERT^{Cre}*::A-MuLV pro-B cells were harvested, washed with PBS, lysed using a varied concentration of Glycerol, NP-40 and DTT in the lysis buffer, sonicated and proteins were Co-IP using Protocol 2. CCND3 mouse monoclonal antibodies were coupled to A/G PLUS-agarose, normal mouse IgG antibodies coupled to A/G PLUS agarose, were used as isotype control (IC). Protein elution was verified via Western blot analysis, FT- flow through..... 150

Figure 6-1 CCND RNA expression in Bone marrow and immune system (Uhlen, Fagerberg et al. 2015)..... 155

Figure 6-2 CCND3 expression in *Ebf1^{fl/fl}RERT^{Cre}*::A-MuLV pro-B and MPI-2 cells. Cells were lysed and proteins were separated via acrylamide gel electrophoresis, then proteins were transferred to nitrocellulose membrane and stained for EBF1, CCND3 and GAPDH. (A) Western blot analysis verifies EBF1 and CCND3 expression. (B) Relative CCND3 and EBF1

protein levels. CCND3 and EBF1 protein levels were normalized to GAPDH protein levels. (C) Cells were collected, washed with PBS, fixed in 4% PFA, then permeabilized using Perm buffer. Cells were incubated with primary CCND3 antibodies, followed by incubation with secondary Alexa Fluor 488 antibodies. Stained cells were cytospun onto slides, air-dried and DNA was stained with DAPI. Confocal images of 1_3 *Ebf1^{fl/fl}RERT^{Cre}*::A-MuLV pro-B and MPI-2 cells stained for CCND3 (green) and DAPI (blue). (D) Average total intensity of the CCND3 in the nuclei and cytoplasm (from 50 cells; n = 3 experiments, ×10 magnification)..... 156

Figure 6-3 Verifying CCND3 immunoprecipitation. 1_1, 1_4 *Ebf1^{fl/fl}RERT^{Cre}*::A-MuLV pro-B and MPI-2 cells were harvested and lysed. Lysates were incubated with CCND3 antibody coupled resin. After incubation, flow through was collected, resin was washed and CCND3 was eluted. CCND3 elution from 1_1, 1_4 *Ebf1^{fl/fl}RERT^{Cre}*::A-MuLV pro-B and MPI-2 cells was then assessed *via* acrylamide gel silver staining (B and C). Assessment of the second CCND3 pulldown from 1_4 *Ebf1^{fl/fl}RERT^{Cre}*::A-MuLV pro-B cells (B) *via* acrylamide gel silver staining and (C) Western blot analysis. 158

Figure 6-4 The number of potential binding partners of CCND3 that are unique and common in 1_1 and 1_4 *Ebf1^{fl/fl}RERT^{Cre}*::A-MuLV pro-B cells and MPI-2 cells. 1_1, 1_4 *Ebf1^{fl/fl}RERT^{Cre}*::A-MuLV pro-B and MPI-2 cells were harvested and lysed. Lysates were incubated with CCND3 antibody coupled resin. After incubation, flow through was collected, resin was washed and CCND3 was eluted. The verified eluates were run into 12% acrylamide gel and proteins were in gel digested with trypsin. Peptides were analysed with short-gradient LC-MS/MS. The list of CCND3 potential binding partners (Figure 10-4) in different cell lines was assessed using Venn diagram. 159

Figure 6-5 EBF1 does not interact with ANP32A. 1_4 *Ebf1^{fl/fl}RERT^{Cre}*::A-MuLV pro-B cells were harvested, washed with PBS, lysed and sonicated and proteins were Co-IP using Protocol 2. EBF1 rabbit polyclonal antibodies were coupled to A/G PLUS-agarose, normal rabbit IgG antibodies coupled to A/G PLUS agarose were used as isotype control (IC). Protein elution was verified *via* Western blot analysis, FT- flow through..... 169

Figure 10-1 *Ebf1* qRT-PCR forward and reverse primer aligned on the *Mus musculus Ebf1* transcript variant X1, where in green is shown *Ebf1* gene coding sequence, in grey is forward primer annealing site and in yellow is shown reverse primer annealing site, (NCBI Reference Sequence 030245520.1) (Benson, Cavanaugh et al. 2017). 199

Figure 10-2 <i>Ccnd3</i> qRT-PCR forward and reverse primer aligned on the <i>Mus musculus Ccnd3</i> transcript variant 1 , where in green is shown <i>Ccnd3</i> gene coding sequence, in grey is forward primer annealing site and in yellow is shown reverse primer annealing site, (NCBI Reference NM_007632.2) (Matsushime, Roussel et al. 1991, Benson, Cavanaugh et al. 2017).....	201
Figure 10-3 <i>Hprt</i> qRT-PCR forward and reverse primer aligned on the <i>Mus musculus Hprt</i> , where in green is shown <i>Hprt</i> gene coding sequence, in grey is forward primer annealing site and in yellow is shown reverse primer annealing site, (NCBI Reference NM_013556.2) (Chapman and Shows 1976, Benson, Cavanaugh et al. 2017)	202
Figure 10-4 Potential binding partners of CCND3	203

List of Tables

Table 3-1 Plasmid maps used in plasmid cloning and protein expression in mammalian and bacterial cultures, where WT - Wild type, ΔT <i>Ebf1</i> (dT <i>Ebf1</i>)- <i>Ebf1</i> lacking TAD domain, ΔI <i>Ebf1</i> - <i>Ebf1</i> lacking IPT, $\Delta I\Delta T$ <i>Ebf1</i> - <i>Ebf1</i> lacking IPT and TAD and $\Delta D\Delta I\Delta T$ <i>Ebf1</i> - <i>Ebf1</i> lacking DBD, IPT and TAD.	68
Table 3-2 Primers used in PCR amplification of $\Delta H\Delta T$ <i>Ebf1</i> and ΔD <i>Ebf1</i>	75
Table 3-3 Testing the effect of different concentration of HDAC inhibitors alone and in combination with 2 μ M OHT on <i>Ebf1^{fl/fl}RERT^{Cre}::A-MuLV pro-B</i> cells. The final concentration of HDAC inhibitors, OHT, EtOH and DMSO in each well, where R – RGFP966 and D – Droxinostat.	84
Table 3-4 Primers that were used to test for cleaved and floxed alleles	97
Table 3-5 Primers used in qRT-PCR amplifying <i>Ebf1</i> , <i>Ccnd3</i> and housekeeping gene <i>Hrtp</i> . Primer annealing sites on the respective gene is shown in Appendix (Figure 10-1, Figure 10-2 and Figure 10-3).	99
Table 3-6 Primary Antibody concentration used in Western blot analysis	102
Table 6-1 EBF1 binding partners detected via MS in 1_4 <i>Ebf1^{fl/fl}RERT^{Cre}::A-MuLV pro-B</i> cells. EBF1 was immunoprecipitated using Pierce Co-IP kit; eluted samples were sent for MS analysis. Potential EBF1 binding partners were grouped by their primary function. Previously reported NM proteins are presented in red.....	153
Table 6-2 Functions of potential CCND3 binding partners in <i>Ebf1^{fl/fl}RERT^{Cre}::A-MuLV pro-B and MPI-2</i> cells. CCND3 was immunoprecipitated using Pierce Co-IP kit from 1_4 and 1_1 <i>Ebf1^{fl/fl}RERT^{Cre}::A-MuLV pro-B</i> and MPI-2 cells, eluted samples were sent for MS analysis. Potential CCND3 binding partners were grouped by their primary function. In bold are presented newly detected, and cell type unique proteins, highlighted in yellow are previously reported CCND3 binding partners. Previously reported NM proteins are presented in red.	160
Table 6-3 Comparison of CCND3 and EBF1 binding partners. CCND3 and EBF1 were immunoprecipitated using Pierce Co-IP kit from 1_4 <i>Ebf1^{fl/fl}RERT^{Cre}::A-MuLV pro-B</i> cells,	

eluted samples were sent for MS analysis. Potential CCND3 and EBF1 binding partners were grouped by their primary function. Here are presented common binding partners of EBF1 and CCND3,. Previously reported NM protein is presented in red..... 168

List of Abbreviations

γ c	Common cytokine receptor γ -chain
A-MuLV	Abelson murine leukaemia virus
ABC	Ammonium bicarbonate
ABL1	Abelson murine leukaemia viral oncogene homolog 1
AHCY	Adenosyl homocysteinase
AK2	Adenylate kinase 2
AKT	Protein kinase B
ALDH1B1	Aldehyde dehydrogenase 1 family member B1
ALL	Acute Lymphoblastic Leukaemia
ANP32A	Acidic nuclear phosphoprotein 32 family member A
ANXA1	Annexin A1
ARHGDI1B	Rho GDP-dissociation inhibitor 2
AS	ammonium sulfate
ASNS	Asparagine synthetase
ATIC	5-aminoimidazole-4-carboxamide ribonucleotide formyl transferase/IMP cyclohydrolase
ATIC	
AURKB	Aurora Kinase B
BCAT1	Branched-chain aminotransferase 1
BCP-ALL	B-Cell Precursor Acute Lymphoblastic Leukaemia
BCR	The B-cell receptor
bp	Base pair
BSA	Bovine Serum Albumin
CASC5	Cancer susceptibility candidate protein 5
CCNA	Cyclin A
CCNB	Cyclin B
CCND	Cyclin D
CCNE	Cyclin E
<i>Cd40</i>	Custer of differentiation 40
<i>Cd79a</i>	Cluster of differentiation 79A, known as well as Ig α
<i>Cd79a</i>	Cluster of differentiation 79A gene known as well as <i>mb-1</i> gene
<i>Cd79b</i>	Cluster of differentiation 79B, known as well as Ig β)
CDK	Cyclin dependent kinases
CDKN1A	Cyclin dependent kinase inhibitor 1 alpha
CDKN2C	Cyclin-dependent kinase inhibitor 2C
CENPA	Centromere protein A
CENPL	Centromere protein L
CENPM	Centromere Protein M
C _H	Immunoglobulin heavy chain constant segment
C _L	Immunoglobulin light chain constant segment
CLP	Common lymphoid progenitors
CMP	Common myeloid progenitor
Co-IP	Co-Immunoprecipitation
COP9	Constitutive photomorphogenesis 9

COS1	Fibroblast-like cell lines derived from monkey kidney tissue
COSP4	COP9 signalosome subunit 4
CREB2	Cyclic AMP-Responsive Element-Binding Protein 2
CRM1	Chromosomal Maintenance 1
CS	Citrate synthase
CSE1L	Chromosome segregation 1 like
CTCF	CCCTC-binding factor
CTH	Cystathionine gamma-lyase
CUL3	Clullin 3
CUX1	Cut Like Homeobox 1
D	Diversity segment
DACH1	Dachshund Family Transcription Factor 1
DAPI	4',6-diamidino-2-phenylindole
DBD	DNA binding domain
DDX39B	DExD-box helicase 39B
DDX3X	DEAD-Box Helicase 3 X-Linked
DES	Desmin
D _H	Immunoglobulin heavy chain diversity segment
D _H J _H	The first immunoglobulin heavy chain diversity and joining segment
DLBCL	Diffuse large B-cell Lymphoma
DMEM	Dulbecco's Modified Eagle Medium
DMEM FBS p/s	DMEM with 4.5g/l glucose media, supplemented with 10% FBS, 1% v/v penicillin and streptomycin
DMSO	Dimethyl sulfoxide
DTT	Dithiothreitol
DUSP7	Dual specificity Phosphate 7
E-BOX	Enhancer box
E2F1	E2F Transcription Factor 1
EBF1	Early B-cell factor 1
<i>Ebf1</i> ^{+/-}	Heterozygous <i>Ebf1</i> allele
<i>Ebf1</i> ^{+/+} <i>RERT</i> ^{Cre}	Conditional knockout mouse pro-B cells, which expresses the Cre recombinase under the control of a tamoxifen-inducible promoter and does not deplete floxed <i>Ebf1</i>
<i>Ebf1</i> ^{+/+} <i>RERT</i> ^{Cre} ::A-MuLV	Immortalized <i>Ebf1</i> ^{+/+} <i>RERT</i> ^{Cre} with A-MuLV
<i>Ebf1</i> ^{fl/fl} <i>RERT</i> ^{Cre}	Conditional knockout mouse pro-B cells, which expresses the Cre recombinase under the control of a tamoxifen-inducible promoter and deplete floxed <i>Ebf1</i>
<i>Ebf1</i> ^{fl/fl} <i>RERT</i> ^{Cre} ::A-MuLV	Immortalized <i>Ebf1</i> ^{fl/fl} <i>RERT</i> ^{Cre} with A-MuLV
EDTA	Ethylenediaminetetraacetic acid
EdU	5-Ethynyl-2'-deoxyuridine
eIF-3	Eukaryotic translation initiation factor 3
EIF3E	Eukaryotic Translation Initiation Factor 3 Subunit E
EIF3K	Eukaryotic translation initiation factor 3 subunit K
EIF6	Eukaryotic Translation Initiation Factor 6

ELK1	ETS Transcription Factor ELK1
ER	Estrogen receptor protein
ERAP1	Endoplasmic reticulum aminopeptidase 1
ERG3	Transforming Protein ERG
ERM	Ezr, Radixin and Msn (ERM) proteins
ERO1L	Endoplasmic reticulum oxidase 1-alpha
EtOH	Ethanol
ETS	E26 transformation-specific
EZR	Ezrin
FBS	Foetal bovine serum
FITC	Fluorescein isothiocyanate
FLAG Δ D EBF1	FLAG EBF1 lacking DNA binding
FLAG Δ D Δ I Δ T EBF1	FLAG EBF1 lacking DNA binding, "immunoglobulin, plexins, transcription factors-like" and Transactivation domain
FLAG Δ H Δ T EBF1	FLAG EBF1 lacking Helix-loop-helix and Transactivation domain
FLAG Δ I EBF1	FLAG EBF1 lacking "immunoglobulin, plexins, transcription factors-like"
FLAG Δ T EBF1	FLAG EBF1 lacking transactivation domain
FLAG EBF1 Δ I Δ T	FLAG EBF1 lacking "immunoglobulin, plexins, transcription factors-like" and Transactivation domain
FLNA	Filamin a
FoxO1	Forkhead Box O1
FT	Flow-through
GADD45B	Growth arrest and DNA damage inducible beta
GAPDH	Glyceraldehyde 3-phosphate dehydrogenase
GC	Germinal centre
GM-CSF	Granulocyte-macrophage colony-stimulating factor
GS3K3 β	Glycogen synthase kinase-3 beta
H3ac	Acetylated histone H3
H3K4me2	Dimethylated lysine 4 on histone H3
H3K4me3	Trimethylated lysine 4 on histone H3
H4ac	Acetyl anti-histone H4
HAc	Acetic acid
HDAC1	Histone deacetylase 1
HDAC3	Histone deacetylase 3
HES1	Hairy and enhancer of slip-1
hESC	Human embryonic stem cells
HLH	Helix-loop-helix
HNRNPL	Heterogeneous Nuclear Ribonucleoprotein L
HP1 α	Heterochromatin protein 1 homolog alpha
HSCs	Hematopoietic stem cells
HSP10	Heat shock protein family E
HSPE1	Hsp10 member 1
IC	Isotype control

Ig	Immunoglobulin
Ig α	Immunoglobulin alpha, known as well as Cd79a
Ig β	Immunoglobulin betta, known as well as Cd79b
IGL1	Immunoglobulin lambda-like polypeptide 1
IgH	Immunoglobulin heavy chain
IgL	Immunoglobulin light chain
IL7-R	interleukin 7 receptor
INHAT	The inhibitor of histone acetyltransferase complex
IPT	"Immunoglobulin, plexins, transcription factors-like"
IPTG	Isopropyl- β -D-thiogalactoside
IRF4	Interferon regulatory factor 4
ITGB7	Integrin subunit beta 7
J	Joining segment
J _H	Immunoglobulin heavy chain joining segment
J _L	Immunoglobulin light chain joining segment
Krt17	Keratin 17
L	Lysate
LAP1	Lamina associated polypeptide 1
LAP2 β	Lamina associated polypeptide 2 beta
LB-a/c	LB supplemented with 100 μ g/ml ampicillin and 35 μ g/ml chloramphenicol
LB-amp	LB media with ampicillin
LBR	Lamin B-receptor
LGALS9	Galectin-9
LIS	lithium 3,5-diiodosalicylate
LMNA	Lamin A/C
LMNB1	Lamin B1
MACF1	Microtubule actin crosslinking factor 1 (
MAD2L1	Mitotic arrest deficient 2 like 1
MAML2	Mastermind like transcriptional coactivator 2
MAR	Matrix-attachment regions
MEF	Mouse embryonic fibroblasts
MeOH	Methanol
MHC	The major histocompatibility complex
MPI-2	Max Planck Institute cells 2
MPP	Multipotent progenitor cells
MS	Mass spec
MSN	Moesin
MTDH	Metadherin
MYB	Proto-oncogene like 1 and MYB-related protein B
MYBBP1A	MYB Binding Protein 1a
MYOD	Myoblast determination protein
NCOR2	Nuclear Receptor Corepressor 2
NF- κ B	Nuclear factor kappa B
NK	Natural killer cells
NLS	Nuclear localization signal
NM	Nuclear matrix

NOL8	Nucleolar protein 8
NOL10	Nucleolar protein 10
NOLC1	Nucleolar and Coiled-Body Phosphoprotein 1
Nrf1	Nuclear respiratory factor 1
ns	Not significant
NuMA	Nuclear mitotic apparatus protein
O/N	Overnight
OD	Optical density
OHT	(Z)-4-Hydroxytamoxifen
OTX1	Orthodenticle Homeobox 1
PARP	Poly (ADP-ribose) polymerase
<i>Pax5^{+/-}</i>	Heterozygous paired box 5 allele
PBS	Phosphate-buffer saline
PBX1	PBX Homeobox 1
PCNA	Proliferating cell nuclear antigen
PCV	Packed cell volume
PDCD4	Programmed cell death 4
PE	Phycoerythrin
Phosphatase cocktail	PhosSTOP EASY PACK phosphatase inhibitor cocktail inhibitor
PI	Propidium iodide
PI3K	phosphoinositide 3-kinase
Pigr	Polymeric Immunoglobulin receptor
PKA	Protein kinase A
PMSF	Phenylmethylsulphonyl Fluoride
PP1	Protein phosphatase 1
PPDCD6IP	Programmed cell death 6 interacting protein
Pr	Protocol
PSMA6	Proteasome Subunit alpha 6
PSMB3	Proteasome subunit beta 3
RAD21	RAD21 Cohesin Complex Component
<i>Rag1</i>	Recombinant activation gene 1
RAS	Rat sarcoma
RB	Retinoblastoma
EBBP8	RB binding protein 8
RBM39	RNA Binding Motif Protein 39
RGC	Retinal ganglion cells
RNAP	RNA polymerase
RP	Ribosomal protein
RPL14	Ribosomal protein L14
RPMI	Roswell Park Memorial Institute
RPMI FBS p/s β -m	RPMI medium with L- glutamine supplemented with 10% FBS, 1% v/v penicillin and streptomycin and 0.0004% β -mercaptoethanol
RPMI FBS p/s β -m GM-CSF	RPMI FBS p/s β -m with addition of GM-CSF
RRP12	Ribosomal RNA Processing 12 homolog
RPS15A	Ribosomal protein S15a

RRS1	Ribosome Biogenesis Regulator 1 Homolog
RT	Room temperature
RUNX	Runt-related transcription factor
SAF-A	Scaffold attachment factor A
SAR	Scaffold attachment regions
SATB1	Special AT-Rich Sequence Binding Protein 1
Sept11	Septin 11
SMAD2	SMAD Family Member 2
SMTN	Smoothelin
SOD2	Superoxide dismutase 2, mitochondrial
SOX3	SRY-Box 3
SPI1	Hematopoietic Transcription Factor PU.1
SRSF2	Serine and arginine rich splicing factor 2
STAT5	Signal transducer and activator of transcription 5
TAD	Transactivation domain
TCF3	Transcriptional Factor 3 (also known as E2A)
TCR	T-cell receptor signalling
TF	Transcription factor
THOC1	THO Complex 1
Thr283	The 283 threonine
TIA1	T-cell-restricted intracellular antigen-1
TUBA1A	Tubulin Alpha 1a
TUBB4B	Tubulin Beta 4B class IVb
TXNL1	Thioredoxin Like 1
UB	Unspecific binding
UV	Ultraviolet
V	Variable segment
VARS	Valyl-tRNA synthetase
V _H	Immunoglobulin heavy chain variable segment
V _H D _H J _H	Immunoglobulin heavy chain variable, diversity and heavy chain joining segment
V _k J _k	The immunoglobulin light chain variable and joining kappa locus
V _L	Immunoglobulin light chain variable segment
V _L J _L	Immunoglobulin light chain variable and joining segment
WNT3	Wnt Family Member 3
WT	Wild type
ZFX	Zinc finger X-chromosomal protein

Chapter 1 Introduction

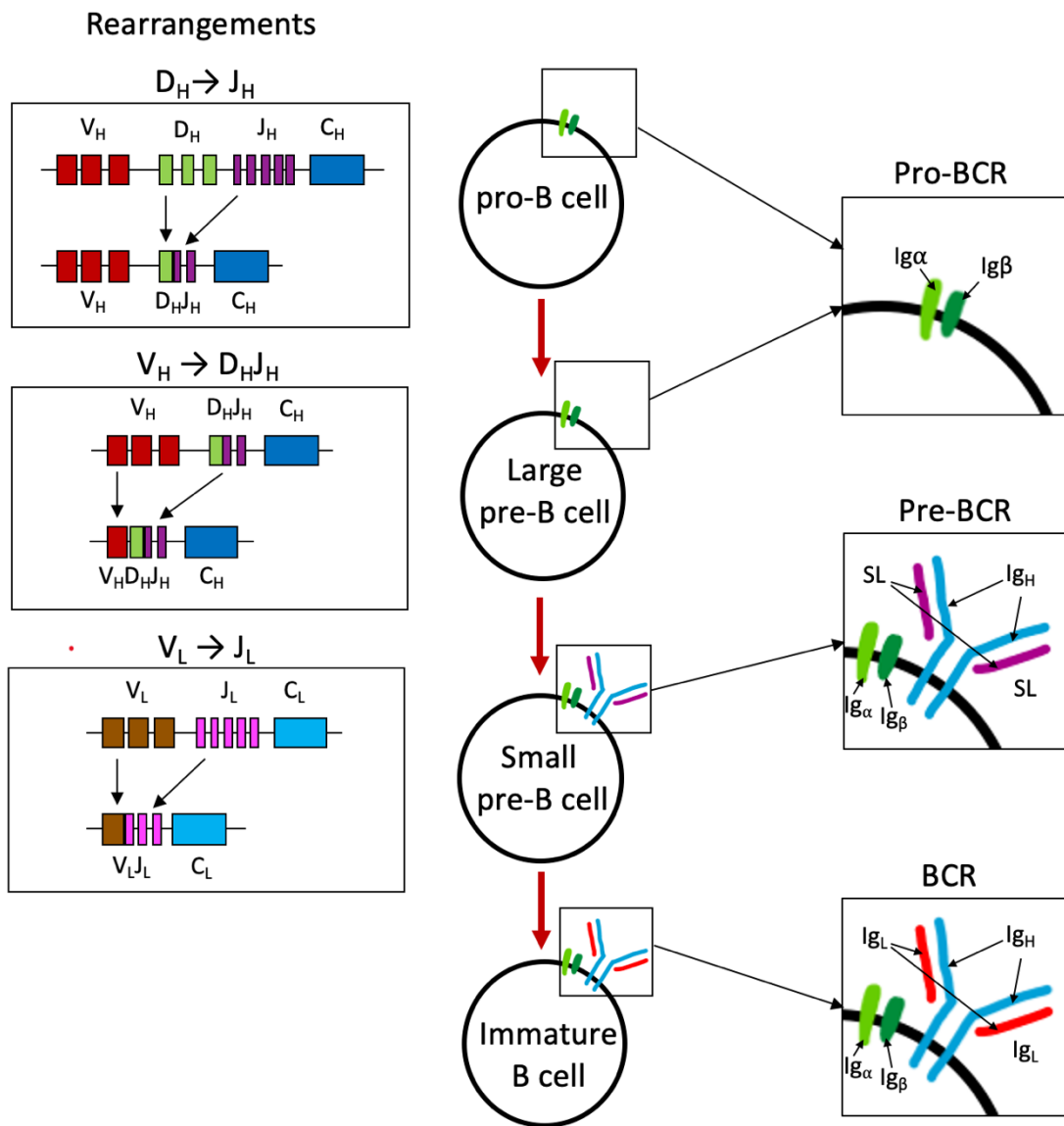
1.1 B-cell development and functions

B-cells are part of the adaptive humoral immune system, their main functions are to produce antibodies, to mature and act as antigen presenting cells (APCs), antibody secreting plasma or memory B-cells (Selvaraj, Poinatte et al. 2016). B-cells differentiate from the hematopoietic stem cell (HSC) in the bone marrow (Till and Mc 1961). Antibody production start in pro-B cells with immunoglobulin heavy chain (IgH) rearrangement, which is followed by immunoglobulin light chain (IgL) rearrangement. Antibody production is completed in immature B-cells when IgH and IgL joins and forms antibody (Figure 1-1) (Winkler and Martensson 2018). Immature B-cells undergo negative selection in the bone marrow and upon binding to self-antigen are marked for apoptosis. Only those immature B-cells, which withstand negative selection, leave the bone marrow (naïve B-cells) and continue their maturation in spleen, forming mature B-cells (Choukrallah and Matthias 2014, Boller, Ramamoorthy et al. 2016). Naïve B-cells upon encounter with antigen may internalized the offending antigen; the digested parts of the antigen are then presented on the surface of the cells. These cells are called APCs and they recognize and fight pathogens by internalizing and digesting them (Fling, Arp et al. 1994). APCs may mature into antibody-secreting plasma and/or memory B-cells (Tangye, Avery et al. 2003). Memory B-cells are able to survive for a long period, their function is to respond on re-infection (McHeyzer-Williams and Ahmed 1999). While, plasma cells are short-lived, their function is to produce and secrete antibodies in order to fight current infection. Secreted antibodies bind to the specific antigens and mark them for phagocytosis (McHeyzer-Williams and Ahmed 1999).

The B-cell receptor (BCR) is responsible for recognition of pathogens, and it consists of membrane-bound antibody molecule and the Cluster differentiation 79 alpha (Cd79a known as well as Ig α) and beta (Cd79b know as well as Ig β) heterodimer (Parkhouse 1990). Pro-BCR and pre-BCR complexes precedes BRC complex formation and are important in B-cell development (Figure 1-1). The driving force of B-cell development is the generation of the antibodies and the BCR repertoire via genetic recombination. The

immunoglobulin expression and variety are regulated by variable (V), diversity (D) and joining (J) gene segment (VDJ) recombination, and it is solely B-cell specific. The staging of B-cell development is based on their developmental phase as well as the level of potency and specialisation towards their future function (specification and commitment) (McCormack, Tjoelker et al. 1991). The BCR complex formation starts with an expression of Cd79a and Cd79b, which forms a signalling complex together with calnexin on the surface of the pro-B cells and large pre-B cells, this complex is called as pro-BCR (Fuentes-Panana, Bannish et al. 2004). Pre-BCR complex consist of IgH and surrogate light chain (SL). SL expression is initiate in pro-B cells and is observed as well in large pre-B cells. Successful IgH chain DJ segment (D_HJ_H) recombination in pro-B cell marks cell progression to pre-B cells (Winkler and Martensson 2018). This leads to joining of IgH chain V segment (V_H) and D_HJ_H , which occurs only in pre-B cells. $V_H D_H J_H$ rearrangements leads to pre-BCR complex is formation and expression on the small pre-B cells (Winkler and Martensson 2018). Pre-BCR complex formation causes repression of SL transcription and activation of IgL chain VJ segment ($V_L J_L$) rearrangement, which leads to the formation of BCR complex on the surface of the immature cells. BCR receptor development and immunoglobulin rearrangements are shown Figure 1-1.

Figure 1-1 Early stages of antibody production and the BCR repertoire via genetic recombination in B-cell development, where V_H – immunoglobulin heavy chain variable, J_H – immunoglobulin heavy chain joining, D_H – immunoglobulin heavy chain diversity gene segment, C_H – immunoglobulin heavy chain constant gene segment, V_L – immunoglobulin light chain variable, J_L – immunoglobulin light chain joining, C_L – immunoglobulin light chain constant gene segment, Ig_H – immunoglobulin heavy chain, Ig_L – immunoglobulin light chain, SL – surrogate light chain, Image adapted from (Parkhouse 1990, Fuentes-Panana, Bannish et al. 2004, Winkler and Martensson 2018).



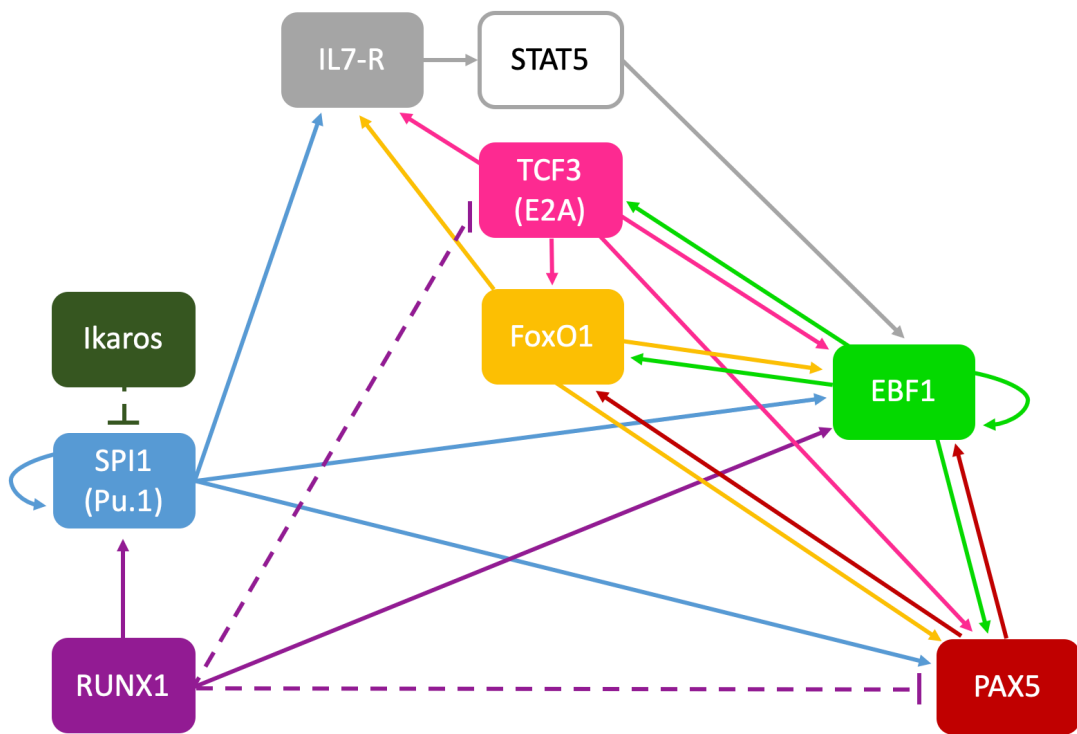
Transcription factors (TFs) are there to make sure that the gene expression program is aligned to B-cell development. It was thought before that the activation of B-cell maturation is linearly regulated, while in recent studies it has been shown that B-cell maturation is regulated by the feed-forward, feedback loops and cross-antagonism (Figure 1-2 A) (Boller and Grosschedl 2014). Hematopoietic transcription factor PU.1 (SPI1) plays an important role B-cell differentiation, it participates in different tasks at specific developmental stages by cooperation with different neighbouring factors (Heinz, Benner et al. 2010). SPI1 knockout in mice results in failure of HSCs to differentiate into macrophages, neutrophils, B, and T cells (McKercher, Torbett et al. 1996). An important observation is that high expression levels of SPI1 leads to HSCs differentiation into macrophages, while low expression levels of SPI1 leads to HSCs differentiation into B-cells (DeKoter and Singh 2000). Ectopic Early B-cell factor 1 (EBF1) expression in SPI1 deficient cells allows them to overcome the developmental block (Medina, Pongubala et al. 2004), suggesting that SPI1 activates EBF1 expression. Ikaros is another important B-lineage TF, which regulates lymphoid-primed multipotent progenitors (LMPPs) maturation into common lymphoid progenitors (CLPs). It has been shown that Ikaros binds to SPI1 promoter and inhibits its auto-regulatory loop (Figure 1-2 A) (Spooner, Cheng et al. 2009, Zarnegar and Rothenberg 2012), causing the low expression levels of SPI1. Moreover, Ikaros depletion lead to cell arrest in LMPP (Figure 1-2 B) (Nichogiannopoulou, Trevisan et al. 1999, Yoshida, Ng et al. 2006). Another crucial task of SPI1 is to activate interleukin 7 receptor (IL7-R) expression in CLPs as IL-7R depletion in mice arrest cells in CLPs (Figure 1-2 A and B) (Kikuchi, Lai et al. 2005).

Transcription factor 3 (TCF3, also known as E2A) has been detected as early as HSCs. TCF3 depletion lead to decreased number of LMPPs (Dias, Mansson et al. 2008). However, TCF3 is more important in pre-pro-B cell maturation (Bain, Maandag et al. 1994, Zhuang, Soriano et al. 1994) as TCF3 and depletion causes developmental arrest at the pre-pro-B cell phase (Figure 1-2 B) (Lin and Grosschedl 1995). EBF1 depletion as well causes developmental arrest at the pre-pro-B cell phase (Györy, Boller et al. 2012), while Paired box 5 protein (PAX5) (Nutt, Urbanek et al. 1997) and Runt-related transcription factor 1 (RUNX1) (Seo, Ikawa et al. 2012) depletion arrests cells at pro-B cell phase (Figure 1-2 B). RUNX1 was shown to be essential for EBF1 expression indirectly, as RUNX1 negative cell

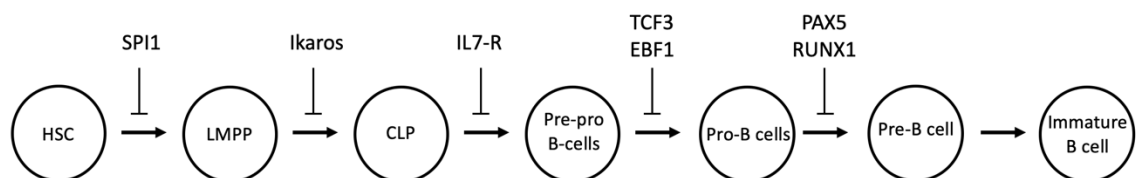
carry the repressive histone mark trimethylated lysine 27 on histone H3 (H3K27me3) in the *Ebf1* promoter. RUNX1 also caused a decrease in the expression of TCF3 and PAX5, thereby further influencing EBF1 expression (Seo, Ikawa et al. 2012). TCF3 and Forkhead Box O1 (FoxO1) have been shown to regulate EBF1 transcription in CLPs directly as well as indirectly through Signal transducer and activator of transcription 5 (STAT5) mediated IL-7 signalling (Kikuchi, Lai et al. 2005, Roessler, Gyory et al. 2007, Rothenberg 2014). Initiation of EBF1 expression leads to activation of positive auto-regulatory feedback (Roessler, Gyory et al. 2007) and multiple positive regulatory feedback loops (Figure 1-2 A), where EBF1 promotes self-expression, expression of PAX5, TCF3 and FoxO1 (Kee and Murre 1998, Roessler, Gyory et al. 2007, Decker, Pasca di Magliano et al. 2009, Mansson, Welinder et al. 2012) as well as FoxO1 feed-forward regulation by TCF3 (Welinder, Mansson et al. 2011). Thus, EBF1 plays an important role in early specification and commitment to B-cell fate. Here, I will explore EBF1 as a potential nuclear matrix protein in the EBF1 conditional knockout mouse pro-B cells.

Figure 1-2 Transcription factor network that regulates B-cell specification, commitment and development. (A) The schematic depicts major TFs regulating B-cell specification and commitment, direct positive regulation between two factors at the transcriptional level is indicated by the corresponding arrows, while repression is represented by thin, barred lines that end with a perpendicular line. Image adapted from (Boller and Grosschedl 2014) (B) A schematic view of B-cell lymphopoiesis and developmental arrest upon loss of TFs, where HSC - hematopoietic stem cell, LMPP - lymphoid-primed multipotent progenitor, CLP - common lymphoid progenitor, with lines that end with a perpendicular line depicts the approximate points of the developmental arrest in mice that have defective TFs - SP1, Ikaros, IL-7R, TCF3, EBF1, PAX5 and RUNX1. Image adapted from (Fuxa and Skok 2007, Spooner, Cheng et al. 2009, Zarnegar and Rothenberg 2012, Boller and Grosschedl 2014).

A



B



1.2 EBF1 maintains and regulates B-cell development

EBF1 is a highly conserved transcription factor that plays pivotal roles in the development of normal and malignant B cells. *EBF1* missense mutations or deletions frequently occur in B-Cell Precursor ALL (BCP-ALL) (Ghazavi, Lammens et al. 2015) and mature B lymphomas such as Diffuse large B-cell Lymphoma (DLBCL) (Karube, Enjuanes et al. 2018) and follicular lymphoma (FL) (Okosun, Bodor et al. 2014). The majority of mutations were detected in the DNA binding domain (DBD) of EBF1 (Okosun, Bodor et al. 2014) and typically *EBF1* lesions were heterozygous (Ramirez-Komo, Delaney et al. 2017). EBF1 mutations in FL resulted in the loss of function and a reduction in EBF1 target gene expression (Okosun, Bodor et al. 2014). Loss of *EBF1* disrupts B-cell development, while heterozygosity of a mutant *Ebf1* allele (*Ebf1*^{+/-}) results in decreased pro-B cell numbers and an increase in DNA damage accumulation upon ultraviolet (UV) light exposure in B-cells, suggesting that *Ebf1*^{+/-} B-cells are more likely to develop mutations. A significant increase in pro-B cell leukaemia incidence was observed in *Ebf1*^{+/-} and heterozygous mutant *Pax5 Pax5*^{+/-} (cell line possesses heterozygous mutant *Pax5 allele*) double-heterozygote mice, in contrast, no malignant transformation was observed in single *Ebf1* heterozygote mice (Prasad, Ungerback et al. 2015). Moreover, transgenic constitutive activation of STAT5 in *Ebf1*^{+/-} mice resulted in Acute Lymphoblastic Leukaemia (ALL) (Heltemes-Harris, Willette et al. 2011), suggesting EBF1 as a potential tumour suppressor. This is underscored by the observation that *EBF1* aberrations in BCR-ABL1-like ALL (Abelson murine leukaemia viral oncogene homolog 1 (ABL1)) patients are associated with poor prognosis (Ghazavi, Lammens et al. 2015).

1.2.1 EBF1 is an important transcriptional factor

It has been shown that EBF1 targets are involved in metabolism, membrane transport, maintaining cell structure and cellular signal transduction machinery, such as BCR and T-cell receptor (TCR) signalling (Treiber, Mandel et al. 2010). EBF1 activates transcription of many B-cell specific TFs such as PAX5, TCF3 and FOXO1 (Kee and Murre 1998, Roessler, Gyory et al. 2007, Decker, Pasca di Magliano et al. 2009, Mansson, Welinder et al. 2012) and EBF1 has been proposed to co-regulate transcription of B-cell specific targets together with TFs such as E26 transformation-specific (ETS), Enhancer box (E-BOX), STAT1, Nuclear factor kappa-light-chain-enhancer of activated B cells (NF- κ B), RUNX, Nuclear respiratory factor 1 (NRF1), PAX5 (Treiber, Mandel et al. 2010) and TCF3 (Zhao, Vilardi et al. 2001, Song, Cooperman et al. 2004). For example, EBF1 and RUNX1 binds at *Cd79a* (known as well as *mb-1* gene) promoter (Maier, Ostraat et al. 2004), while EBF1 interplay together with TCF3 causes activation of Immunoglobulin lambda-like polypeptide 1 (*IGL1*) expression and controls VDJ recombination (Goebel, Janney et al. 2001, Hsu, Luring et al. 2003, van Zelm, van der Burg et al. 2005, Perez-Vera, Reyes-Leon et al. 2011). Such membrane transport proteins as Integrin subunit beta 7 (ITGB7), Smoothelin (SMTN) and metabolic proteins as Aldehyde Dehydrogenase 3 Family Member B1 (ALDH3B1) and Dual specificity Phosphate 7 (DUSP7) were reported as important EBF1 targets. EBF1 is involved in multiple cross-regulatory feedback loops (Figure 1-2 A), which controls B-cell fate maturation. Thus, it is not surprisingly that half of all EBF1 targets belong to BCR signalling.

1.2.2 EBF1 poises chromatin prior transcription

It has been shown that sometimes EBF1 binding to DNA results in the establishment of accessible chromatin (Maier, Ostraat et al. 2004, Treiber, Mandel et al. 2010). During pro-B cell phase EBF1 binds to chromatin in the vicinity of these genes to form conformational alterations. The expression of these genes, such as transforming protein ERG 3 (*Erg3*) and Cluster of differentiation 40 (*Cd40*) is “poised” by EBF1. This process is initiated by dimethylated lysine 4 on histone H3 (H3K4me2) modification during cell transition from pre-pro-B to pro-B cells, while gene activation is associated with H3K4me3 and acetylation of histone H3 (H3ac). Gene downregulation is associated with H3K27me3 modification (Treiber et al., 2010). Moreover, it was shown that demethylation of the *Cd79a* promoter occurs in the TCF3 or EBF1 expressing cells and depletion of PAX5 didn't affect demethylation, evidenced by demethylation not occurring in TCF3 or EBF1 deficient cells (Maier, Ostraat et al. 2004, Hagman and Lukin 2006, Lukin, Fields et al. 2008).

VDJ recombination is regulated by changes in the target site accessibility such as histone modification of chromatin looping (Nakase, Takahama et al. 2003, Choukrallah and Matthias 2014, Bolland, Koohy et al. 2016). For example, It has been shown that methylation at specific sites results in reduced recombination (Nakase, Takahama et al. 2003). PAX5/IRF4 (Interferon regulatory factor 4 (IRF4)) and CTCF/RAD21 (CCCTC-binding factor (CTCF), RAD21 Cohesin Complex Component (RAD21)) are involved in local chromatin regulation of V_H in B cells, while RUNX1 was proposed to be involved in local and the long-range looping in TCR recombination (Bolland, Koohy et al. 2016). PAX5 and RUNX1 bind to DNA in the vicinity of EBF1 binding site at the *Cd79a* promoter site (Nutt and Kee 2007), thus EBF1 might be involved in looping required for VDJ recombination or might be involved in chromatin reorganisation prior VDJ recombination.

1.2.3 EBF1 restricts lineage potential

PAX5 was previously proposed as the main factor that restricts alternative lineage choices in early B cells, as PAX5 negative cells were not able to differentiate beyond the pro B cell stage, but were able to differentiate into functional macrophages, osteoclasts, dendritic cells, granulocytes and natural killer cells. PAX5 overexpression allowed pro-B cells to overcome the arrest and re-establish a full commitment to the B-cell lineage (Nutt, Heavey et al. 1999). However, EBF1, but not PAX5 was able to overcome developmental block of TCF3 deficiency (Seet, Brumbaugh et al. 2004), indicating that EBF1 is an essential factor in B-cell development. (Lin and Grosschedl 1995, Zhang, Cotta et al. 2003, Seet, Brumbaugh et al. 2004, Hagman and Lukin 2006, Nutt and Kee 2007, Lukin, Fields et al. 2008, Györy, Boller et al. 2012, Vilagos, Hoffmann et al. 2012).

EBF1 depletion results in cell arrest at pre-pro-B cell phase, profound proliferation and survival defect at multiple developmental stages (Györy and Grosschedl 2013). Also, BCR and Protein kinase B (AKT) signalling becomes impaired upon tamoxifen-induced EBF1 depletion in the conditional knockout mouse pro-B cells, which expresses the Cre recombinase under the control of a tamoxifen-inducible promoter and depletes floxed *Ebf1* (*Ebf1^{fl/fl}RERT^{Cre}*). Györy and Grosschedl showed that transformation with ABL1 did not rescue *Ebf1^{fl/fl}RERT^{Cre}* (*Ebf1^{fl/fl}RERT^{Cre}::A-MuLV*) pro-B cells from proliferative defect upon EBF1 depletion (Györy, Boller et al. 2012, Györy and Grosschedl 2013), however, pro-B cell clones are arrested at G1 and few but not all clones appear to increase DNA content, indicating that EBF1 depleted pro-B cells clones continue cycling, and are rescued by the EBF1 target - Myb-related proto-oncogene (MYB). Although MYB rescued the survival defect of *Ebf1^{fl/fl}RERT^{Cre}::A-MuLV*, it was not able to overcome EBF1 requirement in cell progression in primary *Ebf1^{fl/fl}RERT^{Cre}* cells. Thus, EBF1 was shown to have non-redundant functions in pro-B and pre-B cell development, suggesting that EBF1 is the essential transcription factor required for early B cell development (Lin and Grosschedl 1995, Seet, Brumbaugh et al. 2004, Hagman and Lukin 2006, Lukin, Fields et al. 2008), proliferation and survival (Györy, Boller et al. 2012).

The arrest at the G1 phase was not accompanied by early and consistent changes in pro-B cell gene expression (Dr Ildiko Györy unpublished observations). A consistent change in

the expression of many EBF1 targets that are involved in metabolism, membrane transport, maintaining cell structure and cellular signal transduction machinery was observed five days after (Z)-4-Hydroxytamoxifen (OHT) addition (Treiber, Mandel et al. 2010), suggesting that changes in the EBF1 target transcription is a secondary event. In preliminary experiments, nuclear collapse upon EBF1 depletion was observed in *Ebf1^{fl/fl}RERT^{Cre}::A*-MuLV cells (Dr Shiqiu Xiong/Ildiko Györy unpublished observations), suggesting that EBF1 might activate transcription of nuclear matrix structural proteins, or it might be part of the pro-B cell structural matrix itself.

The fact that pro-B cell arrest at G1 phase upon EBF1 depletion led to thinking that EBF1 might interact with cell cycle regulating proteins. After probing important cell regulators it was found that in primary B-cells and transformed pro-B cell lines, EBF1 associates with cyclin A2 (CCNA2) and cyclin D3 (CCND3), while no association of EBF1 and cyclin dependent kinase 4 (CDK4) was detected, suggesting a new, potential cell cycle unrelated function of CCNA2 and CCND3 (Dr Shiqiu Xiong/Ildiko Györy unpublished observations). In order to understand the molecular function of CCNA2 and CCND3 binding to EBF1, it was thought to investigate the structural requirements of EBF1 to allow CCNA2 and CCND3 binding.

1.2.4 EBF1 structure

The Gene encoding EBF1 protein is located on human chromosome 5, band q34, and proximal mouse chromosome 11 (Milatovich, Qiu et al. 1994). The expressed EBF1 protein is 591 amino acid large with a molecular weight of 64.5kDa (Figure 1-3 A). EBF1 belongs to the EBF/COE together with three other members. Human EBF/COE members hold over 80% sequence identity, while mouse and human EBF1 proteins are 100% identical. The EBF1, EBF2 and EBF3 proteins are expressed in adipocytes and neuronal cells (Hagman, Belanger et al. 1993, Lin and Grosschedl 1995, Kieslinger, Folberth et al. 2005). Only EBF1 is expressed in B-lymphocytes (Kieslinger, Folberth et al. 2005).

Gene transcription requires transcriptional factor binding to a specific DNA sequence adjacent to the genes that they regulate. EBF1 binds to variations of the palindromic sequence 5'-ATTCCCNNGGGAATT-3' via DBD (Figure 1-3 B). EBF1 zinc coordination motif

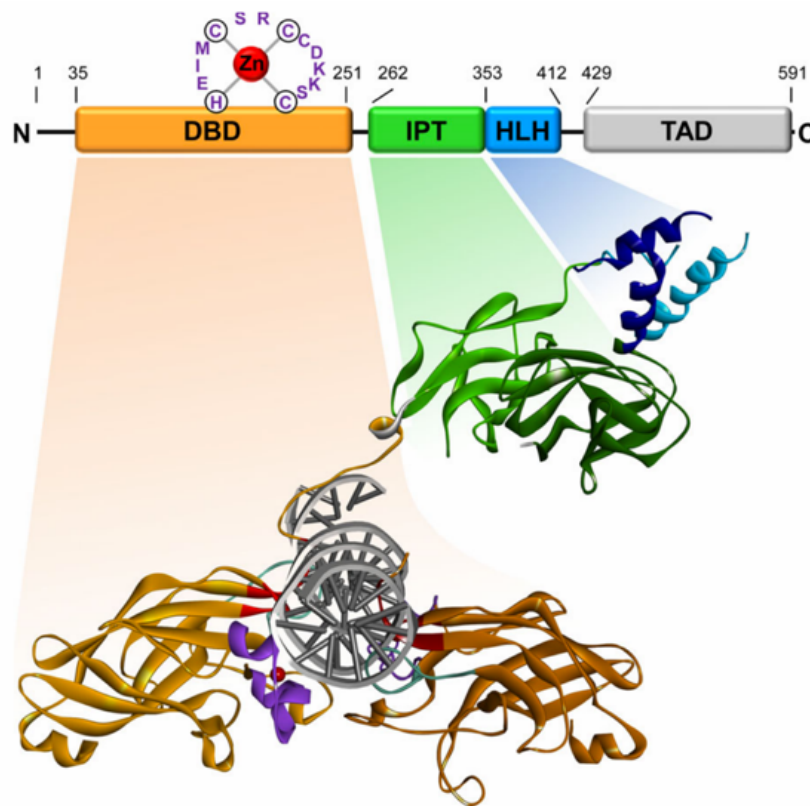
that is located in DBD is necessary for the DNA binding, while helix-loop-helix (HLH) dimerization domain aids in EBF1 binding to DNA. A three-fold decrease in DNA binding has been shown for mutant EBF1 that lacked the HLH domain in reporter gene assays (Hagman, Belanger et al. 1993, Hagman, Gutch et al. 1995, Hagman and Lukin 2006). EBF1 possesses an “immunoglobulin, plexins, transcription factors-like” (IPT) domain, whose function is not yet known, and a transactivation domain (TAD). Colour coded EBF1 domain representation is shown in Figure 1-3 B (Boller and Grosschedl 2014). When other transcription factors are cooperatively binding to DNA in the vicinity of the EBF1 binding site, TAD seems dispensable (Boller, Ramamoorthy et al. 2016). While TAD of EBF1 participates in the gene transcriptional activation in the absence of other TFs in the vicinity of the EBF1 binding site.

Figure 1-3 Sequence and structural representation of EBF1 (A) EBF1 protein sequence, where DBD - DNA binding domain is represented in yellow, IPT – immunoglobulin in green, plexins, transcription factors-like domain in blue, HLH - a helix-loop-helix dimerization domain and TAD - transactivation domain in grey (B) The structure of DNA bound EBF1, where DBD - DNA binding domain, IPT - immunoglobulin, plexins, transcription factors-like domain, HLH - a helix-loop-helix dimerization domain and TAD - transactivation domain. Images taken from (Boller and Grosschedl 2014).

A

1	MFGIQESIQR	SGSSMKEEPL	GSGMNAVRTW	MQGAGVLDAN	TAAQSGVGLA	50
51	RAHFEKQPPS	NLRKSNFFHF	VLALYDRQGQ	PVEIERTAFV	GFVEKEKEAN	100
101	SEKTNNGIHY	RLQLLYSNGI	RTEQDFYVRL	IDSMTKQAIV	YEGQDKNPEM	150
151	CRVLLTHEIM	CSRCCDKKSC	GNRNETPSDP	VIIDRFFLFK	FLKCNQNCLK	200
201	NAGNPRDMRR	FQVVVSTTVN	VDGHVLAVSD	NMFVHNNSKH	GRRARRLDPS	250
251	EGTPSYLEHA	ATPCIKAIISP	SEGWTTGGAT	VIIIGDNFFD	GLQVIFGTML	300
301	VWSELITPHA	IRVQTPPRHI	PGVVEVTLST	KSKQFCKGTP	GRFIYTALNE	350
351	PTIDYGFQRL	QKVIPRHFGD	PERLPKEVIL	KRAADLVEAL	YGMPHNNQEI	400
401	ILKRAADIAE	ALYSVPRNHN	QLPALANTSV	HAGMMGVNSF	SGQLAVNVSE	450
451	ASQATNQGFT	RNSSSVSPHG	YVPSTTPQQT	NYNSVTTSMN	GYGSAAMSNL	500
551	GGSPFTLNGS	AANSPYAIVP	SSPTMASSTS	LPSNCSSSSG	IFSFSPANMV	560
561	SAVKQKSAFA	PVVRPQTSPP	PTCTSTNGNS	LQAISGMIVP	P	591

B



1.3 Cell cycle regulating proteins and their functions in B-cell development

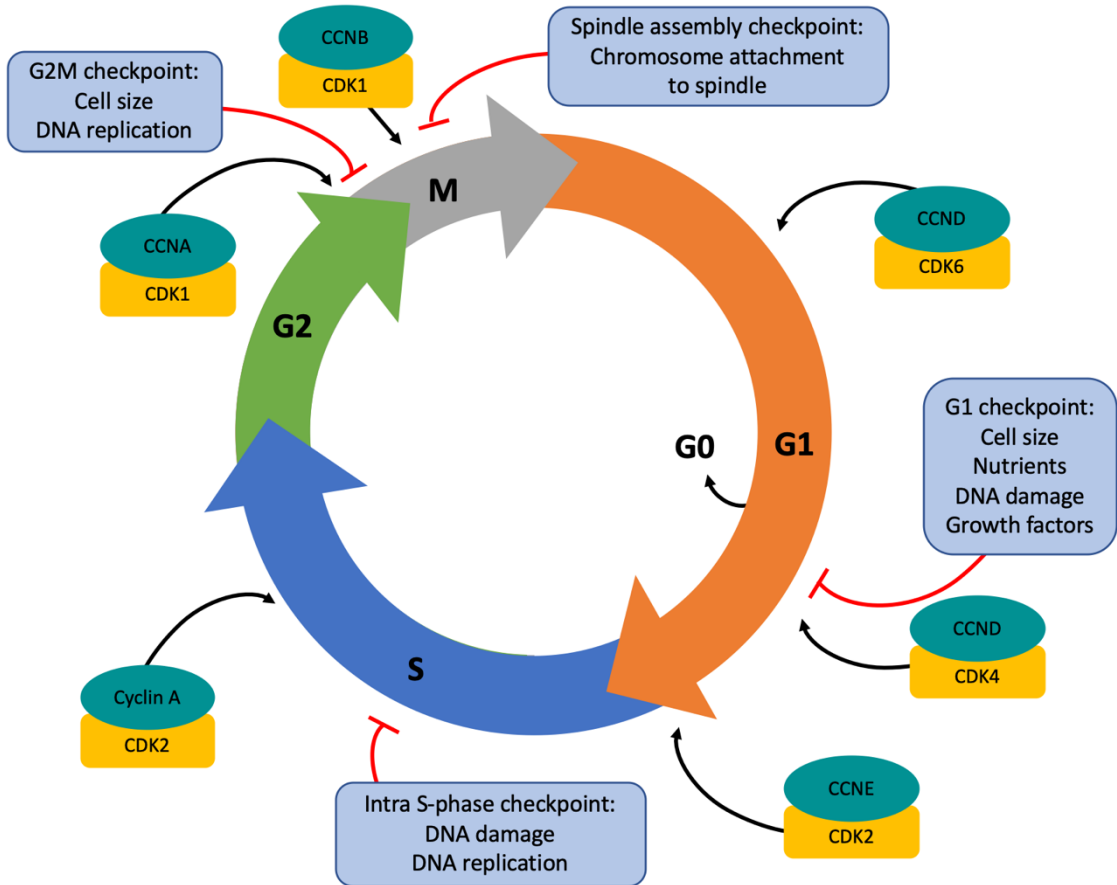
The cell cycle comprises a set of events responsible for cell replication (MacLachlan, Sang et al. 1995). DNA duplication occurs in S phase and during M phase DNA is evenly split between two daughter cells. The S and M phases are separated by gap phases G1 and G2 (Figure 1-4 A). Cyclins (CCNs), cyclin-dependent kinases (CDKs) and their inhibitors regulate cell cycle progression. Most of the CCNs are expressed and degraded in the specific cell cycle phase (Figure 1-4 B) and binds to a corresponding CDK. CDKs upon binding CCNs become activated and phosphorylate substrates allowing cell cycle to progress (MacLachlan, Sang et al. 1995, Pucci, Kasten et al. 2000). Cells that are nutrient deprived or undergo differentiation exit cell cycle and enter the G0 phase. When cells are ready for re-entering cell cycle, CCND/CDK complex is activated by mitogenic stimuli (Kozar, Ciemerych et al. 2004).

Upon deregulation of some cellular processes the cell is arrested at the respective cell cycle checkpoint (G1, Intra-S phase, G2 or Metaphase checkpoint) and is subjected to apoptosis, or it may undergo malignant overdrive, where cell continue to proliferate (Figure 1-4 A). At the G1 checkpoint the levels of DNA damage and growth conditions such as cell size, sufficient nutrients and presence of growth factors are assessed. CCND regulates G1 phase progression by association with CDK4 and CDK6 and induces CCNE/CDK2 and CCNA/CDK2 complex activation via recruiting p21 and p27 – the inhibitors of CCNE/CDK2 and CCNA/CDK2 complexes (Kozar, Ciemerych et al. 2004). CCNE/CDK2, CCND/CKD4 and CCND/CDK6 have been reported to participate in Retinoblastoma protein (RB) phosphorylation. Phosphorylation of RB marks the G1/S transition due to cells lacking RB, p170 and p130 were able to divide in the absence of mitogenic stimuli (Dannenberg, van Rossum et al. 2000, Sage, Mulligan et al. 2000). Upon G1/S transition CCNE/CDK2 complex initiates DNA replication (Hwang and Clurman 2005) and in order to avoid re-replication of DNA CCNE is degraded as soon as cell enters the S phase (Hwang and Clurman 2005). Released CDK2 associates with CCNA and CCNA/CDK2 complex regulates completion and exit from S-phase. At the end of the S phase CCNA associates with CKD1. Due to CCNA/CDK1 and CCNA/CDK2 share a lot of substrates, it is not clear whether they have different role during S to G2 transition. Although it has been

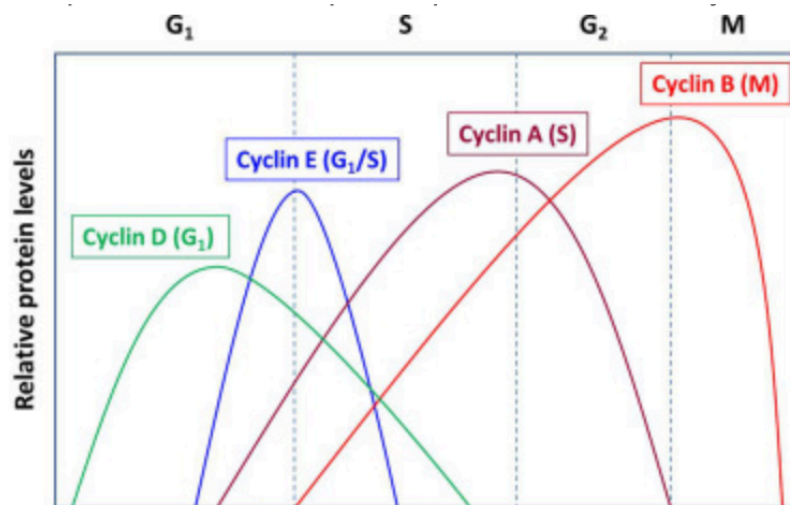
reported that CCNA/CDK2 is G2 DNA damage checkpoint (Lim and Kaldis 2013). Verification of correct DNA replication and cell size at the G2 checkpoint triggers CCNB expression and cell transition into M phase. CCNB/CDK1 complex is essential in cell mitosis and is involved in such processes as breakdown of nuclear lamina, fragmentation of Golgi complex, chromosomal condensation, proteolysis, replication and translation (Harper, Burton et al. 2002). Finally, CCNB is degraded prior exit from mitosis. Proper spindle assembly and correct attachment to centromeres are assessed at the Metaphase checkpoint. New daughter cell, upon exit from M phase, may continue cycling or enter G0.

Figure 1-4 Cell cycle regulation via CCN and CDK interaction and cell cycle checkpoint regulation (A) Cell cycle phases and checkpoints (B) Cyclin expression throughout cell cycle. Image taken from (Yang 2018).

A



B



1.3.1 Structure of Cyclins

Two isoforms of CCNA and CCNE and three isoforms of CCNB and CCND have been discovered (Figure 1-5). All CCNs share a conserved domain, named - cyclin box, while the other regions of the CCNs are very diverse (Brown, Noble et al. 1995). The cyclin box is responsible for binding many CCN partners, including CDKs while the other region diversity may explain the CCN tissue-specific functions (Malumbres and Barbacid 2005).

Figure 1-5 CCN sequence alignment. The first line shows the amino acid conservation index (> 5). The sequences were automatically aligned against CCND2 (the eleventh line). Representative sequences of CCNA1 (the sixth line), CCNA2 (the fifth line), CCNB1 (the eighth line), CCNB2 (the seventh line), CCNB3 (the fourth line), CCND1 (the tenth line), CCND2 (the eleventh line), CCND3 (the ninth line), CCNE1 (the second line) and CCNE2 (the third line) coloured according to predicted secondary structures (red: alpha-helix, blue: beta-strand). Consensus_aa -Consensus amino acids: identical amino acids are presented in bold and uppercase letters, l-aliphatic residues, @- aromatic residues, h- hydrophobic residues, o - alcohol residues, p - polar residues, t - tiny residues, s - small residues, b - bulky residues, “+” - positively charged residues, “-“ -negatively charged residues, c - charged). Consensus_ss -Consensus secondary structures, where h – alpha-helix, e- beta-strand (Pei, Kim et al. 2008).

Conservation:	9		
CCNE2	1	MSR-----RSSLQAKQQPQPSQTESPQEAQ--	26
CCNE1	1	MFR-----ERRERDAKERD TMK ---EDGGAEF--	24
CCNB3	1	MLLPLPPQSSKVPVKKSQSSKIVPSHHDPEKTGENCQTKI---SPSSLQE---SPS---SLQ-----	54
CCNA2	1	MLG-----NSAP-----GPATREAGSALLALQQ---TALQEDQEN	32
CCNA1	1	METGFPAIMYPGSFIGGWGEEYLSWEGPGLPDFVFVQQQPVESAMHCSNPKSGVVLA---TVARGPDAC	66
CCNB2	1	MA-----LLRRPTVSDLENIDT---GVNSK----	23
CCNB1	1	MA-----LRVTRNSKINAENKAK---INMAGAKRV	27
CCND3	1	M-----	1
CCND1	1	M-----	1
CCND2	1	M-----	1
<u>Consensus_aa:</u>		M	
<u>Consensus_ss:</u>		hhhhhhh	
Conservation:	27	-----IIQAKKRKTQDVKKRRE-----EVTKK-HQYEIRNC-----	57
CCNE1	25	-----SARSRKRKANVTVFLQDPDEEMAKIDRT-ARDQCGSQ-----	60
CCNB3	55	-----GALKKRSAFEDLTNASQ-----CQPVPKKEANKEFVKVVS SKINR NTHALGLAKNKRNL	110
CCNA2	33	INPEKAAPVQQPRTRAALAVLKSGNP-----RGLAQ-QQRPKTRRVAPLKDLPVNDEHVTVPWPKANSKQ	96
CCNA1	67	QILTRAPLGQDPPQRTVLGLLTANGQ-----YRRTC-GQGITRIRCYSGSENAFPPAGKKALPDCGVQEP	130
CCNB2	24	-----VKSHVTIRR TVLEE IGNRVT-----TRAAQ-VAKKAQNTKVPVQPTKTTNVNKQLKPTASVKPV	81
CCNB1	28	PTAPAATSKPGLRPTALGDI GNKVS -----EQLQA-KMPMKKEAKPSATGKVIDKLLPKPLEKVPMLVP	91
CCND3		-----	
CCND1		-----	
CCND2		-----	
<u>Consensus_aa:</u>		
<u>Consensus_ss:</u>		
Conservation:		-----	
CCNE2		-----	
CCNE1		-----	
CCNB3	111	KWHKLEVTPVVASTTVVPNIMEKPLILDISTTSKTPNTEEASLFRKPLVLKKEPTIEDETLINKSLSKK	180
CCNA2	97	PAFTIHVDE-----	105
CCNA1	131	PKQGFDIY-----	138
CCNB2		-----	
CCNB1	92	VPVSEPVPE-----	100
CCND3		-----	
CCND1		-----	
CCND2		-----	
<u>Consensus_aa:</u>		
<u>Consensus_ss:</u>		

Continued...

Continued...

Conservation:
CCNE2 -----
CCNE1 -----
CCNB3 181 CSNHEEVSLLEKQLPQEESDSDDAFVIEPMTFKKTHKTEEAAITKKTLSLKKKMCASQRKQSCQEEESLA 250
CCNA2 -----
CCNA1 -----
CCNB2 -----
CCNB1 -----
CCND3 -----
CCND1 -----
CCND2 -----
[Consensus aa:](#)
[Consensus ss:](#)

Conservation:
CCNE2 -----
CCNE1 -----
CCNB3 251 VQDVNMEEDSFFMESMSFKKKPKTEESIPTHKLSLKKKCTIYGKICHFRKPPVLQTTICGAMSSIKKPT 320
CCNA2 -----
CCNA1 -----
CCNB2 -----
CCNB1 -----
CCND3 -----
CCND1 -----
CCND2 -----
[Consensus aa:](#)
[Consensus ss:](#)

Conservation:
CCNE2 -----
CCNE1 -----
CCNB3 321 TEKETLFQELSVLQEKHTEHEMSILKKSALQKTNFKEDSLVKESLAFKKKPTTEEAIMMPVILKEQCM 390
CCNA2 -----
CCNA1 -----
CCNB2 -----
CCNB1 -----
CCND3 -----
CCND1 -----
CCND2 -----
[Consensus aa:](#)
[Consensus ss:](#)

Conservation:
CCNE2 -----
CCNE1 -----
CCNB3 391 TEGKRSRLKPLVLQEIITSGEKSILMKPLSIKEKPKSTEKESFSQEPSALQKKHTTQEEVSIKPEPSSLLKS 460
CCNA2 -----
CCNA1 -----
CCNB2 -----
CCNB1 -----
CCND3 -----
CCND1 -----
CCND2 -----
[Consensus aa:](#)
[Consensus ss:](#)

Conservation:
CCNE2 -----
CCNE1 -----
CCNB3 461 PTEESPFDEALAFTKKCTIEEAPPKPLIILKRKHATQGTMSHLKPLIQLQTTSGEKSILKEPLPFKEEK 530
CCNA2 -----
CCNA1 -----
CCNB2 -----
CCNB1 101 -----PEPEPEPE 108
CCND3 -----
CCND1 -----
CCND2 -----
[Consensus aa:](#)
[Consensus ss:](#)

Continued...

Continued...

Conservation:
CCNE2
CCNE1
CCNB3 461 PTEESPFDEALAF~~TKKCTIEE~~AP~~TKKPLILKRKHATQGTMSHLKKPLILQTTSGEKSLIKEPLPFKEEK~~ 530
CCNA2
CCNB2
CCNB1 101 -----PEPEPEPE 108
CCND3
CCND1
CCND2
[Consensus_aa:](#)
[Consensus_ss:](#)

Conservation:
CCNE2
CCNE1
CCNB3 531 VSLKKKCTTQEMMSICPELLDFQDMIGEDKNSFFMEPMSFRKNPTTEETVLT~~TKTSLSLQEKKITQGKMSH~~ 600
CCNA2
CCNB2
CCNB1
CCND3
CCND1
CCND2
[Consensus_aa:](#)
[Consensus_ss:](#)

Conservation:
CCNE2
CCNE1
CCNB3 601 LKKPLVLQKITSEESFYKLLPFKMKSTTEEKFLSQEPSALKEKHTTLQEVSLSKESLAIQEKATTEEE 670
CCNA2
CCNB2
CCNB1
CCND3
CCND1
CCND2
[Consensus_aa:](#)
[Consensus_ss:](#)

Conservation:
CCNE2
CCNE1
CCNB3 671 FSQELFSLHVKHTNKSGSLFQEALVLQEKTD~~AEEDSLKNLLALQEKSTMEEESL~~IN~~KLLALKEEL~~-~~SAEA~~ 739
106 -----~~AEKEAQKPAE~~ 116
CCNA2
CCNB2
CCNB1 109 -----PV~~KEE~~KLSP-- 117
CCND3
CCND1
CCND2
[Consensus_aa:](#)
[Consensus_ss:](#)

Conservation:
CCNE2
CCNE1
CCNB3 740 ATNIQTQLSLKKKSTSHGKVFFLKKQLALNETINEEEFLNKQPLALEGYPSIAEGETL~~FKLLAMQE~~EPS 809
117 ~~S~~----- 117
CCNA2
CCNB2
CCNB1
CCND3
CCND1
CCND2
[Consensus_aa:](#)
[Consensus_ss:](#)

Continued...

Continued...

```
Conservation:
CCNE2 -----
CCNE1 -----
CCNB3 810 IEKEAVLKEPTIDTEAHFKEPLALQEEPSSTEKEAVLKEPSVDTEAHFKETLALQEKPSIEQEALFKRHSA 879
CCNA2 -----
CCNB2 -----
CCNB1 -----
CCND3 -----
CCND1 -----
CCND2 -----
Consensus_aa: .....
Consensus_ss: .....
```

```
Conservation:
CCNE2 -----
CCNE1 -----
CCNB3 880 LWQEPSTEKETIFKESLDLQEKPSIKKETLLKKPLALKMSTINEAVLFEDMIALNEKPTTGKELSFKEPL 949
CCNA2 -----
CCNB2 -----
CCNB1 -----
CCND3 -----
CCND1 -----
CCND2 -----
Consensus_aa: .....
Consensus_ss: .....
```

```
Conservation:
CCNE2 -----
CCNE1 -----
CCNB3 950 ALQESPTYKEDTFLKTLVLPQVGTSPNVSSSTAPESITSKSSIATMTSVGKSGTINEAFLFEDMITLNEKP 1019
CCNA2 118 -----QKI 120
CCNB2 -----
CCNB1 -----
CCND3 -----
CCND1 -----
CCND2 -----
Consensus_aa: .....
Consensus_ss: .....
```

```
Conservation:
CCNE2 58 -----WPPVLSGGISPCIIIET----- 74
CCNE1 61 -----PWDNNAVCADPCSLIPT----- 77
CCNB3 1020 TTGKELSFKEPLALQESPTCKEDTFLFETFLIPQIGTSPYVFSTTPESITEKSSIATMTSVGKSRTTTESS 1089
CCNA2 121 ER---EDALAFNSAISLPGPRKPLV----- 142
CCNA1 139 -----MDELEQDRDSCSVREGMA----- 157
CCNB2 82 -----QMEKLAPKGFSPPTPEDV----- 98
CCNB1 118 -----EPILVDTASPSMETSG----- 134
CCND3 -----
CCND1 -----
CCND2 -----
Consensus_aa: .....
Consensus_ss: .....
```

```
Conservation:
CCNE2 75 -----PHKEIGTSDFSRFTNYRFKLNLFINP-----5-----SPLPDLSSWGC-SKEVWLNMLKK 120
CCNE1 78 -----PDKEDDRVPNSTCKPRI IAPSRG-----SPLPVLSWAN-REEVWKIMLNK 123
CCNB3 1090 ACESASDKPVSPQAKGTPKEITPREDIDED-----SSDPSFNPMY-AKEIFSYMKER 1140
CCNA2 143 ---PLDYPMDGSFESPHTMDSII LEDEK-----PVSVNEVPDY-HEDIHTYLREM 189
CCNA1 158 ---FEDVYEVDGTGLKSDLHFLDFNTVSPMLVDSLLSQSEDISSLGTDVINVTEY-AEEIYQYLREA 222
CCNB2 99 ---SMKEENLCQAFSDALLCKIEDIDNED-----WENPQLCSDY-VKDIYQYLRQL 145
CCNB1 135 ---CAPAEEDLCQAFSDVILAVNDVDAED-----GADPNLCSEY-VKDIYAYLRQL 181
CCND3 2 -----ELLCCEGTRHAP-----RAGPDRLLG-DQRVLSLLRL 34
CCND1 2 -----EHQLLCCVEVETI-----RRAYPDANLL-NDRVLRAMLKA 34
CCND2 2 -----ELLCHEVDVP-----RRAVRDRNLLRDDRVLQNLTI 33
Consensus_aa: .....p.....s.....s..h..cclh..h.p.
Consensus_ss: .....hhh hhhhhhhhhhh
```

Continued...

Continued...

Conservation: 9 6 5 55 99 77 597579 5 5 9755765 9766 6 99959
CCNE2 121 ESRYVHDKHFEV-LHSDLEPQ **MRSILLD**DWLLVEVCEVYTLRHRETFYLAQDFDFRMLTQKDINKNMLQLIG 189
CCNE1 124 EKTYLDRDQHFE-QHPLLQPK **MRAILLD**DWLMVEVCEVYKLRHRETFYLAQDFDFRYMATQENVVKTLLQLIG 192
CCNB3 1141 EEQFILT-DYMN-RQIEITSD **MRAILLD**DWLVVEVQVSEFEMTHETLYLAVKLVLDLYLMAK-VCKKDKLQLLG 1207
CCNA2 190 EVKCKPKVGYMK-KQPDITNS **MRAILLD**DWLVVEVGEYKLNQETLHLAVNYIDRFLSSM-SVLRGKQLQVVG 257
CCNA1 223 EIRHRPKAHYMK-KQPDITEG **MRTILLD**DWLVVEVGEYKLRRAETLYLAVNFLDRFLSCM-SVLRGKQLQVVG 290
CCNB2 146 EVLQSIINPHFL--DGRDINGR **MRAILLD**DWLVQVHSHFRLLQETLYMCEVIMDRFLVQV-PVSRKKLQLQVVG 212
CCNB1 182 EEEQAVRPKYL--LGREVTGN **MRAILLD**DWLVQVQMKFRLLQETMYMTVSIIDRFMQNN-CVPKMKLQVVG 248
CCND3 35 EERYVPRASYFQCVQREIKPH **MKRMLAY**WMLEVCCEEQRCCEEEVFPPLAMNYLDRFLSVCV-PTRKAQLQLLG 103
CCND1 35 EETCAPSVSYFKCVQKEVLP **MRKIVAT**WMLEVCCEEQKCEEEVFPPLAMNYLDRFLSLE-PVKSRSLQLLG 103
CCND2 34 EERYLPQCSYFKCVQKDIQPY **MRRMVA**TWMLEVCCEEQKCEEEVFPPLAMNYLDRFLAGV-PTPKSHLQLLG 102
Consensus aa: E.p...p.p@hp...-lpsh**MR.I**LhsWhlpV...bch.pEhh.ht.shhDR@h...sh.+bLQLIG
Consensus ss: hhh hhhh hhhhhhhhhhhhhhh hhhhhhhhhhhhhhh hhhhhhhhhhhhhhh

Conservation: 5555979 59 57 755579 557 79 56 9 5 7 5 77
CCNE2 190 **ITSLFI**ASKLEEIYAPKLOEFAYVTDGACSEEDIIRMEILII **KALKWEL**CPVTIISWLNLFQVDALKDA 259
CCNE1 193 ISSLFIAAKLEEIYPPKLHQFAYVTDGACSGDEIILTMELMIM **KALKWRL**SPLTIVSWLNVMYQVAYLNDL 262
CCNB3 1208 **ATAFMIA**AKFEEHNSPRVDDFVYICDDNYQRSEVLSMEINIL **NVLKCD**INIPIAYHFLRRYARCIHTN-- 1275
CCNA2 258 **TAAMLL**ASKFEEIYPPEVAEFVYITDDTYTKKQVLRMEHLVL **KVLTFD**LAAPTIVNQFLTQYFLHQQFAN- 326
CCNA1 291 **TAAMLL**ASKYEEIYPPEVDEFVYITDDTYTKRQLKMEHLIL **KVLAFL**DLTVPTTNQFLQLYLRQVGC-- 358
CCNB2 213 **ITALL**LASKYEEFMSPNIEDFVYITDNAYTSSQIREMETLII **KELKFE**LGRPLPLHFLRRASKAGEVD-- 280
CCNB1 249 **VTAMFI**ASKYEEYMPPEIGDFAFVTDNTYTKHQIRQMEMKII **RALNFG**LGRPLPLHFLRRASKIGEVD-- 316
CCND3 104 **AVCMFL**ASKLRETTPLTIEKLCIYTDHAVSPRQLRDWEVLVI **GKLNWDL**AAVIAHDFLAFILHRLSLPRD 173
CCND1 104 **ATCMFV**ASKMKETIPLTAEKLCIYTDNSIRPEELQOMELLLV **NKLNWLA**AMT **PHDFIE**HFLSKMPEAEE 173
CCND2 103 **AVCMFL**ASKLKETSPLTAEKLCIYTDNSIRPEELQOMELLLV **NKLNWLA**AVT **PHDFIE**HLRKLPOORE 172
Consensus aa: hhhhAtKhcEh.s.pl.chhhhTdsshp.ppl.pMEh.lLp.Lp@Ls.sh.p@Lp.h.p...s..
Consensus ss: hhhhhhhhhhh hhhhhhhh hhhhhhhhhhhhh hhhhhhhhhhhhh

Conservation: 55 575 5 56 57556 55 5 7
CCNE2 260 **PKVLLP**QYSQETFIQIAQLDLCILAID-SLEFQYRILTAALCHFTS-----IEVVKK 312
CCNE1 263 **HEVLLP**QYPQQIFIQIAELDLCLVDLDV-CLEFPYGILAAALYHFS-----SELMQK 315
CCNB3 1276 -----**MKTLT**LSRYICEMTLQEYH-YVQEKASKLAAASLLALYMKLGY-----WVPFLEH 1326
CCNA2 327 -----**CKVESL**AMFLGELSILIDADPYLKYLPSVIAAGAAFLHALYTVTGQS-----WPESLIR 378
CCNA1 359 -----**VRTENL**AKYVAELSLEADPFLKYLPSLIAAAAFCLANYTVNKHG-----WPETLAA 410
CCNB2 281 -----**VEQHTL**AKYLMELTLDYD-MVHYHPSKVAAAASCLSQKVLGQK-----WNLKQQY 331
CCNB1 317 -----**VEQHTL**AKYLMELTLDYD-MVHFPPSQIAAGAFCLALKILDNGE-----WPTPLQK 367
CCND3 174 **R-----**QALVKKHAQTFALCATDYT-FAMYPSPMIATGSIGAAVQGLGACSMG----DELTELLAG 231
CCND1 174 **N-----**KQIIRKHAQTFALCATDVK-FISNPPSMVAAGSVAAVQGLNLRSPNNFLSYRYLRTFLSR 235
CCND2 173 **K-----**LSLIRKHAQTFALCATDFK-FAMYPSPMIATGSVGAACGLQODEEVSSLTCDALTELLAK 234
Consensus aa:b...h..hh.Lshh-hc.hlpb..tblAttthhhh...l.....hs..h..
Consensus ss: hhhhhhhhhhhhhhh hh hh hhhhhhhhhhhhhhh hhhhhhhhhhhhhhh

Conservation: 5 5 5 6 5
CCNE2 313 **ASGLEW**DSISECVDMVVPFVNVVKSTSPVKLKTFFKKIPMEDRHNIQHTNYLAMLEEVNYINTFRKGGQL 382
CCNE1 316 **VSGYQW**CDIENCVMWVPFAMVIRETGSSK**LKHFR**GVADEDAHNIQTHRDSLDLLDKARAKKAMLSEQNR 385
CCNB3 1327 **YSGYSI**SELHPLVRQLNKLITFSSY--DSLKAVYKYKSHPVFFFEVAKIPALDMKLEEIILNCDCEAQG-- 1392
CCNA2 379 **KTGYT**LESCLKPCLMDLHQYTIKAPQ--HAQQSIREKYKNSKYHGV**SVLLN**PPETLNL----- 432
CCNA1 411 **FTGYSL**SEIVPCLSELHKAYLIDIPH--RPQQAIREKYKASKYLCVSLMEPPAVLLQ----- 465
CCNB2 332 **YTGYTE**NEVLEVMQHMKNVVKVNEENLTKFIAIKNKYASSKLLKISMIQPLNSKAVKDLASPLIGRS--- 398
CCNB1 368 **YLSYTE**ESLPLVMQHLAKNVVMVNOGLTKHMTVKNKYATSKHAKISTLPQLNSALVQDLAKAVAKV--- 433
CCND3 232 **ITGTEV**DCLRACQEQIEAALRESLR-----EASQTSSSP-----APKAPRGSSSQGPS----- 279
CCND1 236 **VIKCDP**DCLRACQEQIEAALRESLR--**QAQNM**DPKAAEEEEEEEEVSD----- 282
CCND2 235 **ITNTDV**DCLRACQEQIEAVLLNSLQ--QYRQD----QRDGSKSEDELSD----- 276
Consensus aa: hothp.p.l.h.p.h...h...p.p.b.h.ph.....p.h.....
Consensus ss: hh hhhhhhhhhhhhhhhhh hhhhhhh hhhhh hhhhh

Conservation:
CCNE2 383 SPVCNGGIMTPPKSTKPPGKH--- 404
CCNE1 386 ASPLPSGLLTPPQSGKKQSSGPEMA 410
CCNB3 1393 -----LVL----- 1395
CCNA2 -----
CCNA1 -----
CCNB2 -----
CCNB1 -----
CCND3 280 QTSTPTDVTA-----IHL-- 292
CCND1 283 LACTPTDVRD-----VDI-- 295
CCND2 277 QASTPTDVRD-----IDL-- 289
Consensus aa:
Consensus ss:

N-terminal cyclin box
C-terminal cyclin box

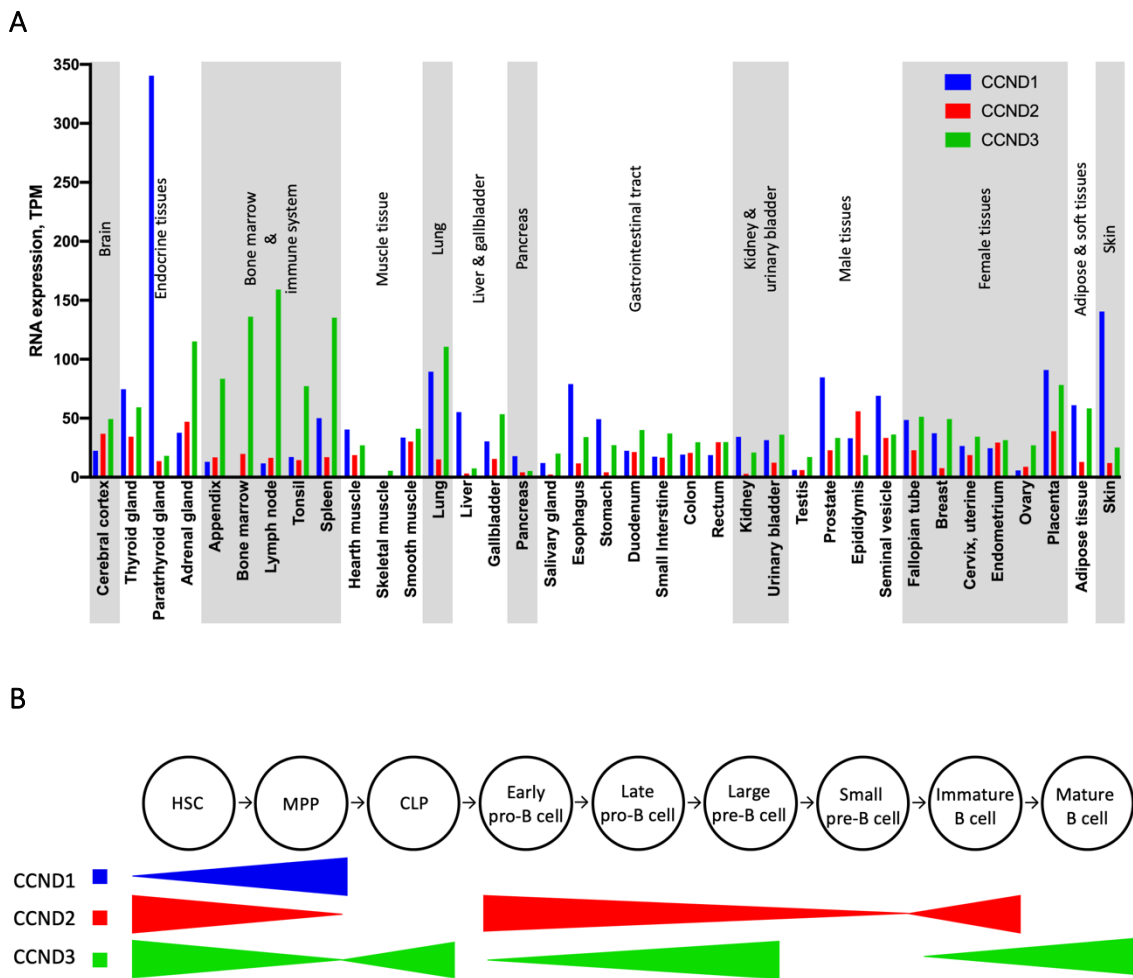
1.3.2 CCND3 is indispensable in B-cell development

CCND1 is expressed and plays a vital role in many cell lines. When it comes to bone marrow and immune system cells CCND2 and CCND3 play a more important role (Passegue, Wagers et al. 2005), although CCND3 expression in the bone marrow and immune system cells is more profound compared to CCND2 expression (Uhlen, Fagerberg et al. 2015) (Figure 1-6 A). CCND2 is expressed in myeloid lineage cells, while CCND3 is expressed in lymphocytic lineage cells (Passegue, Wagers et al. 2005). In order to promote B-cell maturation, CCND3 is expressed in pro-B, large pre-B cells, immature and mature B cells (Cooper, Sawai et al. 2006) (Figure 1-6 B). It has been shown that loss of the one of the CCND can be compensated by overexpression of the other. It seems that CCNDs play a cell type-specific role (Peled, Yu et al. 2010). CCND1 depletion causes neurobiological abnormalities, affects retinas and mammary glands (Sicinski, Donaher et al. 1995). CCND2 depletion affects reproduction of mice (Sicinski, Donaher et al. 1996), cerebral abnormalities (Huard, Forster et al. 1999) and impaired B-cell proliferation (Lam, Glassford et al. 2000), while B-cell differentiation was not affected by CCND2 depletion (Cooper, Sawai et al. 2006, Peled, Yu et al. 2010). Moreover, CCND2 overexpression in HSCs results in a higher percentage of myeloid cells compared to a control HSCs (Cooper, Sawai et al. 2006). CCND3 is important in B-cell and T cell expansion (Sicinska, Aifantis et al. 2003, Cooper, Sawai et al. 2006), germinal centre formation (Cato, Chintalapati et al. 2011) and metabolism (Aguilar & Fajas, 2010) and regulation and modulation of V_H gene expression (Powers, Mandal et al. 2012, Karki, Kennedy et al. 2018).

CCND3 depletion leads to an incomplete block at pro-B and pre-B cell phase (Peled, Yu et al. 2010). The number of total bone marrow cell as well as the number of immature B-cells decreased upon CCND3 depletion, while the number of pro-B cells increased. Thus, it was suggested that CCND3 is required for the differentiation of pro-B cells after cell commitment to the B-cell lineage (Cooper, Sawai et al. 2006). CCND3 depletion in Naïve B-cells cells showed that CCND2 and CCND3 are not required for the initiation. However, CCND3 is indispensable for germinal centre (GC) maturation as CCND2 cannot compensate the loss of CCND3 (Cato, Chintalapati et al. 2011). The double depletion of CCND3 and CCND2 (Cooper, Sawai et al. 2006) and triple depletion of all three CCNDs

potentiated the effect seen in the single depleted CCND cells (Kozar, Ciemerych et al. 2004). Moreover, *Rag1^{-/-}γc^{-/-}* (Recombinant activation gene 1 (Rag1), common cytokine receptor γ-chain (γc)) mouse injected with HSCs that lacks all three CCNDs were not able to produce T-cells, B-cells, and NK cells (Kozar, Ciemerych et al. 2004).

Figure 1-6 CCND expression in different tissues and during B cell maturation phases (A) CCND expression in different tissues (Uhlen, Fagerberg et al. 2015) (B) CCND expression in different B cell maturation phases, where HSC – hematopoietic stem cell, MPP – multipotent progenitor, LMPP - lymphoid-primed multipotent progenitor, CLP – common lymphoid progenitor (Cooper, Sawai et al. 2006, Fuxa and Skok 2007, Lukin, Fields et al. 2008, Perez-Vera, Reyes-Leon et al. 2011, Boller and Grosschedl 2014, Choukallah and Matthias 2014).



1.3.3 CCND transcription activity

Transcriptional activity of CCND1 and CCND3 has been reported, while no information of CCND2 transcriptional activity has been found. All three CCNDs have been seen to reside on chromatin in human embryonic stem cells (hESCs), however only CCND1 activated transcription of gene encoding Aurora Kinase B (AURKB), Centromere Protein M (CENPM), PAX2, SRY-Box 3 (SOX3), PBX Homeobox 1 (PBX1), Dachshund Family Transcription Factor 1 (DACH1), Orthodenticle Homeobox 1 (OTX1), while repressing SOX18, Wnt Family Member 3 (WNT3) and SMAD Family Member 2 (SMAD2) proteins (Pauklin, Madrigal et al. 2016). CCND1 activates transcription of many proteins like Estrogen receptor protein (ER) (Neuman, Ladha et al. 1997, Zwijsen, Wientjens et al. 1997), ATF5 (Liu, Sun et al. 2004), Cyclic AMP-Responsive Element-Binding Protein 2 (CREB2), ETS Transcription Factor ELK1 (ELK1), Cut Like Homeobox 1 (CUX1) (Bienvenu, Jirawatnotai et al. 2010), SUV9, Heterochromatin protein 1 homolog alpha (HP1 α), p300, Histone deacetylase 1 (HDAC1) and HDAC3 (Fu, Rao et al. 2005) independently of CDK4 and represses such proteins as v-MYB (Ganter, Fu et al. 1998), STAT3 (Bienvenu, Gascan et al. 2001), DMP1 (Inoue and Sherr 1998), SPI1 and Myoblast determination protein (MYOD) (Rao, Chu et al. 1994). As well as CCND1 was found to bind at the promoters of such genes as *Ctcf*, Zinc finger X-chromosomal protein (*Zfx*), *Spi1*, E2F Transcription Factor 1 (*E2f1*), *Creb1* (Casimiro, Crosariol et al. 2012). CCND1 transcriptional activity is usually supported by the recruitment of other transcriptional factors.

CCND3 transcriptional activity was shown in COS1 cells (fibroblast-like cell lines derived from monkey kidney tissue), where CCND3 activated transcription of Cyclin dependent kinase inhibitor 1 alpha (CDKN1A), Clullin 3 (CUL3), Growth arrest and DNA damage inducible beta (GADD45B), Programmed cell death 4 (PDCD4), Branched-chain aminotransferase 1 (BCAT1) and T-cell-restricted intracellular antigen-1 (TIA1) (Liu, Sun et al. 2004) and in pancreatic ductal adenocarcinoma (Radulovich, Pham et al. 2010) CCND3 potentiated transcriptional activity of hATF5. While Powers and colleagues showed that CCND3 does not act as a transcriptional factor in B-cells, but rather regulates post-translational processes (Powers, Mandal et al. 2012). Overexpression of CCND3 in myoblasts through epigenetic modifications activated muscle-specific genes and

repressed Ig V (Athar and Parnaik 2015), while in pro-B cells Ig V repression is not associated with epigenetic modifications (Powers, Mandal et al. 2012). CCND3 has been shown to colocalise at the nuclear matrix (NM) together with RNA polymerase (RNAP). CCND3 localization on the NM prevents the IgL chain V kappa locus (V_k) gene association with transcriptional factories, thus causes repression of V_k gene transcription in pro-B cells. While, CCND3 release from the V_k gene sites results in monoallelic V_k gene transcription (Karki, Kennedy et al. 2018). It seems that CCND3 localisation and interaction with cell type-specific proteins governs CCND3 cell type-specific function.

1.3.4 CCND3 localisation and degradation

In pro-B cells, CCND3 is found as bound to CDK4, the nuclear matrix (NM) or regulated by phosphoinositide 3-kinase (PI3K). While CCND2 localizes throughout nucleus unbound to CDK4. Subcellular localisation of CCND2 did not overlap with the CCND3 (Powers, Mandal et al. 2012). Moreover, subcellular localization for CCND3 in B-cell differs from its localization in mouse embryonic fibroblasts (MEFs), suggesting that CCND3 localization is essential for specific function activation. PI3K inhibition caused a reduction in total levels of the CCND3, while the amount of CCND3 associated with CDK4 or CCND3 colocalization with RB was not altered, indicating that PI3K protects CDK4 free CCND3 fraction from degradation (Powers, Mandal et al. 2012). The loss of the pre-BCR on the surface of the cell or inhibition of PI3K decreases CCND3 half-life 4-fold, suggesting that PI3K inhibits CCND3 proteasomal degradation through pre-BCR signalling (Cooper, Sawai et al. 2006).

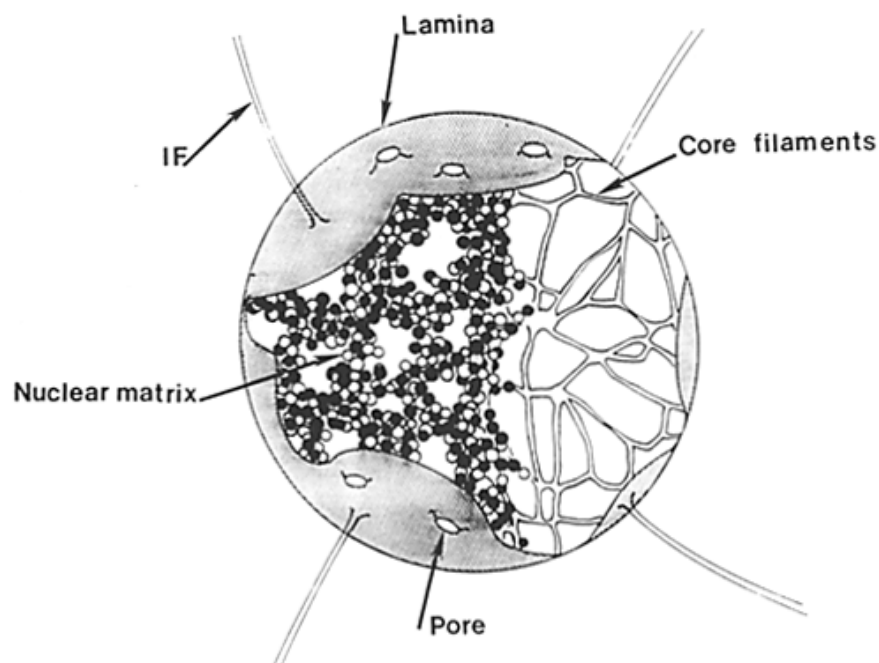
CCND3 is degraded in proteasome or in nuclei. Proteasomal degradation requires CCND3 phosphorylation at the 283 threonine (Thr283) (Naderi, Gutzkow et al. 2004), while nuclear CCND3 degradation does not require phosphorylation of the CCND3 at the Thr283 (Lahne, Kloster et al. 2006). Glycogen synthase kinase-3beta (GS3K3 β) phosphorylates CCND3 and CCND1 respectively at Thr283 and Thr286, thus marking CCND3 and CCND1 for proteasomal degradation (Lahne, Kloster et al. 2006). During mitosis CCND3 is targeted by E3 ligase family proteins such as F-box protein (FBXL2) for ubiquitination (Chen and Mallampalli 2013).

Overexpression of CCND1, together with Chromosomal Maintenance 1 (CRM1) and GSK3 β in NIH-3T3 cells, leads to CCND1 relocation to the cytoplasm and is subjected to further degradation (Lu, Gladden et al. 2003). It was shown that inhibition of Protein phosphatase 1 (PP1) causes CCND3 depletion regardless of GSK-3 β activity or phosphorylation status at Thr283 of CCND3. Whereas PP1 and proteasome inhibition resulted in the accumulated CCND3 in the nuclei, indicating that PP1 protects CCND3 from nuclear proteasomal degradation (Lahne, Kloster et al. 2006). GSK3 β is less active in GC B-cells, thus allows for CCND3 accumulation. Moreover, PI3K inhibition did not increase CCND3 degradation in GC B cells, suggesting that in GC CCND3 might not be regulated by PI3K. CCND3 degradation was induced by inhibition of Protein kinase A (PKA) in GCs, suggesting that PKA activity and inhibition of GSK3 β results in CCND3 accumulation in GCs (Cato, Chintalapati et al. 2011). Overall that CCND3 localization is tightly regulated with its stability and function.

1.4 Nuclear matrix

The NM is the biochemical entity that resist stringent extraction of intact nuclei procedures with non-ionic detergents, DNase I and hypotonic salt. It is believed that NM is protein network, which maintains structure of nuclei and regulates chromatin organisation (Engelke, Riede et al. 2014). After NM isolation, the shape of nuclei remains unchanged and some morphological features such as a presence of nuclear lamina, residual nucleoli, ribonucleoprotein complex and the nuclear pore complexes can be observed as well (Berezney and Coffey 1977, Stuurman, Van Driel et al. 1989). Although after chromatin removal as well was observed filamentous network (Berezney and Coffey 1974), it was proposed to be an artificial formation. For example, it could be a result of embedded plastic (Penman 1995), a ribonucleoprotein network (Fey, Krochmalnic et al. 1986) or spontaneous filament formation created by viral pre-mRNA transcripts after a release from their RNA binding partners (Heaphy, Finch et al. 1991). Schematic representation of Nm is shown in Figure 1-7.

Figure 1-7 Nuclear matrix schematic representation, where IF – intermediate filaments. (Figure taken from Frey and Penman, 1988).



NM and chromatin occupy, respectively, 10% and 35% of the nuclei (Coffey 2002). About 400 proteins were found to associate with NM. From which 50% of the proteins are

temporarily associated with the NM, and their association depends on the cellular processes (Mika and Rost 2005). Moreover, the same origin cells have a higher number of shared proteins, while the NM proteins from different origin cells were more diverse (Fey and Penman 1988). NM is involved in DNA metabolism (Verheijen, van Venrooij et al. 1988), DNA replication, chromosomal organisation (Vemuri, Raju et al. 1993), DNA transcription, processing and transport of RNA (Zeitlin, Parent et al. 1987), steroid hormone action (Diamond and Barrack 1984), viral replication (Simard, Bibor-Hardy et al. 1986) and carcinogenesis (Elcock and Bridger 2008).

Nuclear lamina along, with NM is responsible for nuclear contents organization. The nuclear lamina consists of A-type or B-type lamins and nuclear lamin-associated membrane proteins such as lamina associated polypeptides 1 and 2 (LAP1, LAP2), emerin, lamin B-receptor (LBR) and MAN (Gant, Harris et al. 1999, Dechat, Shimi et al. 2007).

Mutation in nuclear lamina results in laminopathies which are observed as nuclear dysmorphism with severe nuclear blebbing (Eriksson, Brown et al. 2003, Vergnes, Peterfy et al. 2004, Taimen, Pflieger et al. 2009). Structural changes in the nucleus affect the cell cycle, chromatin organisation, transcription and differentiation (Csoka, English et al. 2004, Dechat, Shimi et al. 2007, Briand and Collas 2018) and result in various tissue-specific diseases and premature ageing (Worman and Schirmer 2015). Thus, observation of nuclear blebbing in the EBF1 depleted cell lead to think that EBF1 might be a nuclear matrix protein.

1.4.1 Nuclear matrix history

The foundation of NM research began with observation of fibro-granular non-chromatin structure in the nuclei via electron microscopy (Fawcett 1966). Smetana and colleagues observed that these structures contains ribonucleoproteins and RNA (Smetana and Hermansky 1963). Later on it was shown that RNA or ribonucleoproteins are present in the nuclear remainder (which in later research is caller NM) after the removal of the nuclear envelope or gentle homogenization of the nucleus (Herman, Weymouth et al. 1978) as well as after digestion with DNase I (Narayan, Steele et al. 1967, Herman, Weymouth et al. 1978), suggesting that ribonucleoproteins form some structure that

does not require association with DNA. The release of RNA or ribonucleoproteins was observed only after digestion with ribonucleases (Narayan, Steele et al. 1967, Herman, Weymouth et al. 1978) and severe mechanical extraction (Faiferman and Pogo 1975).

The next step in NM discovery was the isolation and biochemical characterization of the non-chromatin structures observed via electron microscopy (Nickerson 2001). Initial biochemical isolation of NM revealed that non-chromatin structures in the nucleus are resistant to DNase and RNase digestion (Berezney and Coffey 1974). The structural elements seen via electron microscopy consisted of RNA or ribonucleoproteins, thus it was suggested that NM isolated by Berezney and Coffey rather revealed an underlying RNase-resistant scaffolding, but not the whole proteome of NM (Hendzel, Boisvert et al. 1999). Thus, RNase cannot be used for isolation of whole NM (ribonucleoprotein network or non-chromatin structure) (Nickerson 2001). The NM research progressed with the observation that chromatin attaches to NM via loop domains (Flavell 1994, Brouwer, Bruce et al. 2002) and the discovery of spatially distinct functional domains in the nucleus that remain in place after the removal of soluble proteins and chromatin (Dickinson, Dickinson et al. 1997, Nickerson 2001, Karki, Kennedy et al. 2018).

1.4.2 Nuclear matrix is a non-chromatin structure in the nuclei not an artefact

There is much discussion for and against the existence of NM. The cytoskeleton is a fixed system and molecule movement along actin strands can be observed in immunofluorescence, while nothing similar is observed in nuclei (Hancock 2000, Martelli, Falcieri et al. 2002). Although some might think that the nuclear shape is contained by the nuclear membrane, the studies have been shown that the nuclear membrane adapts to the change in the volume or shape of the nuclei (Spector 1993, Richter, Nessling et al. 2007). Thus, the nuclear membrane is more like fluid-like and does not contribute significantly to nuclear shape stability (Rowat, Lammerding et al. 2008). Existence of the rigid NM is opposed by the observation of oligonucleotide diffusion in the nuclei (Politz, Browne et al. 1998), suggesting that the protein remainder after extraction might be an artefact. However, it might be that the NM is rather a dynamic protein system which undergoes changes regulated by the cellular process (Martelli, Falcieri et al. 2002). The dynamic processes of the NM are supported by the observation that upon induced heat

shock proteins that undergo thermal denaturation adsorb to the NM in time and temperature-dependent manner. The protein adsorption on the NM induces inhibition of DNA supercoiling and results in the change in protein association (Tomasovic, Turner et al. 1978, Roti Roti and Wright 1987, Lepock, Frey et al. 2001). Another fact in favour of NM existence is that chromatin motions were seen to be restricted via Brownian motions. Chromosome density and non-chromosomal structures within the nuclei are not enough to constrain the chromosome motions. It was proposed that NM causes the chromosome motion restriction (Henzel, Boisvert et al. 1999, Martelli, Falcieri et al. 2002).

There are a number of methods reported for ribonucleoprotein network or non-chromatin structure isolation (Narayan, Steele et al. 1967, Herman, Weymouth et al. 1978, Nickerson 2001, Sawasdichai, Chen et al. 2010, Engelke, Riede et al. 2014). Most of these methods employ non-ionic detergents, DNase I and hypotonic salt washes to remove cytoplasmic, loosely and tightly held nuclear proteins and DNA from the intact cell (Narayan, Steele et al. 1967, Herman, Weymouth et al. 1978, Nickerson 2001, Sawasdichai, Chen et al. 2010, Engelke, Riede et al. 2014). Some NM critics speculate that high salt concentration and Triton used for NM isolation causes proteins precipitation (Pederson 2000). However, NM isolation using low salt concentrations and avoiding detergents revealed similar structural features as were seen using other NM isolation protocols (Jackson and Cook 1988, Wan, Nickerson et al. 1999).

Another reason to believe in the existence of the NM is that NM changes (Getzenberg, Pienta et al. 1991) upon cell malignant transformation (Elcock and Bridger 2008), apoptosis (Earnshaw 1995) or viral infection (Zhai, Nickerson et al. 1987). For example, such NM proteins as RPL4 and TXNL1 are elevated in Prostate cancer (Engelke, Riede et al. 2014, Filella, Fernandez-Galan et al. 2018). Moreover, the change in NM was observed as well in the normal bladder cells that were adjacent to bladder cancer cells compared to cells from the healthy tissues. This suggests that cancer cells induce a change in the NM of the neighbour hooding healthy cell and subsequently causes these normal cells to undergo malignant transformation (Getzenberg, Konety et al. 1996, Coffey 2002). Thus, NM proteins can be potential cancer biomarkers (Elcock and Bridger 2008).

In the recent study three different, previously described NM extraction buffers were compared: lithium 3,5-diiodosalicylate (LIS), NaCl and ammonium sulfate (AS). Briefly, PD36 pre-B cell nuclei were isolated and purified, followed by nuclei disruption in hypotonic buffer and DNA digestion. Further, NM were extracted using 25mM LIS, 2M NaCl or 250mM AS. 0.71 to 0.95 high correlation was shown comparing the three NM isolation methods (Engelke, Riede et al. 2014). Only those proteins that were detected by all three extraction methods were classified as NM proteins. Moreover, Engelke and colleagues classified the detected proteins by their retention at the NM only (classifier I) or by protein retention and abundance (classifier II). 272 and 351 protein were identified assigned to classifier I and classifier II, respectively. Most of the proteins overlapped, while some of the proteins were classified only into one of the groups. For example, HDAC3 and Nuclear Receptor Corepressor 2 (NCOR2), have a lower significance in the classifier II due to their low abundance in the NM, while RUNX1 and THO complex 1 protein (THOC1) have a higher significance in the classifier II due to their high abundance in the NM (Engelke, Riede et al. 2014).

It was suggested that matrix-attachment regions (MARs) and scaffold attachment regions (SARs) of the DNA sequences that are located at the border of gene domains are responsible for chromatin organization within the nucleus (Flavell 1994); they may act as repressors or gene activators (Brouwer, Bruce et al. 2002). For example, it was shown that Special AT-Rich Sequence Binding Protein 1 (SATB1) of NM protein binds the μ -immunoglobulin MAR (Dickinson, Dickinson et al. 1997) and regulates gene activation in pro-B cells and gene repression in non-pro-B cells (Cunningham, Purucker et al. 1994). Engelke and colleagues observed that many of the NM classified I proteins were previously reported to associate with S/MAR (Engelke, Riede et al. 2014). Moreover, the detected NM proteins in this study were comparable with the previously reported data, suggesting that NM does exist. However, some of the NM extraction methods may lead to false-positive results (Engelke, Riede et al. 2014). One of the causes is usage NM stabilization techniques, such as NM crosslinking after DNA digestion and prior NM extraction (Martelli, Falcieri et al. 2002).

Xiong and colleagues have observed EBF1 and CCND3 association and nuclear collapse upon EBF1 depletion in pro-B cells (Dr Shiqiu Xiong/Ildiko Györy unpublished

observations). This led to few possible hypotheses. One possible hypothesis is that EBF1 activates transcription of a NM protein, which supports CCND3 attachment to the NM in pro-B cells. EBF1 downregulated and upregulated proteins (Treiber, Mandel et al. 2010) was compared were searched against the reported nuclear matrix proteins (Engelke, Riede et al. 2014). EBF1 depletion in *Ebf1^{fl/fl}RERT^{Cre}::A-MuLV* cells resulted in downregulation and upregulation of genes that have previously been reported to encode nuclear matrix proteins Cancer susceptibility candidate protein 5 (CASC5), Lamin B1 (LMNB1), Mastermind like transcriptional coactivator 2 (MAML2), RB binding protein 8 (RBBP8), Centromere protein A (CENPA), Ribosomal RNA Processing 12 homolog (RRP12), Nucleolar protein 8 (NOL8) and 10 (NOL10) and Microtubule actin crosslinking factor 1 (MACF1), Mitotic arrest deficient 2 like 1 (MAD2L1), MYB binding protein 1a (MYBBP1A), and Centromere protein L (CENPL) (Treiber, Mandel et al. 2010, Engelke, Riede et al. 2014). However, the change in these protein levels is observed five days after EBF1 depletion, suggesting that changes in the EBF1 target transcription is a secondary event. The other possible hypothesis is that EBF1 as a structural matrix protein supports CCND3 attachment to the nuclear matrix in the pro-B cells. As well it was hypothesized that if EBF1 is genuinely a nuclear matrix protein, it should co-immunoprecipitated with known NM proteins.

Chapter 2 The aims of the project

- To investigate whether EBF1 is a nuclear matrix protein
- To investigate EBF1 structural requirements for CCNA2 and CCND3 binding
- To identify EBF1 and CCND3 common NM binding partners

Chapter 3 Materials and Methods

3.1 Cell lines used and cell culture conditions

3.1.1 Conditional *Ebf1* depleted mouse pro-B cell lines

The conditional knockout mouse pro-B cells (from the foetal liver), which expresses the Cre recombinase under the control of a tamoxifen-inducible promoter and depletes floxed *Ebf1* (*Ebf1^{fl/fl}RERT^{Cre}*) after tamoxifen-induced Cre recombinase expression were immortalized with Abelson murine leukaemia virus (A-MuLV). These cell lines are referred to as *Ebf1^{fl/fl}RERT^{Cre}::A-MuLV*. Control cell lines lacking floxed *Ebf1*, which maintain *Ebf1* expression after tamoxifen exposure are referred to as *Ebf1^{+/+}RERT^{Cre}::A-MuLV*. Both were generated by Dr Ildiko Györy (Györy, Boller et al. 2012).

Single cell clones of the *Ebf1^{fl/fl}RERT^{Cre}::A-MuLV* and *Ebf^{+/+}RERT^{Cre}::A-MuLV* cells were derived from foetal liver of the conditional knockout mouse. In my experiments I have used different sub-clones, namely 1_1, 1_3, 1_4 pro-B *Ebf1^{fl/fl}RERT^{Cre}::A-MuLV* and c3_4 *Ebf1^{+/+}RERT^{Cre}::A-MuLV*. Gene expression of *Ebf1^{fl/fl}RERT^{Cre}::A-MuLV* pro-B cells were tested *via* microarray (Dr Ildiko Györy unpublished observations). Gene expression pattern in pro-B *Ebf1^{fl/fl}RERT^{Cre}::A-MuLV* after 5 days upon *Ebf1* depletion was previously reported (Györy, Boller et al. 2012). While, at early time point pro-B *Ebf1^{fl/fl}RERT^{Cre}::A-MuLV* have different gene expression pattern.

Murine *Ebf1^{fl/fl}RERT^{Cre}::A-MuLV* and *Ebf1^{+/+}RERT^{Cre}::A-MuLV* pro-B cells were grown in Roswell Park Memorial Institute (RPMI) medium with L- glutamine (BE12-752F, Lonza, USA) supplemented with 10% Foetal bovine serum (FBS) (Lonza), 1% v/v penicillin and streptomycin (p4458, Sigma) and 0.0004% β -mercaptoethanol (Sigma, Germany) (This medium is abbreviated as RPMI FBS p/s β -m).

3.1.2 MPI-2 GM-CSF dependent macrophages

Granulocyte-macrophage colony-stimulating factor (GM-CSF)-dependent, differentiated macrophages Max Planck Institute (MPI) cells are self-renewing, non-transformed, GM-CSF-dependent phagocytes that do not express EBF1 (Fejer et al., 2013). MPI-2 were grown in RPMI FBS p/s β -m and 20–50 ng/mL murine GM-CSF (Zal, Volkmann et al. 1994) (RPMI FBS p/s β -m GM-CSF).

3.1.3 293T cells

293T cells (DuBridge, Tang et al. 1987) were grown in Dulbecco's Modified Eagle Medium (DMEM) supplemented with 4.5g/l glucose (12-604F Lonza, USA), 10 % FBS, 1% v/v penicillin and streptomycin (DMEM FBS p/s).

In order to detach adherent MPI-2 or 293T cells, media was removed, and cells were washed with Phosphate-buffer saline (PBS) (P4417, Sigma-Aldrich), then cells were incubated with 2.5% trypsin (15090-46, Gibco, UK) or 0.5% trypsin-EDTA (ethylenediaminetetraacetic acid) (15090-54, Gibco, UK), respectively. Detached MPI-2 and 293T cells were resuspended, respectively in RPMI FBS p/s β -m GM-CSF or DMEM FBS p/s.

3.1.4 DH5 and BL21 pLysS alpha Competent bacteria preparation

100 μ l of frozen DH5 α (18265017, Termofisher, UK) and BL21 pLysS (L1195, Promega, UK) were inoculated in 500ml LB media (1% tryptone, 1% NaCl, 5% yeast extract), cells were grown at 37°C until they reached optical density (OD) 0.3-0.4. Cells then were centrifuged at 500rpm for 10min at 4°C. 100mM CaCl₂ and 100mM MgCl₂ buffers were precooled. The bacterial pellet was resuspended in 0.25 packed cell volume (PCV) precooled 100mM MgCl₂ for 5min, then centrifuged at 400rpm for 10min. The bacterial pellet was then resuspended in 0.05 PCV precooled 100mM CaCl₂. Then additional 0.45PCV of CaCl₂ was added to the resuspended pellet and incubated on ice for 20min. The cell suspension was centrifuged at 400rpm for 10min and resuspended in 0.02PCV cold 85mM CaCl₂ and 15% glycerol w/v. Cells were dispensed as 100 μ l aliquots and frozen down at -80°C.

3.2 Drug preparation

(Z)-4-Hydroxytamoxifen (OHT) (13258, Cayman Chemical Company, USA) was diluted as 10mM in ethanol (EtOH) (64-175, VWR).

Droxinostat (23869, Cayman Chemical Company, USA) is a selective inhibitor of HDAC3, HDAC6 and HDAC8 and RGFP966 (16917, Cayman Chemical Company, USA) is a selective inhibitor of HDAC3. Droxinostat and RGFP966 were diluted as 5mM in dimethyl sulfoxide (DMSO) (276855, Sigma-Aldrich).

3.3 Plasmids

pMYs FLAG Wild type (WT) *Ebf1* (pMYs FLAG WT *Ebf1*), pMYs FLAG *Ebf1* lacking TAD (pMYs FLAG Δ T *Ebf1*) (Boller, Ramamoorthy et al. 2016), pMys FLAG *Ebf1* lacking IPT (pMys FLAG Δ I *Ebf1*) (Yang, Ramamoorthy et al. 2016), pMys FLAG *Ebf1* lacking IPT and TAD (pMys FLAG Δ I Δ T *Ebf1*) (Treiber, Treiber et al. 2010), pMYs FLAG *Ebf1* lacking DBD, IPT and TAD (pMYs FLAG Δ D Δ I Δ T *Ebf1*) and pMYs Hairy and enhancer of slip-1 (*Hes1*) (cloned by Dr Ildiko Gyory, unpublished) were available in house. pET 21d bovine His-tagged *Ccna2* which lacks the first 169 amino acids including the destruction box (pET 21d *CCNA2 His*) was given by Dr Echaliere (Bettayeb, Oumata et al. 2008). pMYs FLAG *Ebf1* lacking HLH and TAD (pMYs FLAG Δ H Δ T *Ebf1*) and pMYs FLAG *Ebf1* lacking DBD (pMYs FLAG Δ D *Ebf1*) were cloned (see below). Schematic representation of FLAG-tagged WT and mutant proteins is represented in Figure 3-1. pCR II TOPO Δ H Δ T *Ebf1* and pCR II TOPO Δ D are ligates of pCR II TOPO (Termofisher, UK) and a PCR product. pCR II TOPO plasmid has 3'-T overhangs, which allows for a directly cloning of PCR products from a PCR reaction. The PCR products that were cloned into pCR II TOPO vector were re-cloned into a retroviral expression vector pMys IRES GFP (Sekine, Kitamura et al. 2008). All plasmid maps are presented in Table 3-1.

Figure 3-1 WT and mutant FLAG EBF1 schematic representation. DNA binding domain (D) is necessary for EBF1 binding to DNA, helix-loop-helix (H) dimerization domain aids in EBF1 binding to DNA, an “immunoglobulin, plexins, transcription factors-like” (I) domain, whose function is not yet known, and a transactivation domain (T), which participates in the gene transcriptional activation in the absence of other TFs. FLAG and streptavidin (ST) - protein tags

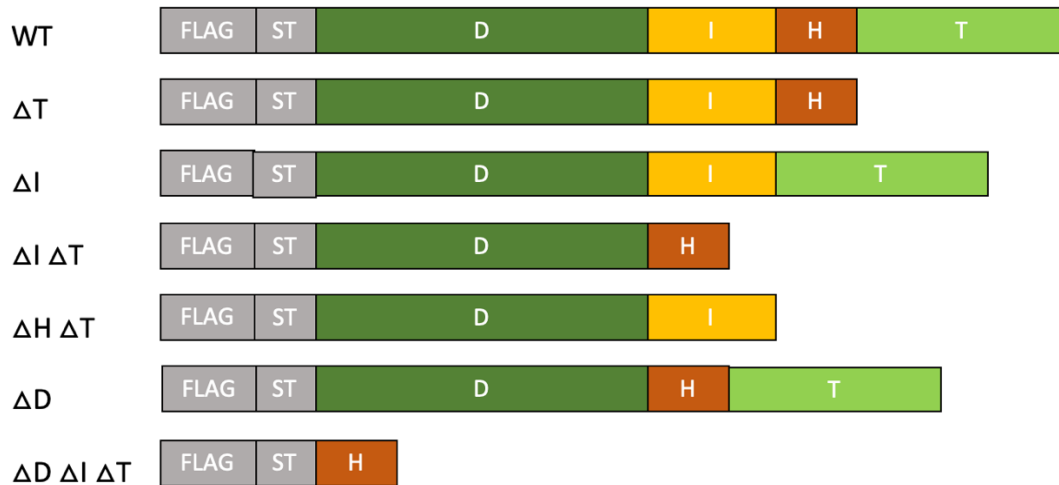
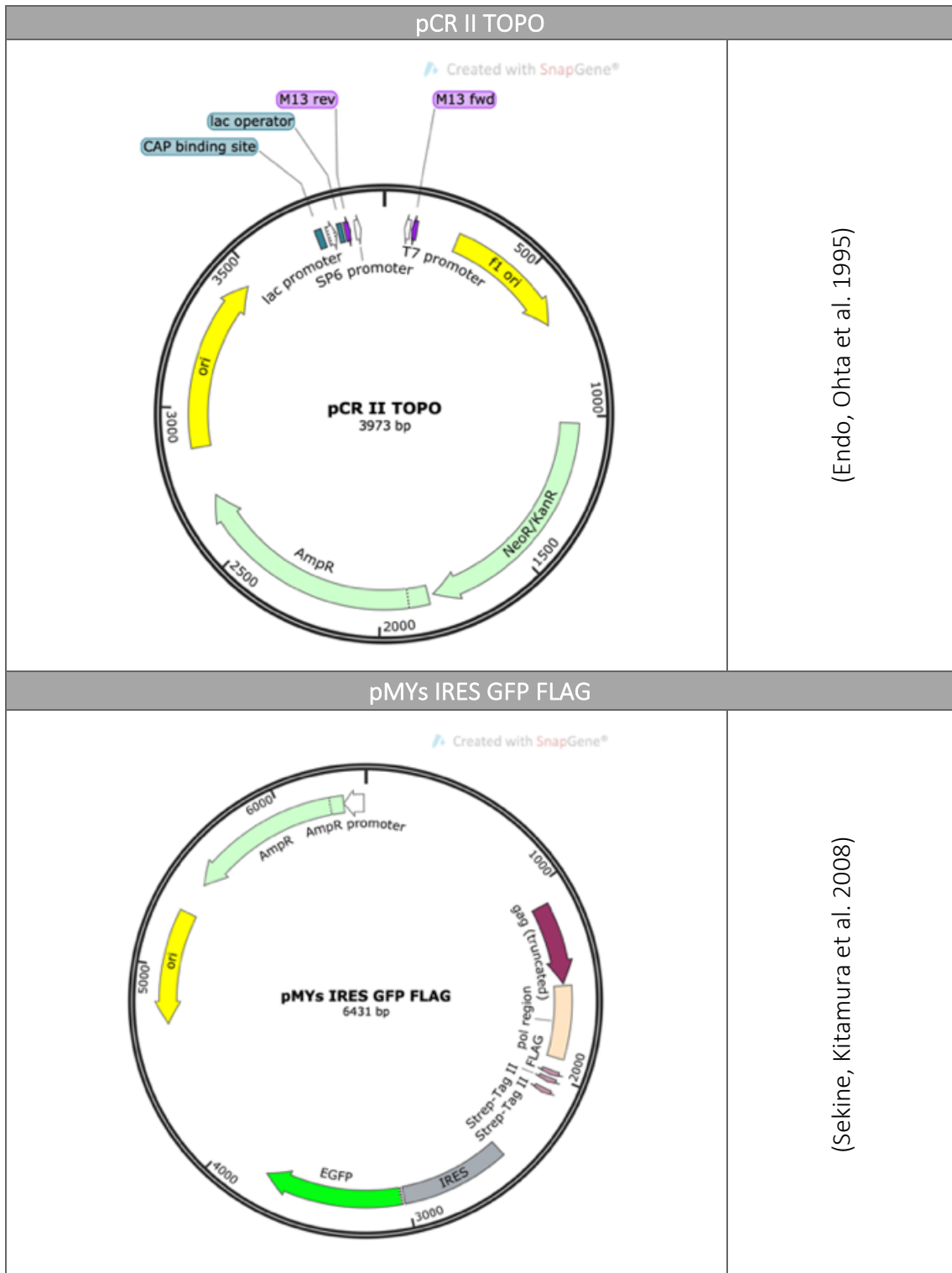
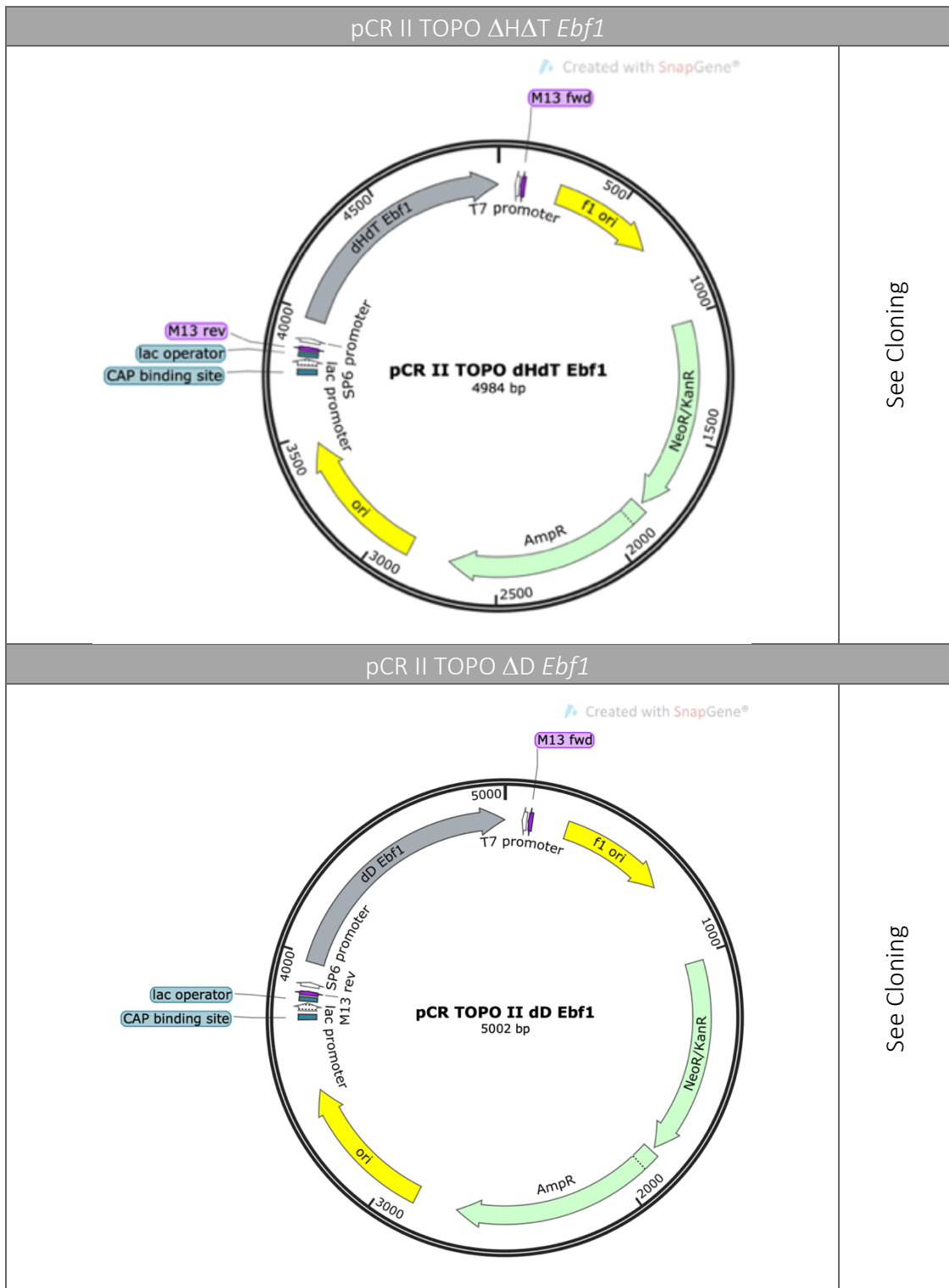


Table 3-1 Plasmid maps used in plasmid cloning and protein expression in mammalian and bacterial cultures, where WT - Wild type, $\Delta T Ebf1$ ($dT Ebf1$)- *Ebf1* lacking TAD domain, $\Delta I Ebf1$ - *Ebf1* lacking IPT, $\Delta I \Delta T Ebf1$ - *Ebf1* lacking IPT and TAD and $\Delta D \Delta I \Delta T Ebf1$ - *Ebf1* lacking DBD, IPT and TAD.



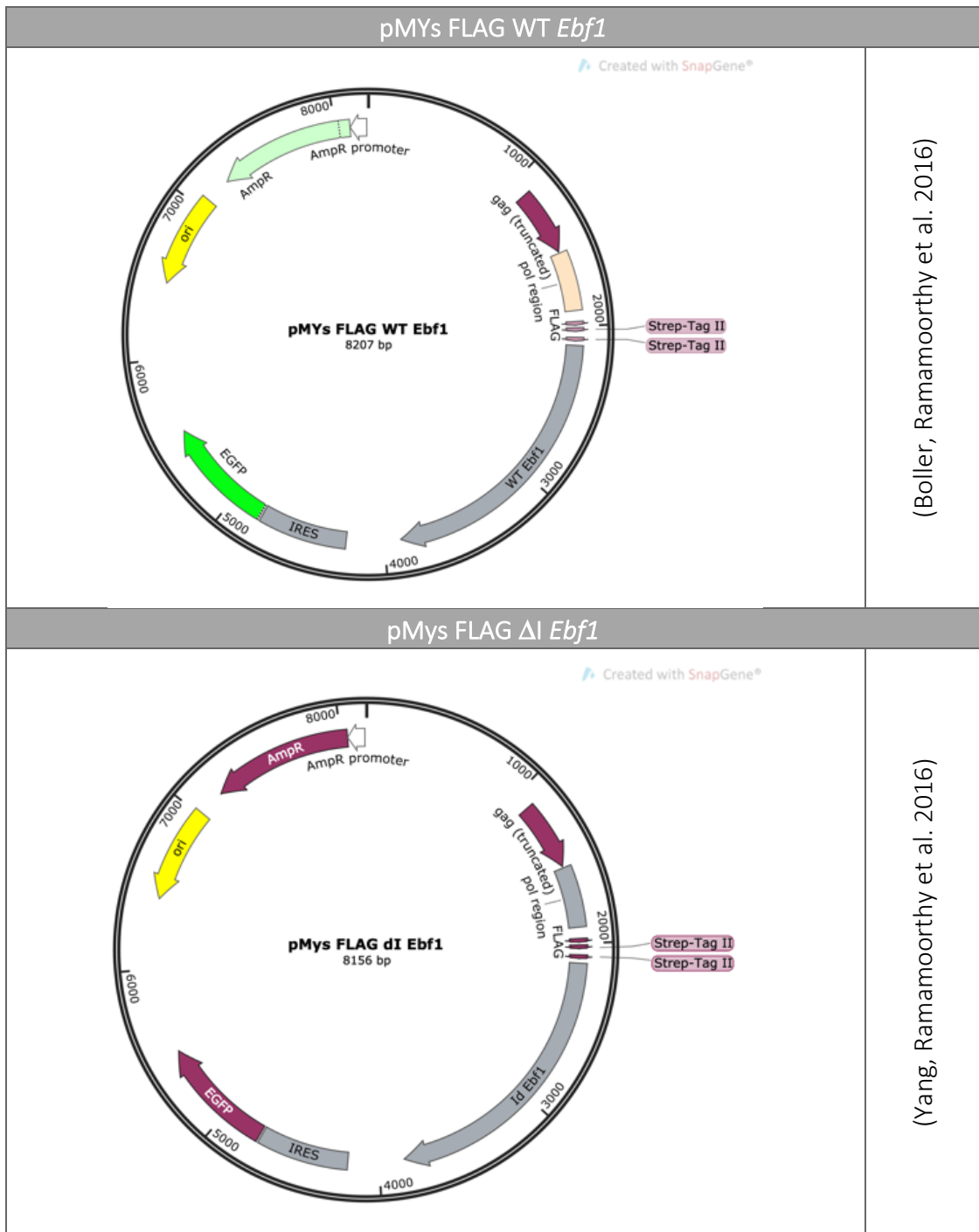
Continued...

Continued...



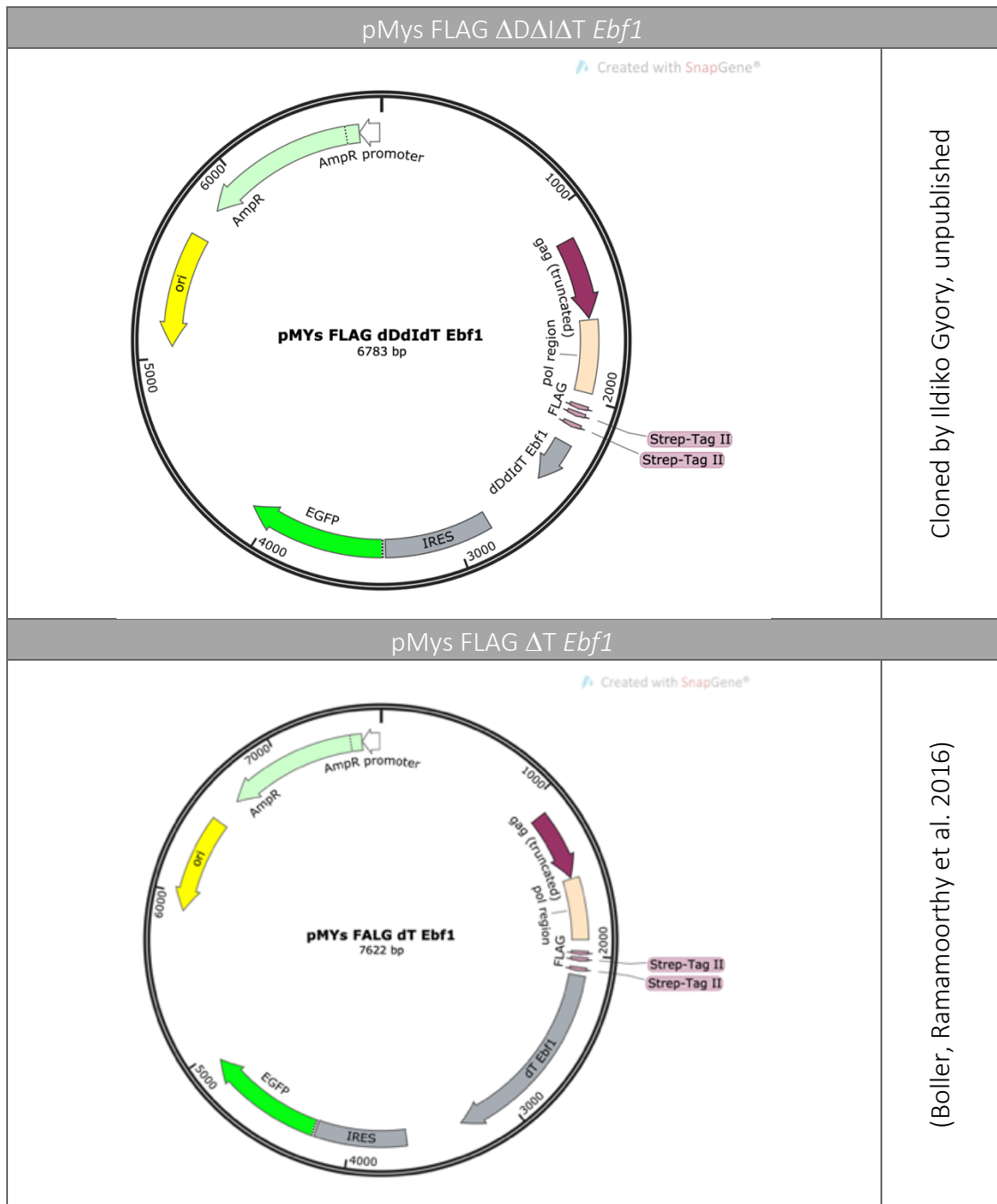
Continued...

Continued...



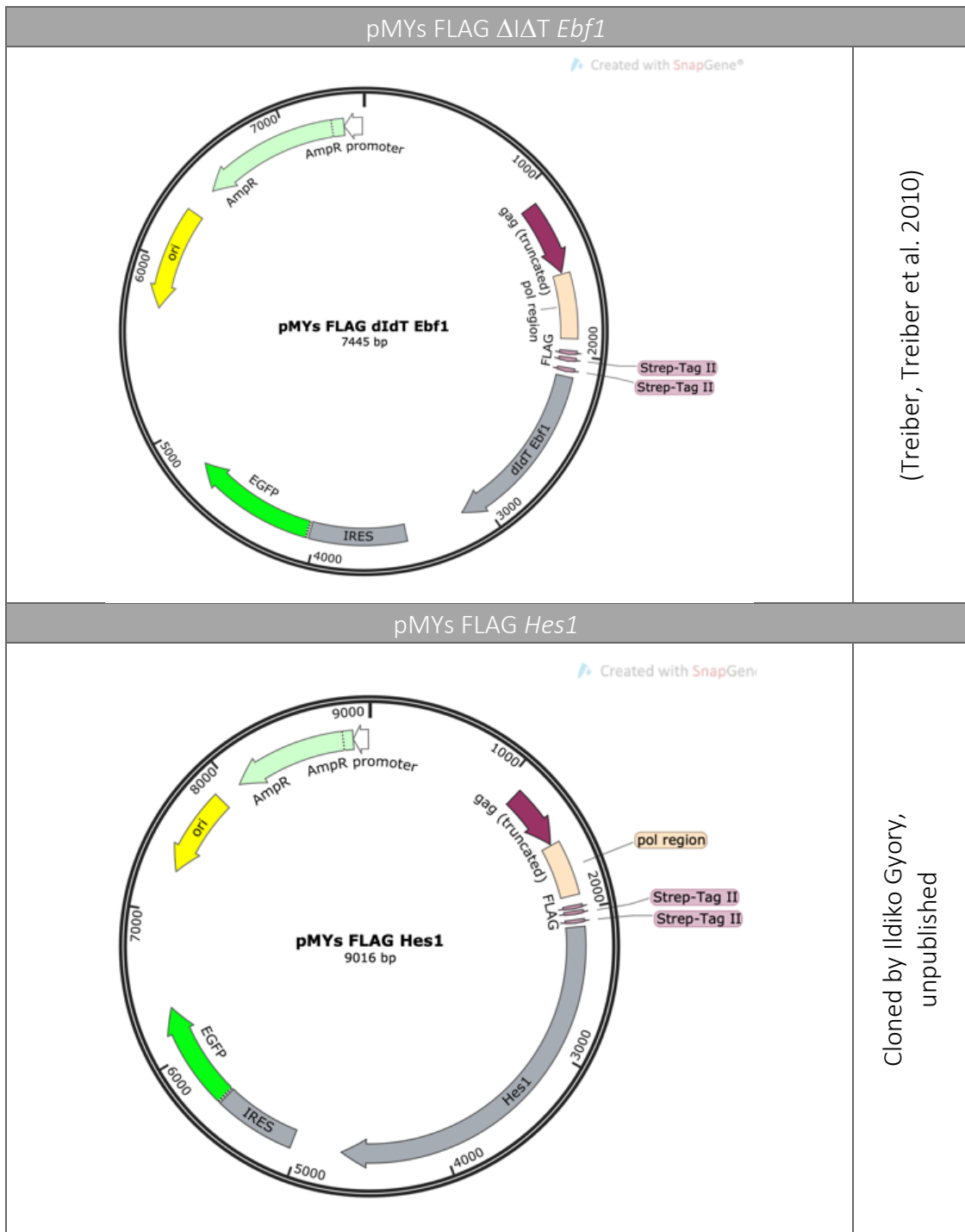
Continued...

Continued...



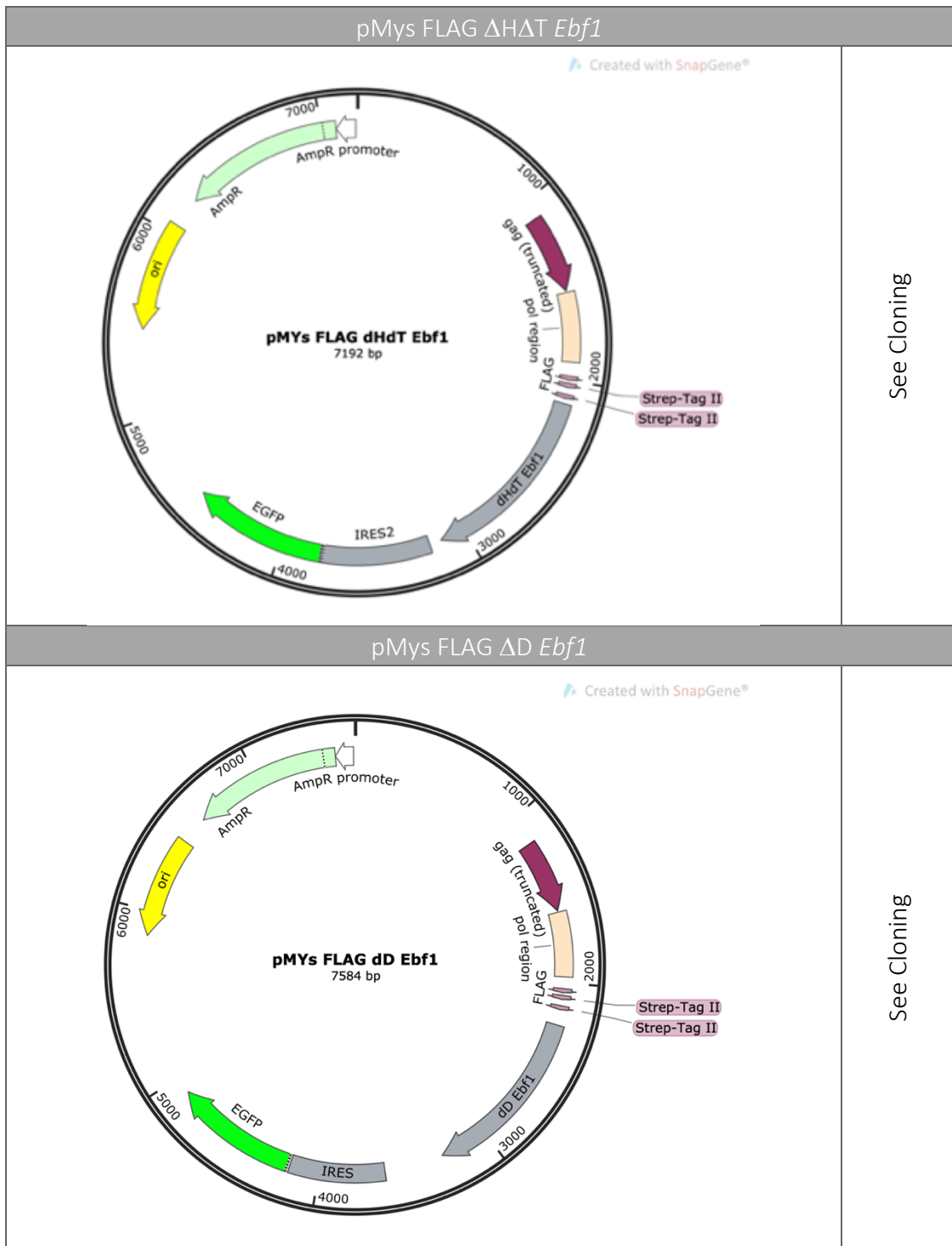
Continued...

Continued...



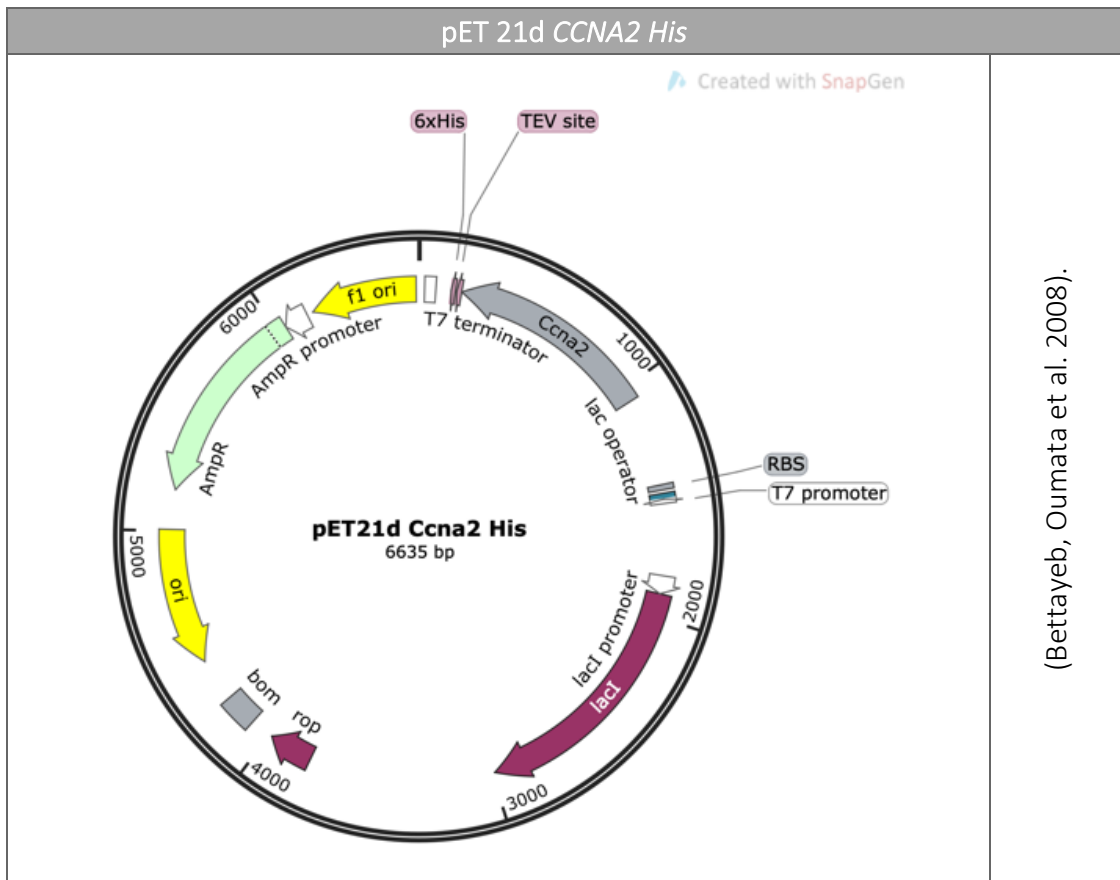
Continued...

Continued...



Continued...

Continued...



3.4 Cloning

3.4.1 PCR amplification of Δ H Δ T *Ebf1* and Δ D *Ebf1*

pMYs FLAG WT *Ebf1* was diluted to 10ng/ml. 1 \times PCR mix was prepared by adding 3 μ l 10 \times Paq 5000 DNA polymerase buffer (#600682-51, Agilent), 1 μ l 10 μ M dNTP (DNTP100-1KT, Sigma), 0.5 μ M Paq 5000 polymerase (#600680-52), 1 μ l 10 μ M reverse and 1 μ l 10 μ M forward primer (Table 3-2) and 21.5 μ l H₂O (for one sample). To 2 μ l DNA 1 \times PCR mix was added. DNA was amplified in the PCR cycle. DNA denaturation was initiated at 95°C for 3min, then followed with 35 cycles of denaturation, annealing and extending stages. DNA was denaturised at 95°C for 40 s, annealed at 60°C for 45 s and extended at 72°C for 3min 20 s for 35 cycles. The PCR final extension was performed at 72°C for 4min.

Table 3-2 Primers used in PCR amplification of Δ H Δ T *Ebf1* and Δ D *Ebf1*

Δ H Δ T <i>Ebf1</i>	
FW primer	CAGGATCCTTTGGGATTCAGGAAAGCATCC
Reverse primer	CTCGAGTCAGTCGATGGTGGGTTTCATTGAGTGCTGTGT
Δ D <i>Ebf1</i>	
FW primer	CAGGATCCGAAGGTACGCCCACGACGGGAG
Reverse primer	CGGTGCGACTCACATAGGAGGAACAATCATG

3.4.2 PCR product purification

The PCR product was excised from 1% agarose gel and purified using QIAquick Gel Extraction Kit (28706, BioRad, USA). Briefly, the excised one volume of agarose gel slice containing PCR product was solubilized in three-volume of QG Buffer and incubated at 50°C for 10min. One volume of isopropanol was added to the solubilized PCR product and added to the spin column. The column was centrifuged for 1min at 13 000 rpm, flow-through was discarded and washed once with 500 μ l of QG buffer and once with 750 μ l PE Buffer by centrifuging at 13 000 rpm for 1min. In order to remove the residual buffer, the empty column was spun down at 13 000 rpm for 1min, and PCR product was eluted with 30 μ l H₂O by centrifuging at 13 000 rpm for 1min. 6 μ l of 5 \times DNA gel loading buffer (5% β -

Mercaptoethanol, 0.02% Bromophenol blue, 30% Glycerol, 10% Sodium dodecyl sulphate, 250mM Tris-HCl pH6.8) was added to the 30µl of each PCR product and samples were load on the 1% agarose gel (containing 0.2µg/µl ethidium bromide (E/P800/03, Fisher Chemicals, UK). Agarose gel electrophoresis was performed in 1×TBE buffer (1M Tris base, 1M Boric acid, 0.02 M EDTA) at 120V for 1h.

3.4.3 PCR product recombination into pCR II TOPO vector

0.5µl of pCR II TOPO vector (45-0640, Invitrogen, USA) was added to 4.5µl of PCR product and incubated at RT for 15min. Ligated material was added to 20µl DH5α competent cells and incubated on ice for 20min. Cells were heat-shocked for 45s at 42°C and transferred on ice. 1ml of LB media was added to the cells and cells were incubated at 37°C for 1h shaking at 225 rpm. 100µl of transformed DH5α cells were spread on one and 900µl on the second LB media plate supplemented with 100µg/ml ampicillin (Leicester, UK) (L-amp). Plates were incubated at 37°C overnight (O/N).

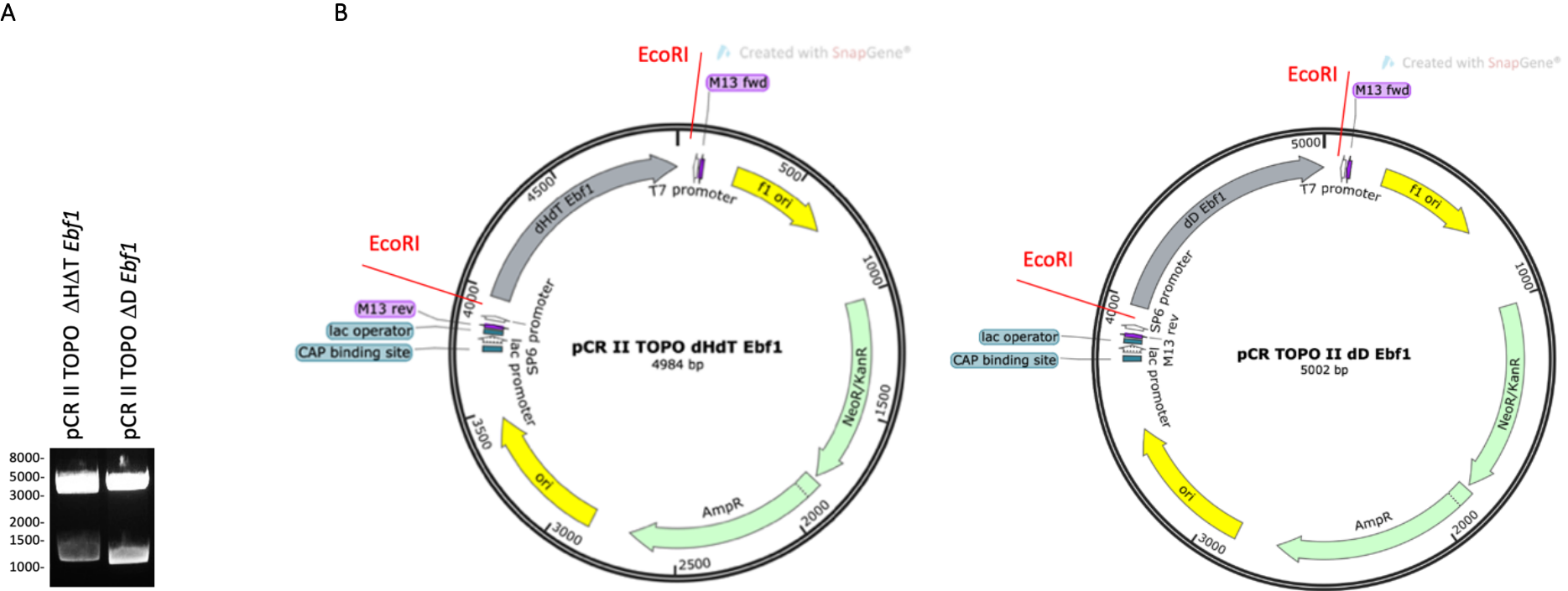
The following day colonies were picked, resuspended in 3ml LB-amp and incubated at 37°C O/N. DNA purification was done accordingly to the protocol using QIAprep Spin Miniprep Kit (27104, BioRad, USA), briefly the O/N cultures were pelleted at 4000rpm for 30min at room temperature (RT). The bacterial pellet was resuspended in 250µl P1 Buffer and transferred to a microcentrifuge tube, followed by addition of 250µl P2 Buffer. Microcentrifuge tubes were inverted six times and incubated for about 5min until the solution became clear. Then 350µl of N3 Buffer was added, and the solution was mixed by inverting microcentrifuge tube six times. Lysates were spun down for 10min at 13 000rpm. The supernatant was applied to the spin column and centrifuged for 1min at 13 000rpm. After flow-through was discarded, the column was washed with 750µl of PE Buffer and centrifuged for 1min at 13 000rpm. After flow-through was discarded, the spin column was spun once again to remove residual wash buffer. The plasmid was eluted with 30µl H₂O for 1min at 13 000rpm.

PCR product ligation into pCR II TOPO vector was confirmed by enzymatic digest of pCR II TOPO FLAG ΔHΔT *Ebf1* and pCR II TOPO FLAG ΔD *Ebf1* using EcoRI (R6011, Promega,

UK) (Figure 3-2). 13µl of H₂O, 1µl of EcoRI and 2µl of the ×10 Buffer H (Promega, UK) was added to 4µl of 0.25µg/ml DNA and incubated at 37°C for 1h. 5µl of ×5 DNA gel loading buffer was added to the 20µl of the digest product and samples were load on the 1% agarose gel containing 0.2µg/µl ethidium bromide. Agarose gel electrophoresis was performed in 1×TBE buffer at 120 V for 1h.

In order to assess *Ebf1* sequence for mutation, all plasmids were sequenced.

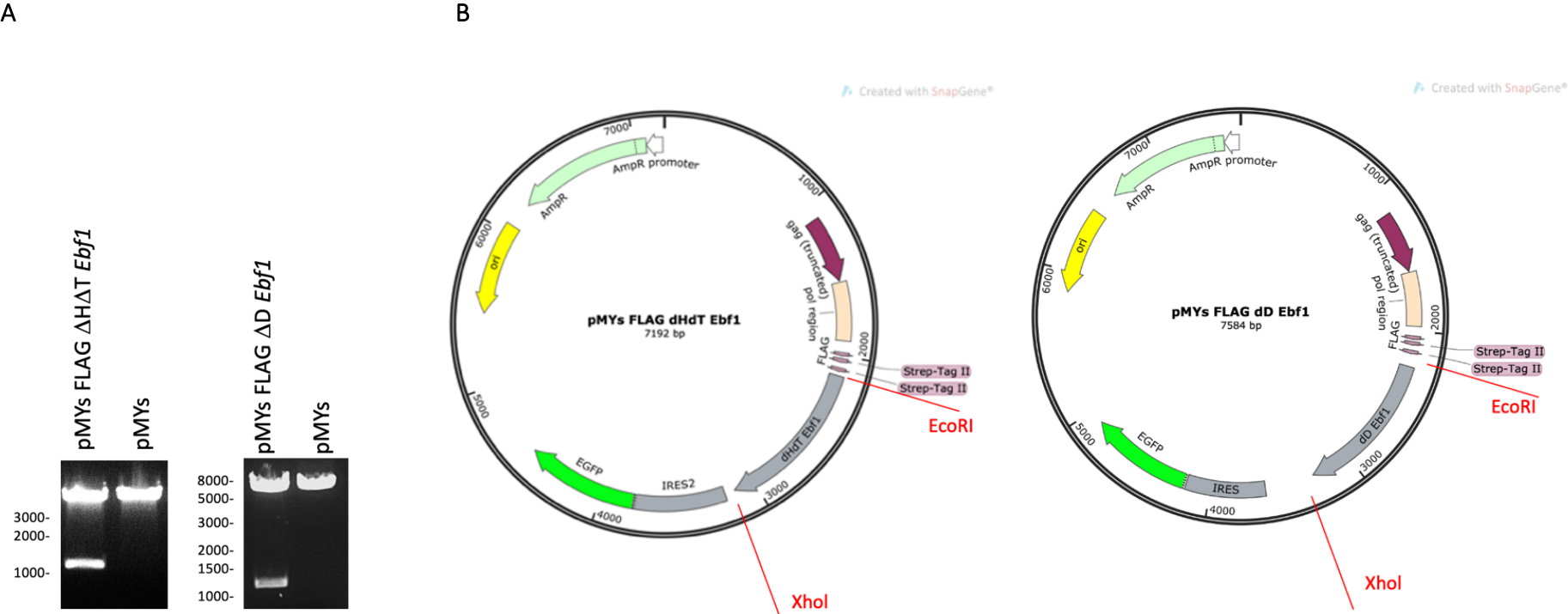
Figure 3-2 Verification of pCR II TOPO ΔHΔT *Ebf1* and pCR II TOPO ΔD *Ebf1* cloning. ΔHΔT *Ebf1* and ΔD *Ebf1* were PCR amplified and ligated into pCR II TOPO vector. PCR product ligation into pCR II TOPO vector was confirmed by enzymatic digest of pCR II TOPO FLAG ΔHΔT *Ebf1* and pCR II TOPO FLAG ΔD *Ebf1* using *EcoRI*. (A) Agarose gel image, where ΔHΔT *Ebf1* and ΔD *Ebf1* fragments are 1094 and 1053bp large. (B) Schematic representation of pCR II TOPO ΔHΔT *Ebf1* and pCR II TOPO ΔD *Ebf1*, where *EcoRI* digestion sites are shown in red.



3.4.4 PCR product recombination from pCR II TOPO vector into retroviral expression vector pMYs IRES GFP

pCR II TOPO FLAG Δ H Δ T *Ebf1* and pCR II TOPO FLAG Δ D *Ebf1* and pMys FLAG *Ebf1* vectors were digested with EcoRI and XhoI (P6161, Promega). 12.5 μ l of H₂O, 1 μ l of EcoRI, 0.5 μ l of XhoI and 2 μ l of the \times 10 Buffer H was added to 4 μ l of 0.25 μ g/ml DNA and incubated at 37°C for 1.5h. DNA digests were separated *via* agarose gel electrophoresis. The linearized pMys FLAG vectors, Δ H Δ T *Ebf1* and FLAG Δ D *Ebf1* inserts were excised of the agarose gel and purified as described above. The concentration of DNA was calculated using the Nano Drop Lite Spectrophotometer (Thermo Scientific). DNA concentration of the vector and insert were taken at the ratio 1:3. 2 μ l \times 10 T4 DNA ligase buffer (#B02026, Biolabs) and 1 μ l ligase T4 (#M0202T, Biolabs) were added to the vector and insert mix. H₂O was added to the total 20 μ l volume and incubated for 2h at RT. Ligate was transformed into DH5 α bacteria and produced and purified as described before. Religation of *Ebf1* inserts into pMys FLAG vector was confirmed by the enzymatic digest of pMYs FLAG Δ H Δ T *Ebf1* pMYs FLAG Δ D *Ebf1* using EcoRI and XhoI (Figure 3-3). As described above. pMYs IRES GFP was used as a control. DNA digests were separated *via* agarose gel electrophoresis, and digest products were visualized and imaged using Gel Doc \times R⁺ with Lab Image Lab Software.

Figure 3-3 Verification of pMYs FLAG Δ H Δ T Ebf1 and pMYs FLAG Δ D Ebf1 cloning. pCR II TOPO FLAG Δ H Δ T Ebf1 and pCR II TOPO FLAG Δ D Ebf1 and pMYs FLAG Ebf1 vectors were digested with EcoRI and XhoI. Δ H Δ T Ebf1 and Δ D Ebf1 fragments were relegated into pMYs vector. Ligation was confirmed by enzymatic digest of pMYs FLAG Δ H Δ T Ebf1 and pMYs FLAG Δ D Ebf1 using EcoRI and XhoI. (A) Agarose gel image, where Δ H Δ T Ebf1 and Δ D Ebf1 fragments are 1088 and 1047bp large. (B) Schematic representation of pCR II TOPO Δ H Δ T Ebf1 and pCR II TOPO Δ D Ebf1, where EcoRI and XhoI digestion site are shown in red.



3.5 *Ebf1* depletion in transformed murine *Ebf1^{fl/fl}RERT^{Cre}::A*-MuLV pro-B cell lines

Cre recombinase under the control of a tamoxifen-inducible promoter by addition of OHT depletes floxed *Ebf1* in *Ebf1^{fl/fl}RERT^{Cre}*. Cre recombinase expression in *Ebf1^{+/+}RERT^{Cre}::A*-MuLV where *Ebf1* gene lacks floxed sites, do not activate *Ebf1* depletion (Györy, Boller et al. 2012). *Ebf1^{fl/fl}RERT^{Cre}::A*-MuLV and *Ebf1^{+/+}RERT^{Cre}::A*-MuLV pro-B cells were split as 1×10^6 cells/ml the day before treatment with 2 μ M OHT. The Day 0 sample was collected prior addition of OHT. Untreated control samples and OHT treated samples were collected every day for four days, and cell cycle phases were assessed *via* Flow cytometry as described below. *Ebf1* gene depletion was verified *via* floxed and cleaved allele PCR gene amplification (Described below). The decrease in EBF1 protein levels was verified using Western blot analysis. Changes in RNA levels were analyzed using RT-qPCR.

3.6 Subcellular fractionation

1×10^9 *Ebf1^{fl/fl}RERT^{Cre}::A*-MuLV pro-B cells were harvested, spun down and washed with PBS. 50 μ l of cells (approx. 2.5×10^7 cells) were collected (total lysate) for analysis. For buffer exchange cells were resuspended in 5 PCV of Buffer A (10mM Hepes (pH 7.6), 1.5mM MgCl₂, 10mM KCl, pH 7.9 with 10M KOH at RT to 100ml and filter sterilize) with addition of 1 μ M dithiothreitol (DTT), 0.2mM Phenylmethylsulphonyl Fluoride (PMSF) (Sc-3597, Santa Cruz, USA) and 1 tablet of PhosSTOP EASY PACK phosphatase inhibitor (Phosphatase cocktail) cocktail inhibitor (04906845001, Roche, Germany) per 10 ml of lysis buffer, vortexed and spun down at 1200 rpm for 7min at 4°C, then resuspended in 2 PCV of hypotonic buffer A and left for 30min to swell. Resuspended cells were disrupted with B-type pestle Dounce homogenizer (Nilsen 2013) 25 times. Cells were then transferred into two microcentrifuge tubes and spun down at 1200 rpm for 10min. The supernatant collected after spin down is a cytoplasmic fraction, the pellet consists of nuclei. 1.1 PCV of Buffer B (0.3M Hepes (pH 7.9), 1.4M KCl, 0.03 M MgCl₂) was added to the cytoplasmic fraction and frozen down at -80°C until further analysis. The nuclei fraction was resuspended in 0.9 PCV of Buffer C (20mM Hepes pH 7.9, 25% glycerol, 0.42 M NaCl, 1.5 mM MgCl₂, 0.2 mM EDTA, , 1mM Sodium metabisulfite) with addition of 1mM DTT, 0.5mM PMSF and 1 tablet Phosphatase inhibitor per 10 ml of lysis buffer. 250 μ l of

resuspended nuclei were collected into a separate microcentrifuge tube (CLS3620, Sigma, UK) for further analysis. The remaining nuclei were disrupted mechanically with B-type pestle Dounce homogenizer 25 times, then transferred into a 5ml beaker and incubated with mixing for 45min at 4°C. After the incubation the mixture was spun down at 14000rpm for 30min at 4°C. The supernatant was considered to be the soluble nuclear extract, while the pellet was considered to be the insoluble chromatin fraction.

The collected cell, nuclei and chromatin were lysed in 3 PCV RIPA buffer (10mM Tris pH 8.0, 1mM EDTA, 1% Triton X-100, 0.1% Sodium deoxycholate, 0.1% SDS, 140mM NaCl) with addition of 1mM PMSF and 1 tablet of Phosphatase inhibitor per 10 ml of lysis buffer. Lysates were sonicated three times at ten amplitude microns for 15s with 15s break in between each sonication using Soniprep 150 MSE (MSE Scientific Instruments, Crawley, UK). Protein concentrations were determined in all collected samples using the Bradford assay (Bradford 1976) and used in further Western Blot analysis. Glyceraldehyde 3-phosphate dehydrogenase (GAPDH) antibody (2118S, Cell Signalling Biotechnology) was used as a cytoplasmic control (Sawasdichai, Chen et al. 2010), Acetyl anti-histone H4 (Lys5) (H4ac) (07-327, Millipore) (Laham-Karam, Lalli et al. 2015) and LAP2 β (611000, BD Biosciences, USA) (Gant, Harris et al. 1999) were used as Chromatin fraction control, and THOC1 (sc514123, Santa Cruz Biotechnology) and RUNX1 (sc365644, Santa Cruz, USA) were used as NM controls (Engelke, Riede et al. 2014).

3.7 NM isolation via *in situ* fractionation

NM protein isolation in *Ebf1^{fl/fl}RERT^{Cre}* pro-B cells was performed using *In situ* fraction as per Sawasdichai *et al.* protocol (Sawasdichai, Chen et al. 2010). Briefly, coverslips were coated with poly-L lysine solution (P4707, Signa-Aldrich) according to manufacturer instruction. 0.7×10^6 *1_3 Ebf1^{fl/fl}RERT^{Cre}::A-MuLV* pro-B cells were seeded on poly-L lysine coated coverslips in a 12 well plate. After 24-hour incubation at 37°C in 5% CO₂ on coverslips, seeded cells were washed once with 1ml cold PBS. Control samples were then prepared for confocal microscopy. The rest samples were treated in order to remove cytoplasmic, loosely and tightly held nuclear proteins and DNA.

Cytoplasmic and loose nuclear proteins were removed by incubating *1_3 Ebf1^{fl/fl}RERT^{Cre}::A-MuLV* pro-B cells in 200µl CSK buffer (10mM PIPES, 300mM Sucrose, 100mM NaCl, 3mM MgCl₂, 1mM EGTA) with addition of 0.1% (v/v) Triton X-100 for 1min on ice. *1_3 Ebf1^{fl/fl}RERT^{Cre}::A-MuLV* pro-B cells were then washed three times with 1ml cold PBS. Tightly held nuclear proteins were removed by incubating *1_3 Ebf1^{fl/fl}RERT^{Cre}::A-MuLV* pro-B cells with 200µl CSK buffer with addition of 0.5% (v/v) Triton X-100 for 20min on ice. *1_3 Ebf1^{fl/fl}RERT^{Cre}::A-MuLV* pro-B cells were then washed three times with 1ml cold PBS. DNA digest was performed by incubating *1_3 Ebf1^{fl/fl}RERT^{Cre}::A-MuLV* pro-B cell in 200µl CSK buffer with addition of 100µg/ml of DNase I (D4263, Sigma, USA) for 30min at 37°C in 5% CO₂, *1_3 pro-B Ebf1^{fl/fl}RERT^{Cre}::A-MuLV* cells were then washed three times with 1ml cold PBS.

In situ fractionated cells were stained, and fractionation was assessed *via* confocal imaging (see Chapter 2.11.2.3)

3.8 Testing the effect of different concentration of HDAC inhibitors alone and in combination with OHT.

1_1 and 1_3 pro-B *Ebf1^{fl/fl}RERT^{Cre}::A*-MuLV cells were split as 1×10^6 cells/ml and seeded as 200 μ l into 96 well plate. Some of the wells were treated with 2 μ M OHT. OHT was diluted in 100% EtOH. In order to confirm that the effects I observe are OHT induced, EtOH was used as a control. After 8h, Droxinostat and RGFP966 were added at different concentrations from 0.02 μ M to 5 μ M to the untreated and OHT treated cells (Table 3-3) 5 μ M DMSO was added to EtOH treated cells. Twenty-four hours after OHT addition cells were spun down and resuspended in RPMI FBS p/s β -m. Droxinostat, RGFP966 and DMSO were added at the same concentration to the same well as before. After two days cells were prepared for flow cytometry analysis.

Table 3-3 Testing the effect of different concentration of HDAC inhibitors alone and in combination with 2 μ M OHT on *Ebf1^{fl/fl}RERT^{Cre}::A*-MuLV pro-B cells. The final concentration of HDAC inhibitors, OHT, EtOH and DMSO in each well, where R – RGFP966 and D – Droxinostat.

Control	D 0.020 μ M	D 0.039 μ M	D 0.078 μ M	D 0.16 μ M	D 0.31 μ M	D. 0.63 μ M	D 1.25 μ M	D 2.5 μ M	D 5 μ M
OHT 2 μ M	D 0.020 μ M OHT 2 μ M	D 0.039 μ M OHT 2 μ M	D 0.078 μ M OHT 2 μ M	D 0.16 μ M OHT 2 μ M	D 0.31 μ M OHT 2 μ M	D 0.63 μ M OHT 2 μ M	D 1.25 μ M OHT 2 μ M	D 2.5 μ M OHT 2 μ M	D 5 μ M OHT 2 μ M
Control	R 0.020 μ M	R 0.039 μ M	R 0.078 μ M	R 0.16 μ M	R 0.31 μ M	R 0.63 μ M	R 1.25 μ M	R 2.5 μ M	R 5 μ M
OHT 2 μ M	R 0.020 μ M OHT 2 μ M	R 0.039 μ M OHT 2 μ M	R 0.078 μ M OHT 2 μ M	R 0.16 μ M OHT 2 μ M	R 0.31 μ M OHT 2 μ M	R 0.63 μ M OHT 2 μ M	R 1.25 μ M OHT 2 μ M	R 2.5 μ M OHT 2 μ M	R 5 μ M OHT 2 μ M
EtOH 2 μ M	EtOH 2 μ M DMSO 5 μ M								

3.8.1 Pro-B cell treatment with HDAC inhibitors and OHT

1_3 and 1_1 *Ebf1^{fl/fl}RERT^{Cre}::A*-MuLV pro-B cells were split as 1×10^6 cells/ml and seeded as 25ml into seven 75cm² flasks. Three flasks were treated with 2 μ M OHT. One flask was treated with 2 μ M EtOH. *Ebf1^{fl/fl}RERT^{Cre}::A*-MuLV pro-B cells were incubated with or without 2 μ M OHT or 2 μ M EtOH for 8h prior HDAC inhibitor addition in order to allow for the initiation of *Ebf1* depletion. Droxinostat or RGFP966 was added as 2.5 μ M to one of the untreated flasks, and one of the OHT treated flask and 2.5 μ M DMSO was added to EtOH treated cells. On the next day after addition of OHT cells were spun down at 1200 rpm for 5min at 4°C and resuspended in RPMI FBS p/s β -m. 2.5 μ M Droxinostat, 2.5 μ M RGFP966 and 2.5 μ M EtOH were added to the same flasks as before. After two days, samples were collected for Western blot analysis and confocal imaging.

3.9 Protein expression and affinity purification

3.9.1 His-tagged CCNA2 expression in BL21 pLysS

pET 21d *CCNA2 His* was transformed into BL21 pLysS. Colonies were inoculated in 50ml LB supplemented with 100 μ g/ml ampicillin and 35 μ g/ml chloramphenicol (C0378, Sigma, Demark) (LB-a/c) at 37°C media O/N. The overnight culture was resuspended in 0.5l LB-a/c and incubated at 37°C. The culture was tested for OD, and when OD reached 0.5-0.6, culture was incubated for 15min at 25°C, then 50 μ M Isopropyl- β -D-thiogalactoside (IPTG) (final concentration 100 μ M) was added and culture was incubated at 30°C for 3h and spun down at 4000rpm at 4°C for 20min in SLC-6000 rotor. The pellet was resuspended in cold Ni-NTA lysis buffer (50mM NaH₂PO₄, 300mM NaCl, 10mM imidazole, 1 mg/ml Lysozyme, 1 tablet cOmplete™, EDTA-free Protease Inhibitor Cocktail (1187358001, Roche) per 10 ml of lysis buffer, pH 8.00) (as 3ml of buffer per gram wet weight), sonicated six times and spun down at 4000rpm for 30min. The supernatant was collected and frozen down till further CCNA2 His purification.

3.9.2 FLAG EBF1 protein expression in 293T cells

293T cells were grown in DMEM FBS p/s. 70-80% confluent 293T cells were split as 1 in 2 and grown for a day prior transfection. 5µg of pMYs WT and mutant FLAG *Ebf1*, pMYs, pMYs FLAG *Hes1* were added to 300µl OPTIMEM (31985-062, Gibco, USA). 10µl of Turbofect transfection reagent (#R0532, Thermo Scientific, Lithuania) were added to the mix and incubated for 20min. After incubation, the transfection mix was added dropwise to the 293T cells. On day four, cells were harvested and lysed with RIPA buffer. Cell lysates were diluted as 1mg/ml in PBS and used fresh for FLAG-EBF1 affinity purification together with CCNA2 His using Ni-NTA resin.

3.9.3 Co-purification of mammalian and bacterial proteins

20µl of FLAG-EBF1 and CCNA2 His lysates were collected for further western blot analysis. 250µl of Super Nickel NTA Affinity Resin (Super-NiNTAA10, Generon) was added to a microcentrifuge tube. Ni-NTA resin was equilibrated by washing twice with 1.5ml H₂O and twice with Wash buffer (50mM NaH₂PO₄, 300mM NaCl, 20mM imidazole, pH 8.00) by spinning for 3min at 3500rpm. 1ml CCNA2 His lysate was incubated together with the equilibrated Ni-NTA resin in an end-over-end rotor at 4°C for 60min. The lysate/Ni-NTA mixture was loaded to a column with a capped bottom. The cap was removed and flow-through was collected in a microcentrifuge tube and saved for further analysis. The column was washed twice with 1ml Ni-NTA Wash buffer. The column was capped, and 1ml of 1mg/ml FLAG-EBF1 lysate was added to the CCNA2 His bound Ni-NTA resin and incubated for 20min at 4°C. The column was washed twice with 1ml PBST (PBS with the addition of 0.05% Tween20). FLAG EBF1 was purified together with CCNA2 His using 200µl Ni-NTA elution buffer (50mM NaH₂PO₄, 300mM NaCl, 250mM imidazole, pH 8.00).

3.10 Protein immunoprecipitation

Protein interactions were verified by their co-immunoprecipitation (Co-IP) using Protein A/G PLUS-agarose (sc-2003, Santa Cruz Biotechnology) and corresponding antibodies (see below).

Immunoglobulin precipitation is seen in the eluted fraction when Protein A/G PLUS-agarose are used for protein Co-IP. For the Mass spec (MS) analysis in order to avoid immunoglobulin detection in the eluted fraction Pierce Co-IP Kit (26149, Thermo Scientific, USA) was used.

3.10.1 Co-IP protocol 1

100µl of Protein A/G PLUS-agarose (sc-2003, Santa Cruz Biotechnology) were washed three times with PBST, resuspended in 1ml 5% milk in TBS and incubated rotating O/N at 4°C. After incubation, beads were washed three times with PBST and resuspended in 75µl of Co-IP buffer. 500µl of 1_4 *Ebf1^{fl/fl}RERT^{Cre}*::A-MuLV pro-B cell lysate was precleared with 20µl of resuspended beads by incubating rotating for 1h at 4°C, then spun down at 300rpm for 3min. 20µl of the precleared sample was saved for future Western blot analysis. 200µl of lysates were put into two microcentrifuge tubes, 4µg of CCND3 mouse monoclonal or EBF1 rabbit polyclonal antibodies were added to one of the lysates, 4µg normal mouse IgG or normal rabbit IgG antibodies were added to the other lysate and incubated O/N at 4°C. 40µl of resuspended beads were added to each of the microcentrifuge tubes containing primary antibody and lysate and incubated for 0.5h at 4°C rotating. Then spun down at 1800rpm for 3min and washed three times with PBST. Proteins were eluted by incubating with 50µl of 0.1M glycine (pH 2.4) for 10min and spinning down at 1800rpm for 3min. The supernatant was collected into a microcentrifuge tube and 50µl of 1M Tris (pH 8.5) was added. The beads were incubated with 50µl X2 SDS loading gel (100mM Tris-HCl pH6.8, 4% (w/v) SDS, 0.2% (w/v) bromophenol blue, 20% glycerol) at 50°C for 10min. Samples were spun down at 1800rpm for 3min. The supernatant was collected into a microcentrifuge tube, 5µl of 1M DTT and 45µl H₂O was added to the eluate. The beads were incubated with 50µl X2 SDS

loading gel and 5µl 1M DTT at 100°C for 10min. 45µl of H₂O was added to the beads. Protein Co-IP was verified *via* gel electrophoresis.

3.10.2 Co-IP protocol 2

200×10⁶ 1_4 *Ebf1^{fl/fl}RERT^{Cre}*::A-MuLV pro-B cells were harvested and lysed with 1.4ml of modified Co-IP buffer, containing 0.1% or 1% NP-40, 0%, 5% or 10% glycerol and 0 or 1µM DTT. 50µl Protein A/G PLUS-agarose were added into two microcentrifuge tubes, washed twice with 200µl PBST and centrifuged at 1800rpm for 3min after each wash. 4µg of CCND3 mouse monoclonal or EBF1 rabbit polyclonal antibodies were added to one of the microcentrifuge tubes, and 4µg normal mouse IgG or normal rabbit IgG control antibodies were added to the other microcentrifuge tube and incubated for 1h at RT, then centrifuged at 1800rpm for 3min. Antibody-linked beads were washed once with PBST and centrifuged at 1800rpm for 3min. 600µl of lysate was added to each microcentrifuge tube and incubated O/N at 4°C. Then spun down at 1800rpm for 3min and washed three times with PBST. Proteins were eluted by incubating with 50µl X2 SDS loading gel at 50°C for 10min and spinning down at 1800rpm for 3min. The supernatant was collected into a microcentrifuge tube, 5µl of 1M DTT and 45µl of H₂O was added to the eluate. The beads were incubated with 50µl X2 SDS loading gel and 5µl 1M DTT at 100°C for 10min. 45µl of H₂O was added to the beads. Protein Co-IP was verified *via* gel electrophoresis.

3.10.3 Protein immunoprecipitation for the MS analysis using Pierce Co-IP Kit

3.10.3.1 Antibody coupling to the resin

50µl of the resin slurry was added to the Pierce Spin Column and centrifuged at 1000g for 1min, flow-through was discarded, and the resin was washed twice by adding 200µl of ×1 Coupling Buffer, the column was centrifuged, and flow-through was discarded. 50µg of EBF1 rabbit polyclonal (AB10523, Millipore, Germany) or CCND3 mouse monoclonal (sc-6283, Santa Cruz Biotechnology), or normal rabbit IgG (2729S, Cell Signalling Biotechnology) or normal mouse IgG (sc-2025, Santa Cruz Biotechnology) antibody was mixed together with ×20 Coupling Buffer and water up to final volume of 200µl, so that

solution consists of ×1 Coupling Buffer. Diluted antibodies in Coupling buffer were added to the column. 3µl of the Sodium Cyanoborohydride Solution was added to the column and incubated on an end-over-end rotor at RT for 120min. The flow-through was discarded, and the column was washed twice with 200µl of ×1 Coupling Buffer and once with 200µl of Quenching Buffer. The column was centrifuged at 1000g for 1min after each wash. 200µl of Quenching Buffer and 3µl of Sodium Cyanoborohydride Solution was added to the column and incubated for 15min with end-over-end mixing, then centrifuged at 1000g for 1min and flow-through was discarded. The resin was washed twice with 200µl of ×1 Coupling Buffer, and six times with 150µl of Wash Solution, centrifuging after each wash at 1000g for 1min.

3.10.3.2 Co-IP for the MS analysis

200×10⁶ – 400×10⁶ 1_1, 1_4 *Ebf1^{fl/fl}RERT^{Cre}*::A-MuLV pro-B and MPI-2 cells were harvested and lysed with 500-1ml Co-IP buffer (150mM NaCl, 50mM Tris-HCl pH7.4, 1% NP-40, 0.25% Sodium Deoxycholate, 1mM EGTA, 10% glycerol) with addition of 1mM PMSF and 1 tablet Phosphatase inhibitor per 10 ml of lysis buffer. 500µl of lysate was added to the column and incubated for 2h at 4°C. The flow-through was discarded. The column was washed three times with 200µl of IP Lysis/Wash Buffer, once with 100µl of ×1 Conditioning Buffer and centrifuged at 1000g for 1min after each wash. For buffer exchange, 10µl of Elution Buffer was added to the column and centrifuged at 1000g for 1min. Proteins were eluted by incubating resin with 50µl of Elution Buffer for 5min at RT three times. CCND3 or EBF1 elution was then assessed *via* acrylamide gel silver staining and/or Western Blot analysis.

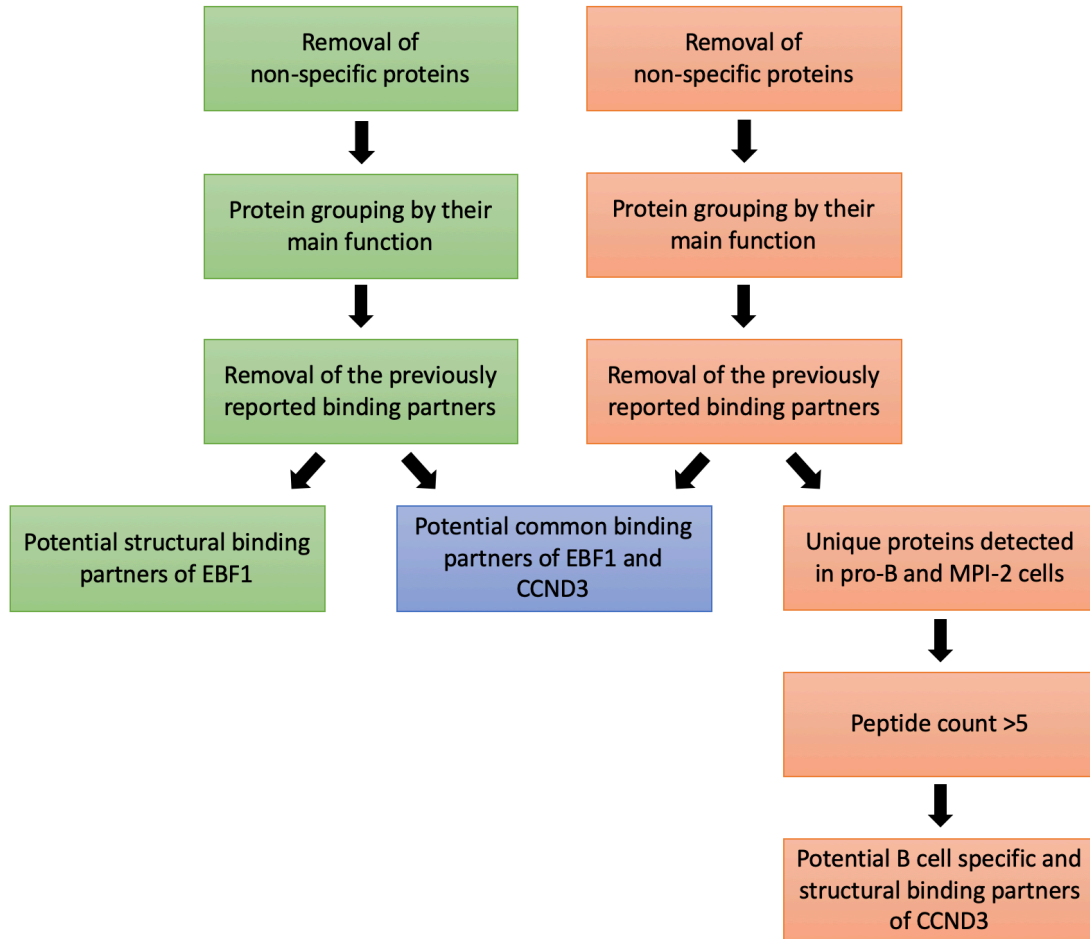
3.10.3.3 Sample preparation for MS and data analysis

The verified eluates were run into 12% acrylamide gel and send to PROTEX (Leicester, UK) for MS analysis. In the PROTEX facility, the gel slices were diced into cubes of 2-4 mm, transferred into a 1.5ml tube and destained three times in Destain solution (50% ethanol and 50mM ammonium bicarbonate (ABC)) for 20min at RT. Then gel was dehydrated in 100% ethanol for 5min in RT and treated with Reduction/alkylation buffer (10mM tris(2-carboxyl)phosphine and 40mM 2-chloroacetamide) for 5min at 70°C. The gel bands were

washed twice with Wash solution (50% ethanol, 50mM ABC) for 20min at RT followed by dehydration with 100% ethanol for 5min at RT. The gel and proteins were digested with 2.5ng/ μ l trypsin for 10min at RT, then 50mM ABC was added, and peptide mix was incubated O/N at 37°C. Peptide extraction buffer (25% Acetonitrile, 5% Formic acid) was added to the O/N solution and sonicated twice in a bath for 5-10min at RT. Then peptides were concentrated in Speed-Vac for 40-50min and volume was brought down to 20 μ l. Peptides were resuspended in 2% CAN and 0.1% Trifluoroacetic acid buffer to the final volume of 50 μ l and analysed with short-gradient LC-MS/MS. The data were searched against protein databases to provide protein identification.

The protein lists were then read *via* Scaffold4 (Proteome software, UK). The non-specific proteins were removed from the provided list of the potential EBF1 and CCND3 binding partners. Protein functions were determined *via* GeneCards Human database (Stelzer G 2016) and UniProt database (UniProt Consortium 2018). Previously reported binding partners of EBF1 and CCND3 were removed from the lists. Common binding partners were determined from the EBF1 and CCND3 potential binding partners lists. In order to determine potential B-cell specific and structural binding partners of CCND3, the binding partners of CCND3 in 1_1 and 1_4 *Ebf1^{fl/fl}RERT^{Cre}::A-MuLV* pro-B cells were compared to binding partners in MPI-2 cells. Then proteins whose peptide count was below five were removed. The ratio of the peptide number of the pulldown prey protein and the bait protein was calculated and used for further analysis. The flow chart of the MS data analysis is presented in Figure 3-4.

Figure 3-4 Flow chart of the MS data analysis identifying potential B-cell unique and structural binding partners of EBF1 and CCND3. Analysis of the EBF1 or CCND3 binding partners is color-coded, respectively, in green and orange, while analysis of potential binding partners of EBF1 and CCND3 is shown in blue.



3.11 Flow cytometry and confocal microscopy

3.11.1 Reagent preparation

3.11.1.1 4% PFA

20g of paraformaldehyde powder (Fisher #04042) were added to 60°C heated up 450 ml of water. Five drops of 2N NaOH (1 drop per 100ml) were added and heated until paraformaldehyde dissolved. 50ml of 10×PBS was added to the solution and pH was adjusted to pH7.2. 4% PFA was aliquoted, stored frozen at -20°C and thawed before use.

3.11.1.2 Hard mounting buffer

21g of Polyvinyl alcohol (Sigma Chemical Cat. #P-8136), 42ml of glycerol and 52ml of H₂O were mixed. Few sodium azide crystals and 106ml of 0.2M Tris pH8.5 were add (Fisher Chemical Cat. #S227-100) to the solution. The solution was mixed at low heat until reagents dissolved. The mixture was clarified by centrifugation at 5000g for 15min.

3.11.2 Sample preparation

3.11.2.1 5-Ethynyl-2'-deoxyuridine (EdU) combining Propidium iodide (PI) staining

150µl of OHT and/or Droxinostat and/or RGFP966 treated and control cells were seeded into 96 round bottom well plate (650185, CellStar). EdU was added as 0.5µM to each well and incubated for 3h at 37°C, then spun down at 350g for 5min, washed once with 150µl cold PBS and spun down at 350g for 5min. 150µl of 4% PFA was added dropwise to the cells and cells were incubated at RT for 10min. After incubation cells were spun down at 350g for 5min and washed three times with 150µl Perm buffer (PBS, 20% FBS, 1% triton X-100), each time plate was spun down at 350g for 5min, flipped and tapped on the filter paper to remove the excess liquid, then gently vortexed. Cells were resuspended in 150µl Perm and incubated for 20min at RT, then spun down at 350g for 5min. Cells were stained with Click-iT EdU Alexa Fluor 488 Imaging Kit (C10337, Invitrogen, USA). EdU staining buffer was prepared by mixing 43µl of Tris buffer, 2µl 100mM CuSO₄ of 0.12µl AF488-azide and 5µl of additive buffer (per well). 50µl of EdU staining buffer was added to each

well and incubated in the darkroom at RT for 30min. EdU staining buffer was removed by washing cells with 150µl Perm buffer three times. Then to each well was added 50µl of 50µg/ml Propidium iodide (PI) in PBS and incubated in the darkroom at RT for 20min. The PI excess was removed by washing cells 150µl Perm buffer three times. Cells were resuspended in 150µl Perm buffer and analysed using flow cytometer. In order to set up compensation matrix for Phycoerythrin (PE) and Fluorescein isothiocyanate (FITC) channels on flow cytometry, one of the control samples was left unstained, one was stained only with EdU, and one was stained only with PI.

3.11.2.2 Nuclear PI staining

1_1 and 1_3 *Ebf1^{fl/fl}RERT^{Cre}::A*-MuLV pro-B cells that were seeded in 96 well plate were spun down at 350g for 5min, then washed once with cold 150µl PBS and spun down at 350g for 5min. Then to each well 50µl of 50µg/ml PI was added and incubated in the darkroom at RT for 20min. Then cells were washed three times with 150µl PBS buffer. Each time plate was spun down at 350g for 5min, flipped and tapped on the filter paper to remove the excess liquid, then gently vortexed. Cells were resuspended in 150µl PBS and analysed using flow cytometer.

3.11.2.3 *In situ* fractionated sample preparation

Both untreated and *in situ* fractionated 1_3 *Ebf1^{fl/fl}RERT^{Cre}::A*-MuLV pro-B cells on coverslips were fixed with 4% PFA for 10min at room temperature (RT), washed three times with 1ml of Perm Buffer, then permeabilized in 1ml Perm Buffer for 20min at RT. For one sample 0.5µg rabbit polyclonal EBF1 or/and mouse monoclonal IgG1 RUNX1 (A-2) (sc365644, Santa Cruz, USA), mouse monoclonal IgG1 LAP2β (611000, BD Biosciences, USA), normal mouse IgG or normal rabbit IgG antibodies were mixed with 100µl Perm Buffer, cells were incubated with the primary antibody diluted in Perm Buffer for 20min at RT. The excess of primary antibodies was washed off three times with 1ml Perm Buffer. Alexa Fluor 488 goat anti-mouse IgG (A11001, Life Technologies, Eugene, USA) or Alexa Fluor 647 goat anti-rabbit IgG (A21244, Life technologies, Eugene, USA) secondary antibodies were diluted as 1 in 200 in Perm Buffer and samples were incubated in 100µl of corresponding diluted secondary antibodies in dark room at RT for 20min. The excess

of secondary antibodies was washed off three times with 1ml of Perm Buffer. Then coverslips were mounted on slides using Hard mounting buffer. Cells were imaged *via* confocal microscope.

3.11.2.4 *Ebf1^{fl/fl}RERT^{Cre}::A*-MuLV Pro-B cell and MPI-2 cell staining

For each sample, 5×10^6 cells were collected, spun down at 1200 rpm for 5min, then washed once with 5ml of cold PBS and spun down at 1200 rpm for 3min. 4% PFA was added dropwise to the cells, gently vortexed and incubated at RT for 10min. After incubation cells were spun down at 2500 rpm for 3min and washed three times with 1ml of Perm buffer, each time spun down at 2500 rpm for 3min. Cells were resuspended in 1ml of Perm and incubated for 20min at RT, then spun down at 2500 rpm for 3min. Cells were resuspended in 100 μ l Perm buffer. To the resuspended cell 0.5 μ g of rabbit polyclonal EBF1, mouse monoclonal CCND3, mouse monoclonal LAP2 β , mouse monoclonal RUNX1, normal mouse IgG or normal rabbit IgG primary antibodies were added and incubated at RT for 20min, then spun down at 2500 rpm for 3min and washed three times with 1ml of Perm buffer, each time spun down at 2500 rpm for 3min. Cells were resuspended in 200 μ l Perm buffer. To the resuspended cell 1 μ l of Alexa Fluor 488 goat anti-mouse IgG or Alexa Fluor 647 goat anti-rabbit IgG were added and incubated in the darkroom at RT for 20min. Then washed three times with 1ml of Perm buffer. Stained cells were cytopspun onto slides, air-dried and stained with 300nM 4',6-diamidino-2-phenylindole (DAPI) in PBS for 5min and washed three times with PBS each time incubating for 5min at RT. 20 μ l of Hard mounting buffer was added on the cells and covered with coverslips. Hard mounting buffer was left to dry out O/N. Cells were imaged with a confocal microscope.

3.11.3 Flow cytometry

Ebf1^{fl/fl}RERT^{Cre}::A-MuLV pro-B cell staining in 96 well plates were analysed using Beckman Coulter Cytoflex. EdU staining was detected *via* the FITC channel, while PI staining was detected *via* the PE channel. Since PE staining can be detected in the FITC channel, the single stained samples with PI and EdU were used to set up a compensation matrix. The compensation matrix was applied for the EdU and PI double-stained samples before flow cytometry analysis. Recorded data were analysed using FlowJo.

All collected events were gated to remove cell cluster and debris, then gated for viable cells. All gated events and the viable cells in the EdU and PI double-stained samples were then gated for G1 and S phases. All gated events in the PI stained samples were gated for PI unstained and Pi stained cells.

3.11.4 Confocal microscopy

Stained cells were imaged using Leica TCS SP5 confocal microscope with HCX PL APO Lambda blue 63.0x1.4D OIL UV lence. 405 Diode was used to excite DAPI and was detected within 415-475nm, Argon laser was used to excite Alexa Fluor 488 and was detected within 495-555nm, HeNe633 laser was used to excite Alexa Fluor 647 and detected within 645-720 nm. 3D images were taken at x2 and x10 magnification. Images were deconvoluted using Hygens Essential using CMLE deconvolution algorithm, 40 maximum iterations. Signal to noise ratio was set at five and the quality threshold at 0.05.

3.11.5 Calculation of cell nuclear blebbing

Nuclear blebbing severity of OHT and/or HDAC inhibitor-treated pro-B cells was assessed from 3D confocal images (>100 cells per each sample) using a scoring system of nuclear blebbing severity: full flower shape - 4, two fissures - 3, one fissure or other cell deformation - 2, normal - 1.

3.12 Sample preparation for Electron microscopy (EM)

1_4 *Ebf1^{fl/fl}RERT^{Cre}::A*-MuLV and C3_4 *Ebf1^{+/+}RERT^{Cre}::A*-MuLV pro-B cells were treated with and without 2 μ M OHT. After two days, cells were resuspended as 1 in 4 in RPMI FBS p/s β -m. the day after resuspension cells were fixed with glutaraldehyde with the addition of 2% of PFA and 0.1M Sodium Cacodylate buffer pH 7.3 for 1h at RT. Fixed cells were sent to EM facility where cells were prepared further and imaged by Straatman-Iwanowska A. Samples were washed three times in 0.1M cacodylate buffer and centrifuged at 800 rpm for 5min. 1_4 *Ebf1^{fl/fl}RERT^{Cre}::A*-MuLV and C3_4 *Ebf1^{+/+}RERT^{Cre}::A*-MuLV pro-B cells were treated with 1% OsO₄ (Agar Scientific, UK), 1.5% potassium ferricyanide in cacodylate buffer for 65h, then washed three times with 0.1M cacodylate buffer and once with H₂O, each times centrifuging at 800 rpm for 5min. The pellet was embedded in 3% agar, cut into small pieces and washed twice H₂O, then kept in 70% EtOH O/N. The agar pieces were then incubated with 90% EtOH for 30min, then with 100% EtOH for 30min, followed with two incubations in 100% analytical EtOH (Sigma Aldrich, UK) for 30min and 25min. Then samples were twice incubated in Propylene oxide (VWR) within 40min. In order to get rid of propylene oxide, samples were incubated in Propylene oxide and Spurr's resin hard mix (Agar Scientific, UK) three times. The ration of Propylene oxide and Spurr's resin and duration were 3:1 (for 1h and 45min), 1:1 (for 80min) and in 1:3 (for 1h 45min). The fresh resin was added to the samples and incubated for 1h and 40min, after reapplying fresh resin samples were incubated for 4h and 40min. Then samples were embedded in fresh resin and polymerised for 16h at 60°C. Samples were sectioned to 70nm thick using a Reichert Ultracut E ultramicrotome, collected onto copper mesh grids and stained with 2% aqueous uranyl acetate for 30min, followed by 5min incubation in lead citrate. Sections were viewed on a JEOL JEM-1400 TEM with an accelerating voltage of 100kV. Digital images were collected with a Megaview III digital camera with iTEM software.

3.13 Genomic DNA PCR

1×10⁶ untreated 1_3 *Ebf1^{f/f}RERT^{Cre}::A*-MuLV pro-B cells and treated with OHT were collected as described and frozen down. The cell pellet was defrosted and resuspended into 500µl Toe buffer (100mM Tris pH 8.0, 200mM NaCl, 5mM EDTA) supplemented with 2.5µM (20mg/ml) proteinase K (25530049, Invitrogen) and incubated at 55-65°C for 1h. After incubation genomic DNA was precipitated by addition of 500µl isopropanol. Samples were spun down at 14000 rpm for 30min at 4°C, and the supernatant was discarded. The DNA was resuspended in 100µl H₂O and incubated at 37°C for 1h. DNA concentration was measured using Nano Drop, and samples were further diluted as 10ng/ml. 1×PCR mix was prepared by adding 3µl of ×10 Paq 5000 DNA polymerase buffer, 1µl of 10µM dNTP, 0.5µM Paq 5000 polymerase and 1µl of 10µM primer mix (Table 3-4) (recipe for one sample). To 2µl DNA 1×PCR mix was added. Floxed and cleaved alleles of genomic DNA was amplified in the PCR cycle. DNA denaturation was initiated at 95°C for 3min, then followed with 35 cycles of denaturation, annealing and extending stages. DNA was denaturised at 95°C for 40s, annealed at 60°C for 45s and extended at 72°C for 3min 20s for 35 cycles. The PCR final extension was performed at 72°C for 4min.

Table 3-4 Primers that were used to test for cleaved and floxed alleles

Name	Forward primer	Reverse primer
Floxed alleles	CAAGCTTTGCCGCACTTC	TCCTGTTCTGTCCGTATCCCT
Cleaved alleles	CCCCCACTTCTTGAGGCCTGTGT TGCTT	CTGGGGGTGGAGGGAGGAAGG AAAAT

6µl of 5×DNA gel loading buffer was added to the 30µl of each PCR product and samples were load on the 1% agarose gel containing 0.2µg/ml ethidium bromide. Agarose gel electrophoresis was performed in 1×TBE buffer at 120 V for 1h.

3.14 RT-qPCR

5×10^6 $Ebf1^{fl/fl}RERT^{Cre}$::A-MuLV pro-B cells were collected after OHT treatment. The pellet was washed with PBS and frozen down. The cell pellet was defroster and resuspended in 1ml cold TRI Reagent (T9424, Sigma, USA) and incubated for 5min at RT, then 200 μ l of chloroform was added, and resuspended pellet was incubated for 3min at RT. Samples were spun down at 12000g for 15min at 4°C. The colourless aqueous top phase was collected and transferred into a new microcentrifuge tube. 500 μ l of isopropanol was added the aqueous phase and incubated at RT for 10min, then spun down at 12000g for 10min at 4°C. The supernatant was discarded and washed with 1ml 75% EtOH and spun down at 7500g for 5min at 4°C. The supernatant was discarded, and pellet was air-dried for 10min. The RNA pellet was solubilized by addition of 30 μ l H₂O and incubation at 65°C for 10min. The RNA concentration was calculated using a Nano Drop. 2 μ g of RNA was diluted in H₂O to final volume 11 μ l. 1 μ l of OligoDT (Sigma Aldrich) was added to the mix and followed by five-minute incubation at 72°C. 4 μ l of M-MLV RT x5 Reaction Buffer (M531A, Promega, USA) and 3 μ l of 10mM dNTPs and 1 μ l of M-MLV Reverse Transcriptase (M170B, Promega, USA) were added to the samples and incubated for 1h at 37°C.

To prepare a standard curve for each set of primers set Day zero control sample cDNA and H₂O were added to 384 well plate at the dilution ratios, 0:2, 2:3, 1:7, 1:3, 1:1, 2:0. All samples were loaded as 1 μ l cDNA and 1 μ l H₂O. To each well 7 μ l of LightCycler 480 SYBER green I Master (04707 516001, Roche, USA) and 1 μ l of *Ebf1* or *Ccnd3* or *Hrpt* primer mix was added (Table 3-5, Figure 10-1, Figure 10-2 and Figure 10-3). Plate was spun down at 1000rpm for 1min prior analysis using Light Cyler 480 Software release 1.5.0 SP3. cDNA was amplified in the PCR cycle. DNA denaturation was initiated at 95°C for 10minutes, then followed with 35 cycles of denaturation, annealing and extending stages. DNA was denaturised at 94°C for 15s, annealed at 66°C for 15s and extended at 72°C for 40s for 35 cycles. The PCR final extension was performed at 72°C for 10minutes.

Table 3-5 Primers used in qRT-PCR amplifying *Ebf1*, *Ccnd3* and housekeeping gene *Hrtp*. Primer annealing sites on the respective gene is shown in Appendix (Figure 10-1, Figure 10-2 and Figure 10-3).

Name	Forward primer	Reverse primer
<i>Ebf1</i> RT-qPCR	TCTACAGCAATGGGATACGGA	GTGTGTGAGCAATACTCGGCA
<i>Ccnd3</i> RT-qPCR	GGCATACTGGATGCTGGAG	CCAGGTAGTTCATAGCCAGAGG
<i>Hrtp</i> RT-qPCR	AGTCCCAGCGTCGTGATTAG	TTTCCAAATCCTCGGCATAATGA

3.15 Western blot analysis

3.15.1 Bradford assay

In order to determine protein concentration in lysates, 10 μ l of 0 μ g/ml, 100 μ g/ml, 200 μ g/ml, 300 μ g/ml, 400 μ g/ml and 500 μ g/ml Bovine Serum Albumin (BSA) (A7906, Sigma, USA) was loaded as a control on to 96 well plate. Lysates were diluted as 1 in 10 and 1 in 20 and loaded as 10 μ l into 96 well plate. 250 μ l of Quick Start Bradford 1 \times Dye Reagent (#500-0205, BioRad, USA) was added to each well and protein concentration was measured using HIDEX software at 595nm. A graph was drawn from the BSA standards, and lysate protein concentration was determined from the graph.

3.15.2 Coomassie Blue staining of acrylamide gel

After gel electrophoresis acrylamide gel was stained in Coomassie blue (50% (v/v) methanol (MeOH), 10% (v/v) acetic acid, 0.05% (w/v) Coomassie Brilliant blue (10233, AnalaR, UK)) O/N. The stain was removed, and the gel was incubated in Destain (7% (v/v) acetic acid, 5% (v/v) MeOH) until most of the gel was transparent. The proteins on the gel were imaged using Gel Doc xR⁺ with Lab Image Lab Software.

3.15.3 Silver staining of acrylamide gel

After gel electrophoresis acrylamide gel was fixed with Fixer Buffer (50% MeOH 12% Acetic acid (HAc), 0.018% Formaldehyde (F8775, Sigma, Germany)), then washed three times with 35% EtOH for 20min. After washing, the gel was sensitised with 0.02% Na₂S₂O₃ for 2min, then washed three times with H₂O for 5min. After washing, the gel was incubated with Staining Buffer (0.2% (w/v) AgNO₃, 0.27% formalin) for 20min, then washed twice with H₂O for 1min. In order to see protein bands gel was incubated in Developer Buffer (6% (w/v) Na₂CO₃, 1.75% formalin, 0.0004% Na₂S₂O₃). As soon as protein bands were developed, the gel was incubated in Stop Buffer (50% MeOH, 12% HAc) for 5min. The proteins on the gel were imaged using Gel Doc xR⁺ with Lab Image Lab Software.

3.15.4 Protein transfer from acrylamide gel to nitrocellulose membrane

Pure nitrocellulose membrane (T71514, Pall Corporation, Mexico) and two pieces of Whatman paper (GB003, Scientific laboratory supplies, UK) per gel were soaked in Transfer Buffer (3.02% (w/v) Tris base, 14.4% (w/v) glycine, 20% MeOH). The transfer was set up as follows: black part of the transfer cassette, a piece of filter paper on the bottom, gel, nitrocellulose membrane, a piece of Whatman paper on the top and closed with the red part of the transfer cassette. Transfer cassette was inserted into the box, and Transfer buffer was poured to cover the cassettes. Protein transfer was performed at 30V O/N. Membranes then were stained for analysis with Curix 60 developer (AGFA, Mortsel, Belgium) or ODYSSEY CLX (Li-COR).

3.15.5 Membrane staining and protein analysis

After transfer, the membrane was washed three times in TBST (20mM tris HCl pH 7.6, 8% (w/v) NaCl, 0.1% Tween20) for 5min. The membrane was blocked in 10ml 5% dried skimmed milk (Marvel, UK) in TBST (Blotto) at RT for 30min. Then the membrane was incubated with primary antibody diluted in Blotto for 2h at RT or O/N at 4°C. Please see Table 3-6 for all the primary antibodies used. The excess of the primary antibodies was removed, washing the membrane three times in TBS-T for 5min. The membrane was incubated in anti-mouse (BS-029G-HRP, Bioss), anti-rat (A10-137P, Bethyl) secondary antibodies diluted as 1 in 1000 or anti-rabbit (A16096, Invitrogen) secondary antibodies diluted as 1 in 10 000 in 10ml 5 % Blotto (for further membrane development with Curix 60 developer) or IRDye 680RB goat anti-rabbit (LiCOR, USA) or IRDye 800CW goat anti-mouse (LiCOR, USA) antibodies diluted as 1 in 1000 in 10ml Odyssey Blocking Buffer (PBS) (927-40000, LiCOR, USA) (for further membrane analysis using at ODYSSEY CLx ((Li-COR) the Near-Infrared Fluorescence Imaging System) at RT for 1h. The excess of the secondary antibodies was removed, washing the membrane three times in TBST for 10min. The membrane incubated with IRDye secondary antibodies was washed once in TBS for 10min prior analysis using ODYSSEY CLx (Li-COR)).

SuperSignal West Pico Plus (Thermo Scientific, USA) stable peroxide solution and Luminal/Enhancer solution were mixed 1:1. The membranes incubated in horseradish peroxide conjugated antibodies were incubated in the 1ml of the prepared mix for 5min. The excess of the mix was drained off. The membrane was wrapped in cling film and taped down into a film cassette. The membrane was exposed for a different time to photographic film (Kodak, Rochester, NY, USA) and developed using AGFA Curix 60 developer.

Table 3-6 Primary Antibody concentration used in Western blot analysis

Primary Antibodies	Species	Dilution	Company
CCNA2	mouse monoclonal IgG _{2a}	1:500	sc-53230, Santa Cruz Biotechnology
CCND3	rat monoclonal	1:500	sc453, Santa Cruz Biotechnology
CCND3	mouse monoclonal	1:500	sc-6283, Santa Cruz Biotechnology
EBF1	rabbit polyclonal	1:1000	AB10523, Millipore, Germany
FLAG M2	mouse monoclonal	1:1000	F3165, Sigma
GAPDH (14C10)	rabbit monoclonal	1:1000	2118S, Cell Signalling Biotechnology
H4ac	rabbit polyclonal	1:500	07-327, Millipore
His	mouse IgG ₁	1:1000	11922416001, Roche
LAP2 β	mouse monoclonal IgG1	1:500	611000, BD Biosciences, USA
PARP	rabbit polyclonal	1:1000	#9542, Cell signalling
RUNX1 (A-2)	mouse monoclonal IgG1	1:500	sc365644, Santa Cruz, USA
THOC1	mouse monoclonal IgG1	1:1000	sc-514123, Santa Cruz Biotechnology

3.16 P-value calculation

P-values were using non-parametric paired, two-tailed t-test using Prism 8 (GraphPad Software, Inc.). P values for the change in protein levels, cell viability, cell percentage in G1 and S phases were calculated between the untreated control sample and OHT treated samples incubated for one to four days. P-values for the change in nuclear blebbing severity were calculated taking each of the experiments for both pro-B cell lines as a separate replicate experiment for the same sample. This was due to I have performed only two separate experiments for each of the pro-B cell lines. In order to assess the significance of the reduction of the cells with normal nuclei and increase in nuclear blebbing upon treatments, t-test was performed to compare untreated control samples with OHT, Droxinostat or RGFP966 and to compare OHT treated samples with samples treated with drug combinations.

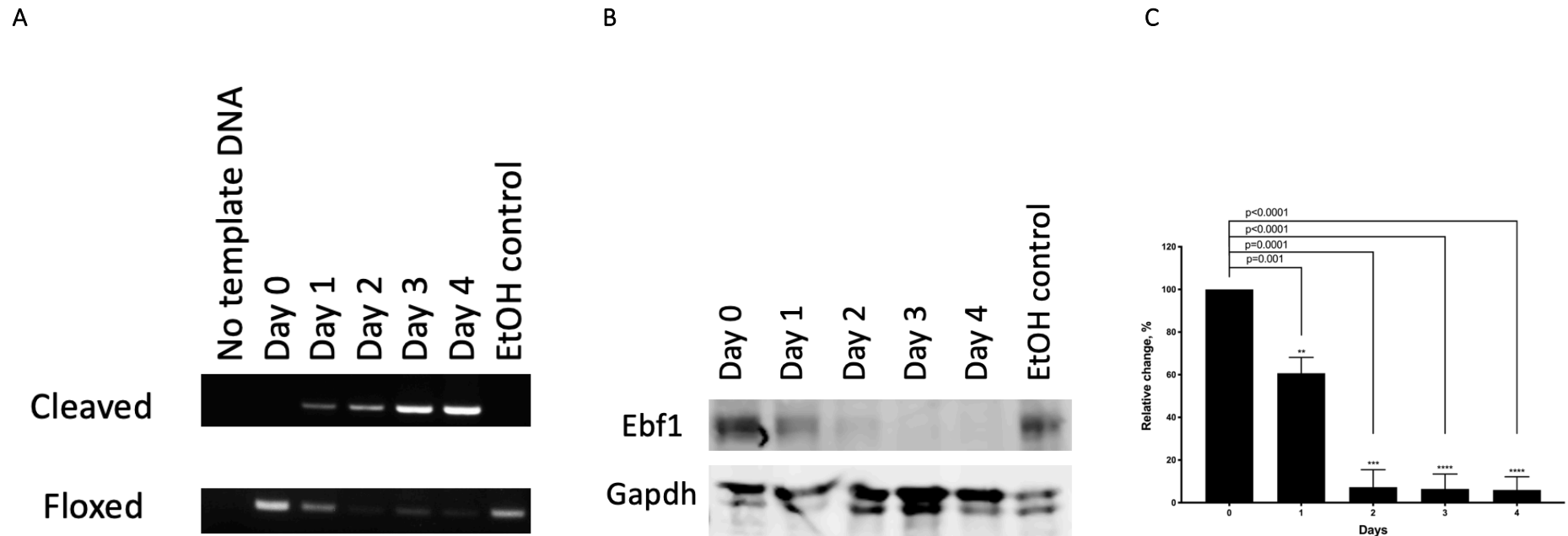
Chapter 4 Effect of acute EBF1 depletion on Abelson transformed mouse pro-B cells

4.1 Acute EBF1 depletion in Abelson transformed mouse pro-B cells results in cell cycle arrest and cell death

Ebf1^{fl/fl}RERT^{Cre} pro-B cells were derived from foetal liver and immortalized with A-MuLV, as described by Treiberg and colleagues. In order to test that EBF1 is depleted in house generated 1_3 *Ebf1^{fl/fl}RERT^{Cre}::A-MuLV* pro-B cells, cells were treated with 2 μ M OHT, EtOH was used as a control. Samples were collected every day for four days for flow cytometry, Western blot, PCR and qRT PCR analysis. *Ebf1* gene depletion was verified *via* gene amplification using primers against floxed and cleaved alleles (Figure 4-1).

The increase in cleaved alleles and decrease in floxed alleles over time was observed, indicating that OHT induced *Ebf1* gene depletion. On day four, a faint band of the PCR amplified floxed alleles was observed, indicating that some cells did not undergo *Ebf1* gene depletion (Figure 4-1 A). Western blot analysis showed that the *Ebf1* gene depletion results in a decrease in EBF1 protein levels (Figure 4-1 B). On day one EBF1 protein levels decreased to 60.7 \pm 7.4% (p=0.01), while on the day two EBF1 levels dropped down to 6.5 \pm 7.0% (p=0.001) (Figure 4-1 C).

Figure 4-1 Verifying OHT induced EBF1 depletion via PCR amplification and Western Blot analysis. 1_3 *Ebf1^{fl/fl}RERT^{Cre}::A*-MuLV pro-B cells were treated with 2 μ M OHT, EtOH was used as a control. Samples were collected every day for four days (A) Genomic DNA was purified from the collected samples. *Ebf1* gene cleavage was verified via PCR amplification of floxed and cleaved alleles. (B) Cells were lysed and proteins were separated via acrylamide gel electrophoresis, then proteins were transferred to nitrocellulose membrane and stained for EBF1 and GAPDH. Representative Western blot image of the change in EBF1 protein levels upon OHT treatment over time using GAPDH as a loading control. (C) Relative change in EBF1 protein levels upon EBF1 depletion over time. EBF1 protein levels were normalized to GAPDH protein levels, where *** - $p < 0.001$, **** - $p < 0.0001$ (n = 4 experiments).



In order to assess the effects of EBF1 depletion on the cell cycle, samples were fixed, permeabilized and stained for EdU and PI before Flow cytometry analysis. No cells were detected in the G2/M phase (Figure 4-2) suggesting that after EdU incorporation during S phase, cells were not able to go through the full cell cycle. This can be improved by incubating cells with EdU longer.

Acute EBF1 depletion resulted in cell death; the percentage of viable 1_3 *Ebf1^{fl/fl}RERT^{Cre}*::A-MuLV pro-B cells decreased from 88.5±7.3% on day zero to 31.0±8.9% (p=0.006) on day four (Figure 4-1 B and C). Similarly, acute EBF1 depletion resulted in G1 cell cycle arrest (Figure 4-2). On day zero 33.3±8.1% viable cells were in G1 and 40.4±7.9% in S phase (Figure 4-3 A). OHT treatment caused an increase in viable G1 phase cells, respectively, to 89.1±4.4% (p=0.02), and a decrease in viable S phase cells, 1.9±1.9% (p=0.008) on day four. An increase in the G1 phase cells and a decrease in the number of dividing cells indicated that OHT did not allow cells to go through G1/S checkpoint (Figure 4-2 and Figure 4-3). Comparing phases of the cells in all detected events (Figure 4-2 (gate C) and Figure 4-3 B) with cell phases of the viable cells (Figure 4-2 (gate B) and Figure 4-3 A), it was observed that the dead cells are accumulated in the G1 phase. This suggests that prolonged arrest in G1 phase leads to an increase in cell death.

Figure 4-2 EBF1 depletion causes 1_3 *Ebf1^{f/f}*RERT^{Cre}::A-MuLV pro-B cells arrest in the G1 phase. Representative flow cytometry images of 1_3 *Ebf1^{f/f}*RERT^{Cre}::A-MuLV pro-B cells upon EBF1 depletion over time, where collected events are gated for single cells (gate A), viable and healthy cells (gate B) and all events (gate C). The percentage of cells in the S and G1 phase for B gated and C gated cells is, respectively, shown in blue and red. Cells were treated with 2 μ M OHT; and collected every day for four consecutive days. 0.5 μ M EdU was added 3hours prior sample collection in order to allow for its incorporation into newly synthesized DNA. After sample collection, harvested cells were washed in PBS and fixed in 4% PFA, then cells were permeabilized using Perm buffer. Incorporated EdU was stained with Click-iT EdU Alexa Fluor 488. In order to separate cells by their DNA content cells were stained with PI and samples were analysed using flow cytometer. Alexa Fluor 488 is detected in FITC channel (EdU FITC), while PI in PE channel (PI PE).

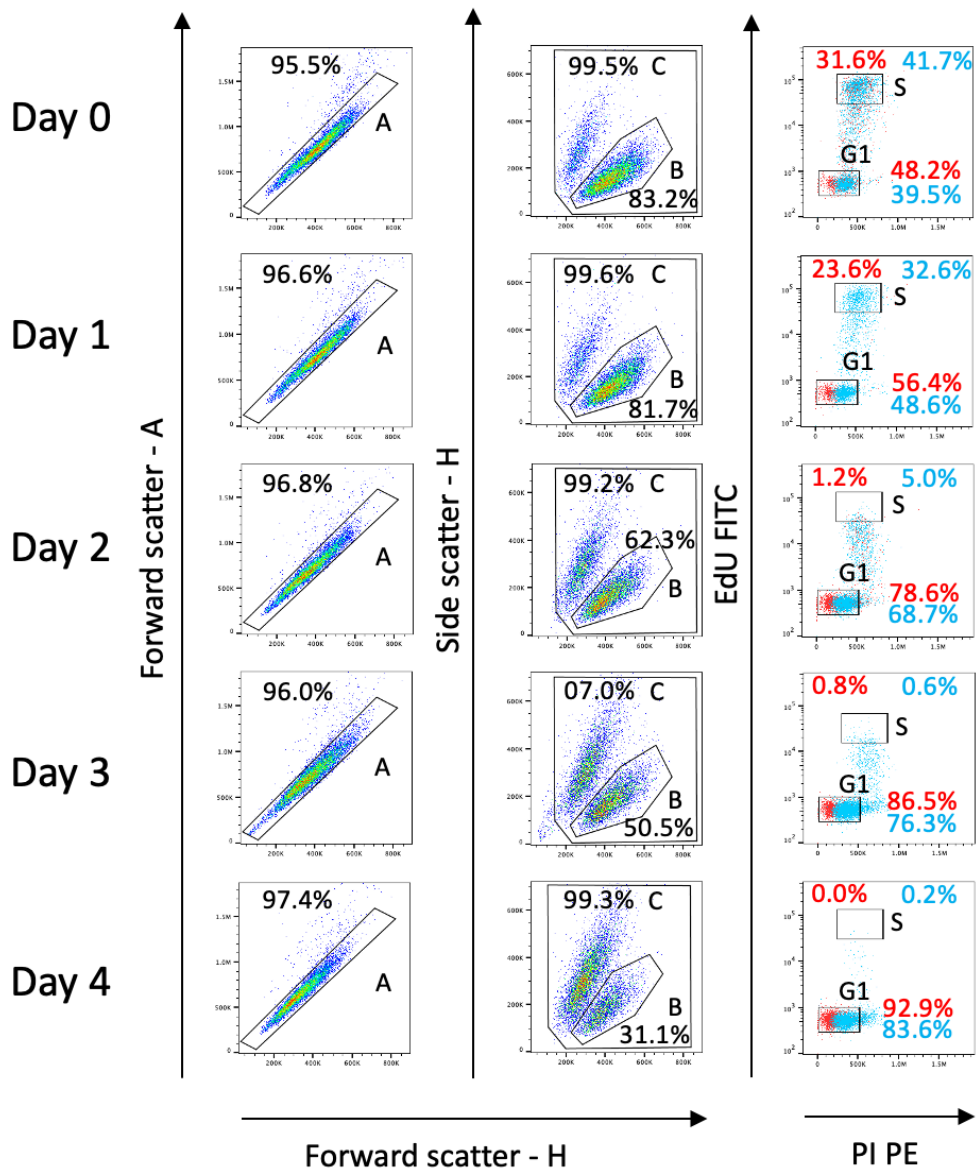
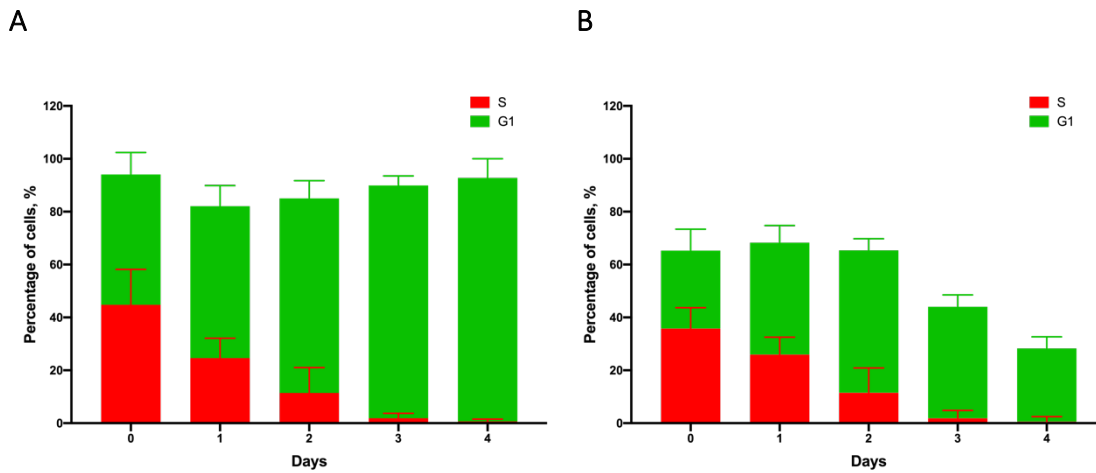


Figure 4-3 The change in cell viability and percentage of 1_3 *Ebf1^{fl/fl}RERT^{Cre}::A-MuLV pro-B* cells in G1 and S phase upon OHT treatment over time. Cells were treated with 2 μ M OHT; and collected every day for four consecutive days. 0.5 μ M EdU was added 3hours prior sample collection in order to allow for its incorporation into newly synthesized DNA. After sample collection, harvested cells were washed in PBS and fixed in 4% PFA, then cells were permeabilized using Perm buffer. Incorporated EdU was stained with Click-iT EdU Alexa Fluor 488. In order to separate cells by their DNA contain cells were stained with PI and samples were analysed using flow cytometer. Alexa Fluor 488 is detected in FITC channel (EdU FITC), while PI in PE channel (PI PE). G1 and S distribution in (A) all detected events and (B) healthy and viable cells, where percentage of cell in S phase is shown in red and in G1 phase in green. ns – not significant, * - $p < 0.05$, ** - $p < 0.01$ (n = 4 experiments).



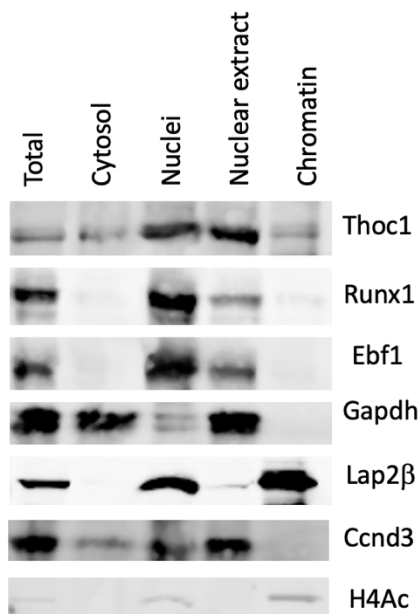
4.2 EBF1 depletion in pro-B cells results in rapid CCND3 degradation

CCND3/CDK4 or CCND3/CDK6 complexes regulate the progression from the G1 phase to the S phase. CCND3/CDK4 and CCND3/CDK6 complexes phosphorylate RB, thus inactivating RB and causing progression from G1 to S phase. An inability of EBF1 depleted pro-B cells to progress from G1 phase to S might be caused by the decrease in CCND3, CDK4 or/and CDK6. Since it was previously seen in our lab that EBF1 binds to CCND3, but not CDK4 (Dr Shiqiu Xiong/Ildiko Györy unpublished observations) and fraction of CCND3 in pro-B cells is localized on the NM (Karki, Kennedy et al. 2018), I hypothesized that CCND3 might interact with EBF1 at the NM.

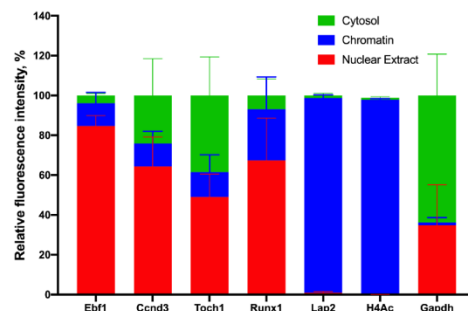
The distribution of EBF1 and CCND3 was assessed *via* 1_3 *Ebf1^{fl/fl}RERT^{Cre}::A-MuLV* pro-B cells subcellular fractionation (Figure 4-4) and confocal imaging (Figure 4-5). Protein fractions were analysed *via* Western blot analysis. GAPDH was used as a cytoplasmic control, while H4ac was used as chromatin fraction control, and THOC1 and RUNX1 were used as NM controls. During cell disruption, the broken cell walls stick to the nuclei and thus can cause some cytoplasmic protein contamination in the nuclear fraction. Western blot analysis showed that GAPDH is present in cytoplasmic fraction and nuclear extract fraction, but was not detected in nuclei (Figure 4-4). The presence of GAPDH in nuclear extract fraction might be due to the contamination from cell walls. LAP2 β is an integral NM protein that binds chromatin (Gant, Harris et al. 1999), and as it was expected to be detected in the nuclei and chromatin fraction. H4ac as well was detected in the nuclei and chromatin fraction, indicating that there was a good separation between the fractions (Figure 4-4).

Figure 4-4 Subcellular localization of CCND3 and EBF1 in 1_3 *Ebf1^{fl/fl}RERT^{Cre}*::A-MuLV pro-B cells.** Cells were harvested and washed with PBS. Total lysate sample was collected prior subcellular fractionation (Total). Then cells were resuspended in hypotonic buffer A and cell walls were disrupted mechanically. The mixture was spun down and supernatant was collected into a new microcentrifuge tube and resuspended in Buffer B (Cytosol). The nuclei fraction was resuspended in Buffer C (Nuclei) and were disrupted mechanically. The homogenized nuclei were spun down and the supernatant (Nuclear extract) and the pellet (Chromatin) were collected. The “Total”, “Nuclei” and “Chromatin” samples were lysed in RIPA buffer and proteins in all collected samples were separated via acrylamide gel electrophoresis. Then proteins were transferred to nitrocellulose membrane and stained for EBF1 and CCND3. GAPDH was used as a cytoplasmic control, H4ac and LAP2 β were used as chromatin fraction control, and THOC1 and RUNX1 were used as NM controls. (A) Representative Western blot image of the subcellular fractionation of 1_3 *Ebf1^{fl/fl}**RERT^{Cre}*::A-MuLV pro-B cells. (B) Fluorescence intensity of the bands was measured and average intensity was calculated for each of the protein in each fraction, where protein levels in the Nuclear Extract is represented in red, in the Chromatin in Blue and in the Cytosol in Green, Protein levels in the Nuclei is the combination of the protein levels in the Nuclear extract and Chromatin, while Total levels are combination of the protein levels in the all three presented fractions (n=3 experiments).

A



B



THOC1 and RUNX1 have been reported as NM proteins (Engelke, Riede et al. 2014). The majority of THOC1 and RUNX1, respectively, about 49% and 67% were detected in nuclear extract fraction (Figure 4-4). About 25% of RUNX1 protein were found in the

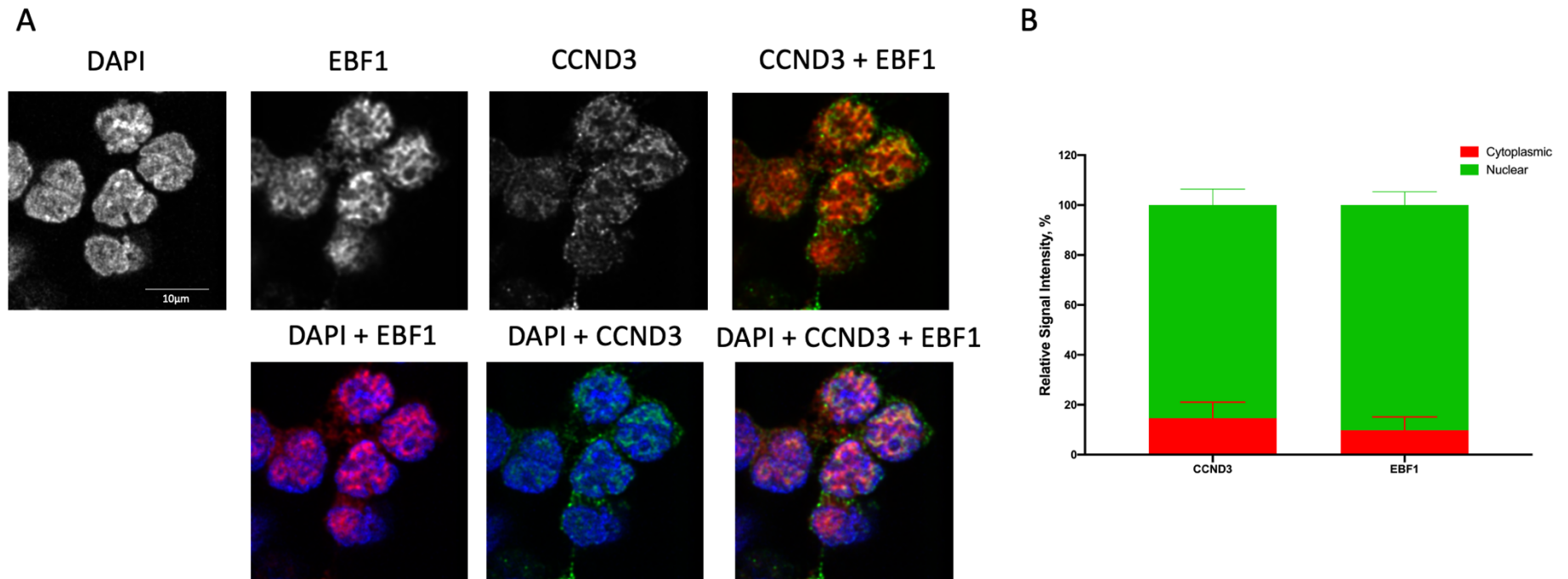
chromatin fraction, which is not surprising as RUNX1 is a transcriptional factor, while 39% of THOC1 were detected in cytosol fraction (Figure 4-4). Although THOC1 is reported to be nuclear, its localization in the cytosol was previously shown in U2 lymphocytes (Thul, Akesson et al. 2017). Thus, THOC1 presence in the cytosol might be lymphocyte-specific. It is expected to see NM proteins mostly in the nuclei and nuclear extract, and partially or not at all in the chromatin fraction. However, the presence in these fractions and absence in the chromatin fraction does not mean that protein is a NM structural protein.

EBF1 and CCND3 were predominantly detected in the nuclear extract, respectively, 84.7% and 64.3%. About 11% of both CCND3 and EBF1 were detected in the chromatin fraction. This was expected as EBF1 and CCND3 transcriptional activity was previously reported (Liu, Sun et al. 2004, Radulovich, Pham et al. 2010, Athar and Parnaik 2015, Pauklin, Madrigal et al. 2016). 25% of the CCND3 was detected in the cytoplasmic fraction (Figure 4-4 B).

Confocal images were taken at X10 magnification in order to get a general view of the distribution of the CCND3 and EBF1 in the cell population (Figure 4-5 A). CCND3 and EBF1 has been seen to colocalise in the nucleus (Figure 4-5) suggesting potential CCND3 and EBF1 interaction.

Total signal intensity for CCND3 and EBF1 was measure in cytoplasm and nuclei and plotted in the Figure 4-5 B. About 85% of total CCND3 and 90% of total EBF1 are localized in the nuclei (Figure 4-5 B), EBF1 amount seen in the nuclei is consistent with the Western blot analysis of subcellular fractionated samples (Figure 4-4 A and B), while via calculation from confocal imaging there is about 10% more nuclear CCND3 than it was calculated from WB.

Figure 4-5 CCND3 and EBF1 localization in 1_3 *Ebf1^{fl/fl}RERT^{Cre}::A*-MuLV pro-B cells via confocal imaging. Cells were collected, washed with PBS, fixed in 4% PFA, then permeabilized using Perm buffer. Cells were incubated with primary EBF1 and CCND3 antibodies, followed by incubation with secondary Alexa Fluor 488 or Alexa Fluor 647 antibodies. Stained cells were cytospun onto slides, air-dried and DNA was stained with 300nM DAPI. (A) Confocal images of 1_3 *Ebf1^{fl/fl}RERT^{Cre}::A*-MuLV pro-B cells stained for EBF1 (red), CCND3 (green) and DAPI (blue). (B) Fluorescence intensity of the CCND3 and EBF1 in the nuclei and whole cell was measured. Average total intensity of the EBF1 and CCND3 in the nuclei and Cytoplasm represents their protein level distribution between these two compartments. (from 50 cells; n = 3 experiments, ×10 magnification).

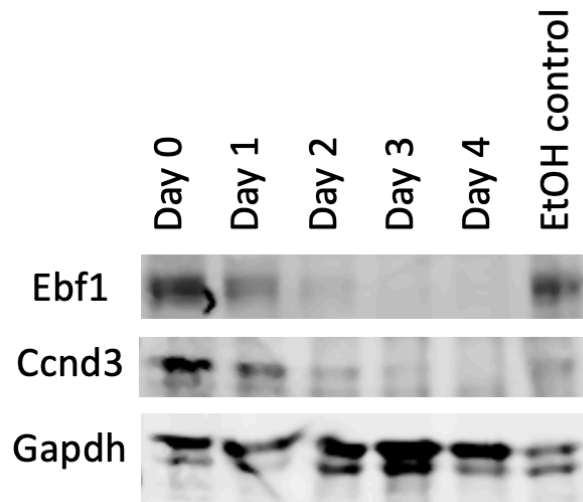


In order to assess the change in CCND3 protein levels upon EBF1 depletion, immunoblot (Figure 4-6) and confocal analyses were performed (Figure 4-7). *Via* Western blot analysis a $65\pm 24.9\%$ decrease in CCND3 protein levels was observed upon EBF1 depletion on the day three (Figure 4-6 A and B). Calculating the change in the fluorescence intensity of the CCND3 from Confocal imaging $40.0\pm 5.16\%$ decrease in total CCND3 protein levels was observed (Figure 4-8).

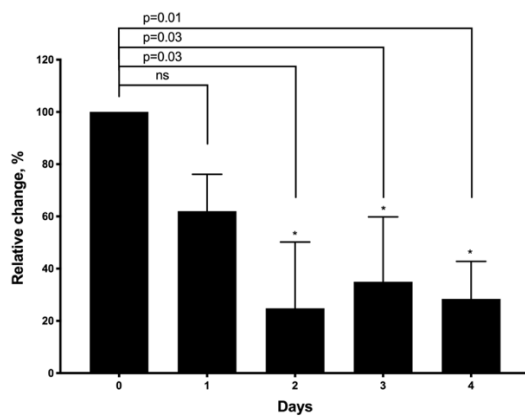
CCND3 is subjected to proteasomal degradation (Cooper, Sawai et al. 2006, Powers, Mandal et al. 2012). Thus, it might be that by binding to CCND3, EBF1 protects CCND3 from degradation. However, EBF1 is a transcriptional factor, and the decrease in CCND3 levels might be because EBF1 is involved in *Ccnd3* gene transcription (Song, Cooperman et al. 2004), causing the decrease in the *Ccnd3* RNA levels and subsequent CCND3 protein levels. In order to test this, RNA was purified from OHT treated and untreated samples, reverse transcribed into cDNA and levels of *Ccnd3* mRNA assessed by RT-qPCR amplification of cDNA. No substantial change in the *Ccnd3* RNA levels was observed upon OHT treatment for four days (Figure 4-6 C), which is consistent with the reported observation in bone marrow transformed primary pro-B cells (Györy, Boller et al. 2012).

Figure 4-6 EBF1 depletion causes a substantial decrease in CCND3 protein levels, but not in *Ccnd3* RNA levels. 1_3 *Ebf1*^{fl/fl}*RERT*^{Cre}::A-MuLV pro-B cells were treated with 2 μ M OHT, EtOH was used as a control. Samples were collected every day for four days (A) Cells were lysed and proteins were separated via acrylamide gel electrophoresis, then proteins were transferred to nitrocellulose membrane and stained for EBF1, CCND3 and GAPDH. Representative Western blot image of the change in CCND3 protein levels upon OHT treatment over time using GAPDH as a loading control. (B) Relative change in CCND3 protein levels upon EBF1 depletion over time. CCND3 protein levels were normalized to GAPDH protein levels, where ns – not significant, * - p<0.05. (C) The change in Ct value of *Ccnd3* upon EBF1 depletion over time. *Ccnd3* Ct values were normalized to *Hrtp* Ct value (n = 4 experiments).

A



B



C

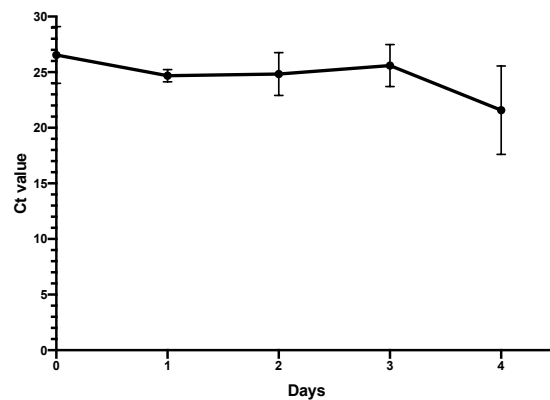


Figure 4-7 EBF1 Depletion causes a decrease in CCND3 protein levels. 1_1 and 1_3 *Ebf1^{fl/fl}RERT^{Cre}::A*-MuLV pro-B cells were treated with 2μM OHT and samples were collected on the third day, washed with PBS, fixed in 4% PFA, then permeabilized using Perm buffer. Cells were incubated with primary CCND3 antibodies, followed by incubation with secondary Alexa Fluor 488. Stained cells were cytospun onto slides, air-dried and DNA was stained with DAPI. (A) Representative confocal images of 1_1 and 1_3 *Ebf1^{fl/fl}RERT^{Cre}::A*-MuLV pro-B cells stained for CCND3 (green) and DNA (blue)

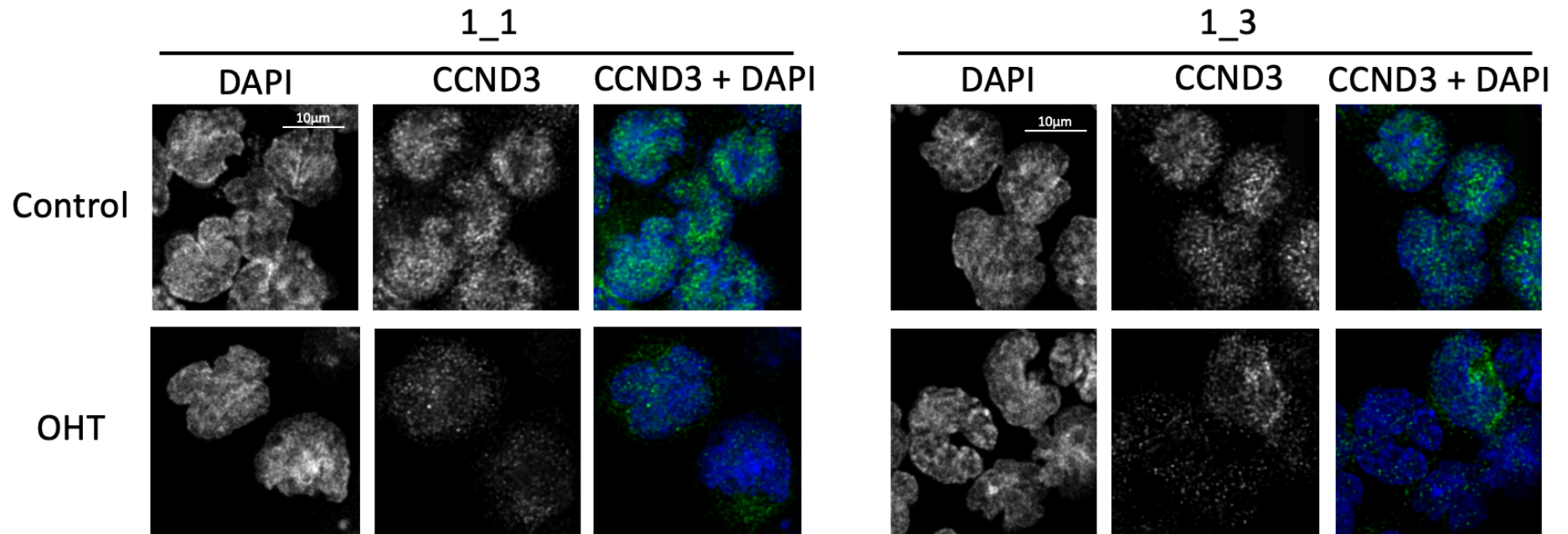
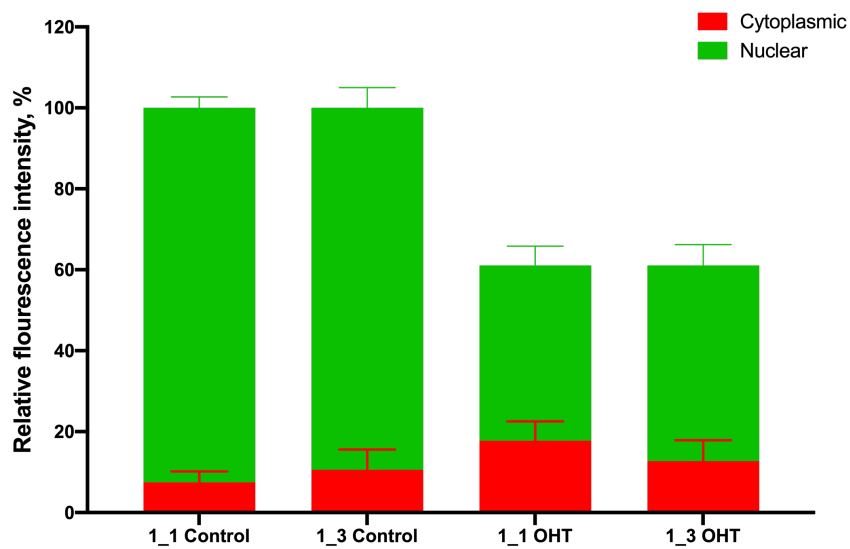


Figure 4-8 Depletion causes a decrease in CCND3 protein levels. 1_1 and 1_3 *Ebf1^{fl/fl}RERT^{Cre}*:A-MuLV pro-B cells were treated with 2 μ M OHT and samples were collected on the third day, washed with PBS, fixed in 4% PFA, then permeabilized using Perm buffer. Cells were incubated with primary CCND3 antibodies, followed by incubation with secondary Alexa Fluor 488. Stained cells were cytopspun onto slides, air-dried and DNA was stained with DAPI. Fluorescence intensity of the CCND3 in the nuclei and whole cell was measured. Average total intensity of CCND3 in the nuclei and cytoplasm represents CCND3 protein level distribution between these two compartments before and after EBF1 depletion (from 25 cells; n = 4 experiments, $\times 10$ magnification)



4.3 EBF1 is a potential NM structural protein in pro-B cells

A part of CCND3 is located in the NM of pro-B cells, CCND3 detachment from NM led to CCND3 degradation and pro-B cell maturation into pre-B cells (Powers, Mandal et al. 2012). EBF1 depletion in pro-B cells resulted in the rapid CCND3 degradation. However, no change in CCND3 RNA levels was observed upon Ebf1 depletion. Thus, the decrease in CCND3 levels might be caused by impaired translation or decreased stability of CCND3. It was hypothesized that EBF1 depletion may cause CCND3 detachment from NM and consequent CCND3 degradation. Thus, here I tested whether EBF1 is a NM protein.

Ebf1^{fl/fl}RERT^{Cre}::A-MuLV 1_1, 1_3 and 1_4 pro-B cells were treated with 2 μ M OHT. Due to the majority of EBF1 is depleted in two to four days after OHT addition in *Ebf1^{fl/fl}RERT^{Cre}* and *Ebf1^{fl/fl}RERT^{Cre}::A-MuLV* (Györy, Boller et al. 2012), cells were harvested after three days. LAP2 β is an integral membrane protein which binds to chromatin (Gant, Harris et al. 1999). In order to test for pro-B cell nuclear blebbing upon EBF1 depletion *Ebf1^{fl/fl}RERT^{Cre}::A-MuLV 1_1 and 1_3* pro-B cells were stained for Lap2 β and DAPI. Images were taken *via* confocal microscope at $\times 10$ magnification in order to assess the percentage of cells with deformed nuclei.

In confocal images stained with LAP2 β , OHT-dependent EBF1 depletion caused nuclear blebbing in 1_1 and 1_3 *Ebf1^{fl/fl}RERT^{Cre}::A-MuLV* pro-B cells after three days (Figure 4-9). Nuclear blebbing severity was assessed from 3D confocal images using a scoring system: full flower shape - 4, two fissures -3, one fissure or another cell deformation - 2, normal - 1 (Figure 4-10). In 77-86% of control and EtOH treated 1_1 and 1_3 *Ebf1^{fl/fl}RERT^{Cre}::A-MuLV* pro-B cells the shape of the nuclear membrane is close to round or oval shape (score 1 or 2). 14-23% of control and EtOH treated 1_1 and 1_3 *Ebf1^{fl/fl}RERT^{Cre}::A-MuLV* pro-B cells display higher nuclear blebbing - a few parts of the nuclear membrane were brought closer to the center of the nuclei forming a more deformed shape nuclei (score 3) or flower-like structure (score 4). Cells with the score 3 and 4 seen in the control and EtOH sample might be apoptotic as via flow cytometry analysis there is always detected population of apoptotic cells.

Due to each of the cell lines treatment and confocal imaging was performed only twice, the p values were calculated taking each of the experiments for both pro-B cell lines as a separate replicate experiment for the same sample. OHT treatment caused a 24-35% ($p=0.009$) decrease in the percentage of nuclei with normal shape pro-B cells (score 1 and 2) and 11-20% ($p=0.006$) increase in the number of moderate and major deformations (score 3 and 4), indicating that OHT treated cells have a collapsed nucleus (Figure 4-10).

Control 1_3 *Ebf1^{fl/fl}RERT^{Cre}::A*-MuLV pro-B cells have a greater number of cells with some minor nuclear deformations compared to 1_1 *Ebf1^{fl/fl}RERT^{Cre}::A*-MuLV pro-B cell, respectively, $9.8\pm 0.5\%$ and $6.2\pm 1.5\%$. As well in 1_3 *Ebf1^{fl/fl}RERT^{Cre}::A*-MuLV pro-B cells was observed almost twice higher number of cell with high nuclear blebbing upon EBF1 depletion compared to 1_1 *Ebf1^{fl/fl}RERT^{Cre}::A*-MuLV pro-B cell, respectively, $24.6\pm 2.2\%$ and $14.0\pm 2.0\%$ (Figure 4-10). This suggests that the cells with the initially deformed nuclei might be more prone to nuclear blebbing upon EBF1 depletion.

More than 90% of EBF1 protein was depleted after three days (Figure 4-1), while major nuclear deformation were observed in about 25-35% of OHT treated cells (Figure 4-10), indicating that nuclear blebbing occurs with a delay upon EBF1 depletion. Thus, EBF1 depletion might indirectly affect nuclear blebbing. Moreover, five days after Ebf1 depletion in pro-B *Ebf1^{fl/fl}RERT^{Cre}::A*-MuLV a change in expression of genes involved in BCR signalling, proliferation, survival, differentiation at multiple cell stages was observed (Györy, Boller et al. 2012). While, no specific gene expression pattern was detected upon EBF1 depletion in 1_1 and 1_3 *Ebf1^{fl/fl}RERT^{Cre}::A*-MuLV at early time point, (Ildiko Györy unpublished observations), suggesting that change in gene expression is a consequence not a cause of pro-B cell nuclear blebbing upon EBF1 depletion.

Figure 4-9 EBF1 depletion in *Ebf1^{fl/fl}RERTCre::A*-MuLV pro-B cells causes nuclear blebbing. 1_1 and 1_3 *Ebf1^{fl/fl}RERTCre::A*-MuLV pro-B cells were treated with 2μM OHT, EtOH was used as a control. Samples were collected on the third day, washed with PBS, fixed in 4% PFA, then permeabilized using Perm buffer. Cells were incubated with primary Lap2β antibodies, followed by incubation with secondary Alexa Fluor 488. Stained cells were cyospun onto slides, air-dried and DNA was stained with DAPI. Representative confocal images of 1_1 and 1_3 *Ebf1^{fl/fl}RERTCre::A*-MuLV pro-B cells stained for Lap2β (green) and DNA (blue). Representative cells with the nuclear blebbing severity: full flower shape - 4, two fissures -3, one fissure or another cell deformation - 2, normal – 1, are shown with the red arrows and corresponding number.

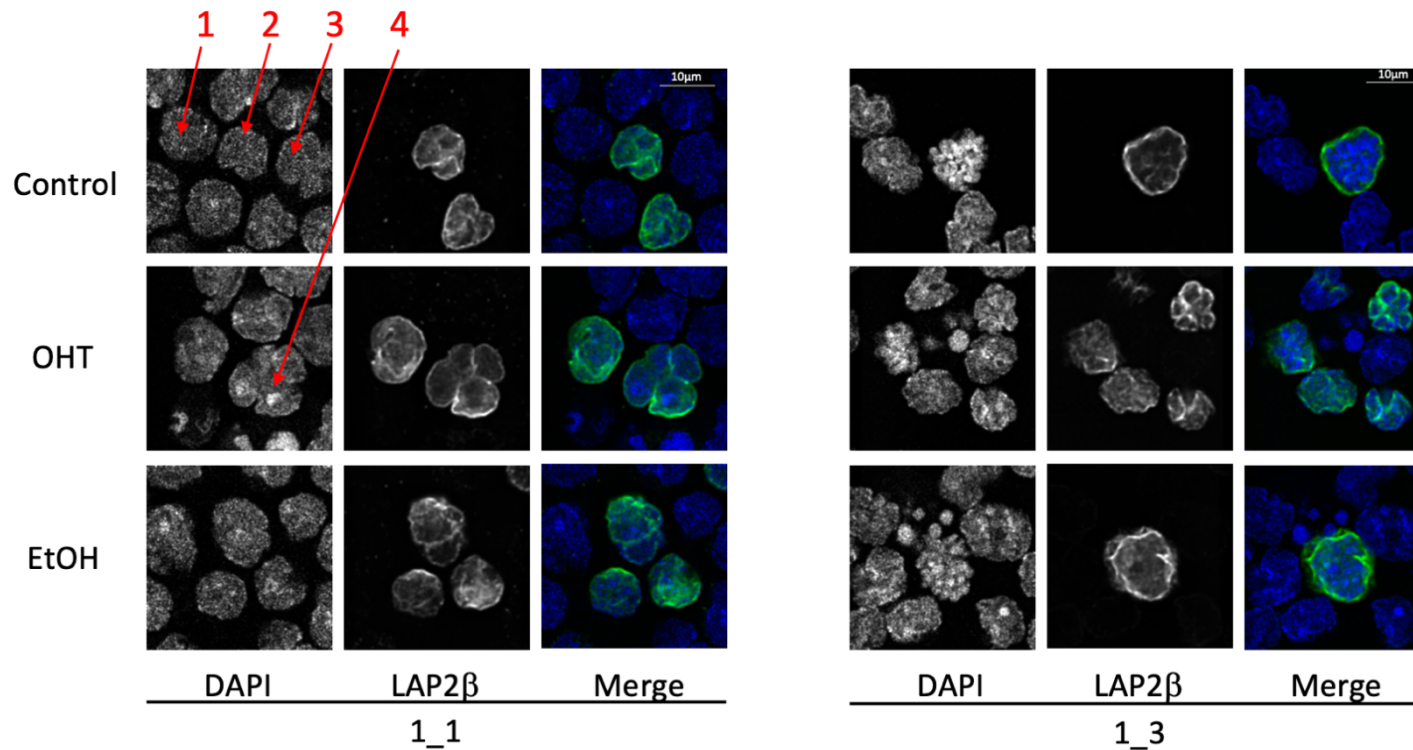
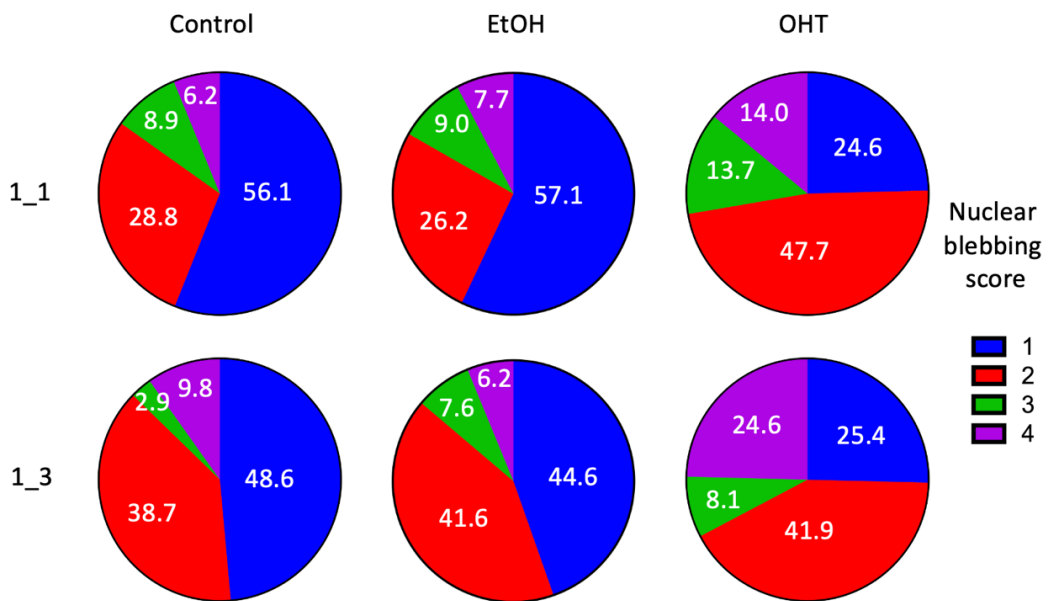


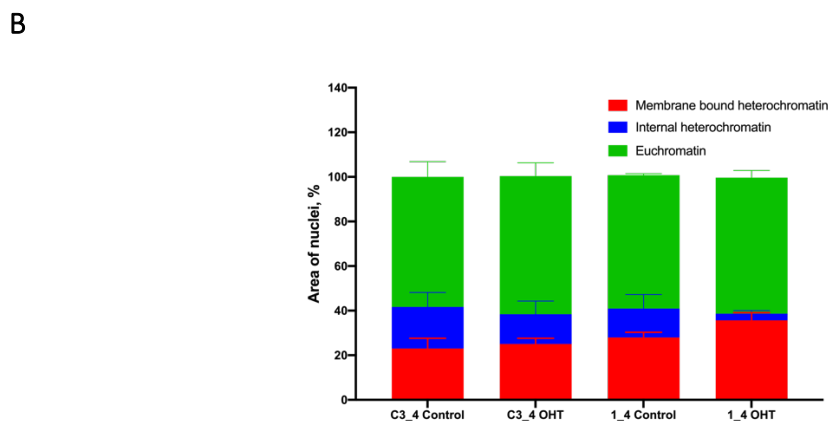
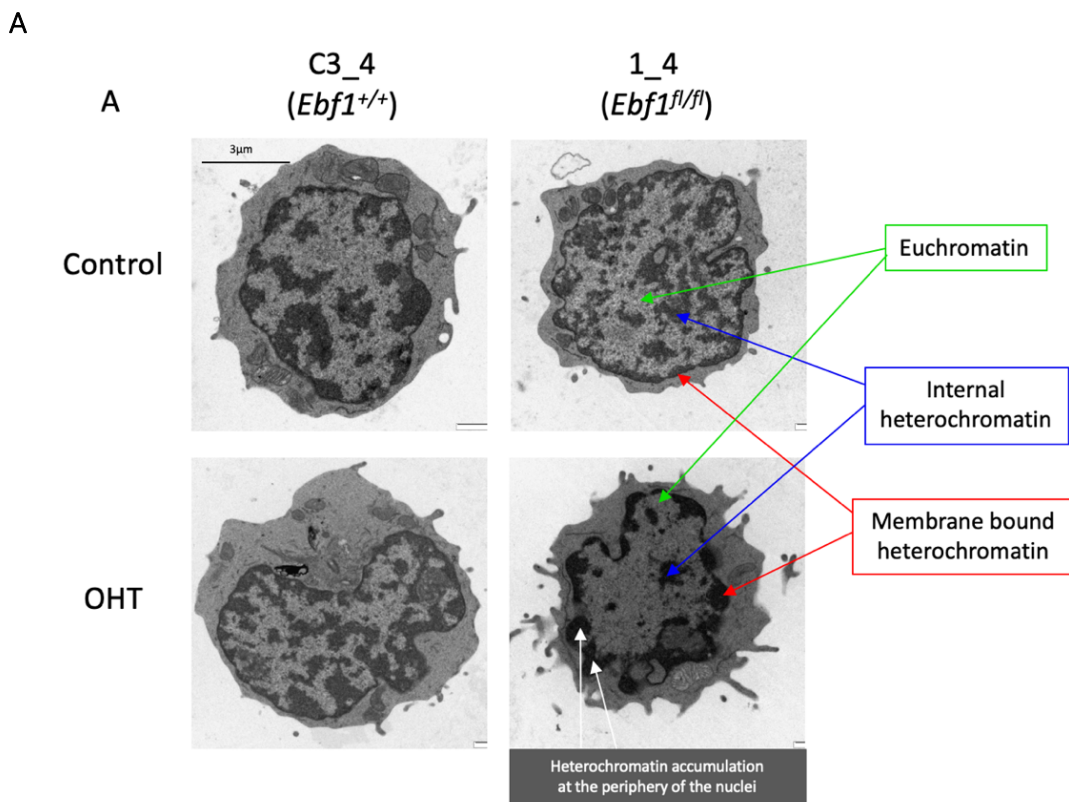
Figure 4-10 Assessment of nuclear blebbing upon OHT-induced EBF1 depletion. 1_1 and 1_3 *Ebf1^{fl/fl}RERT^{Cre}*::A-MuLV pro-B cells were treated with 2 μ M OHT, EtOH was used as a control. Samples were collected on the third day, washed with PBS, fixed in 4% PFA, then permeabilized using Perm buffer. Cells were incubated with primary Lap2 β antibodies, followed by incubation with secondary Alexa Fluor 488. Stained cells were cytopspun onto slides, air-dried and DNA was stained with DAPI. Nuclear blebbing of 1_1 and 1_3 *Ebf1^{fl/fl}RERT^{Cre}*::A-MuLV pro-B cells was assessed from 3D confocal images using a scoring system of nuclear blebbing severity: full flower shape - 4, two fissures -3, one fissure or another cell deformation - 2, normal – 1. (>50 cells per each sample).



From confocal imaging it was not clear if there is any change in euchromatin and heterochromatin localization upon EBF1 depletion, thus I used transmission electron microscopic imaging to assess potential changes. Due to cell availability at the time of the experiment, only 1_4 *Ebf1^{fl/fl}RERT^{Cre}::A-MuLV* and c3_4 *Ebf1^{+/+}RERT^{Cre}::A-MuLV* pro-B control cells were treated with 2 μ M OHT. It was previously observed that more than 90% of EBF1 is depleted after two days of OHT treatment, thus 1_4 *Ebf1^{fl/fl}RERT^{Cre}::A-MuLV* and c3_4 *Ebf1^{+/+}RERT^{Cre}::A-MuLV* pro-B cells were harvested after two days and were processed and submitted for transmission electron microscopic imaging. Significant changes in euchromatin and heterochromatin localizations were observed upon EBF1 depletion (Figure 4-11). In control 1_4 *Ebf1^{fl/fl}RERT^{Cre}::A-MuLV* pro-B cells and OHT treated and control c3_4 *Ebf1^{+/+}RERT^{Cre}::A-MuLV* pro-B cells heterochromatin localized proportionally at the periphery of the nuclei and throughout the inner body of the nucleus. In contrast, in OHT treated 1_4 *Ebf1^{fl/fl}RERT^{Cre}::A-MuLV* pro-B cells strikingly most of the heterochromatin localized at the periphery of the nuclei (Figure 4-11 A).

Calculating the euchromatin and heterochromatin area in the nucleus, it was observed that euchromatin occupies around 60% of the nucleus in control cells and EBF1 depleted cells. In control 1_4 *Ebf1^{fl/fl}RERT^{Cre}::A-MuLV* and c3_4 *Ebf1^{+/+}RERT^{Cre}::A-MuLV* heterochromatin localized at the periphery of the nuclei occupies, respectively 28.0% and 23.0% of the nuclei. There is only 2% increase in area membrane bound heterochromatin occupies upon OHT treatment in c3_4 *Ebf1^{+/+}RERT^{Cre}::A-MuLV*. While OHT induced EBF1 depletion caused 7.7% increase in the area that membrane bound heterochromatin occupies (Figure 4-11 B).

Figure 4-11 EBF1 depletion in *Ebf1^{fl/fl}RERT^{Cre}::A-MuLV* pro-B cells causes heterochromatin localization at the nuclear membrane. 1_4 *Ebf1^{fl/fl}RERT^{Cre}::A-MuLV* (*Ebf1^{fl/fl}*) and c3_4 *Ebf1^{+/+}RERT^{Cre}::A-MuLV* (*Ebf1^{+/+}*) pro-B cells were treated with 2 μ M OHT for two days prior cell fixation. (A) Transmission electron images of 1_4 *Ebf1^{fl/fl}RERT^{Cre}::A-MuLV* pro-B cells and c3_4 *Ebf1^{+/+}RERT^{Cre}::A-MuLV* pro-B cells Heterochromatin accumulation at the periphery of the nuclei in the OHT depleted 1_4 *Ebf1^{fl/fl}RERT^{Cre}::A-MuLV* pro-B cells is show via white arrows. (B) The area euchromatin and heterochromatic occupied within the nuclei was calculated. Euchromatin and heterochromatin distribution in the nuclei before and after EBF1 depletion, where euchromatin, heterochromatin localized in the nuclear body (internal heterochromatin) and at the periphery of the nuclei (membrane bound heterochromatin) are show, respectively, via green, blue and red (from 10 cells; n = 1 experiments).



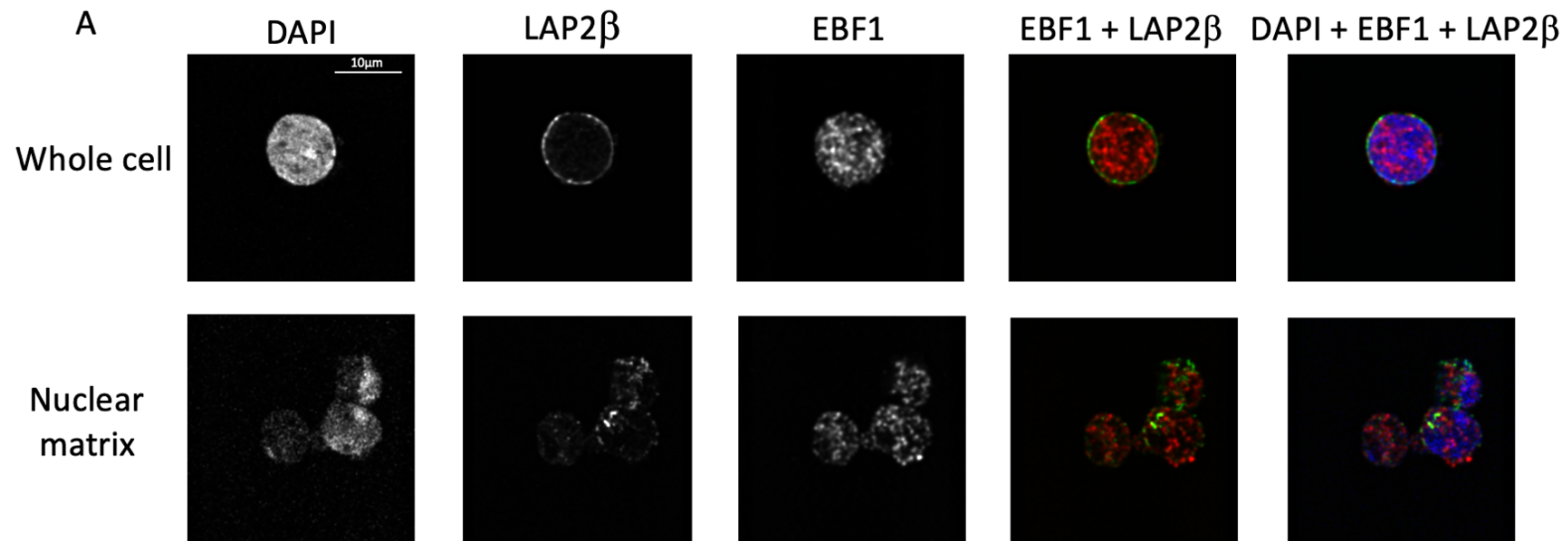
The nuclear blebbing and heterochromatin reorganization upon EBF1 depletion, suggests that EBF1 is important for NM maintenance. EBF1 might directly or indirectly affect the change in the NM proteome, causing nuclear blebbing, or it might be a NM protein itself. *In situ* fractionation (Figure 4-12) was performed in order to begin to understand the role EBF1 plays in NM maintenance. For *in situ* fractionation experiments antibodies against THOC1 and RUNX1 - NM proteins were tested for confocal imaging. Only RUNX1 antibody worked for confocal microscopy staining and was used as a NM control in the *in situ* fractionation experiments.

In situ fraction was performed as per Sawasdichai *et al.* protocol (Sawasdichai, Chen *et al.* 2010). Confocal imaging confirmed EBF1 and RUNX1 nuclear localization. Confocal imaging of the *in situ* fractionated 1_3 *Ebf1^{fl/fl}RERT^{Cre}::A*-MuLV pro-B cells showed partial DNA digestion, decrease in LAP2 β protein level at the nuclear envelope and increase in LAP2 β localization in the nuclear body (Figure 4-12 A) This might be due to DNA digestion, and the subsequent washes caused undigested DNA and LAP2 β that is bound to DNA to relocate from the periphery of the nuclei to the inner body of nuclei. For the full DNA digestion, protocol requires optimization by increasing DNase I concentration. Nevertheless, EBF1 and RUNX1 were detected in the part of the nuclei where the most of the DNA was digested (Figure 4-12 A and B), suggesting that at least some EBF1 may be a component of the NM. In order to assess EBF1 and RUNX1 protein levels in NM, mean fluorescence intensity of the EBF1 and RUNX1 in the nuclei and in the DNA free NM area was calculated. A small - 10.8% decrease in the mean intensity of RUNX1 was observed in the NM compartment compared to the mean intensity calculated in the whole nuclei (Figure 4-12 C). RUNX1 was previously reported a NM protein, although it was not reported what percentage of total RUNX1 is a part of NM. Nevertheless, detecting RUNX1 in the part of nuclei that is DNA free, suggests that DNA free area is the NM and can be used for assessment whether EBF1 is a NM protein. Comparing EBF1 intensity in whole nuclei and in the NM (DNA free nuclei area after *in situ* fractionation), 37.2% of total EBF1 intensity in whole nuclei was detected in the NM (Figure 4-12 C), suggesting that part of EBF1 may be a component of the NM.

EBF1 and RUNX1 colocalised in the nuclei, while no colocalisation of the EBF1 and RUNX1 proteins was detected in the NM, supporting the hypothesis by Hagman and colleagues that the functions of EBF1 and RUNX1 are non-redundant at the molecular level but affecting the same set of target genes (Lukin, Fields et al. 2008).

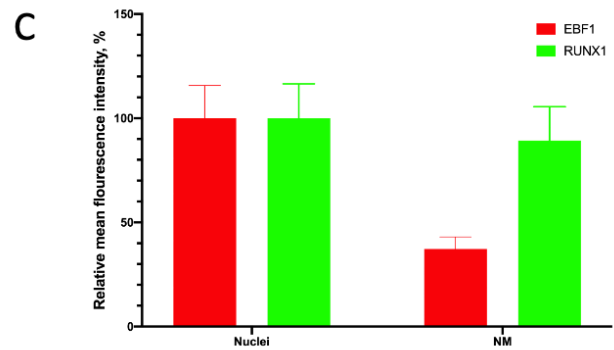
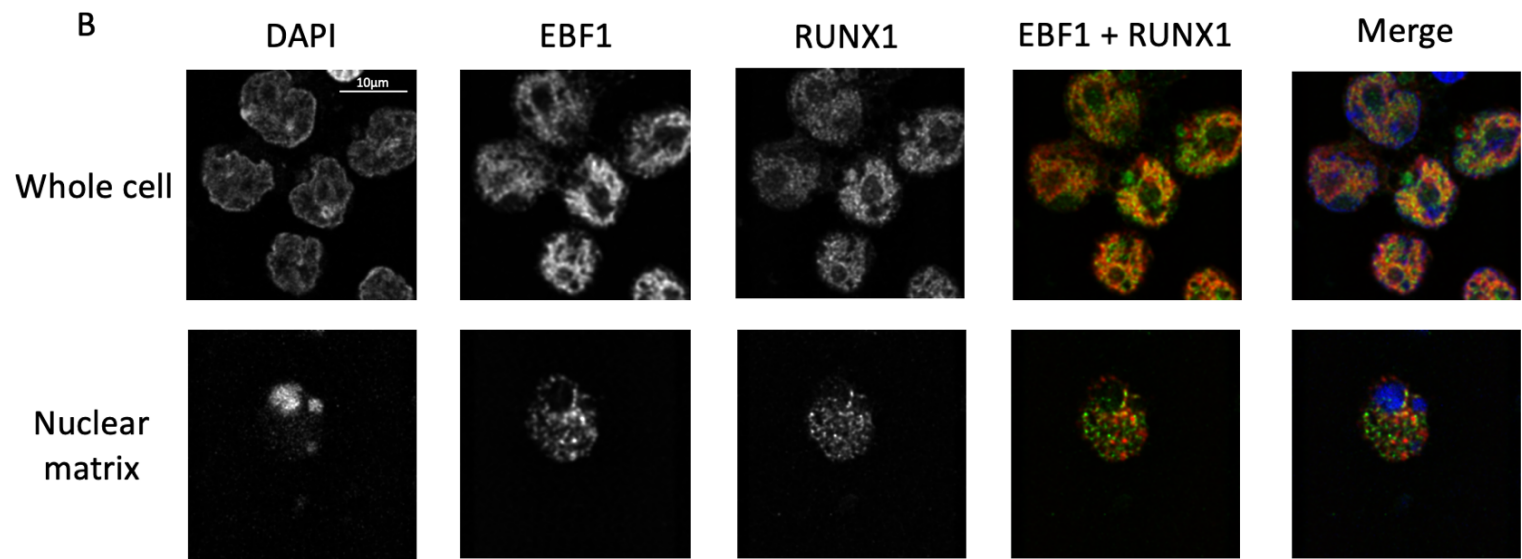
The in situ fractionation suggests that EBF1 might be NM protein, however, the in situ protocol needs optimization in order to be certain.

Figure 4-12 EBF1 is a potential NM protein in *Ebf1^{fl/fl}RERT^{Cre}::A*-MuLV pro-B cells. 1_3 *Ebf1^{fl/fl}RERT^{Cre}::A*-MuLV pro-B cells were seeded on poly-L lysine coated coverslips day before *in situ* fractionation. Briefly, cells were treated with CSK buffer supplemented with 0.1% (v/v) Triton X-100, followed by treatment with CSK buffer supplemented with 0.5% (v/v) Triton X-100 and with CSK buffer supplemented with 100µg/ml of DNase I. Then cells were fixed in 4% PFA and permeabilized using Perm buffer. Cells were incubated with primary Lap2β, RUNX1 and EBF1 antibodies, followed by incubation with secondary Alexa Fluor 488 or Alexa Fluor 647 and DNA staining with DAPI. Mean intensity of the EBF1 and RUNX1 in the nuclei (from whole cell images) and in the NM (the parts that are free from DNA) were calculated. Representative confocal images of 1_3 *Ebf1^{fl/fl}RERT^{Cre}::A*-MuLV pro-B cells before (Whole cell) and after *in situ* fractionation (Nuclear matrix) stained for (A) Lap2β (green), EBF1 (red) and DNA (blue) and for (B) RUNX1 (green), EBF1 (red) and DNA (blue). (C) Relative mean intensity of the EBF1 and RUNX1 per pixel in the whole nuclei and in the NM (from 25 cells; n = 3 experiments, x10 magnification).



Continued...

Continued...



4.4 HDAC3 inhibitors does not reverse the phenotype of EBF1 depleted pro-B cells

HDAC3 regulates epigenome and gene transcription (Karagianni and Wong 2007), but more particularly, it supports the inner nuclear membrane by association with Lamin A/C (LMNA) (Milon, Cheng et al. 2012), where it acts as a “Velcro” by attaching the silenced genes to the inner nuclear membrane. Moreover, HDAC3 knockout resulted in a dramatic decrease of the heterochromatin at the periphery of the nuclei (Zullo, Demarco et al. 2012). Thus, it was hypothesized that HDAC3 inhibition might cause detachment of the heterochromatin from the nuclear membrane in EBF1 depleted pro-B cells, thus rescue them from the nuclear blebbing.

In order to investigate if the hypothesis is correct, Droxinostat and RGFP966 were used to inhibit HDAC3. RGFP966 has been reported to be a selective HDAC3 inhibitor, while Droxinostat mostly inhibits HDAC6, HDAC8 and HDAC3. Flow cytometry images are shown for 1_1 and 1_3 *Ebf1^{fl/fl}RERT^{Cre}::A*-MuLV pro-B cells treated with 2.5μM Droxinostat or 2.5μM RGFP966 alone or in combination with 2μM OHT (Figure 4-13 A and Figure 4-14 A) with gates set to include viable, apoptotic and dead cells. PI is a membrane impermeant dye that can penetrate only damaged cells. Thus, dead and apoptotic cells have higher mean fluorescent intensity in the PE channel compared to healthy, viable cells.

The effects of the HDAC inhibitors alone and HDAC inhibitor in combination with 2μM OHT on nuclear PI staining was plotted for both HDAC inhibitors (Figure 4-13 B and Figure 4-14 B). Neither Droxinostat nor RGFP966 caused a dramatic dose-dependent change in nuclear PI staining of cells when treated with increasing concentration of the drugs. A similar pattern was observed for double treated 1_3 *Ebf1^{fl/fl}RERT^{Cre}::A*-MuLV pro-B cells with Droxinostat and OHT or RGFP966 and OHT. Cell death caused by 5μM Droxinostat in 1_3 *Ebf1^{fl/fl}RERT^{Cre}::A*-MuLV pro-B cells and by 5μM RGFP966 in 1_1 *Ebf1^{fl/fl}RERT^{Cre}::A*-MuLV pro-B cells was observed to be similar to the cell death caused by 2μM OHT in the same pro-B cells (Figure 4-13 B and Figure 4-14 B). This indicates that both HDAC inhibitors failed to rescue cells from OHT induced cell death. HDAC3 depletion was shown to result in $V_H D_H H$ defect indicating that HDAC3 is essential in the regulation of B cell

development (Stengel, Barnett et al. 2017); thus, no such rescue was expected, only some reversal of heterochromatinization at the periphery of the nucleus and consequent decrease in the nuclear blebbing.

In order to confirm this 1_1 pro-B and 1_3 *Ebf1^{fl/fl}RERT^{Cre}::A*-MuLV pro-B cells were treated with 2 μ M OHT, 2.5 μ M Droxinostat or 2.5 μ M RGFP966 alone and with HDAC inhibitors in combination with 2 μ M OHT. Untreated pro-B cells and cells treated with the combination of EtOH and DMSO were used as controls. OHT-dependent EBF1 depletion in 1_1 and 1_3 pro-B cells was confirmed *via* Western Blot analysis (Figure 4-15). Several HDACs are responsible for histone deacetylation. Inhibition of all HDACs would result in detectable increasing histone acetylation, while inhibition of HDAC3 would cause a substantial change in the levels of histone acetylation that can be detected *via* Western blot; thus, the effect of HDAC3 inhibition with 2.5 μ M Droxinostat or 2.5 μ M RGFP966 was not verified. Due to IC50 for HDAC3 inhibition using Droxinostat is 1.46 μ M (Wood, Dalili et al. 2010) and for HDAC3 inhibition using RGFP966 is 0.08 μ M (Dai, Huang et al. 2019), it was thought that 2.5 μ M and 2.5 μ M RGFP966 would inhibit most of HDAC3.

Nuclear PI staining was detected in less than 30% of untreated cells and less than 40% of EtOH and DMSO treated cells, while 2 μ M OHT, 2.5 μ M Droxinostat and 2.5 μ M RGFP966 caused increase in *Ebf1^{fl/fl}RERT^{Cre}::A*-MuLV pro-B cell nuclear staining (cell death), 55%, 50% and 47%, respectively. The addition of HDAC inhibitor to 2 μ M OHT treatment caused a slight decrease in the percentage of the viable cells from 45% to 37% and 30% for the combination of 2.5 μ M Droxinostat and 2 μ M OHT, and 2.5 μ M RGFP966 and 2 μ M OHT (Figure 4-13 A and Figure 4-14 A).

Figure 4-13 Combined treatment of Droxinostat and OHT causes an increase in the cell death compared to a cell death in single treated cells with Droxinostat or OHT . *1_1* and *1_3 Ebf1^{fl/fl}RERT^{Cre}*:A-MuLV pro-B cells were treated with and without 2 μ M OHT on day zero after 8h of Droxinostat was added at different concentrations, combination of EtOH and DMSO was used as a control. Cells were collected three days after OHT treatment and stained with PI. (A) Representative flow cytometry images of untreated, single or double treated pro-B cells with 2 μ M OHT and 2.5 μ M Droxinostat. Collected events are gated for all events (gate A), single cells (gate B), PI unstained cells (gate C) and PI stained cells (Gate D). (B) The change in nuclear PI staining in OHT untreated and treated pro-B cells upon an increase in Droxinostat dose. (n = 4 experiments)

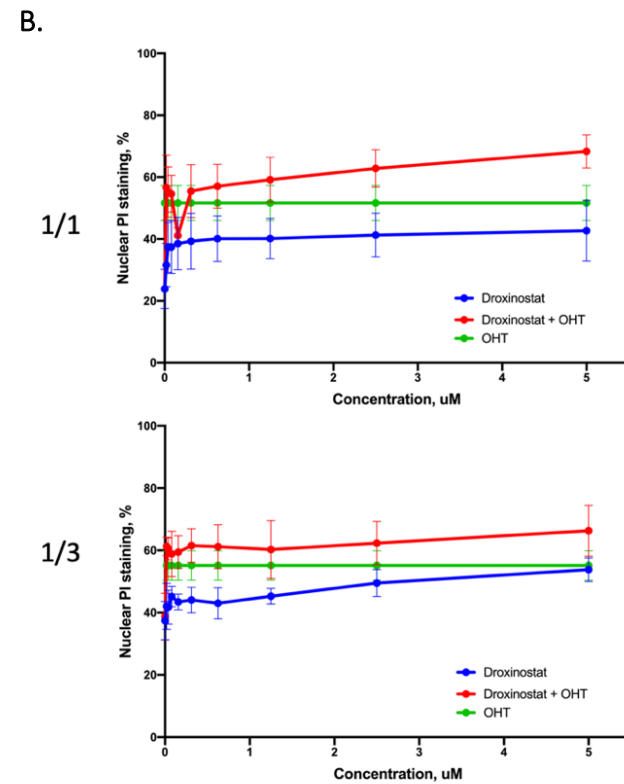
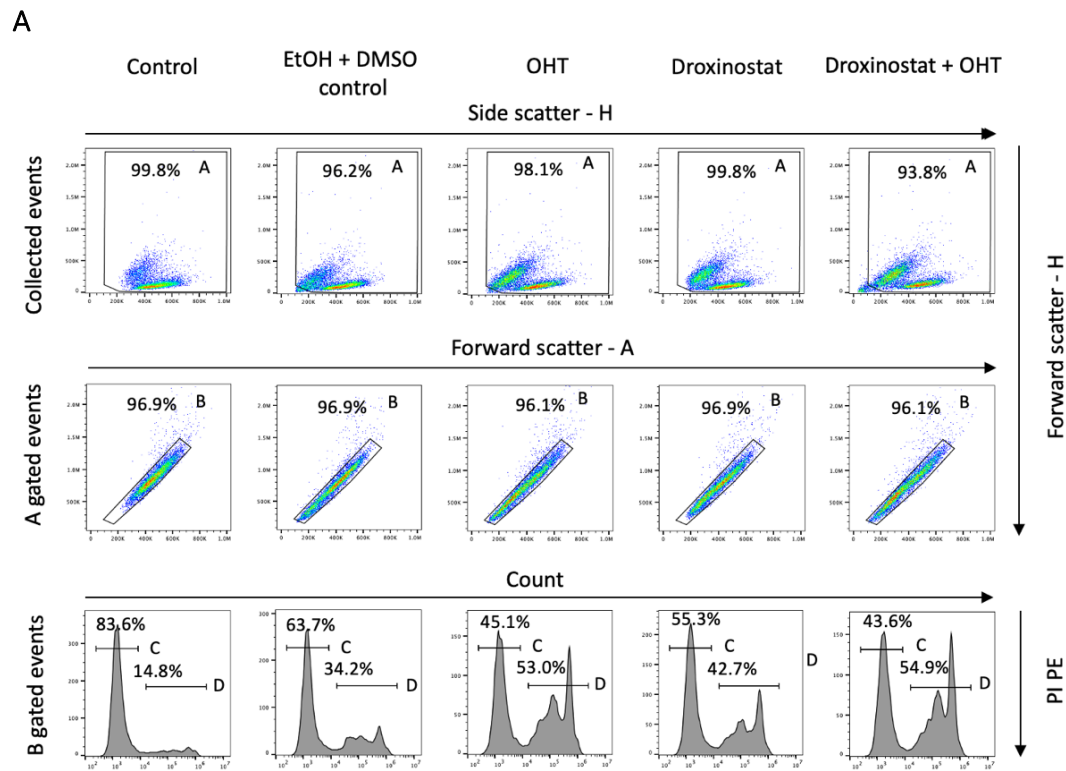


Figure 4-14 Combined treatment of RGFP966 and OHT causes an increase in the cell death compared to a cell death in single treated cells with RGFP966 or OHT. 1_1 and 1_3 *Ebf1^{fl/fl}RERT^{Cre}*:A-MuLV pro-B cells were treated with and without 2μM OHT on day zero, after 8h of RGFP966 was added at different concentrations, combination of EtOH and DMSO was used as a control. Cells were collected three days after OHT treatment and stained with PI. (A) Representative flow cytometry images of untreated, single or double treated pro-B cells with 2μM OHT and 2.5μM RGFP966. Collected events are gated for all events (gate A), single cells (gate B), PI unstained cells (gate C) and PI stained cells (Gate D). (B) The change in nuclear PI staining in OHT untreated and treated pro-B cells upon an increase in RGFP966 dose. (n = 4 experiments)

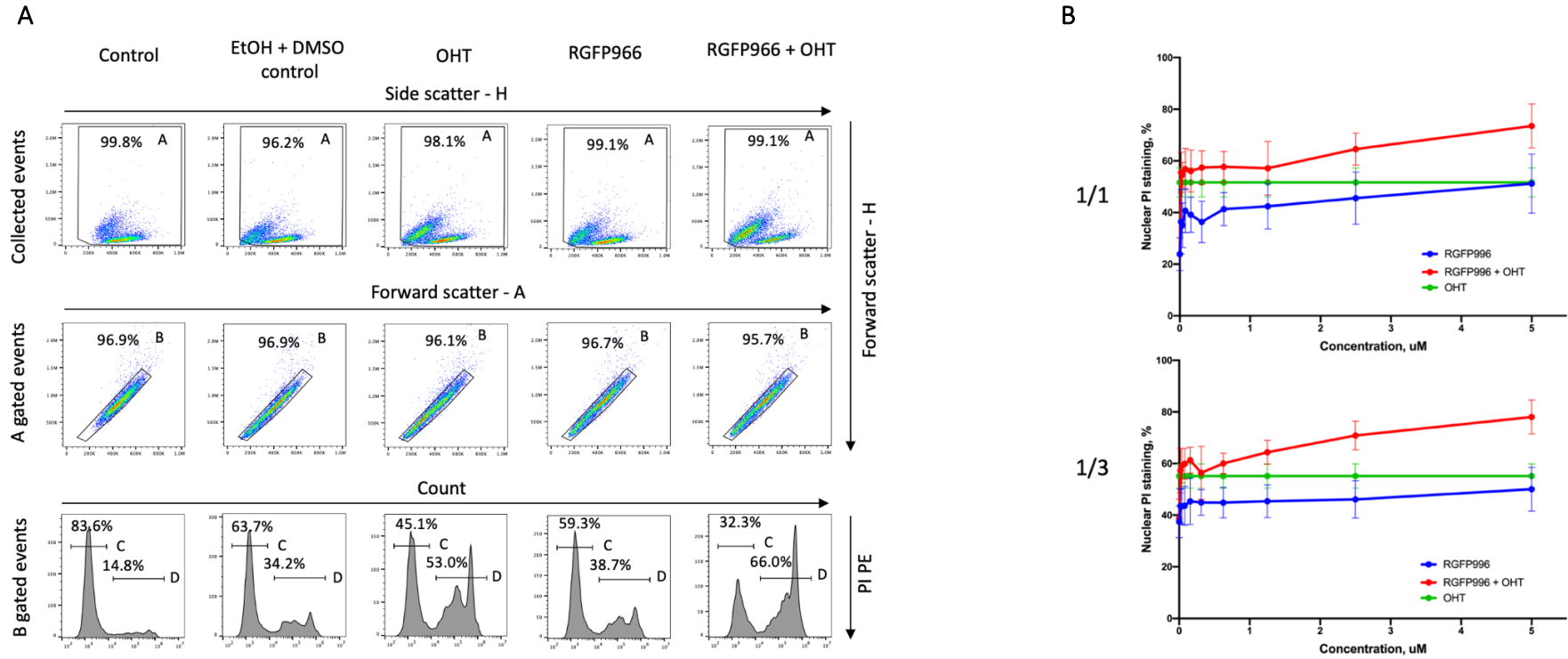
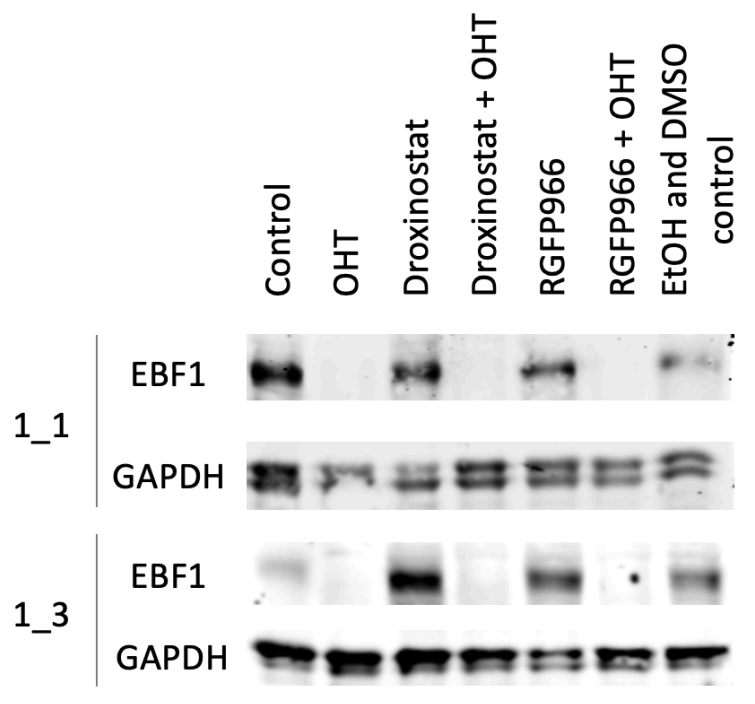


Figure 4-15 Verification of EBF1 depletion in *Ebf1^{fl/fl}RERT^{Cre}::A*-MuLV pro-B cells after OHT and/or HDAC3 inhibitor treatment. 1_1 and 1_3 *Ebf1^{fl/fl}RERT^{Cre}::A*-MuLV pro-B cells were treated with and without 2 μ M OHT on Day zero, 2.5 μ M RGFP966 was added 8h after OHT addition, combination of EtOH and DMSO was used as a control. Cells were collected three days after OHT treatment, lysed and proteins were separated via acrylamide gel electrophoresis, then proteins were transferred to nitrocellulose membrane and stained for EBF1 and GAPDH.



The nuclear shape upon drug treatments was observed *via* Confocal imaging. Samples for confocal imaging were stained for LAP2 β , RUNX1 and DNA with DAPI. The nuclear blebbing severity was assessed from 3D confocal images using a scoring system. Due to each of the cell lines treatment and confocal imaging was performed only twice, the p values were calculated taking each of the experiments for both pro-B cell lines as a separate replicate experiment for the same sample. Droxinostat and RGFP966 alone and in combination with OHT caused nuclear blebbing similar to the nuclear blebbing seen in OHT treated pro-B cells (Figure 4-16 and Figure 4-17). Upon EBF1 depletion severe nuclear blebbing was observed in 25-35% of cells, while normal shape nuclei were observed in about 25% of cells. In some of the Droxinostat and RGFP966 treated cells, the nuclear membrane appeared wavy. This effect was more prominent in the 1_3 *Ebf1^{fl/fl}RERT^{Cre}::A-MuLV* pro-B cells (Figure 4-17). The wavy nuclear membrane was previously reported upon HDAC3 knockdown in Retinal ganglion cells (RGCs) (Schmitt, Pelzel et al. 2014).

Droxinostat, RGFP966 and OHT alone caused, respectively, 13-20% (p=0.008), 15-22% (p=0.04) and 24-35% (p=0.009) decrease in the percentage of cell with normal shaped nuclei (Figure 4-18) and, respectively, 2-10% (p=0.1, not significant (ns)), 20% (p=0.02) and 11-20% (p=0.006) increase in the percentage of cell with moderate to high nuclear blebbing. Addition of Droxinostat or RGFP966 to OHT treated cells caused, respectively, a 6% (p=0.4, ns) and 3-10% (p=0.4, ns) decrease in the percentage of cells with normal nuclei and 15% (p=0.2, ns) and 18% (p=0.03) increase in the percentage of cell with the moderate to high nuclear blebbing (Figure 4-18). Thus, HDAC3 inhibition does not rescue pro-B cell phenotype induced by EBF1 depletion

Figure 4-16 HDAC3 inhibitors do not rescue 1_1 *Ebf1^{fl/fl}RERT^{Cre}*::A-MuLV pro-B cells from OHT induced nuclear blebbing collapse. 1_1 *Ebf1^{fl/fl}RERT^{Cre}*::A-MuLV pro-B cells were treated with and without 2μM OHT on Day zero, 2.5μM RGFP966 or 2.5μM Droxinostat was added 8h after OHT addition, combination of EtOH and DMSO was used as a control. Cells were collected three days after OHT treatment, washed with PBS, fixed in 4% PFA, then permeabilized using Perm buffer. Cells were incubated with primary Lap2β antibodies, followed by incubation with secondary Alexa Fluor 488. Stained cells were cytospun onto slides, air-dried and DNA was stained with DAPI. Representative confocal images of 1_1 and *Ebf1^{fl/fl}RERT^{Cre}*::A-MuLV pro-B cells stained for Lap2β (green) and DNA (blue).

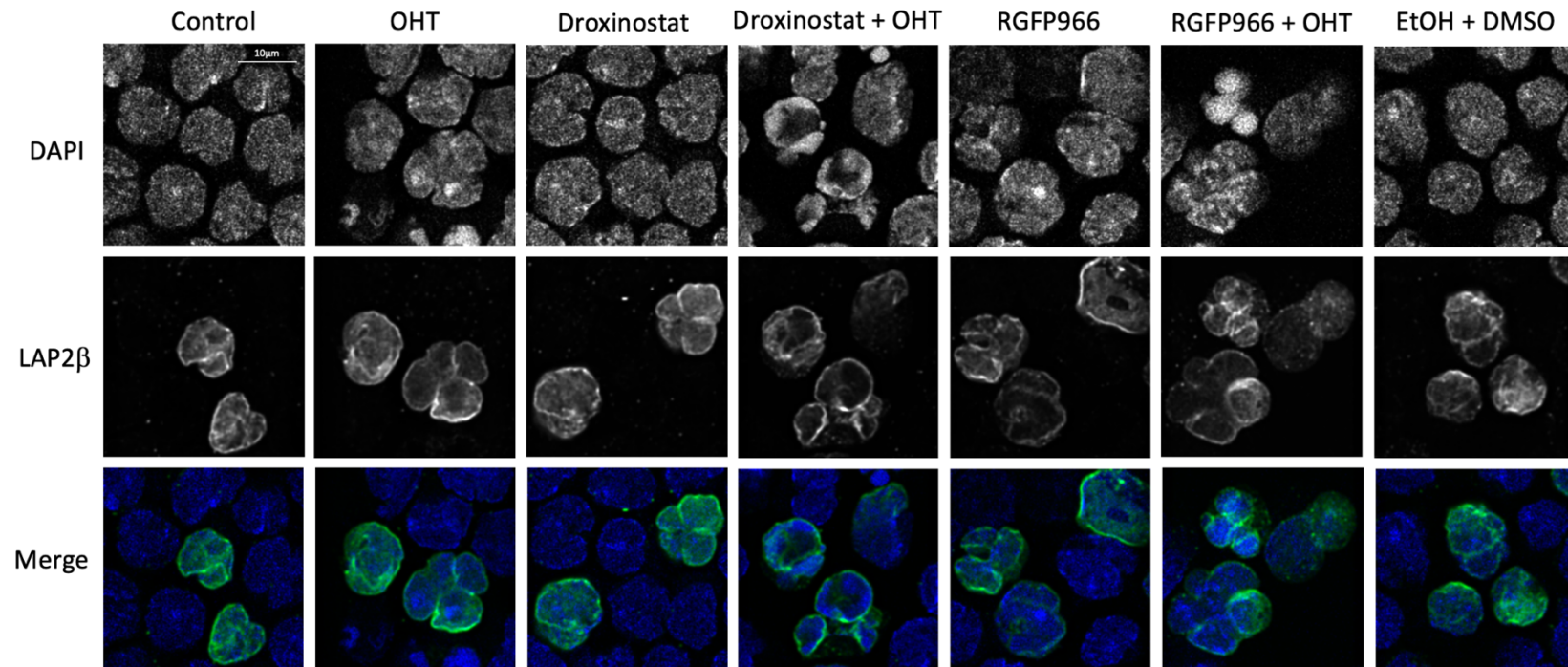


Figure 4-17 HDAC3 inhibitors does not rescue 1_3 *Ebf1^{fl/fl}RERT^{Cre}::A*-MuLV pro-B cells from OHT induced nuclear blebbing collapse. 1_3 *Ebf1^{fl/fl}RERT^{Cre}::A*-MuLV pro-B cells were treated with and without 2 μ M OHT on Day zero, 2.5 μ M RGFP966 or 2.5 μ M Droxinostat was added 8h after OHT addition, combination of EtOH and DMSO was used as a control. Cells were collected three days after OHT treatment, washed with PBS, fixed in 4% PFA, then permeabilized using Perm buffer. Cells were incubated with primary Lap2 β antibodies, followed by incubation with secondary Alexa Fluor 488. Stained cells were cytospun onto slides, air-dried and DNA was stained with DAPI. Representative confocal images of 1_3 and *Ebf1^{fl/fl}RERT^{Cre}::A*-MuLV pro-B cells stained for Lap2 β (green) and DNA (blue).

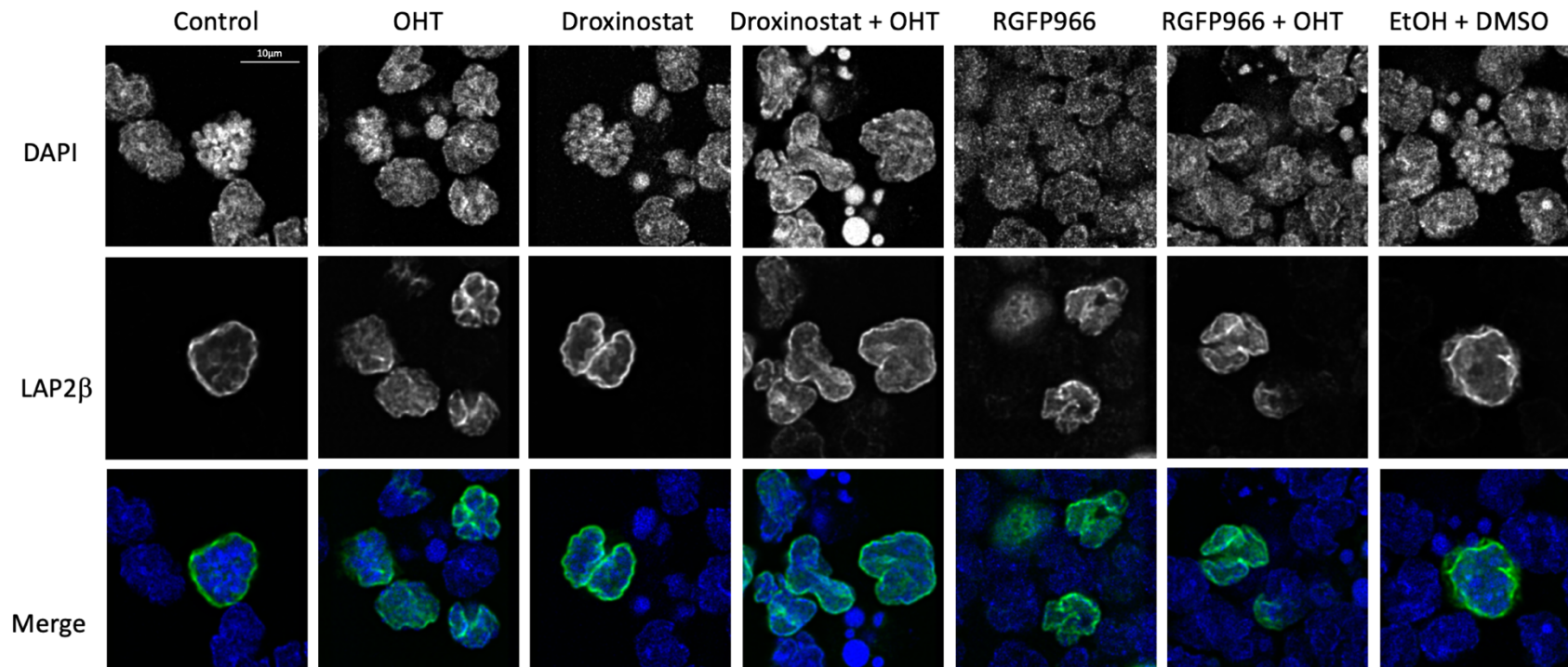
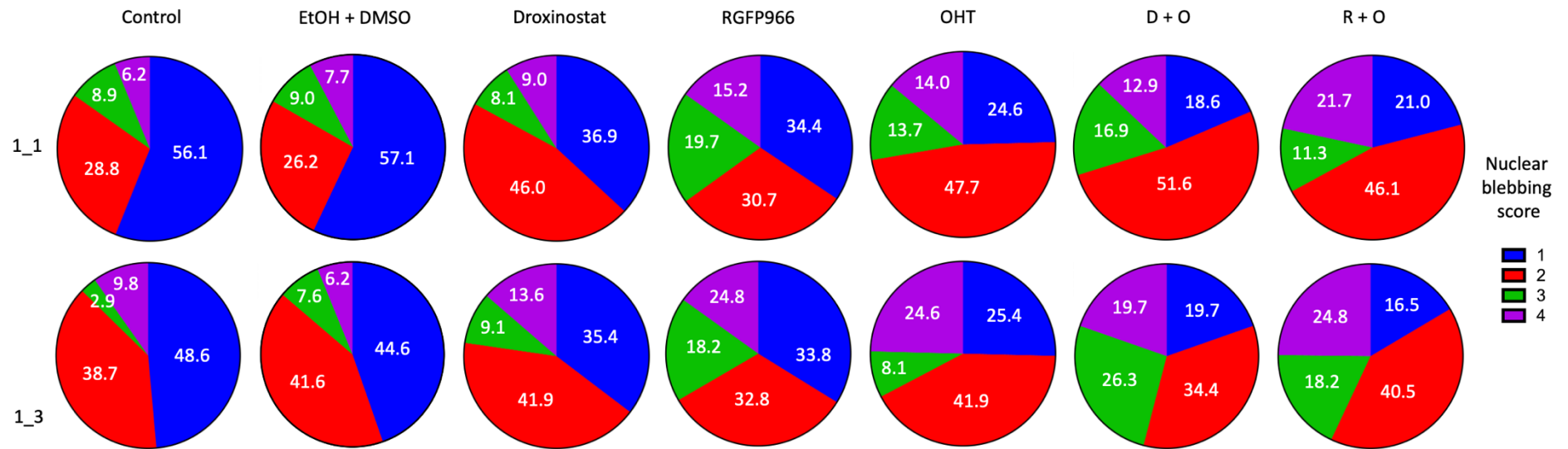


Figure 4-18 Assessment of nuclear blebbing upon pro-B cell treatment with OHT, Droxinostat or RGFP966 alone or their combination. 1_1 and 1_3 *Ebf1^{fl/fl}RERT^{Cre}*::A-MuLV pro-B cells were treated with and without 2μM OHT on Day zero, 2.5μM RGFP966 or 2.5μM Droxinostat was added 8h after OHT addition, combination of EtOH and DMSO was used as a control. Cells were collected three days after OHT treatment, washed with PBS, fixed in 4% PFA, then permeabilized using Perm buffer. Cells were incubated with primary Lap2β antibodies, followed by incubation with secondary Alexa Fluor 488. Stained cells were cytopun onto slides, air-dried and DNA was stained with DAPI. Nuclear blebbing of 1_1 and 1_3 *Ebf1^{fl/fl}RERT^{Cre}*::A-MuLV pro-B cells was assessed from 3D confocal images using a scoring system of nuclear blebbing severity: full flower shape - 4, two fissures -3, one fissure or another cell deformation - 2, normal – 1. (>100 cells per each sample).



During *In situ* fractionation, EBF1 and RUNX1 colocalization was observed within intact nuclei but not in the NM fraction. To assess whether EBF1 depletion might affect RUNX1 protein levels or/and localization immunofluorescent microscopy has been performed (Figure 4-19 and Figure 4-20). A 50% increase in the fluorescence intensity of RUNX1 upon EBF1 depletion was observed, suggesting that there is an increase in RUNX1 protein levels upon EBF1 depletion (Figure 4-21 A and B). Droxinostat, RGFP966 or their combination with OHT did not cause a change in the fluorescence intensity of RUNX1 in 1_1 *Ebf1^{fl/fl}RERT^{Cre}::A*-MuLV pro-B cells. While in the 1_3 *Ebf1^{fl/fl}RERT^{Cre}::A*-MuLV pro-B cells, RGFP966 causes a decrease in the fluorescence intensity of RUNX1 and combination of RGP966 and OHT cause an increase in the fluorescence intensity of RUNX1. In the calculation were used only RUNX1 positive cells, thus it is unclear if this difference in the RUNX1 levels in 1_1 and 1_3 *Ebf1^{fl/fl}RERT^{Cre}::A*-MuLV pro-B cells is genuine. The data needs verification.

No change in RUNX1 localization was observed upon treatments with either OHT, Droxinostat, RGFP966 or combination of these drugs (Figure 4-19 and Figure 4-20). Colocalization in between two protein *via* confocal imaging does not necessarily indicate protein-protein interaction. Moreover, the lack of change in RUNX1 localization suggests that RUNX1 does not depend on the EBF1 NM structure.

Figure 4-19 EBF1 depletion in 1_1 *Ebf1^{fl/fl}*RERT^{Cre}::A-MuLV pro-B cells does not cause a change in Runx1 nuclear localisation. 1_1 *Ebf1^{fl/fl}*RERT^{Cre}::A-MuLV pro-B cells were treated with and without 2µM OHT on Day zero, 2.5µM RGFP966 or 2.5µM Droxinostat was added 8h after OHT addition, combination of EtOH and DMSO was used as a control. Cells were collected three days after OHT treatment, washed with PBS, fixed in 4% PFA, then permeabilized using Perm buffer. Cells were incubated with primary RUNX1 antibodies, followed by incubation with secondary Alexa Fluor 488. Stained cells were cytospun onto slides, air-dried and DNA was stained with DAPI. Representative confocal images of 1_1 and *Ebf1^{fl/fl}*RERT^{Cre}::A-MuLV pro-B cells stained for RUNX1 (green) and DNA (blue).

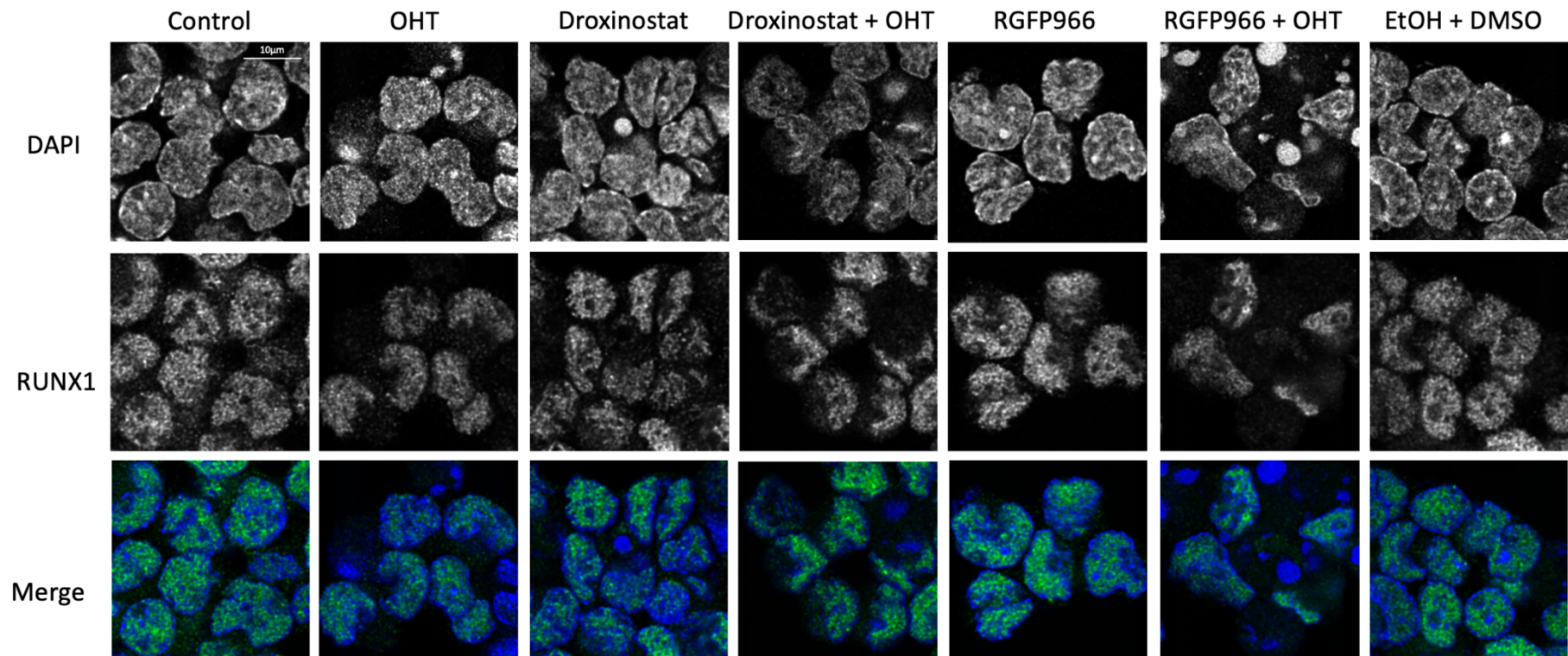


Figure 4-20 EBF1 depletion in 1_3 *Ebf1^{fl/fl}RERT^{Cre}*::A-MuLV pro-B cells does not cause a change in Runx1 nuclear localisation. 1_3 *Ebf1^{fl/fl}RERT^{Cre}*::A-MuLV pro-B cells were treated with and without 2µM OHT on Day zero, 2.5µM RGFP966 or 2.5µM Droxinostat was added 8h after OHT addition. Cells were collected three days after OHT treatment, washed with PBS, fixed in 4% PFA, then permeabilized using Perm buffer. Cells were incubated with primary RUNX1 antibodies, followed by incubation with secondary Alexa Fluor 488. Stained cells were cytopspun onto slides, air-dried and DNA was stained with DAPI. Representative confocal images of 1_3 and *Ebf1^{fl/fl}RERT^{Cre}*::A-MuLV pro-B cells stained for RUNX1 (green) and DNA (blue).

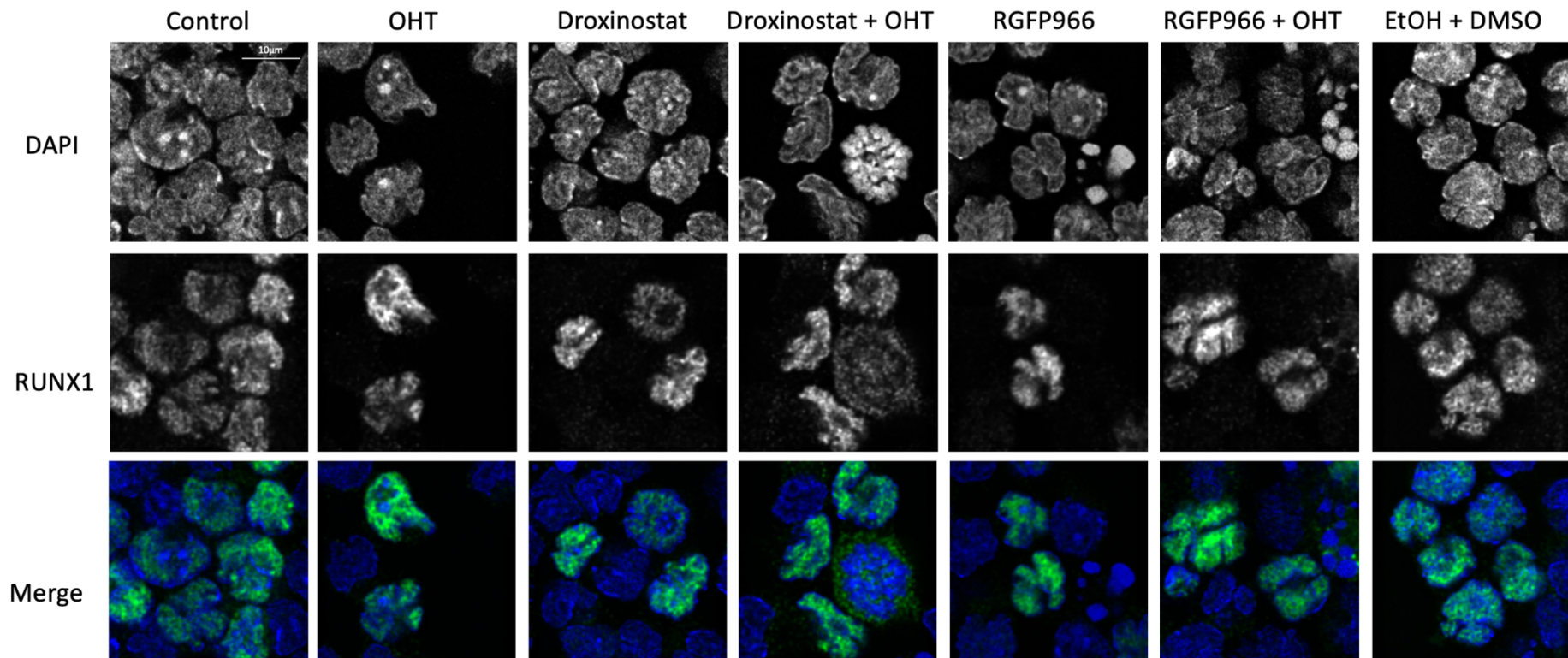
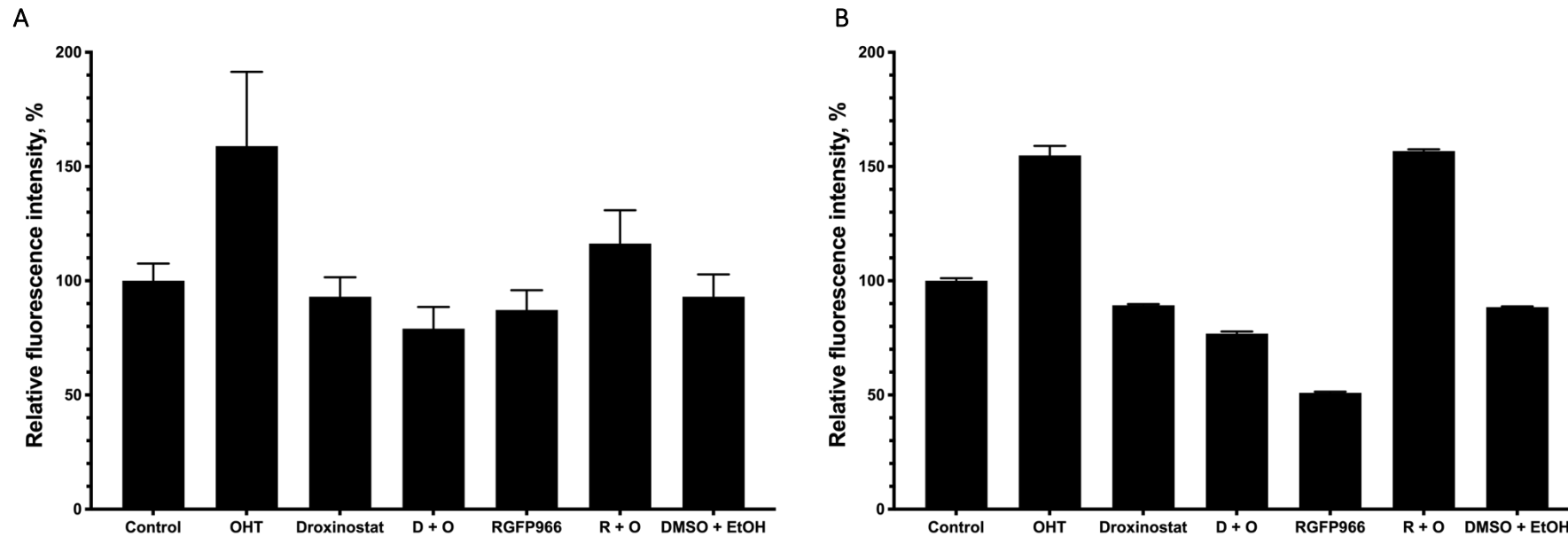


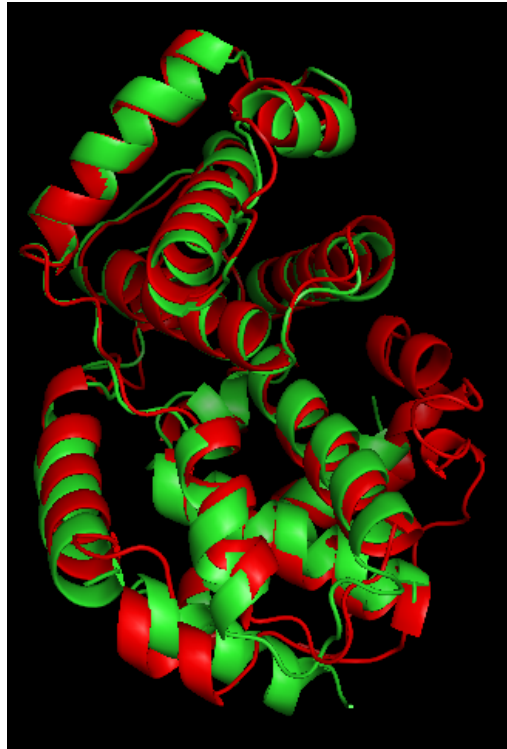
Figure 4-21 RUNX1 protein levels increase upon EBF1 depletion in *Ebf1^{fl/fl}RERT^{Cre}::A*-MuLV pro-B cells. 1_1 and 1_3 *Ebf1^{fl/fl}RERT^{Cre}::A*-MuLV pro-B cells were treated with and without 2 μ M OHT on Day zero, 2.5 μ M RGFP966 or 2.5 μ M Droxinostat was added 8h after OHT addition, combination of EtOH and DMSO was used as a control. Cells were collected three days after OHT treatment, washed with PBS, fixed in 4% PFA, then permeabilized using Perm buffer. Cells were incubated with primary RUNX1 antibodies, followed by incubation with secondary Alexa Fluor 488. Stained cells were cytopun onto slides, air-dried and DNA was stained with DAPI. Fluorescence intensity of the RUNX1 was measured in each RUNX1 stained cell. The change in relative intensity of RUNX1 upon different treatments of (A) 1_1 and (B) 1_3 *Ebf1^{fl/fl}RERT^{Cre}::A*-MuLV pro-B cells (from 50 cells; n = 2 experiments).



Chapter 5 EBF1 does not interact with CCNA2 and CCND3

A postdoctoral researcher in our lab suggested that EBF1 co-localizes and interacts with CCND3 and CCNA2. Thus, I planned to explore the structural requirements for EBF1 association with CCND3 and CCNA2. CCNA2 can be stably expressed in bacteria. In contrast, CCND3 degrades rapidly and can only be successfully expressed in a complex with CKD4 in a baculovirus expression system (Takaki, Echaliier et al. 2009). CCNA2 and CCND3 hold only 23% sequence identity, while the C terminal and N-terminal cyclin box of these protein hold, 18% and 40% sequence identity, respectively (Figure 5-2). CCNA2 and CCND3 have a similar alignment of the alpha-helices, which result in their structural similarity (Figure 5-1). Thus, it was hypothesized that CCND3 and CCNA2 might bind to the same structural domain of EBF1.

Figure 5-1 CCNA2 and CCND3 are highly similar by structure. Comparison of CCNA2 (in green) (PBD ID: 3DOG) (Bettayeb, Oumata et al. 2008) and CCND3 (in red) (PBD ID: 3G33) (Takaki, Echaliier et al. 2009) protein structure. Protein sequences were downloaded from RCSB PBD database and aligned via PyMOL.



5.1 DBD of EBF1 might be required for CCNA2 binding

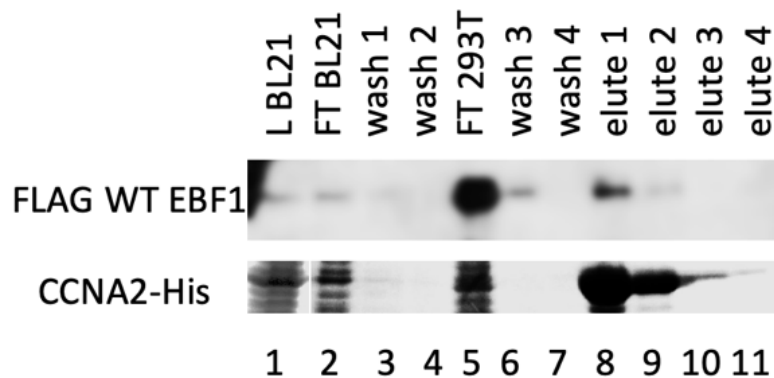
At first, EBF1 structural requirements for CCNA2 binding was investigated using EBF1 constructs described in Materials and Methods (Figure 3-1). Cloning of the WT and mutant *Ebf1* constructs into the pCR II TOPO vector (Invitrogen) consecutive sub-cloning into pMYs vector was verified by a set of restriction enzymatic digest (Figure 3-2 and Figure 3-3).

FLAG WT EBF1 and FLAG Δ T EBF1 were purified together with His-tagged CCNA2 using Ni-NTA resin. Four eluate fractions were collected for each protein affinity purification. The FLAG-WT EBF1 affinity purification was assessed via Western blot analysis, while the expression of CCNA2 His was assessed *via* Coomassie gel staining (Figure 5-3). Most of the CCNA2 His was eluted in the first two Fractions (Figure 5-3 A (lane 8 and 9) and B (lane 9 and 10)) and some of the CCNA2 His was detected in both bacterial (Figure 5-3 A (lane 2)) and mammalian flow-through (Figure 5-3 A (lane 5)), suggesting that Ni-NTA resin amount should be increased in order to bind all CCNA2 His. In the FLAG WT EBF1 affinity purification together with CCNA2 His a similar size band as FLAG WT EBF1 was detected in bacterial lysate and flow-through (Figure 5-3 A lane 1 and 2). It is possible that the FLAG M2 antibody non-specifically binds to a bacterial protein. Thus, it is unclear whether a band seen in the eluted fraction is FLAG WT EBF1 or it is a bacterial protein. FLAG Δ T EBF1 is smaller than FLAG WT EBF1. Thus, the band did not interfere with the observations. Although FLAG Δ T EBF1 was purified together with CCNA2 His (Figure 5-3 B (lane 9)), some of the FLAG Δ T EBF1 was detected in the flow-through (Figure 5-3 B (lane 5)). This might be due to this FLAG Δ T EBF1 was bound to the Ni-NTA uncaptured CCNA2 His or that the binding of CCNA2 His and FLAG Δ T EBF1 is weak.

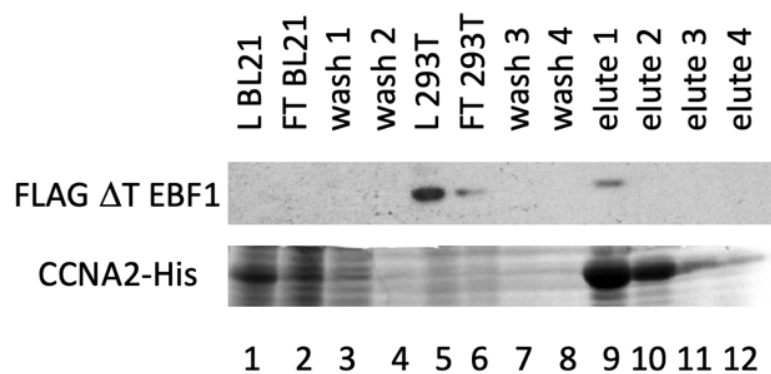
Most of the FLAG WT and mutant EBF1 were expressed at much higher levels than FLAG WT EBF1 (Figure 5-4 A), while FLAG Δ H Δ T EBF1 failed to express (Data not shown). It was previously reported that the HLH domain is required for EBF1 protein stability. Thus, it is possible that FLAG Δ H Δ T EBF1 degrades upon its expression in 293T cells.

Figure 5-3 Recombinant FLAG WT EBF1 and FLAG Δ T EBF1 affinity purification together with recombinant CCNA2 His using Ni-NTA resin. CCNA2 His was expressed in bacteria, while FLAG WT EBF1 and FLAG Δ T EBF1 were expressed in 293T cells. Bacterial lysate containing CCNA2 His was incubated together with the equilibrated Ni-NTA resin, flow through was collected and column was washed twice. Mammalian lysate containing FLAG-EBF1 was added to the CCNA2 His bound Ni-NTA resin. After incubation, flow through was collected and column was washed twice. FLAG EBF1 was purified together with CCNA2 His using Ni-NTA elution buffer. (A) FLAG WT EBF1 and (B) FLAG Δ T EBF1 affinity purification was verified via Western blot analysis, CCNA2 His affinity purification via Coomassie staining, where L BL21 – bacterial lysate containing recombinant CCNA2 His, L 293T – mammalian lysate containing FLAG WT EBF1 or FLAG Δ T EBF1 protein, FT BL21 – flow through after addition of bacterial lysate containing recombinant CCNA2 His, FT 293T – flow-through after addition of mammalian lysate containing FLAG WT EBF1 or FLAG Δ T EBF1 protein.

A

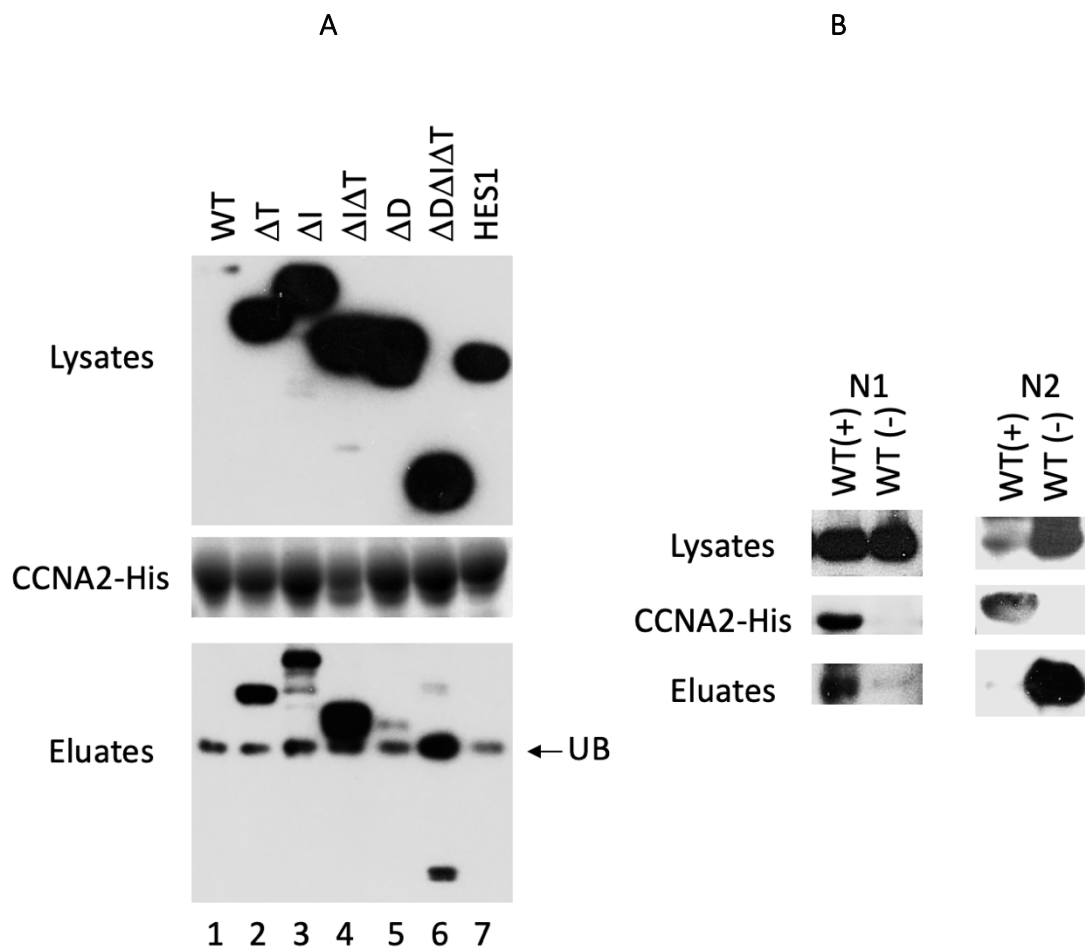


B



Affinity purification of FLAG WT and mutant EBF1 protein together with CCNA2 His was performed as described before and verified via Western blot analysis (Figure 5-4 A). HES1 is a transcriptional gene repressor which does not bind to CCNA2, thus FLAG HES1 was used as a negative control. In order to test whether FLAG WT EBF1 binds to CCNA2 His or sticks to Ni-NTA beads FLAG-WT EBF1 was purified together with bacterial lysate that does not contain CCNA2 His (FLAG-WT Ebf1 (-)) (Figure 5-4 B). CCNA2 His affinity purification was verified *via* Coomassie gel staining (Figure 5-4). No FLAG HES1 was eluted together with CCNA2 His (Figure 5-4 A), indicating that FLAG tag does not bind to CCNA2 His. FLAG WT EBF1 and FLAG Δ I EBF1, FLAG Δ T EBF1, FLAG Δ I Δ T EBF1 and FLAG Δ D Δ I Δ T EBF1 were purified together with CCNA2 His. Due to all of the proteins possessed DNA binding domain, it was thought that EBF1 DBD is required for CCNA2 binding. However, in the experiments where FLAG-WT EBF1 (-) was used as a control, FLAG WT EBF1 was detected in the eluted fraction, suggesting that EBF1 binds to the Ni-NTA, making it difficult to assess whether the two proteins indeed associate (Figure 5-4 B).

Figure 5-4 Recombinant FLAG WT and mutant EBF1 affinity purification together with recombinant CCNA2 His using Ni-NTA resin. CCNA2 His was expressed in bacteria, while FLAG WT EBF1 and FLAG Δ T EBF1 were expressed in 293T cells. Bacterial lysate containing CCNA2 His was incubated together with the equilibrated Ni-NTA resin, flow through was collected and column was washed twice. Mammalian lysate containing FLAG-EBF1 was added to the CCNA2 His bound Ni-NTA resin. After incubation, flow through was collected and column was washed twice. FLAG EBF1 was purified together with CCNA2 His using Ni-NTA elution buffer. Protein expression and affinity purification were verified via Western blot analysis. (A) FLAG WT and mutant EBF1 affinity purification together with CCNA2 His, where UB – unspecific binding. (B) FLAG WT EBF1 affinity purification with and without CCNA2 His, where N1 and N2 are two separate experiments. FLAG WT (+) EBF1 – FLAG WT EBF1 affinity purification together with CCNA2 His (n=5 experiments), FLAG WT (-) EBF1 – FLAG WT EBF1 affinity purification with bacterial lysate (n=3), FLAG Δ T EBF1 (n=6), FLAG Δ I EBF1 (n=7), FLAG Δ I Δ T EBF1 (n=7), FLAG Δ D EBF1 (n=5) FLAG Δ D Δ I Δ T EBF1 (n=4), FLAG HES1 (n=4).



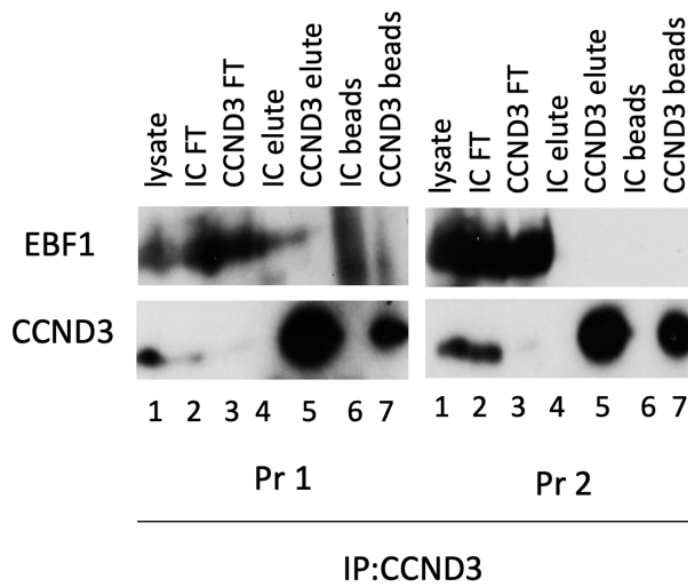
5.2 EBF1 does not interact with CCND3 and CCNA2 in *Ebf1^{fl/fl}RERT^{Cre}::A-MuLV* pro-B cells

Due to FLAG EBF1 was found to bind Ni-NTA resin, it was thought to pulldown endogenous CCNA2 together with overexpressed FLAG WT and mutant EBF1 in HEK293 using FLAG M2 beads and FLAG WT and mutant EBF1 together with CCNA2 using Co-IP protocol 1 (see materials and Methods). However, pulldowns failed to work (Data not shown). In order to optimize Co-IP pulldown and protein elution from the beads I performed pulldown of endogenous EBF1 and CCNA2 or CCND3 from 1_4 *Ebf1^{fl/fl}RERT^{Cre}::A-MuLV* pro-B cells using two standard protocols, both used by multiple laboratories at University of Leicester (see Material and Methods).

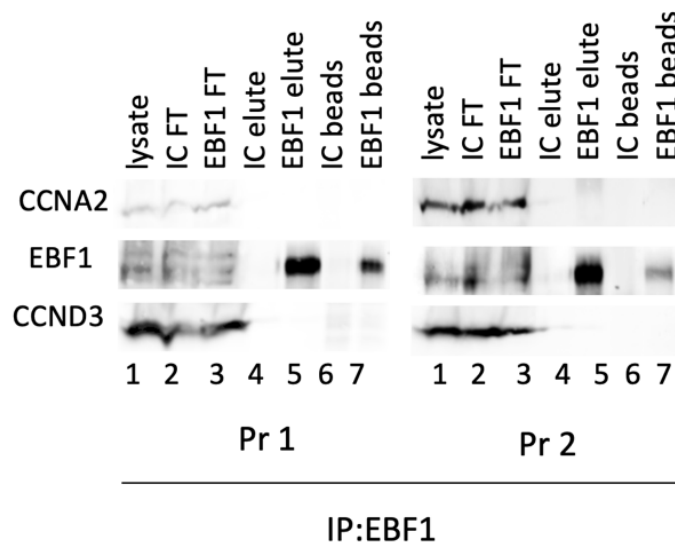
1_4 *Ebf1^{fl/fl}RERT^{Cre}::A-MuLV* pro-B cells were harvested and lysed using freshly prepared Co-IP buffer and sonicated. For CCND3 pulldowns, CCND3 mouse monoclonal antibodies were coupled to A/G PLUS-agarose, normal mouse IgG antibodies coupled to A/G PLUS agarose were used as isotype control. CCND3 immunoprecipitation was verified *via* Western blot analysis, while EBF1 was detected in the flow-through for both CCND3 immunoprecipitated fraction and the control (Figure 5-5 A). For EBF1 pulldown EBF1 rabbit polyclonal antibodies were coupled to A/G PLUS-agarose, normal rabbit IgG antibodies coupled to A/G PLUS agarose were used as isotype control. EBF1 immunoprecipitation was verified *via* Western blot analysis, while CCND3 and CCNA2 were detected in the flow-through using both protocols (Figure 5-5 A).

Figure 5-5 Optimizing Co-IP protocol for (A) EBF1 Co-IP together with CCND3 and (B) CCNA2 and CCND3 Co-IP together with EBF1. 1_4 *Ebf1^{fl/fl}RERT^{Cre}::A*-MuLV pro-B cells were harvested, washed with PBS, lysed and sonicated and proteins were Co-IP using Protocol 1 (Pr1) and Protocol 2 (Pr2). For CCND3 pulldown CCND3 mouse monoclonal antibodies were coupled to A/G PLUS-agarose, normal mouse IgG antibodies coupled to A/G PLUS agarose were used as isotype control (IC). For EBF1 pulldown EBF1 rabbit polyclonal antibodies were coupled to A/G PLUS-agarose, normal rabbit IgG antibodies coupled to A/G PLUS agarose were used as isotype control (IC). Protein elution was verified via Western blot analysis, FT- flow through.

A



B

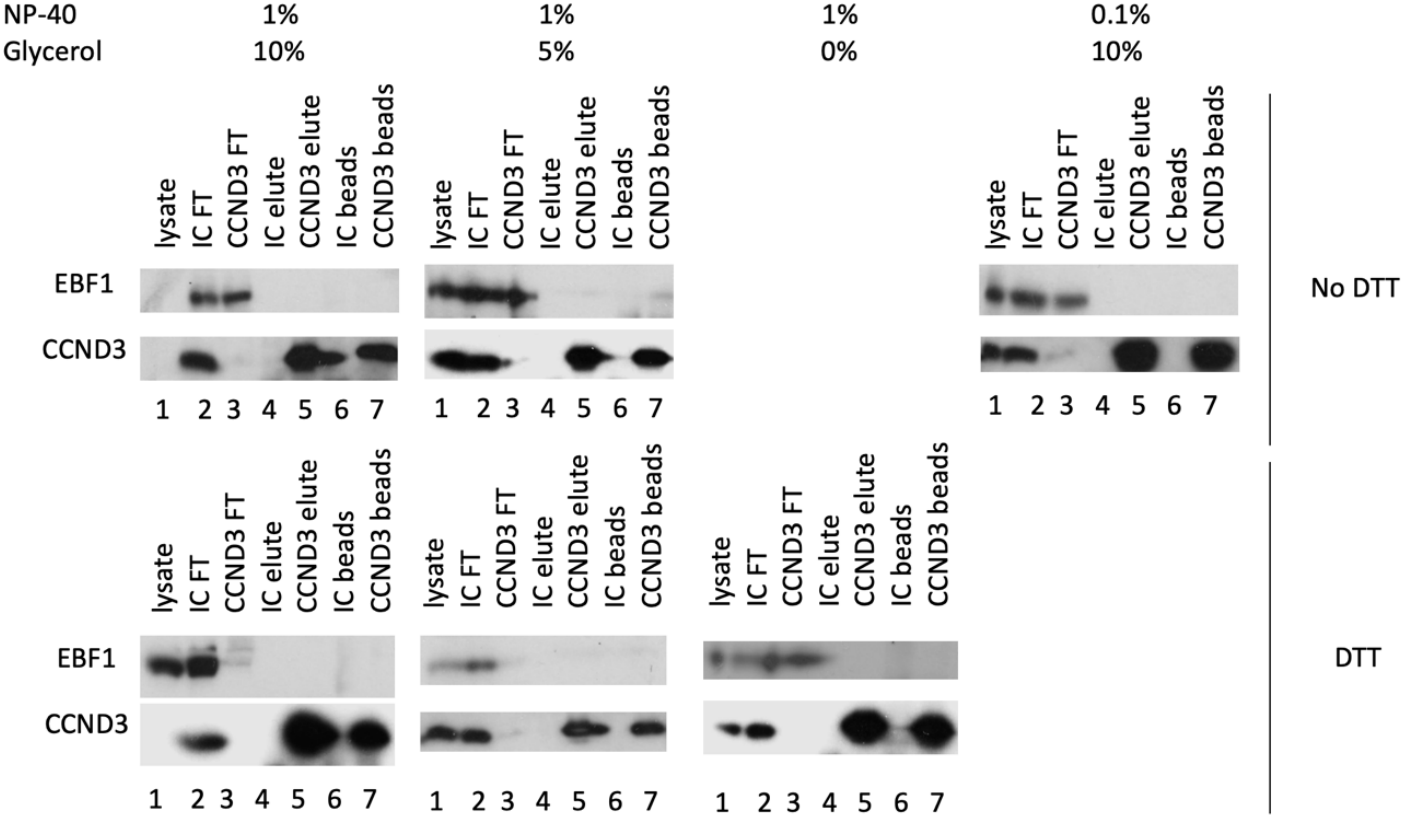


It was thought that optimizing Co-IP conditions could improve the detectability of the co-immunoprecipitated prey proteins. CCND3 immunoprecipitation was performed using Protocol 2 from 1_4 *Ebf1^{f/f}RERT^{Cre}*:A-MuLV pro-B cell lysates. Glycerol addition into lysis buffer stabilizes proteins and prevents their aggregation (Vagenende, Yap et al. 2009), however glycerol may slow down protein binding to antibody coupled beads or interaction with other proteins (Miernyk and Thelen 2008), thus it was thought to that decrease of glycerol percentage in the lysis buffer may help in protein Co-IP. NP-40 is non-ionic, mild detergent. Addition of NP-40 in lysis buffer breaks cell membranes and aids in protein extraction from cells (Burgess 2009), however non-ionic detergent can cause change in protein conformation, thus disrupting their binding to other proteins (Tan and Ting 2000). DTT reduces the disulfide bonds of protein, in the lysis buffer it prevents non-specific intramolecular disulfide linkage, respectively to reduce protein non-specific binding in the eluate and prevents the change in protein conformation (Burgess 2009). It was thought that decrease in NP-40 concentration and/or addition of DTT in the lysis buffer may prevent potential change in the protein conformation. 0.1% and 1% NP-40, 0%, 5% and 10% glycerol, as well as none or 1 μ M DTT were used in modified Co-IP buffer in order to improve the detectability of the co-immunoprecipitated prey proteins. Protein Co-IP was verified via Western blot analysis. About 3% from total lysate was used as input control, and the rest of the sample was utilized in the CCND3 immunoprecipitation experiment, this might be the reason why CCND3 was not detected in all lysate fractions (Figure 5-6 Column 1). CCND3 was detected in eluted fraction and as bound to beads, in flow-through of isotype control, and lysate (4 out of 6 immunoprecipitations) (Figure 5-6 Column 2 to 4), indicating that CCND3 immunoprecipitation worked. EBF1 was not co-immunoprecipitated together with CCND3 in any of the used condition, it was detected in the flow-through of CCND3 immunoprecipitation and isotype control. This suggests that glycerol does not affect EBF1 and CCND3 binding as removal of the glycerol from the lysis buffer did not result in EBF1 pulldown together with CCND3 (Figure 5-6 Column 3, Row 2). Decrease in NP-40 or addition of DTT did not result in EBF1 pulldown together with CCND3 (Figure 5-6 Column 4, Row 1 and Row 2), suggesting that 1% NP-40 does not induce the change in conformation that prevents binding of CCND3 and EBF1. Moreover, CCND3 and EBF1

potentially does not form non-specific intramolecular disulfide linkage that may prevent their interaction, because no prey protein was detected in the eluate, when 1 μ M DTT was add to lysis buffer.

I was not able to reproduce observations reported by a postdoc using the same protocol and in the modified conditions. It might be that CCND3 and EBF1 do not associate directly or that their binding is cell phase specific. This, needs further investigation.

Figure 5-6 Optimizing EBF1 elution together with CCND3. *1_4 Ebf1^{fl/fl}RERT^{Cre}*:A-MuLV pro-B cells were harvested, washed with PBS, lysed using a varied concentration of Glycerol, NP-40 and DTT in the lysis buffer, sonicated and proteins were Co-IP using Protocol 2. CCND3 mouse monoclonal antibodies were coupled to A/G PLUS-agarose, normal mouse IgG antibodies coupled to A/G PLUS agarose, were used as isotype control (IC). Protein elution was verified via Western blot analysis, FT- flow through.



Chapter 6 Investigating whether the unique NM function of EBF1 and CCND3 is mediated by B-cell specific CCND3 and/or EBF1 association partners

In the data reported above I have shown that EBF1 depletion causes *Ebf1^{fl/fl}RERT^{Cre}::A-*MuLV pro-B nuclear collapse. As well EBF1 seems to be a NM protein, suggesting unanticipated functions for EBF1. Here I have shown that *Ebf1^{fl/fl}RERT^{Cre}::A-*MuLV pro-B cells are arrested at the G1 phase and CCND3 level decreased upon EBF1 depletion and EBF1 co-localized with nuclear CCND3. Although, I was not able to reproduce EBF1 interaction with CCND3 seen by a postdoctoral researcher in Gyory lab, it was hypothesized that EBF1 and CCND3 might have a common B-cell unique NM binding partner, through which EBF1 supports the pro-B cell nuclear structure.

6.1 Possible B-cell specific EBF1 association partners identified by immunoprecipitation and MS

In order to investigate NM binding partners of EBF1 in pro-B cells, EBF1 was immunoprecipitated from 1_4 *Ebf1^{fl/fl}RERT^{Cre}::A-*MuLV pro-B cells. EBF1 rabbit polyclonal antibodies were cross-linked to Pierce Co-IP kit beads. Due to some proteins may bind unspecifically to the beads or to the rabbit IgG, normal rabbit IgG antibodies crosslinked with beads and beads on their own were used as control. The list of the proteins obtained after MS analysis then were assessed and the non-specific proteins that were detected in the bead and isotype controls were removed from the list of proteins that were pulldown using beads crosslinked with EBF1 antibodies. This gave a total of 39 potential EBF1 binding partners (Table 6-1). None of these proteins was previously reported to be EBF1 binding partners. CCND3 was not detected. This might be due to the overall sensitivity of the experiment being low, having returned only six peptides of the bait EBF1 protein. For most of the detected proteins, the total unique peptide count for individual protein was below five. The experiment may need to be scaled up to detect less abundant binding partners.

Serine and arginine-rich splicing factor 2 (SRSF2) and Ribosomal protein L14 (RPL14) that were previously reported as NM structural proteins (Engelke, Riede et al. 2014) were found as potential EBF1 binding partners, suggesting that these might be involved in the nuclear blebbing upon EBF1 depletion. Structural proteins such as Galectin-9 (LGALS9), Metadherin (MTDH), Rho GDP-dissociation inhibitor 2 (ARHGDIB, also known as RHOGDI2), Septin 11 (SEPT11), Keratin 78 (KRT78), Keratin 17 (KRT17) were identified as potential EBF1 binding partners, but none of these proteins were reported as NM protein. The ratio between peptide numbers of the pulldown structural protein to that of bait protein EBF1 is above 0.5, where the ration for SRSF2 and LGALS9 binding to EBF1 is 1.2 and for MTDH 0.9, suggesting their strong association with EBF1. LGALS9 and MTDH are localized to the nuclei. ARHGDIB, KRT78, KRT17 and SEPT11 are mostly cytoplasmic but are detected to a lesser extent in nuclei. The high ratio of the peptide number of LGALS or MTDH and EBF1 might be due to these proteins are predominantly nuclear. In order to test whether one of these proteins support EBF1 structural matrix function, their association with EBF1 needs to be verified independently by further Co-IP studies followed by Western blotting.

Table 6-1 EBF1 binding partners detected via MS in 1_4 *Ebf1^{f/f}RERT^{Cre}::A-MuLV pro-B cells*. EBF1 was immunoprecipitated using Pierce Co-IP kit; eluted samples were sent for MS analysis. Potential EBF1 binding partners were grouped by their primary function. Previously reported NM proteins are presented in red.

Functions	EBF1 potential binding partners
Apoptosis	SOD2
Chromatin reorganisation	ANP32A, PSMB3
Metabolism	DLAT, IDH3B, HADHB, SLC25A5, P4HB, ATIC
Protein folding	HSPE1
Replication and transcription	MCM7
Signalling	EWSR1
Splicing	PPP1R12A, <i>SRSF2</i> , DDX39B
Structural	LGALS9, MTDH, ARHGDIB, ATP5O, SEPT11, KRT78, KRT17
Transcription	SUB1, TARDBP, EIF1AX
Translation	FAU, YBX2, RPL22L1, <i>RPL14</i> , RPS15, EIF2S1, EIF4G1, POLDIP3, GM8994, EIF3K, LYAR
Transportation	CAPRIN1, PDCD6IP

6.2 Possible B-cell specific CCND3 association partners identified by immunoprecipitation and MS

CCND2 is ubiquitously expressed in various cell types. CCND1 expression is enhanced in the parathyroid gland, while CCND3 is expressed higher in lung tissues, adrenal glands, placenta, bone marrow and immune system (Figure 1-6 A). In bone marrow and immune system, CCND1 and CCND2 expression is low (Uhlen, Fagerberg et al. 2015) (Figure 6-1).

CCND expression is dependent on the differentiation status of hematopoietic cells. CCND3 is expressed in HSCs and MPP at low levels; its levels increase three times in CLP (Passegue, Wagers et al. 2005). Low levels of CCND3 are detected in the early pro-B cell and the expression increases during the pro-B cell maturation into pre-B cells and in GC cells (Cooper, Sawai et al. 2006) (Figure 1-6 B). Moreover, it was previously shown that CCND3 is localized to the NM in pro-B cells and CCND3 detachment from NM leads to the IgL chain V and J kappa locus ($V_{\kappa}J_{\kappa}$) recombination and subsequent pro-B cell maturation into pre-B cells (Karki, Kennedy et al. 2018).

CCND3 might have B cell unique functions. I, therefore, sought B-cell specific binding partner using immunoprecipitation and MS. B-cell specific partners of CCND3 detected in the pro-B cells were compared to CCND3 binding partners from MPI-2 - another immature haematopoietic cell type in which EBF1 is not expressed (Fejer et al., 2013).

Western blot analysis showed that CCND3 in 1_1, 1_3, 1_4 *Ebf1^{fl/fl}RERT^{Cre}::A*-MuLV pro-B cells is expressed at higher levels than in MPI-2 cells (Figure 6-2 A). Moreover, confocal imaging has shown that CCND3 in 1_3 *Ebf1^{fl/fl}RERT^{Cre}::A*-MuLV pro-B cells is mostly localized to the nuclei, while in MPI-2 the distribution between the cytoplasm and the nuclei varied from the individual cell to cell (Figure 6-2 B). The reason for the observed CCND3 localization in MPI-2 cells was not investigated.

Figure 6-1 CCND RNA expression in Bone marrow and immune system (Uhlen, Fagerberg et al. 2015)

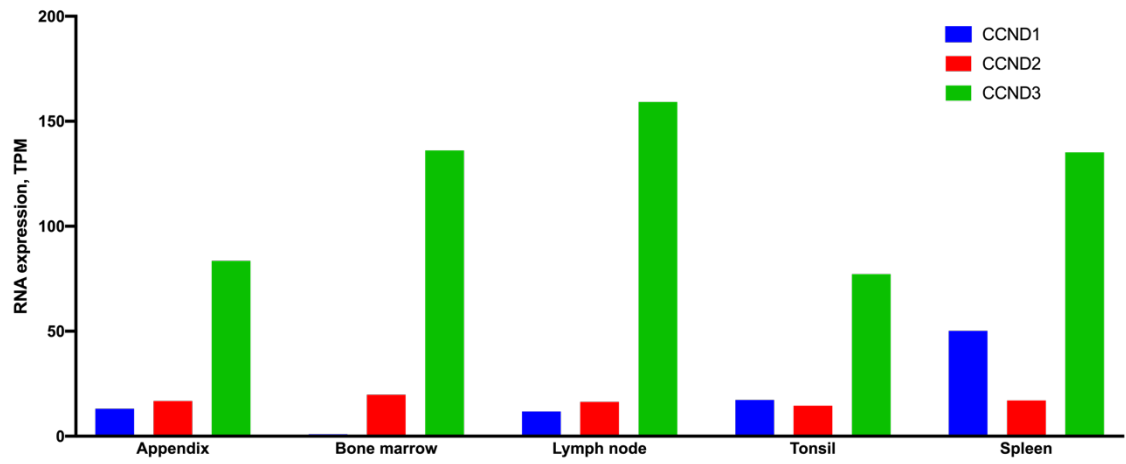
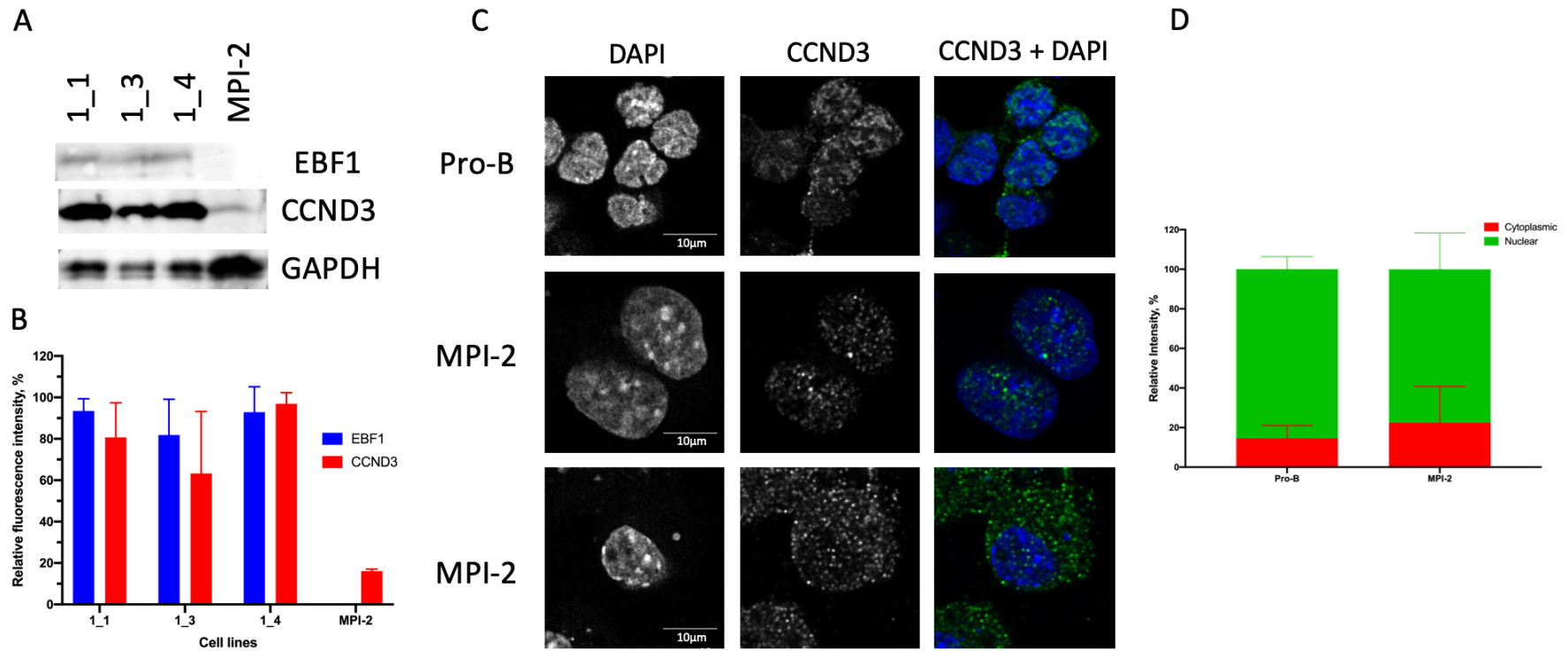


Figure 6-2 CCND3 expression in *Ebf1^{fl/fl}RERT^{Cre}::A-MuLV pro-B* and MPI-2 cells. Cells were lysed and proteins were separated via acrylamide gel electrophoresis, then proteins were transferred to nitrocellulose membrane and stained for EBF1, CCND3 and GAPDH. (A) Western blot analysis verifies EBF1 and CCND3 expression. (B) Relative CCND3 and EBF1 protein levels. CCND3 and EBF1 protein levels were normalized to GAPDH protein levels. (C) Cells were collected, washed with PBS, fixed in 4% PFA, then permeabilized using Perm buffer. Cells were incubated with primary CCND3 antibodies, followed by incubation with secondary Alexa Fluor 488 antibodies. Stained cells were cytopspun onto slides, air-dried and DNA was stained with DAPI. Confocal images of 1_3 *Ebf1^{fl/fl}RERT^{Cre}::A-MuLV pro-B* and MPI-2 cells stained for CCND3 (green) and DAPI (blue). (D) Average total intensity of the CCND3 in the nuclei and cytoplasm (from 50 cells; n = 3 experiments, ×10 magnification).

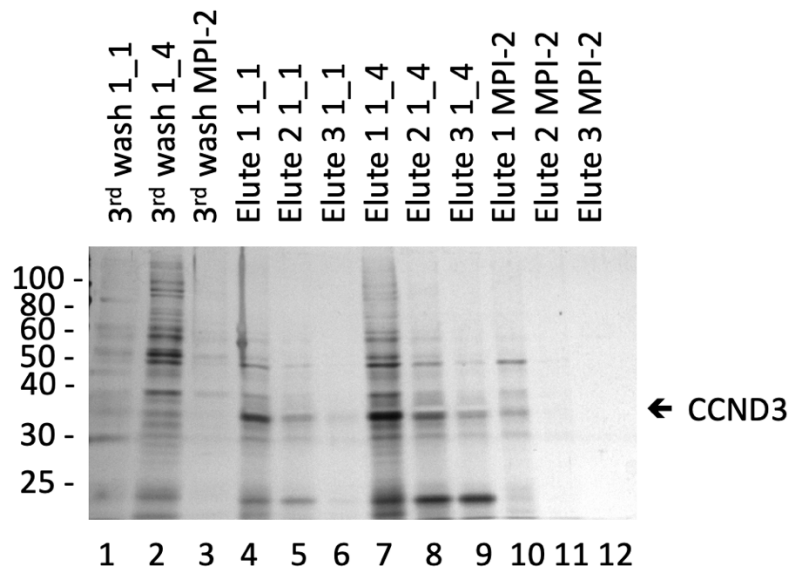


CCND3 was immunoprecipitated from 1_1 *Ebf1^{fl/fl}RERT^{Cre}::A*-MuLV pro-B cells (once), 1_4 *Ebf1^{fl/fl}RERT^{Cre}::A*-MuLV pro-B cells (three times) and MPI-2 cells (once). CCND3 immunoprecipitation was confirmed via gel silver staining (Figure 6-3 A). After the first exploratory experiment, the two follow-up CCND3 immunoprecipitations from 1_4 *Ebf1^{fl/fl}RERT^{Cre}::A*-MuLV pro-B cells were performed using isotype and bead controls. CCND3 elution was verified *via* acrylamide gel silver staining (Figure 6-3 B). Although CCND3 size band was detected *via* acrylamide gel silver staining in the first eluted fractions of isotype (Figure 6-3 B, lane 3) and bead control (Figure 6-3 B, lane 1), *via* Western blot analysis CCND3 was detected only in the eluted fraction of CCND3 immunoprecipitation (Figure 6-3 C). The initial experiment is considered as preliminary, the Gyory lab will perform fully controlled pulldown experiments in the future to find out which association partners are shared between parallel pro-B cell lines and which are unique to B cells or MPI cells. The current work focuses on the association partners of CCND3 in 1_4 *Ebf1^{fl/fl}RERT^{Cre}* cells.

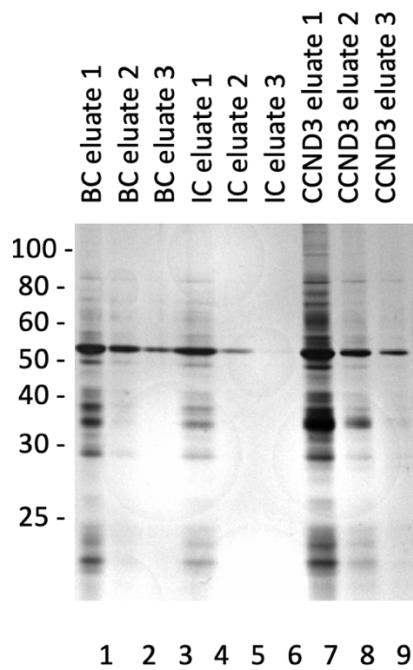
The total peptide count for CCND3 and total peptide count for all detected proteins was much higher in 1_4 *Ebf1^{fl/fl}RERT^{Cre}::A*-MuLV pro-B cells CCND3 immunoprecipitation compared to 1_1 *Ebf1^{fl/fl}RERT^{Cre}::A*-MuLV pro-B and MPI-2 cells, which resulted in the higher number of detected potential binding partners in 1_4 *Ebf1^{fl/fl}RERT^{Cre}::A*-MuLV pro-B cells (Figure 6-4 and Figure 10-4). It was expected as CCND3 was detected in three elution fractions, when CCND3 was immunoprecipitated from 1_4 *Ebf1^{fl/fl}RERT^{Cre}::A*-MuLV pro-B (Figure 6-3 A), while from 1_1 *Ebf1^{fl/fl}RERT^{Cre}::A*-MuLV pro-B CCND3 was eluted in the two first fraction and from MPI-2 cell lysates CCND3 was detected only in the first eluate. The following immunoprecipitation of CCND3 from 1_4 *Ebf1^{fl/fl}RERT^{Cre}::A*-MuLV pro-B cells detected lower levels of CCND3 peptides and consequently lower levels of total peptide count for all proteins. This suggests that MS experiments need repeating by scaling up the number of cells used in the experiment.

Figure 6-3 Verifying CCND3 immunoprecipitation. 1_1, 1_4 *Ebf1^{fl/fl}RERT^{Cre}*::A-MuLV pro-B and MPI-2 cells were harvested and lysed. Lysates were incubated with CCND3 antibody coupled resin. After incubation, flow through was collected, resin was washed and CCND3 was eluted. CCND3 elution from 1_1, 1_4 *Ebf1^{fl/fl}RERT^{Cre}*::A-MuLV pro-B and MPI-2 cells was then assessed *via* acrylamide gel silver staining (B and C). Assessment of the second CCND3 pull-down from 1_4 *Ebf1^{fl/fl}RERT^{Cre}*::A-MuLV pro-B cells (B) via acrylamide gel silver staining and (C) Western blot analysis.

A



B



C

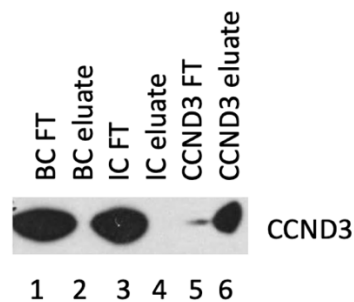
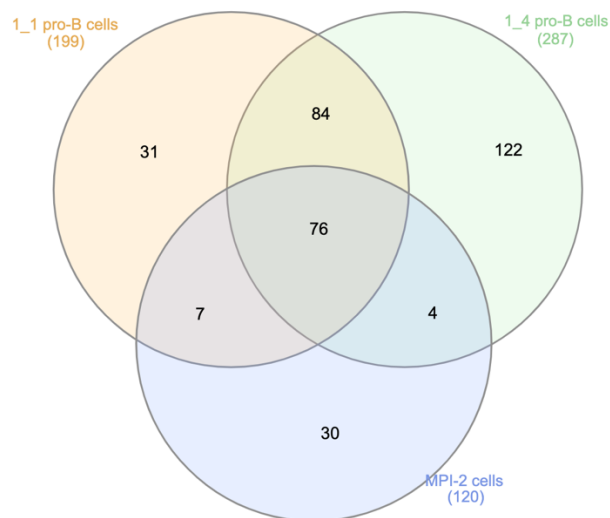


Figure 6-4 The number of potential binding partners of CCND3 that are unique and common in 1_1 and 1_4 *Ebf1^{fl/fl}RERT^{Cre}*::A-MuLV pro-B cells and MPI-2 cells. 1_1, 1_4 *Ebf1^{fl/fl}RERT^{Cre}*::A-MuLV pro-B and MPI-2 cells were harvested and lysed. Lysates were incubated with CCND3 antibody coupled resin. After incubation, flow through was collected, resin was washed and CCND3 was eluted. The verified eluates were run into 12% acrylamide gel and proteins were in gel digested with trypsin. Peptides were analysed with short-gradient LC-MS/MS. The list of CCND3 potential binding partners (Figure 10-4) in different cell lines was assessed using Venn diagram.



MS analysis detected such known CCND3 binding partners as CDK5 (Varjosalo, Keskitalo et al. 2013), CDK4 (Lundberg and Weinberg 1998), Cyclin-dependent kinase inhibitor 2C (CDKN2C) (Huttlin, Ting et al. 2015), CDKN1A and CDKN1B (Datta, Williams et al. 1998), Proliferating cell nuclear antigen (PCNA) (Matsuoka, Yamaguchi et al. 1994), Eukaryotic translation initiation factor 3 subunit K (EIF3K) (Shen, Yang et al. 2004) in 1_1, CDKN1B, CDK4, PCNA, EIF3K in 1_4 and CDK4, CDKN1B in MPI-2 cells. Four, ten and 63 cell-type unique binding partners of CCND3 were detected, respectively, in MPI-2, 1_1 and 1_4 *Ebf1^{fl/fl}RERT^{Cre}*::A-MuLV pro-B cells (Table 6-2).

Table 6-2 Functions of potential CCND3 binding partners in *Ebf1^{fl/fl}RERT^{Cre}::A*-MuLV pro-B and MPI-2 cells. CCND3 was immunoprecipitated using Pierce Co-IP kit from 1_4 and 1_1 *Ebf1^{fl/fl}RERT^{Cre}::A*-MuLV pro-B and MPI-2 cells, eluted samples were sent for MS analysis. Potential CCND3 binding partners were grouped by their primary function. In bold are presented newly detected, and cell type unique proteins, highlighted in yellow are previously reported CCND3 binding partners. Previously reported NM proteins are presented in red.

Functions	1_1 pro-B cells	1_4 pro-B cells	MPI-2 cells
Replication and transcription	PCNA	PCNA , MCM2, MCM3, MCM6, RFC4	
Cell growth and division, cell cycle	PPP2R1A, TPT1, CDK4 , CDK5 , CDKN2C , NUCKS1 , CDKN1A , CDKN1B , FUBP1	BZW2 , PPP2CA, PPP2R1A, PPP2R4 , TPT1, CDK4 , CDK5 , CDKN2C , CDKN1A , CDKN1B , FUBP1, DES	S100A4 , S100A10 , PPP2R1A, TPT1, CDKN2D , CDK4 , CDKN1B ,
Chromatin reorganisation	HMGB2, HIST2H2BE, HIST1H2AA, HIST1H3B , H2AFZ, ANP32A , ANP32B, MAPRE1	HMGB2, HIST1H2AA, HIST1H3B , H2AFZ, ANP32A , ANP32B, NASP , ANP32E , H3F3C , MAPRE1, RPS2 , HIST1H2AB	H1FO , HIST1H2AA, H2AFZ, ANP32B, MAPRE1
Degradation	CNPY2 , KXD1, PSMA2, PSMA3 , PSMA4, PSMA5, PSMA6 , PSMA7, PSMB1 , PSMB2 , PSMB3, PSMB4 , PSMB8 , PSMD1, PSMD11, PSMD12, PSMD13, PSMD5 , PSMD6, PSMD7, PSME1, PSME2, PSME3 , UBA1 , UBE2N , VHL, CAND1 , PSMA1, PREP	KXD1, PREP, PSMA2, PSMA3 , PSMA4, PSMA5, PSMA6 , PSMB1 , PSMB3, PSMB4 , PSMB8 , PSME1, PSME2, PSME3 , PSMA7, PSMC6 , PSMC4 , PSMD1, PSMD11, PSMD12, PSMD13, PSMD3 , PSMD7, UBA1 , UBE2N , UCHL3 , USP14 , VCP, CAND1 , PSMA1, SMR3B , C3	KXD1, PSMA2, PSMA4, PSMA5, PSMA6 , PSMA7, PSMB3, PSMD1, PSMD11, PSMD12, PSMD13, PSMD6, PSMD7, PSME1, PSME2, RPN2 , VCP, VHL, PSMA1, CAPNS1 , LYZ2 , PREP
Splicing	GM6793 , NHP2L1 , SNRPB	ELAVL1 , DDX39B , GM6793 , SF3A3 , SNRPA , SNRPB , SRSF2 , SRSF3 , TARS , RBM3 , PRR4 , SRSF1 , SNRPE , SNRPA1 , RBM39	SRSF1

Continued...

Continued...

Functions	1_1 pro-B cells	1_4 pro-B cells	MPI-2 cells
Signalling	KCTD12, G3BP1, PDCD6, ARHGDIA, ARHGDIB, CAP1, FAM49B, GDI2, GNB2L1, IQGAP1, LCP1, PEBP1, SRI, TAGLN2, STRAP, ANXA5, YWHAB, IPO5, ANXA7, BAX, CALM1, ILF2, ANXA6, ANXA11, YWHAQ, COPS4, COPS8,	ANXA6, G3BP1, PDCD10, PDCD6, PPIB, RCC2, ARHGDIA, ANXA5, ANXA11, LARS, CAMK2D, ARHGDIB, CAP1, FAM49B, GBP2, GDI2, GNB2L1, IQGAP1, LCP1, PEBP1, SRI, TAGLN2, STRAP, YWHAB, YWHAQ, BPIFA2, PIGR, COPS4, COPS8,	ARHGDIA, ANXA5, ANXA1, ARHGDIB, CAP1, GDI2, GNB2L1, IQGAP1, LCP1, REEP5, TAGLN2, STRAP, YWHAB, IGKC, ANXA4, RAB7A, CAPNS1
Metabolism	CS, ADSL, APRT, CTH, DBI, ECHS1, EPRS, ERO1L, ESYT1, ETFA, FDPS, GOT1, GRPEL1, GSTP1, HADHA, IDH3A, MDH1, MTAP, P4HA1, PCMT1, PGAM1, PGAM2, PGD, PGK1, PRDX3, PRDX4, PRDX6, PRKCSH, PSAT1, RARS, SHMT1, TALDO1, HINT1, PRDX5, PCK2, AKR1B1, AHCY, AK2, ATIC, ATP6V1A, ALDH1B1, ALDH2, ACLY, HPRT1, ACAT1	CS, CMPK1, CTH, DARS, DBI, EPRS, ERO1L, ETFA, FASN, FDPS, GM17190, GOT1, GSTP1, HADHA, IARS, IDH3A, MDH1, MTAP, PAFAH1B2, PCMT1, PGD, PGK1, PRDX3, PRDX4, PRDX6, PRKCSH, PTGR1, RANBP1, RARS, SARS, SHMT1, TALDO1, TXNL1, UMPS, YARS, HINT1, PRDX5, ASNS, PCK2, CA2, ADSS, AKR1B1, AHCY, AK2, ATIC, ATP6V1A, ALDH1B1, ACADL, ALDH2, ACO2, ACLY, P4HA1, CLTA, CSE1L, ACAT1, GART, ECHS1, DLD, MTHFD1, PGAM1, CLTA, ZG16B, AMY1A, BLMH, CALML5, CST1, CST4, CA6	CNDP2, ESD, FDPS, PCMT1, PGAM1, PGD, PGK1, TALDO1, ATP6V1A, ALDH2, ACLY, P4HA1
Apoptosis	MZB1, PDCD6IP, SOD1, SOD2, STK26, STK4, API5	MZB1, PDCD6IP, SOD1, SOD2, STK26, STK4, GIMAP4, API5	MZB1, LGALS3, SOD2

Continued...

Continued...

Functions	1_1 pro-B cells	1_4 pro-B cells	MPI-2 cells
Protein folding	HSP90B1, NAP1L4 , CCT6A, CALR, HSPE1 , HSPH1 , PDIA3, PDIA6, PPIA, ERP29 , DNAJC9 , ERAP1	HSP90B1, DNAJB11 , NAP1L4 , STIP1 , CCT6A, CALR, GANAB , HSPE1 , HSPH1 , PDIA3, PDIA4 , PDIA6, PPIA, PPP1R7 , SDF2L1 , ST13 , ERP29 , PPID , DNAJC9 , ERAP1	HSP90B1, CCT6A, CALR, PDIA3, PDIA6, PPIA
Transcription	HDGF , HSPA4 , HYOU1 , NACA , OTUB1 , PARK7 , SARNP , TCEB1 , KHSRP , TCEB2	HDGF , HSPA4 , HYOU1 , MYBBP1A , NACA , OTUB1 , SARNP , SND1 , TCEA1 , TCEB1 , TXNRD1 , DDX3X , KHSRP , TCEB2 , SERPINA1	HSPA4 , HYOU1 , NACA , TCEB1 , TCEB2
Homeostasis	FTH1 , FTL1	FTH1 , FTL1	FTH1
Translation	EEF2 , EIF3E , EIF3F , EIF3K , EIF3L , EIF4A1 , EIF4H , EIF6 , NOLC1 , PCBP2 , RPLP2 , RPS12 , RPS21 , RPS8 , VARS , SAE1 , FAU , GM5039 , HNRNPC , PCBP1 , VAT1 , EIF3H , AHNAK , HNRNPD ,	EEF2 , EIF3A , EIF3B , EIF3C , EIF3E , EIF3F , EIF3K , EIF3L , EIF4A1 , EIF4H , EIF6 , GARS , HNRNPL , NOLC1 , PCBP2 , RPLP2 , RPS12 , RPS15A , RPS21 , RPS24 , RPS28 , RPS8 , VARS , AARS , GM10036 , SAE1 , NAA15 , EIF2S3X , TAF15 , RPS6 , RPL39 , RRS1 , HNRNPD ,	EEF2 , EIF3F , EIF3I , EIF3L , EIF4A1 , EIF6 , RPL13A , RPS11 , RPS12 , RPS6 , RPS8 , HNRNPC , PABPC1 , RPL10A , RPL13 , RPL38 , PCBP1 , VAT1 , AHNAK
Transportation	ARF3 , CLIC1 , RAB11B , RAB5C , SLC3A2 , VAT1 , XPO1 , TOMM34 , COPS3 , ARPC5 , CLTC	BIN1 , ARF4 , ARF3 , CLIC1 , NSFL1C , SLC3A2 , VPS35 , XPO1 , TOMM34 , CLTC , IPO7 , TNPO1 , FKBP4 , IGHA1 , KPNA4 , LCN1 , TF	ARF3 , ANXA4 , CLIC1 , KPNA2 , RAB14 , RAB5C , VAT1 , CLTC
Structural	CFL1 , LGALS1 , PFN1 , VASP , TLN1 , DPYSL2 , EZR , KRT8 , ACTR2 , MSN , DSP , RAC1 , ATP5O	STMN1 , CFL1 , LGALS1 , FERMT3 , CBX3 , PFN1 , VASP , TLN1 , DPYSL2 , PAK2 , EZR , ACTR2 , SEPT2 , SEPT7 , MSN , MYH9 , PRPH , TUBB4B , PKP1	FLNA , CFL1 , LGALS1 , PFN1 , VASP , TLN1 , TUBA1A , DPYSL2 , LGALS3BP , LMNA , ACTR2 , CAPG , JUP , MYH9

Proteasome Subunit Alpha 6 (PSMA6), Thioredoxin Like 1 (TXNL1), SRSF2, SRSF3, SRSF1, RNA Binding Motif Protein 39 (RBM39), DEAD-Box Helicase 3 X-Linked (DDX3X), EIF3E, Eukaryotic Translation Initiation Factor 6 (EIF6), Nucleolar and Coiled-Body Phosphoprotein 1 (NOLC1), Ribosome Biogenesis Regulator 1 Homolog (RRS1), MYBBP1A and Heterogeneous Nuclear Ribonucleoprotein L (HNRNPL) are potential CCND3 binding partner that have been previously reported as NM structural proteins (Engelke, Riede et al. 2014) and might be a part of NM proteome in pro-B cells. PSMA6, SRSF1 and EIF6 have been detected as potential binding partners of CCND3 in pro-B cells and MPI-2 cells. The ratio of the peptide number of the pulldown PSMA6, SRSF1 and EIF6 and the bait protein CCND3 was, respectively, 0.5, 0.4 and 0.2 in pro-B cells and 0.4, 0.2 and 0.3 in MPI-2 cells, suggesting that there is a moderate to strong interaction between the CCND3 and PSMA6 and weak to moderate between CCND3 and SRSF1 and EIF6 in the corresponding cell lines. TXNL1, SRSF2, SRSF3, RBM39, DDX3X, EIF3E, NOLC1, RRS1, MYBBP1A and HNRNPL are pro-B cell unique potential binding partners of CCND3. The ratio between peptide numbers of EIF3E, MYBBP1A and HNRNPL to that of bait protein CCND3 was respectively, 0.7, 0.6 and 0.5, suggesting that there is a moderate to strong interaction between the CCND3 and EIF3E, MYBBP1A and HNRNPL. The ratio between peptide numbers of TXNL1, SRSF2, SRSF3, RBM39, DDX3X, NOLC1, RRS1 and the bait protein CCND3 was below 0.3, suggesting that there is a weak to moderate between CCND3 and TXNL1, SRSF2, SRSF3, RBM39, DDX3X, NOLC1 and RRS1.

Structural regulatory proteins Ezrin (EZR), Moesin (MSN) and Desmin (DES) were detected only in the pro-B cells, while Filamin A (FLNA) and LMNA are MPI-2 specific (Table 6-2). The ratio of the peptide number of the pulldown EZR, MSN, DES, FLNA and LMNA and the bait protein CCND3 was, respectively, 1.6, 2.3 and 0.6 in pro-B cells, 1.6, 0.9 in MPI-2 cells, suggesting that there is a strong interaction between the CCND3 and structural proteins in the corresponding cell lines. It was previously shown that pro-B cells do not express LMNA, and in the previous experiments in our lab, LMNA was not detected in any of pro-B cell lines (Rober, Sauter et al. 1990). FLNA crosslinks actin filaments and links actin filaments to membrane glycoproteins. DES is a cytoskeletal protein that is essential for proper muscular structure and function. Also, it is not clear if DES has a unique function in lymphocytes. MSN and EZR belong to EZR, RADIXIN and MSN (ERM)

proteins which act as a crosslinker between plasma membranes and actin-based cytoskeletons (Neisch and Fehon 2011). MSN was reported to be important in T and B-cell homeostasis and self-tolerance. It might be that CCND3 regulates B-cell self-tolerance and homeostasis through binding to MSN, this needs further investigation.

Endoplasmic reticulum aminopeptidase 1 (ERAP1), Valyl-tRNA synthetase (VARS) and Polymeric Immunoglobulin receptor (PIGR) were identified as CCND3 B-cell specific potential binding partners (Table 6-2). ERAP1 is involved cleaving proteins into peptides prior their exportation and attachment on major histocompatibility complex (MHC) class I molecules, while VARS catalyses the aminoacylation of tRNA and is localized at the regions of the MHC (Klein and Sato 1998). PIGR is a polymeric immunoglobulin receptor, which facilitates transcytosis of IgA and IgM. It was previously reported that CCND3 attaches on the nuclear structural matrix represses pro-B cell differentiation into pre-B cells. It might be that CCND3 through binding to ERAP1, VARS and/or PIGR regulates pro-B cell maturation into pre-B cells. The ratio of the peptide number of the pulldown VARS, ERAP1 or PIGR and the bait protein CCND3 was, respectively, 1.6, 0.7 and 0.9, suggesting that there is a strong interaction between the CCND3 and B-cell specific proteins. Thus, CCND3 interaction with these protein needs further exploration.

Acidic nuclear phosphoprotein 32 family member A (ANP32A) was detected in both 1_1 and 1_4 *Ebf1^{fl/fl}RERT^{Cre}::A*-MuLV pro-B cells, while ANP32B was detected in MPI-2 cells. Although ANP32A and ANP32B hold high sequence identity, ANP32A is a part of the inhibitor of histone acetyltransferase complex (INHAT), while ANP32B does not hold any inhibition properties. Thus, CCND3 binding to this protein might result in different function within the pro-B cells. However, if ANP32A is expressed in MPI-2 cells, it might bind to CCND3 within MPI-2 cells. This could be verified by scaling up immunoprecipitation of CCND3 using MPI-2 cells.

Another exciting and pro-B cell unique binding partner is Chromosome segregation 1 like (CSE1L). CSE1L regulates importin-alfa export from nuclei into the cytoplasm. Protein import from the cytoplasm to nuclei is regulated by importin-alfa binding to nuclear localization signal (NLS) within a protein. CCND3 does not have the NLS, and it is unclear

how CCND3 is imported and exported from nuclei. Exploring CSE1 and CCND3 binding might bring clarity on CCND3 import and export from and to nuclei.

Constitutive photomorphogenesis 9 (COP9) signalosome subunit 4 (COSP4) and COSP8 which are a part of eight subunits composing COP9 signalosome were detected in 1_1 and 1_4 *Ebf1^{fl/fl}RERT^{Cre}*::A-MuLV pro-B cells but were not detected in MPI-2 cells. COP9 signalosome is involved in protein degradation through deactivation of Cullin-RING ubiquitin ligase (Bosu and Kipreos 2008); thus CCND3 bound to COSP4 and COSP8 most likely was marked for degradation.

Although, it seemed that in pro-B cells, CCND3 had a high number of B-cell unique binding partners, some of these proteins share structural and functional similarity with the proteins detected in the MPI-2 cells. To name a few, Tubulin Alpha 1a (TUBA1A) detected in the MPI-2 cells and Tubulin Beta 4B class IVb (TUBB4B) detected in 1_4 *Ebf1^{fl/fl}RERT^{Cre}*::A-MuLV pro-B cell lines are the constituents of the microtubules, Annexin A1 (ANXA1) was detected in the MPI-2 cells only, while a number of Annexing family members were detected as binding partners of CCND3 in the pro-B cells. EIF3E is a component of the eukaryotic translation initiation factor 3 (eIF-3) complex, which is required for several steps in the initiation of protein synthesis, was detected only in 1_4 and 1_1 *Ebf1^{fl/fl}RERT^{Cre}*::A-MuLV pro-B cells. However, the other components of eIF-3 complex EIF3F, EIF3L were detected in both pro-B cells and MPI-2 cells. Due to all these protein belonging to one complex, these binding partners of CCND3 are not considered as cell-specific. Such Ribosomal protein subunits RPS15A (Ribosomal protein S15A), RPS21 were detected in the pro-B cells, while RPL10A, RPL13 RPL38 were detected in MPI-2, are part of ribosome catalyse protein synthesis.

Aldehyde dehydrogenase 1 family member B1 (ALDH1B1) a CCND3 binding partner detected in pro-B cells and ALDH2, a CCND3 binding partner, detected in MPI-2 cells belongs to the aldehyde dehydrogenases family of proteins which are involved in alcohol metabolism. Thus, ALDH1B1 is excluded from the list of B-cell specific CCND3 binding partners. The large number of CCND3 detected potential binding partners have a metabolic function and were detected in both MPI-2 and pro-B cell. Although Endoplasmic reticulum oxidase 1-alpha (ERO1L), Adenosyl homocysteinase (AHCY),

Cystathionine gamma-lyase (CTH), Adenylate kinase 2 (AK2), Asparagine synthetase (ASNS) and Citrate synthase (CS) were detected only in pro-B cells, these proteins are involved in various metabolic processes within the cells. It was previously reported that CCND3 is involved in cell metabolism (Wang, Nicolay et al. 2017), these partners might shed light to a novel function of CCND3, albeit not necessarily specific to the B lineage.

An important observation from the MS results was that EBF1 is absent in the immunoprecipitation of CCND3 and *vice versa*. It might be that the amount of EBF1 immunoprecipitated together with CCND3 bait was below the detection level of MS. Thus, EBF1 might be detected by scaling up the CCND3 Co-IP experiment. However, I was not able to co-immunoprecipitate EBF1 together with CCND3 and CCND3 together with EBF1.

6.3 EBF1 and CCND3 common binding partners

EBF1 depletion caused a decrease in CCND3 protein levels. It might be that EBF1 inhibits a CCND3 degradation activator, thus upon EBF1 depletion CCND3 degradation is activated via previously inhibited protein. On the other hand, EBF1 might stabilise CCND3 by retention in the nucleus by physical association. Thus, EBF1 and CCND3 might interact with the same NM proteins. In order to test this hypothesis, CCND3 and EBF1 were immunoprecipitated, and the eluates were analysed via MS for common CCND3 and EBF1 binding partner.

Superoxide dismutase 2, (SOD2), ANP32A, Heat shock protein family E (HSP10) member 1 (HSPE1), ARHGDIB, 5-aminoimidazole-4-carboxamide ribonucleotide formyl transferase/IMP cyclohydrolase (ATIC), Serine and arginine-rich splicing factor 2 (SRSF2), EIF3K, DExD-box helicase 39B (DDX39B), Programmed cell death 6 interacting protein (PPDCD6IP) and Proteasome subunit beta type-3 (PSMB3) were identified as common binding partners of EBF1 and CCND3 (Table 6-3). The ratio between peptide numbers of binding partner to that of bait protein EBF1 and the ratio between peptide numbers of binding partners - ANP32A, HSPE1, ARHGDIB, ATIC, PPDCD6IP, PSMB3 to that of bait protein CCND3 was above 0.5, suggesting that these proteins might have moderate to strong interaction with EBF1 or CCND3, respectively. The ratio between peptide numbers of the binding partner to that of bait protein CCND3 was below 0.5 for SOD2, PSMB3, SRSF2, DDX39B and EIF3K, suggesting that these proteins and CCND3 might have weak interaction or the binding is non-specific.

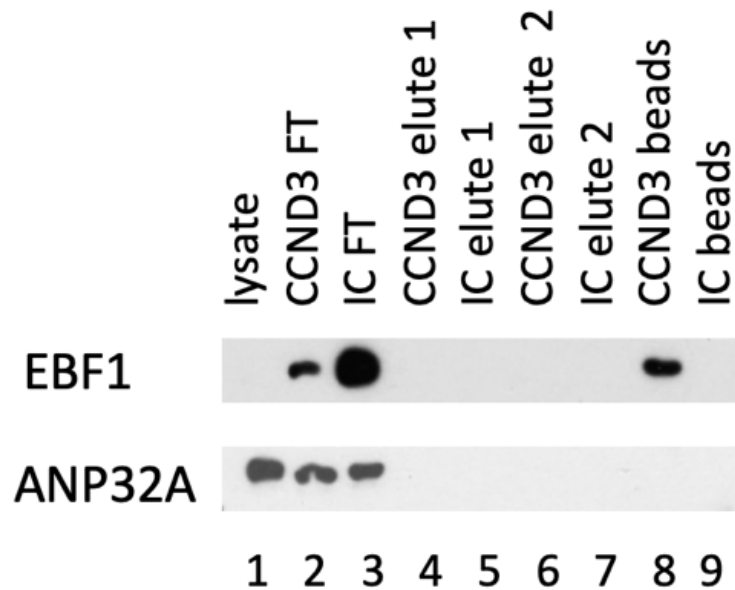
Table 6-3 Comparison of CCND3 and EBF1 binding partners. CCND3 and EBF1 were immunoprecipitated using Pierce Co-IP kit from 1_4 *Ebf1^{fl/fl}RERT^{Cre}::A*-MuLV pro-B cells, eluted samples were sent for MS analysis. Potential CCND3 and EBF1 binding partners were grouped by their primary function. Here are presented common binding partners of EBF1 and CCND3,. Previously reported NM protein is presented in red.

Functions	CCND3 and EBF1 potential common binding partners
Apoptosis	SOD2
Chromatin reorganisation	ANP32A
Degradation	PSMB3
Metabolism	ATIC
Protein folding	HSPE1
Signalling	ARHGDIB
Splicing	SRSF2 , DDX39B
Translation	EIF3K
Transportation	PDCD6IP

SRSF2 is a part of the spliceosome and is involved in splicing and was previously reported as NM protein (Engelke, Riede et al. 2014); thus it might play a role in rapid CCND3 protein level decrease upon EBF1 depletion. ARHGDIB is involved in multiple cellular processes, such as cell signalling, cytoskeletal organization and secretion. Due to its structural function within the cell, it could be that ARHGDIB, together with EBF1, is a structural NM protein. Thus, SRSF2 and ARHGDIB interaction with EBF1 and CCND3 need further investigation. DDX39B is involved in splicing. EIF3K is involved in translation. SOD2 is involved in apoptosis. HSPE1 enhances protein folding. ATIC is involved in de novo purine biosynthetic pathway. PDCD6IP is involved in cytokinesis and endosomal vehicle formation and apoptosis. PSMB3 is a proteasome subunit and is involved in protein degradation, while ANP32A is a part of the INHAT complex. The ratio of the peptide number of the pulldown ANP32 and the bait protein EBF1 or CCND3 was, respectively 0.7 and 0.8, suggesting that there might be a strong interaction between the proteins.

INHAT complex binds to histone tails preventing their acetylation, thus preventing chromatin unwinding. It could be hypothesised that EBF1 or CCND3 binding to ANP32A allows chromatin uncoiling and subsequent binding of transcription factors and transcription activation. EBF1 binding to ANP32A was tested via Co-IP and subsequent Western blot analysis. No binding was detected, indicating that EBF1 and ANP32A do not interact (Figure 6-5). Due to the time constriction, the other potential binding partners of EBF1 and CCND3 were not verified.

Figure 6-5 EBF1 does not interact with ANP32A. 1_4 *Ebf1^{fl/fl}RERT^{Cre}*::A-MuLV pro-B cells were harvested, washed with PBS, lysed and sonicated and proteins were Co-IP using Protocol 2. EBF1 rabbit polyclonal antibodies were coupled to A/G PLUS-agarose, normal rabbit IgG antibodies coupled to A/G PLUS agarose were used as isotype control (IC). Protein elution was verified via Western blot analysis, FT- flow through



Summarizing, the association between either CCND3 or CCNA2 and EBF1 was not detected despite extensive optimization of Co-IP conditions. The alternative approach of detecting the EBF1-CCN interaction by His-tag-pulldown faced the technical challenge of FLAG WT EBF1 binding to the Ni-NTA resin itself, suggesting that FLAG WT or mutant EBF1 purification with CCNA2 His was not a feasible method to detect the interaction. CCND3 or CCNA2 was not detected in the MS of EBF1 immunoprecipitation, and EBF1 was not detected in the MS of CCND3 immunoprecipitation from 1_1, 1_4 *Ebf1^{fl/fl}RERT^{Cre}::A-* MuLV pro-B cells and MPI-2 cells. However, MS analysis revealed 10 potential common binding partners of EBF1 and CCND3.

EBF1 and CCND3 co-localization and CCND3 relocation from the nuclei to the cytoplasm upon EBF1 depletion from pro-B cells could be due to EBF1 potentially has an important nuclear structural matrix function that might regulate CCND3 localization. Binding of EBF1 and CCND3 to a putative common NM structural protein and the complexity and function of their interaction needs further investigation.

Chapter 7 Discussion

EBF1 expression is initiated in CLPs and maintained through-out B-cell differentiation, except plasma cells. EBF1 depletion arrest cells at pro-B cell phase and blocks immunoglobulin rearrangement and suppresses cell differentiation into alternative lineages in both early and late stages of B-cell development, suggesting that EBF1 is essential B-cell fate restricting factor (Lin and Grosschedl 1995, Zhang, Cotta et al. 2003, Seet, Brumbaugh et al. 2004, Hagman and Lukin 2006, Nutt and Kee 2007, Lukin, Fields et al. 2008, Györy, Boller et al. 2012, Vilagos, Hoffmann et al. 2012). Moreover, ectopic EBF1 overcomes TCF3 depletion defect, which cannot be rescued by ectopic TCF3 (Lin and Grosschedl 1995). EBF1 is linked to both positive and negative regulation of genes at the transcriptional level (Treiber, Mandel et al. 2010). EBF1 has been reported to co-activate gene transcription together with RUNX1 (Maier, Ostraat et al. 2004) and TCF3 (Goebel, Janney et al. 2001). While such proteins as ETS, E-BOX, STAT1, NF- κ B, NRF1 and PAX5 have been proposed as EBF1 transcriptional co-regulators (Treiber, Mandel et al. 2010).

V-MuLV immortalized conditional knockout mouse pro-B cells, which expresses the Cre recombinase under the control of a tamoxifen-inducible promoter and depletes floxed *Ebf1* (*Ebf1^{fl/fl}RERT^{Cre}::A-MuLV*) (Treiber, Mandel et al. 2010, Györy, Boller et al. 2012) were used in the experiments. In *Ebf1^{fl/fl}RERT^{Cre}::A-MuLV* pro-B cells EBF1 directly activates transcription of proteins that are involved in cellular signal transduction machinery, metabolism, membrane transport and cytoskeleton and motility as well as causes conformation alternation of chromatin, establishing accessible promoter sites (Treiber, Mandel et al. 2010).

Here I shown EBF1 as a potential nuclear matrix protein in pro-B cells. The supporting findings are following: EBF1 depletion results in nuclear blebbing and increase in the levels of the heterochromatin at the periphery of the nuclei (Figure 4-9 and Figure 4-11) as well as EBF1 has been detected in the NM fraction (Figure 4-12).

7.1 EBF1 depletion causes nuclear blebbing of *Ebf1^{fl/fl}RERT^{Cre}::A-MuLV* pro-B cells and an increase in the levels of the heterochromatin at the periphery of the nuclei

Nuclear blebbing severity upon EBF1 depletion was assessed from 3D confocal images. The percentage of cells with high nuclear blebbing increased more than twice after three days of OHT-induced EBF1 depletion. The change in heterochromatin localization after two days of OHT-induced EBF1 was observed via EM. Heterochromatin in cells is usually localized at the periphery of the nuclei and in the body of the nuclei. EBF1 depletion causes an increase in the levels of the heterochromatin at the periphery of the nuclei and a substantial decrease in the levels of the heterochromatin in the body of the nuclei (Figure 4-9). Heterochromatin compared to euchromatin has a higher density; thus, the activity of the genes in the heterochromatin is modified or suppressed. HDAC3, together with NCOR and SMRT, forms a complex that anchors heterochromatin to the inner side of the nuclear membrane. It was previously reported that in apoptotic cells chromatin condensation is observed as distinct heterochromatin clumps which are localized mostly at the periphery of the nuclei (Widlak, Palyvoda et al. 2002, Schmitt, Pelzel et al. 2014). However, nuclear envelope in apoptotic cells remains morphologically intact (Earnshaw 1995). An important fact is that NM proteins such as topoisomerase II α (Casiano 1997), Nuclear mitotic apparatus *protein* (NuMA) (Gueth-Hallonet, Weber et al. 1997), scaffold attachment factor A (SAF-A) (Kipp, Schwab et al. 2000), Lamin B1 (Dymlacht, Story et al. 1999), LMNA (Takahashi, Alnemri et al. 1996), and SATB1 (Gotzmann, Meissner et al. 2000) are cleaved during apoptosis (Martelli, Bareggi et al. 1997). It is not clear whether proteolysis of NM proteins is the cause or the consequence of the apoptosis (Martelli, Falcieri et al. 2002). There is a possibility that EBF1 depletion causes apoptosis through activation of positive or deregulation of negative regulators of apoptosis. For example, NF- κ B, which has been proposed as potential transcriptional co-activator together with EBF1, has been shown to block apoptosis (Beg and Baltimore 1996). It might be that EBF1 depletion blocks transcription of apoptosis suppressors. However, due to EBF1 depletion results in nuclear blebbing, which was not reported as apoptotic cell feature, it is more likely that EBF1 induces a change in NM proteome, which significantly affects cellular processes and results in apoptosis. This needs further investigation.

7.2 HDAC3 inhibitors does not rescue EBF1 depleted *Ebf1^{fl/fl}RERT^{Cre}::A*-MuLV pro-B cells from nuclear blebbing

In EBF1 depleted cells, more chromatin associated with the nuclear membrane than usually. HDAC3 knockout in fibroblasts resulted in a dramatic decrease of the heterochromatin (Zullo, Demarco et al. 2012). Heterochromatin formation was not observed upon HDAC3 knockdown in apoptotic RGC, but HDAC3 knockdown potentiated cell death (Schmitt, Pelzel et al. 2014). Moreover, recently, it was shown that HDAC3/NCOR/SMRT complex is essential in the regulation of B cell development, due to HDAC3 depletion resulted in $V_{H}D_{H}J_{H}$ defect (Stengel, Barnett et al. 2017). Thus, it was hypothesized that HDAC3 inhibitors would prevent excessive relocation of chromatin to the nuclear periphery and subsequently would rescue from nuclear blebbing, but not cell death. However, HDAC3 inhibition with RGFP966 or Droxinostat did not rescue *Ebf1^{fl/fl}RERT^{Cre}::A*-MuLV pro-B cells from the nuclear blebbing, but seems like potentiated the severity of the nuclear blebbing and cell death (Figure 4-16 and Figure 4-17). Overall the experimental outcome was hard to determine due to HDAC3 inhibitors potentiating cell death of EBF1 depleted *Ebf1^{fl/fl}RERT^{Cre}::A*-MuLV pro-B cells. In order to confirm that HDAC3 inhibition resulted in a decreased amount of the heterochromatin, EM images need to be taken.

7.3 Cells that are at G1 phase during OHT induced EBF1 depletion might not display nuclear blebbing upon EBF1 depletion

As EBF1 depletion is more rapid than NM blebbing it seems that EBF1 indirectly affects NM. However, this timing does not argue either for or against the direct effect of EBF1 depletion on nuclear blebbing of *Ebf1^{fl/fl}RERT^{Cre}::A-MuLV* pro-B cells. It might be that nuclear blebbing depends on which cell phase the cell is during OHT-induced EBF1 depletion. Nuclear lamina disintegrates and rebuilds in every cell cycle. The lamina association domains are established in the G1 phase when the cells “remember” from the previous cell cycle which part of chromatin should be attached to the lamina (Bridger, Kill et al. 1993). It might be that EBF1 depletion does not affect the existing nuclear lamina, but EBF1 absence causes an incorrect NM rebuilding, which results in nuclear blebbing. Thus, nuclear blebbing would not be observed upon EBF1 depletion in the G1 phase cells, which just formed lamina and chromatin attachments while EBF1 depletion at S, G2 or M cell phases would result in nuclear blebbing as EBF1 depletion would happen before nuclear lamina formation. This is supported by the observation that the nuclear envelope is intact in apoptotic cells which undergo substantial changes in NM proteome and needs further investigation. This could be verified via live imaging of *Ebf1^{fl/fl}RERT^{Cre}::A-MuLV* cells expressing fluorescently tagged LMNA and EBF1.

7.4 EBF1 is a potential nuclear matrix proteins

Cellular fractionation of *Ebf1^{fl/fl}RERT^{Cre}::A-MuLV* pro-B cells were performed in order to test EBF1 localisation. Most of the nuclear proteins including NM proteins are found in the nuclear extract, while DNA bound proteins - histones and transcriptional factors and epigenetic modifiers are found in chromatin fraction (Lalonde, Cheng et al. 2014, Herrmann, Avgousti et al. 2017, Gillotin 2018). Due to EBF1 has a role as transcriptional factor, it was expected to detect a prominent fraction of EBF1 in the chromatin fraction. Nevertheless, the most of EBF1 was detected in the nuclear extract with a small fraction in the chromatin fraction (Figure 4-4), which is not surprising as it was previously reported that transcription factors binding at the transcription start sites (TSS) is restricted and regulated in cell-specific manner (Voss and Hager 2014).

NM protein extraction was performed by removal of cytoplasmic proteins, loosely and tightly attached nuclear proteins and DNA. EBF1 was detected in the nuclear matrix fraction (Figure 4-12). EBF1 was detected in the NM fraction. It is unlikely that EBF1 detected in the nuclear matrix fraction might be an *in situ* fractionation artefact as I did not use stabilization techniques, which might cause protein precipitation onto NM. However, for confirmation a negative NM control should be used in the future experiments. My observation suggests that EBF1 might activate transcription of nuclear matrix structural proteins, or it might be part of the pro-B cell structural matrix itself. In order to verify that EBF1 is a genuine NM protein DNA digestion in *in situ* fractionation needs optimization.

An important observation was RUNX1 and EBF1 colocalization in non-fractionated cells, while no colocalization was detected in the NM (Figure 4-12). It was previously reported that RUNX1 and EBF1 co-activate transcription of *Cd79a* (Nutt and Kee 2007). A similar set of genes might be targeted by both factors; thus, they may reside in similar euchromatin territories which is observed as colocalization of EBF1 and RUNX1 seen in the non-fractionated pro-B. RUNX1 has been reported as a nuclear matrix structural protein (Engelke, Riede et al. 2014), thus it might be that RUNX1 and EBF1 are both NM structural proteins, which are not dependent on each other. This is supported by the observation that EBF1 and RUNX1 do not colocalize in the NM fraction. EBF1 depletion caused an increase in RUNX1 protein levels in *Ebf1^{fl/fl}RERT^{Cre}::A-MuLV* pro-B cells (Figure 4-19 and Figure 4-20 and Figure 4-21). It has been shown that RUNX1 directly and indirectly regulates EBF1 expression, thus an increase in the RUNX1 levels upon EBF1 depletion might be an attempt to compensate for EBF1 loss.

7.5 Potential structural binding partners of EBF1

EBF1 depletion in *Ebf1^{fl/fl}RERT^{Cre}::A-MuLV* cells resulted in downregulation and upregulation of genes that have previously been reported to encode nuclear matrix proteins CASC5, LMNB1, MAML2, RBBP8, CENPA, MACF1, MAD2L1, MYBBP1A, NOL8, NOL10, RRP12 and CENPL (Treiber, Mandel et al. 2010, Engelke, Riede et al. 2014). It cannot be excluded that nuclear blebbing is dependent on downregulation or upregulation of target genes encoding NM proteins and not due to EBF1 being a nuclear matrix protein itself. However, target gene analysis has been performed at a much later time point after EBF1 depletion than when the nuclear blebbing becomes obvious (Treiber, Mandel et al. 2010). Gene expression of 1_1, 1_3, 1_4 *Ebf1^{fl/fl}RERT^{Cre}::A-MuLV* pro-B cells had different gene expression pattern upon EBF1 depletion at an early time point (Dr Ildiko Györy unpublished observations), suggesting that change in the gene expression observed by Treiber and colleagues is more likely the consequence not the cause of nuclear matrix collapse.

It was hypothesized that if EBF1 is genuinely a nuclear matrix protein, it should co-immunoprecipitated with known NM proteins. In order to confirm this, MS analysis of EBF1 co-immunoprecipitated proteins from the *Ebf1^{fl/fl}RERT^{Cre}::A-MuLV* pro-B cell was done (Table 6-1). Only six EBF1 peptides were detected in the sample that was analyzed by MS. Moreover, none of the previously reported EBF1 binding partners was detected in the sample, suggesting that either the cell type was different or upscaling of the experiment is necessary. From the single MS analysis that was performed, SRSF2 and RPL14 that were previously reported as NM structural proteins in pre-B cells (Engelke, Riede et al. 2014) were found as potential EBF1 binding partners, suggesting that these might be involved in the nuclear blebbing upon EBF1 depletion. As well structural proteins such as LGALS9, MTDH, ARHGDIB, ATP5O, SEPT11, KRT78 and KRT17 were found to be co-eluted with EBF1, suggesting that they might be EBF1 binding partners, but none of these proteins was reported as NM protein. The ratio of the peptide number of the pulldown structural protein and the bait protein EBF1 suggesting strong interaction between EBF1 and SRSF2, LGALS9 or MTDH. Important to note that usually a bona fide NM protein LMNA, which has been detected in NM of pre-B cells (Engelke, Riede et al.

2014), is not expressed or expressed at low levels in pro-B cells (Rober, Sauter et al. 1990). Although, the same-origin cells have a higher number of shared NM proteins, their NM proteomes are not entirely identical (Fey and Penman 1988). As pro-B cell NM proteomics studies have never been done before, it is not possible to decide whether these proteins are unique pro-B cell NM proteins, yet the possibility is intriguing. Moreover, *Sep11* was upregulated, while *Lgals9* was downregulated upon loss of EBF1 in primary pro-B cells (Treiber, Mandel et al. 2010); thus they might play a role in the nuclear blebbing upon EBF1 depletion. In order to see which of these proteins are dependent on EBF1, NM proteome in the presence and absence of EBF1 could be analyzed via MS.

7.6 Exploring EBF1 and CCND3 relationship in *Ebf1^{fl/fl}RERT^{Cre}::A-MuLV* pro-B and possible cause of decrease in CCND3 levels upon EBF1 depletion

EBF1 depletion caused a decrease in CCND3 protein levels (Figure 4-6 A and B). It was previously reported that EBF1 depletion causes a decrease in *Ccnd3* RNA levels in the *Ebf1^{fl/fl}RERT^{Cre}* primary cells (Treiber, Mandel et al. 2010, Györy, Boller et al. 2012). However, no change in *Ccnd3* RNA levels in *Ebf1^{fl/fl}RERT^{Cre}::A-MuLV* pro-B cells upon EBF1 depletion was detected (Figure 4-6 C). The experimental system used in this work was an A-MuLV transformed cell line, while the published expression analysis was done in primary cells; thus, it is possible that CCND3 expression is differentially regulated in transformed cells. ABL1 has been shown to regulate CCND3 expression before; this might provide an explanation (Vandenberg, Waring et al. 2014). Thus, it is likely that the decrease in CCND3 expression upon EBF1 depletion depends on non-transcriptional mechanisms. Post-transcriptional regulation might manifest in either decreased translation or increased degradation. It has been proposed that EBF1 stabilizes CCND3 by retention in the nucleus. This hypothesis is based on the observation that an early effect of EBF1 depletion is a profound change in the localization of CCND3 that favours the cytoplasmic compartment and this re-distribution is followed by a rapid decrease in the overall CCND3 levels. Physical association between EBF1 and CCND3 has been proposed as the retention mechanism; however, no binding has been detected in Co-IP experiment.

One possible hypothesis is that EBF1 as a structural matrix protein supports CCND3 attachment to the nuclear matrix in the pro-B cells. In order to test this hypothesis, CCND3 and EBF1 were immunoprecipitated, and the eluates were analysed via MS. ARHGDIB and SRSF2 were found as the only potential common binding partners of EBF1 and CCND3. SRSF2 was previously reported as a NM structural protein (Engelke, Riede et al. 2014), while ARHGDIB might be a unique B-cell NM protein. In further studies, ARHGDIB and SRSF2 binding to EBF1 and CCND3 and their role in pro-B cell NM proteome needs to be verified via WB analysis of the EBF1 and CCND3 immunoprecipitation as well as *in situ* fractionation of pro-B cells before and after EBF1 depletion, followed by CCND3, EBF1, ARHGDIB and SRSF2 staining and confocal microscopy imaging.

The other possible hypothesis is that EBF1 activates transcription of a NM protein, which supports CCND3 attachment to the NM in pro-B cells. Thus, I have looked for a pro-B cell unique potential structural binding partners of CCND3. PSMA6, TXNL1, SRSF2, SRSF3, SRSF1, RBM39, DDX3X, EIF3E, EIF6, NOLC1, RRS1, MYBBP1A and HNRNPL are potential CCND3 binding partners that have been previously reported as NM structural proteins (Engelke, Riede et al. 2014). MYBBP1A was previously reported as upregulated upon EBF1 depletion (Treiber, Mandel et al. 2010). Upregulation of the NM protein may lead to upregulated protein expression and to the deformation of the NM and potentially cause nuclear blebbing and/or CCND3 degradation. This needs further investigation.

Although EZR, MSN and DES were not previously reported to be nuclear matrix proteins, they play a structural role in a cell and were detected as potential CCND3 binding partners. EBF1 binds >100bp downstream of TSS of *Ezr* and *Msn* gene (Treiber, Mandel et al. 2010). Moreover, EBF1 gain and loss of function did not affect the mRNA expression of these proteins, suggesting that EBF1 is not involved in the transcription of these genes. Thus, EZR, DES and MSN potential binding partners of CCND3 are less likely to be involved in CCND3 decrease upon EBF1 depletion.

In pro-B cells CCND3 is found as CDK4 bound, bound to the nuclear matrix or regulated by PI3K . PI3K has been shown to protect soluble CCND3 from degradation (Powers, Mandal et al. 2012), while CCND3 bound to matrix represses V gene recombination (Karki, Kennedy et al. 2018). Powers and colleagues have shown that inhibition of PI3K

substantially decrease CCND3 levels, while did not alter the CCND3 levels associated with CDK4 or NM, suggesting that activity of PI3K causes increase in free CCND3. (Powers, Mandal et al. 2012). Thus, upregulation of PI3K inhibitor or downregulation of PI3K upon EBF1 depletion might result in the decrease of the CCND3 levels. EBF1 was reported to bind >100bp downstream of the TSS of the *Pten* gene that encodes a PI3K inhibitor. Moreover, no change in *Pten* mRNA expression was observed upon gain and loss of EBF1 function (Treiber, Mandel et al. 2010). Thus, PI3K is less likely to be involved in the CCND3 decrease upon EBF1 depletion.

Apoptotic cells show features like loose substrate attachment, become rounded and shrink (Pucci, Kasten et al. 2000). Han and colleagues have shown that increased CCND1 protein levels by starvation-induced apoptotic cells (Han, Begemann et al. 1996), while Janicke and colleagues have shown that CCND3 promotes TNF-induced apoptosis (Janicke, Lin et al. 1996), suggesting that increase in CCND3 may activate apoptosis. Due to CCND3 upregulation activates CDKs and subsequent cell progression, it was proposed that the apoptotic effect of CCNs is dependent on other apoptosis-inducing factors (Pucci, Kasten et al. 2000). Here I have shown that EBF1 depleted apoptotic cells are arrested at G1 phase and EBF1 depletion causes decrease in CCND3 levels. It might be that CCND3 degradation is a result of apoptosis activation and less likely that CCND3 degradation causes apoptosis, however, it might be that EBF1 depletion causes an increase in CCND3 protein levels at early time points, which activates apoptosis and cell arrest at G1 phase. Upon cell arrest and/or induction of apoptosis is activated CCND3 degradation, thus need further investigation.

Chapter 8 Summary and Further studies

Summarizing, here I have shown that EBF1 known as a B-cell restricting transcriptional factor is a potential nuclear matrix protein in pro-B cells. EBF1 depletion leads to nuclear blebbing, heterochromatin relocation from the nuclear body to the inner membrane of the nuclei and CCND3 rapid degradation. It was previously shown that EBF1 depletion arrests cells at the pro-B cell phase and blocks immunoglobulin rearrangement and suppresses cell differentiation into alternative lineages in both early and late stages of B-cell development, suggesting that EBF1 is an essential B-cell fate restricting factor (Lin and Grosschedl 1995, Zhang, Cotta et al. 2003, Seet, Brumbaugh et al. 2004, Hagman and Lukin 2006, Nutt and Kee 2007, Lukin, Fields et al. 2008, Vilagos, Hoffmann et al. 2012). Depletion of TF EBF1 might cause suppression of transcription of NM proteins. It might be that due to EBF1 is an essential TF and potentially an essential NM protein, OHT-induced EBF1 depletion causes substantial changes in the NM proteome, which leads to cell arrest at G1 and apoptosis.

As the NM has previously been reported to be involved in the chromosomal organization (Vemuri, Raju et al. 1993), it might be that suppression of immunoglobulin rearrangements is caused by the EBF1 depletion-induced changes in the NM. Moreover, Treiber and colleagues have shown that EBF1 binding to DNA not always results in gene transcription, but rather in the establishment of accessible chromatin. Thus, EBF1 as a NM protein might participate in gene conformational alterations, which results in subsequent gene repression or activation. Although, it was previously shown that CCND3 represses $V_{\kappa}J_{\kappa}$ recombination and subsequent pro-B cell maturation into pre-B cells (Karki, Kennedy et al. 2018), decrease in CCND3 levels and relocation to the cytoplasm upon EBF1 depletion does not result in the pro-B cell maturation into pre-B cells, indicating that CCND3 is rather just a consequence of the nuclear NM reorganization upon EBF1 depletion.

In further studies, it is important to verify that EBF1 is a genuine NM protein. This could be achieved by optimizing DNA digestion in situ fractionation and using a negative NM control. It would be useful to analyze the NM proteome in the pro-B cell before and after

EBF1 depletion using MS. Verifying EBF1 binding to SRSF2, RPL14, SEP11 or LGALS9 and presence of these proteins in the pro-B cell NM proteome would be the first step in understanding EBF1 role as a NM protein. In order to test whether EBF1 is a part of the NM platform that stabilizes and support CCND3 retention in nuclei, ARHGDIB and SRSF2 binding to EBF1 and CCND3 and their presence in NM need verification.

It is important to verify whether EBF1 depleted cells die from apoptosis and whether the change in NM proteome causes apoptosis, or rather apoptosis triggers a change in the NM proteome and what role EBF1 performs in inducing apoptosis. This could be too complicated as it is impossible to obtain 100% apoptotic population. However, some insights could be gained by live imaging observing a change in levels and localisation of fluorescently tagged EBF1, NM proteins and apoptotic markers.

Chapter 9 Bibliography

Athar, F. and V. K. Parnaik (2015). "Association of lamin A/C with muscle gene-specific promoters in myoblasts." Biochem Biophys Res Commun **4**: 76-82.

Bain, G., E. C. Maandag, D. J. Izon, D. Amsen, A. M. Kruisbeek, B. C. Weintraub, I. Krop, M. S. Schlissel, A. J. Feeney, M. van Rooij and et al. (1994). "E2A proteins are required for proper B cell development and initiation of immunoglobulin gene rearrangements." Cell **79**(5): 885-892.

Beg, A. A. and D. Baltimore (1996). "An essential role for NF-kappaB in preventing TNF-alpha-induced cell death." Science **274**(5288): 782-784.

Benson, D. A., M. Cavanaugh, K. Clark, I. Karsch-Mizrachi, D. J. Lipman, J. Ostell and E. W. Sayers (2017). "GenBank." Nucleic Acids Res **45**(D1): D37-D42.

Berezney, R. and D. S. Coffey (1974). "Identification of a nuclear protein matrix." Biochem Biophys Res Commun **60**(4): 1410-1417.

Berezney, R. and D. S. Coffey (1977). "Nuclear matrix. Isolation and characterization of a framework structure from rat liver nuclei." J Cell Biol **73**(3): 616-637.

Bettayeb, K., N. Oumata, A. Echalié, Y. Ferandin, J. A. Endicott, H. Galons and L. Meijer (2008). "CR8, a potent and selective, roscovitine-derived inhibitor of cyclin-dependent kinases." Oncogene **27**(44): 5797-5807.

Biennu, F., H. Gascan and O. Coqueret (2001). "Cyclin D1 represses STAT3 activation through a Cdk4-independent mechanism." J Biol Chem **276**(20): 16840-16847.

Biennu, F., S. Jirawatnotai, J. E. Elias, C. A. Meyer, K. Mizeracka, A. Marson, G. M. Frampton, M. F. Cole, D. T. Odom, J. Odajima, Y. Geng, A. Zagodzón, M. Jecrois, R. A. Young, X. S. Liu, C. L. Cepko, S. P. Gygi and P. Sicinski (2010). "Transcriptional role of cyclin D1 in development revealed by a genetic-proteomic screen." Nature **463**(7279): 374-378.

Bolland, D. J., H. Koohy, A. L. Wood, L. S. Matheson, F. Krueger, M. J. Stubbington, A. Baizan-Edge, P. Chovanec, B. A. Stubbs, K. Tabbada, S. R. Andrews, M. Spivakov and A. E. Corcoran (2016). "Two Mutually Exclusive Local Chromatin States Drive Efficient V(D)J Recombination." Cell Rep **15**(11): 2475-2487.

Boller, S. and R. Grosschedl (2014). "The regulatory network of B-cell differentiation: a focused view of early B-cell factor 1 function." Immunol Rev **261**(1): 102-115.

Boller, S., S. Ramamoorthy, D. Akbas, R. Nechanitzky, L. Burger, R. Murr, D. Schubeler and R. Grosschedl (2016). "Pioneering Activity of the C-Terminal Domain of EBF1 Shapes the Chromatin Landscape for B Cell Programming." Immunity **44**(3): 527-541.

Bosu, D. R. and E. T. Kipreos (2008). "Cullin-RING ubiquitin ligases: global regulation and activation cycles." Cell Div **3**: 7.

Bradford, M. M. (1976). "A rapid and sensitive method for the quantitation of microgram quantities of protein utilizing the principle of protein-dye binding." Anal Biochem **72**: 248-254.

Briand, N. and P. Collas (2018). "Laminopathy-causing lamin A mutations reconfigure lamina-associated domains and local spatial chromatin conformation." Nucleus **9**(1): 216-226.

Bridger, J. M., I. R. Kill, M. O'Farrell and C. J. Hutchison (1993). "Internal lamin structures within G1 nuclei of human dermal fibroblasts." J Cell Sci **104 (Pt 2)**: 297-306.

Brouwer, C., W. Bruce, S. Maddock, Z. Avramova and B. Bowen (2002). "Suppression of transgene silencing by matrix attachment regions in maize: a dual role for the maize 5' ADH1 matrix attachment region." Plant Cell **14**(9): 2251-2264.

Brown, N. R., M. E. Noble, J. A. Endicott, E. F. Garman, S. Wakatsuki, E. Mitchell, B. Rasmussen, T. Hunt and L. N. Johnson (1995). "The crystal structure of cyclin A." Structure **3**(11): 1235-1247.

Burgess, R. D., M. (2009). Guide to Protein Purification. Methods in Enzymology, Academic Press. **463**: 900.

Casiano, R. R. (1997). "Correlation of clinical examination with computer tomography in paranasal sinus disease." Am J Rhinol **11**(3): 193-196.

Casimiro, M. C., M. Crosariol, E. Loro, A. Ertel, Z. Yu, W. Dampier, E. A. Saria, A. Papanikolaou, T. J. Stanek, Z. Li, C. Wang, P. Fortina, S. Addya, A. Tozeren, E. S. Knudsen, A. Arnold and R. G. Pestell (2012). "ChIP sequencing of cyclin D1 reveals a transcriptional role in chromosomal instability in mice." J Clin Invest **122**(3): 833-843.

Cato, M. H., S. K. Chintalapati, I. W. Yau, S. A. Omori and R. C. Rickert (2011). "Cyclin D3 is selectively required for proliferative expansion of germinal center B cells." Mol Cell Biol **31**(1): 127-137.

Chapman, V. M. and T. B. Shows (1976). "Somatic cell genetic evidence for X-chromosome linkage of three enzymes in the mouse." Nature **259**(5545): 665-667.

Chen, B. B. and R. K. Mallampalli (2013). "F-box protein substrate recognition: a new insight." Cell Cycle **12**(7): 1009-1010.

Choukallah, M. A. and P. Matthias (2014). "The Interplay between Chromatin and Transcription Factor Networks during B Cell Development: Who Pulls the Trigger First?" Front Immunol **5**: 156.

Coffey, D. S. (2002). "Nuclear matrix proteins as proteomic markers of preneoplastic and cancer lesions : commentary re: G. Brunagel et al., nuclear matrix protein alterations

associated with colon cancer metastasis to the liver. *Clin. Cancer Res.*, 8: 3039-3045, 2002." *Clin Cancer Res* **8**(10): 3031-3033.

Cooper, A. B., C. M. Sawai, E. Sicinska, S. E. Powers, P. Sicinski, M. R. Clark and I. Aifantis (2006). "A unique function for cyclin D3 in early B cell development." *Nat Immunol* **7**(5): 489-497.

Csoka, A. B., S. B. English, C. P. Simkevich, D. G. Ginzinger, A. J. Butte, G. P. Schatten, F. G. Rothman and J. M. Sedivy (2004). "Genome-scale expression profiling of Hutchinson-Gilford progeria syndrome reveals widespread transcriptional misregulation leading to mesodermal/mesenchymal defects and accelerated atherosclerosis." *Aging Cell* **3**(4): 235-243.

Cunningham, J. M., M. E. Purucker, S. M. Jane, B. Safer, E. F. Vanin, P. A. Ney, C. H. Lowrey and A. W. Nienhuis (1994). "The regulatory element 3' to the A gamma-globin gene binds to the nuclear matrix and interacts with special A-T-rich binding protein 1 (SATB1), an SAR/MAR-associating region DNA binding protein." *Blood* **84**(4): 1298-1308.

Dai, J., Y. J. Huang, X. He, M. Zhao, X. Wang, Z. S. Liu, W. Xue, H. Cai, X. Y. Zhan, S. Y. Huang, K. He, H. Wang, N. Wang, Z. Sang, T. Li, Q. Y. Han, J. Mao, X. Diao, N. Song, Y. Chen, W. H. Li, J. H. Man, A. L. Li, T. Zhou, Z. G. Liu, X. M. Zhang and T. Li (2019). "Acetylation Blocks cGAS Activity and Inhibits Self-DNA-Induced Autoimmunity." *Cell* **176**(6): 1447-1460 e1414.

Dannenberg, J. H., A. van Rossum, L. Schuijff and H. te Riele (2000). "Ablation of the retinoblastoma gene family deregulates G(1) control causing immortalization and increased cell turnover under growth-restricting conditions." *Genes Dev* **14**(23): 3051-3064.

Datta, N. S., J. L. Williams and M. W. Long (1998). "Differential modulation of G1-S-phase cyclin-dependent kinase 2/cyclin complexes occurs during the acquisition of a polyploid DNA content." *Cell Growth Differ* **9**(8): 639-650.

Dechat, T., T. Shimi, S. A. Adam, A. E. Rusinol, D. A. Andres, H. P. Spielmann, M. S. Sinensky and R. D. Goldman (2007). "Alterations in mitosis and cell cycle progression caused by a mutant lamin A known to accelerate human aging." *Proc Natl Acad Sci U S A* **104**(12): 4955-4960.

Decker, T., M. Pasca di Magliano, S. McManus, Q. Sun, C. Bonifer, H. Tagoh and M. Busslinger (2009). "Stepwise activation of enhancer and promoter regions of the B cell commitment gene Pax5 in early lymphopoiesis." *Immunity* **30**(4): 508-520.

DeKoter, R. P. and H. Singh (2000). "Regulation of B lymphocyte and macrophage development by graded expression of PU.1." *Science* **288**(5470): 1439-1441.

Diamond, D. A. and E. R. Barrack (1984). "The relationship of androgen receptor levels to androgen responsiveness in the Dunning R3327 rat prostate tumor sublines." *J Urol* **132**(4): 821-827.

- Dias, S., R. Mansson, S. Gurbuxani, M. Sigvardsson and B. L. Kee (2008). "E2A proteins promote development of lymphoid-primed multipotent progenitors." Immunity **29**(2): 217-227.
- Dickinson, L. A., C. D. Dickinson and T. Kohwi-Shigematsu (1997). "An atypical homeodomain in SATB1 promotes specific recognition of the key structural element in a matrix attachment region." J Biol Chem **272**(17): 11463-11470.
- DuBridge, R. B., P. Tang, H. C. Hsia, P. M. Leong, J. H. Miller and M. P. Calos (1987). "Analysis of mutation in human cells by using an Epstein-Barr virus shuttle system." Mol Cell Biol **7**(1): 379-387.
- Dynlacht, J. R., M. D. Story, W. G. Zhu and J. Danner (1999). "Lamin B is a prompt heat shock protein." J Cell Physiol **178**(1): 28-34.
- Earnshaw, W. C. (1995). "Nuclear changes in apoptosis." Curr Opin Cell Biol **7**(3): 337-343.
- Elcock, L. S. and J. M. Bridger (2008). "Exploring the effects of a dysfunctional nuclear matrix." Biochem Soc Trans **36**(Pt 6): 1378-1383.
- Endo, T., K. Ohta, K. Haraguchi and T. Onaya (1995). "Cloning and functional expression of a thyrotropin receptor cDNA from rat fat cells." J Biol Chem **270**(18): 10833-10837.
- Engelke, R., J. Riede, J. Hegermann, A. Wuerch, S. Eimer, J. Dengjel and G. Mittler (2014). "The quantitative nuclear matrix proteome as a biochemical snapshot of nuclear organization." J Proteome Res **13**(9): 3940-3956.
- Eriksson, M., W. T. Brown, L. B. Gordon, M. W. Glynn, J. Singer, L. Scott, M. R. Erdos, C. M. Robbins, T. Y. Moses, P. Berglund, A. Dutra, E. Pak, S. Durkin, A. B. Csoka, M. Boehnke, T. W. Glover and F. S. Collins (2003). "Recurrent de novo point mutations in lamin A cause Hutchinson-Gilford progeria syndrome." Nature **423**(6937): 293-298.
- Faiferman, I. and A. O. Pogo (1975). "Isolation of a nuclear ribonucleoprotein network that contains heterogeneous RNA and is bound to the nuclear envelope." Biochemistry **14**(17): 3808-3816.
- Fawcett, D. W. (1966). "On the occurrence of a fibrous lamina on the inner aspect of the nuclear envelope in certain cells of vertebrates." Am J Anat **119**(1): 129-145.
- Fey, E. G., G. Krochmalnic and S. Penman (1986). "The nonchromatin substructures of the nucleus: the ribonucleoprotein (RNP)-containing and RNP-depleted matrices analyzed by sequential fractionation and resinless section electron microscopy." J Cell Biol **102**(5): 1654-1665.
- Fey, E. G. and S. Penman (1988). "Nuclear matrix proteins reflect cell type of origin in cultured human cells." Proc Natl Acad Sci U S A **85**(1): 121-125.

- Filella, X., E. Fernandez-Galan, R. Fernandez Bonifacio and L. Foj (2018). "Emerging biomarkers in the diagnosis of prostate cancer." Pharmgenomics Pers Med **11**: 83-94.
- Flavell, R. B. (1994). "Inactivation of gene expression in plants as a consequence of specific sequence duplication." Proc Natl Acad Sci U S A **91**(9): 3490-3496.
- Fling, S. P., B. Arp and D. Pious (1994). "HLA-DMA and -DMB genes are both required for MHC class II/peptide complex formation in antigen-presenting cells." Nature **368**(6471): 554-558.
- Fu, M., M. Rao, T. Bouras, C. Wang, K. Wu, X. Zhang, Z. Li, T. P. Yao and R. G. Pestell (2005). "Cyclin D1 inhibits peroxisome proliferator-activated receptor gamma-mediated adipogenesis through histone deacetylase recruitment." J Biol Chem **280**(17): 16934-16941.
- Fuentes-Panana, E. M., G. Bannish, N. Shah and J. G. Monroe (2004). "Basal Igalpha/Igbeta signals trigger the coordinated initiation of pre-B cell antigen receptor-dependent processes." J Immunol **173**(2): 1000-1011.
- Fuxa, M. and J. A. Skok (2007). "Transcriptional regulation in early B cell development." Curr Opin Immunol **19**(2): 129-136.
- Gant, T. M., C. A. Harris and K. L. Wilson (1999). "Roles of LAP2 proteins in nuclear assembly and DNA replication: truncated LAP2beta proteins alter lamina assembly, envelope formation, nuclear size, and DNA replication efficiency in *Xenopus laevis* extracts." J Cell Biol **144**(6): 1083-1096.
- Ganter, B., S. Fu and J. S. Lipsick (1998). "D-type cyclins repress transcriptional activation by the v-Myb but not the c-Myb DNA-binding domain." EMBO J **17**(1): 255-268.
- Getzenberg, R. H., B. R. Konety, T. A. Oeler, M. M. Quigley, A. Hakam, M. J. Becich and R. R. Bahnsen (1996). "Bladder cancer-associated nuclear matrix proteins." Cancer Res **56**(7): 1690-1694.
- Getzenberg, R. H., K. J. Pienta, E. Y. Huang and D. S. Coffey (1991). "Identification of nuclear matrix proteins in the cancer and normal rat prostate." Cancer Res **51**(24): 6514-6520.
- Ghazavi, F., T. Lammens, N. Van Roy, B. Poppe, F. Speleman, Y. Benoit, P. Van Vlierberghe and B. De Moerloose (2015). "Molecular basis and clinical significance of genetic aberrations in B-cell precursor acute lymphoblastic leukemia." Exp Hematol **43**(8): 640-653.
- Gillotin, S. (2018). "Isolation of Chromatin-bound Proteins from Subcellular Fractions for Biochemical Analysis." Bio-protocol **8**(19): e3035.
- Goebel, P., N. Janney, J. R. Valenzuela, W. J. Romanow, C. Murre and A. J. Feeney (2001). "Localized gene-specific induction of accessibility to V(D)J recombination induced by E2A and early B cell factor in nonlymphoid cells." J Exp Med **194**(5): 645-656.

- Gotzmann, J., M. Meissner and C. Gerner (2000). "The fate of the nuclear matrix-associated-region-binding protein SATB1 during apoptosis." Cell Death Differ **7**(5): 425-438.
- Gueth-Hallonet, C., K. Weber and M. Osborn (1997). "Cleavage of the nuclear matrix protein NuMA during apoptosis." Exp Cell Res **233**(1): 21-24.
- Györy, I., S. Boller, R. Nechanitzky, E. Mandel, S. Pott, E. Liu and R. Grosschedl (2012). "Transcription factor Ebf1 regulates differentiation stage-specific signaling, proliferation, and survival of B cells." Genes & development **26**(7): 668-682.
- Györy, I. and R. Grosschedl (2013). "Regulation of proliferation and survival of B-lymphocytes by Ebf1 - implications in leukaemia." Clinical Epigenetics **5**(Suppl 1).
- Hagman, J., C. Belanger, A. Travis, C. W. Turck and R. Grosschedl (1993). "Cloning and functional characterization of early B-cell factor, a regulator of lymphocyte-specific gene expression." Genes Dev **7**(5): 760-773.
- Hagman, J., M. J. Gutch, H. Lin and R. Grosschedl (1995). "EBF contains a novel zinc coordination motif and multiple dimerization and transcriptional activation domains." EMBO J **14**(12): 2907-2916.
- Hagman, J. and K. Lukin (2006). "Transcription factors drive B cell development." Curr Opin Immunol **18**(2): 127-134.
- Han, E. K., M. Begemann, A. Sgambato, J. W. Soh, Y. Doki, W. Q. Xing, W. Liu and I. B. Weinstein (1996). "Increased expression of cyclin D1 in a murine mammary epithelial cell line induces p27kip1, inhibits growth, and enhances apoptosis." Cell Growth Differ **7**(6): 699-710.
- Hancock, R. (2000). "A new look at the nuclear matrix." Chromosoma **109**(4): 219-225.
- Harper, J. W., J. L. Burton and M. J. Solomon (2002). "The anaphase-promoting complex: it's not just for mitosis any more." Genes Dev **16**(17): 2179-2206.
- Heaphy, S., J. T. Finch, M. J. Gait, J. Karn and M. Singh (1991). "Human immunodeficiency virus type 1 regulator of virion expression, rev, forms nucleoprotein filaments after binding to a purine-rich "bubble" located within the rev-responsive region of viral mRNAs." Proc Natl Acad Sci U S A **88**(16): 7366-7370.
- Heinz, S., C. Benner, N. Spann, E. Bertolino, Y. C. Lin, P. Laslo, J. X. Cheng, C. Murre, H. Singh and C. K. Glass (2010). "Simple combinations of lineage-determining transcription factors prime cis-regulatory elements required for macrophage and B cell identities." Mol Cell **38**(4): 576-589.
- Heltemes-Harris, L. M., M. J. Willette, L. B. Ramsey, Y. H. Qiu, E. S. Neeley, N. Zhang, D. A. Thomas, T. Koeuth, E. C. Baechler, S. M. Kornblau and M. A. Farrar (2011). "Ebf1 or Pax5 haploinsufficiency synergizes with STAT5 activation to initiate acute lymphoblastic leukemia." J Exp Med **208**(6): 1135-1149.

Henzel, M. J., F. Boisvert and D. P. Bazett-Jones (1999). "Direct visualization of a protein nuclear architecture." Mol Biol Cell **10**(6): 2051-2062.

Herman, R., L. Weymouth and S. Penman (1978). "Heterogeneous nuclear RNA-protein fibers in chromatin-depleted nuclei." J Cell Biol **78**(3): 663-674.

Herrmann, C., D. C. Avgousti and M. D. Weitzman (2017). "Differential Salt Fractionation of Nuclei to Analyze Chromatin-associated Proteins from Cultured Mammalian Cells." Bio Protoc **7**(6).

Hsu, L. Y., J. Luring, H. E. Liang, S. Greenbaum, D. Cado, Y. Zhuang and M. S. Schlissel (2003). "A conserved transcriptional enhancer regulates RAG gene expression in developing B cells." Immunity **19**(1): 105-117.

Huard, J. M., C. C. Forster, M. L. Carter, P. Sicinski and M. E. Ross (1999). "Cerebellar histogenesis is disturbed in mice lacking cyclin D2." Development **126**(9): 1927-1935.

Huttlin, E. L., L. Ting, R. J. Bruckner, F. Gebreab, M. P. Gygi, J. Szpyt, S. Tam, G. Zarraga, G. Colby, K. Baltier, R. Dong, V. Guarani, L. P. Vaites, A. Ordureau, R. Rad, B. K. Erickson, M. Wuhr, J. Chick, B. Zhai, D. Kolippakkam, J. Mintseris, R. A. Obar, T. Harris, S. Artavanis-Tsakonas, M. E. Sowa, P. De Camilli, J. A. Paulo, J. W. Harper and S. P. Gygi (2015). "The BioPlex Network: A Systematic Exploration of the Human Interactome." Cell **162**(2): 425-440.

Hwang, H. C. and B. E. Clurman (2005). "Cyclin E in normal and neoplastic cell cycles." Oncogene **24**(17): 2776-2786.

Inoue, K. and C. J. Sherr (1998). "Gene expression and cell cycle arrest mediated by transcription factor DMP1 is antagonized by D-type cyclins through a cyclin-dependent-kinase-independent mechanism." Mol Cell Biol **18**(3): 1590-1600.

Jackson, D. A. and P. R. Cook (1988). "Visualization of a filamentous nucleoskeleton with a 23 nm axial repeat." EMBO J **7**(12): 3667-3677.

Janicke, R. U., X. Y. Lin, F. H. Lee and A. G. Porter (1996). "Cyclin D3 sensitizes tumor cells to tumor necrosis factor-induced, c-Myc-dependent apoptosis." Mol Cell Biol **16**(10): 5245-5253.

Karagianni, P. and J. Wong (2007). "HDAC3: taking the SMRT-N-CoRrect road to repression." Oncogene **26**(37): 5439-5449.

Karki, S., D. E. Kennedy, K. McLean, A. T. Grzybowski, M. Maienschein-Cline, S. Banerjee, H. Xu, E. Davis, M. Mandal, C. Labno, S. E. Powers, M. M. Le Beau, A. R. Dinner, H. Singh, A. J. Ruthenburg and M. R. Clark (2018). "Regulated Capture of κ Gene Topologically Associating Domains by Transcription Factories." Cell Rep **24**(9): 2443-2456.

Karube, K., A. Enjuanes, I. Dlouhy, P. Jares, D. Martin-Garcia, F. Nadeu, G. R. Ordonez, J. Rovira, G. Clot, C. Royo, A. Navarro, B. Gonzalez-Farre, A. Vaghefi, G. Castellano, C.

Rubio-Perez, D. Tamborero, J. Briones, A. Salar, J. M. Sancho, S. Mercadal, E. Gonzalez-Barca, L. Escoda, H. Miyoshi, K. Ohshima, K. Miyawaki, K. Kato, K. Akashi, A. Mozos, L. Colomo, M. Alcoceba, A. Valera, A. Carrio, D. Costa, N. Lopez-Bigas, R. Schmitz, L. M. Staudt, I. Salaverria, A. Lopez-Guillermo and E. Campo (2018). "Integrating genomic alterations in diffuse large B-cell lymphoma identifies new relevant pathways and potential therapeutic targets." Leukemia **32**(3): 675-684.

Kee, B. L. and C. Murre (1998). "Induction of early B cell factor (EBF) and multiple B lineage genes by the basic helix-loop-helix transcription factor E12." J Exp Med **188**(4): 699-713.

Kieslinger, M., S. Folberth, G. Dobreva, T. Dorn, L. Croci, R. Erben, G. G. Consalez and R. Grosschedl (2005). "EBF2 regulates osteoblast-dependent differentiation of osteoclasts." Dev Cell **9**(6): 757-767.

Kikuchi, K., A. Y. Lai, C. L. Hsu and M. Kondo (2005). "IL-7 receptor signaling is necessary for stage transition in adult B cell development through up-regulation of EBF." J Exp Med **201**(8): 1197-1203.

Kipp, M., B. L. Schwab, M. Przybylski, P. Nicotera and F. O. Fackelmayer (2000). "Apoptotic cleavage of scaffold attachment factor A (SAF-A) by caspase-3 occurs at a noncanonical cleavage site." J Biol Chem **275**(7): 5031-5036.

Klein, J. and A. Sato (1998). "Birth of the major histocompatibility complex." Scand J Immunol **47**(3): 199-209.

Kozar, K., M. A. Ciemerych, V. I. Rebel, H. Shigematsu, A. Zagodzdzon, E. Sicinska, Y. Geng, Q. Yu, S. Bhattacharya, R. T. Bronson, K. Akashi and P. Sicinski (2004). "Mouse development and cell proliferation in the absence of D-cyclins." Cell **118**(4): 477-491.

Laham-Karam, N., M. Lalli, N. Leinonen and S. Yla-Herttuala (2015). "Differential Regulation of Vascular Endothelial Growth Factors by Promoter-targeted shRNAs." Mol Ther Nucleic Acids **4**: e243.

Lahne, H. U., M. M. Kloster, S. Lefdal, H. K. Blomhoff and S. Naderi (2006). "Degradation of cyclin D3 independent of Thr-283 phosphorylation." Oncogene **25**(17): 2468-2476.

Lalonde, M. E., X. Cheng and J. Cote (2014). "Histone target selection within chromatin: an exemplary case of teamwork." Genes Dev **28**(10): 1029-1041.

Lam, E. W., J. Glassford, L. Banerji, N. S. Thomas, P. Sicinski and G. G. Klaus (2000). "Cyclin D3 compensates for loss of cyclin D2 in mouse B-lymphocytes activated via the antigen receptor and CD40." J Biol Chem **275**(5): 3479-3484.

Lepock, J. R., H. E. Frey, M. L. Heynen, G. A. Senisterra and R. L. Warters (2001). "The nuclear matrix is a thermolabile cellular structure." Cell Stress Chaperones **6**(2): 136-147.

- Lim, S. and P. Kaldis (2013). "Cdks, cyclins and CKIs: roles beyond cell cycle regulation." Development **140**(15): 3079-3093.
- Lin, H. and R. Grosschedl (1995). "Failure of B-cell differentiation in mice lacking the transcription factor EBF." Nature **376**(6537): 263-267.
- Liu, W., M. Sun, J. Jiang, X. Shen, Q. Sun, W. Liu, H. Shen and J. Gu (2004). "Cyclin D3 interacts with human activating transcription factor 5 and potentiates its transcription activity." Biochem Biophys Res Commun **321**(4): 954-960.
- Lu, F., A. B. Gladden and J. A. Diehl (2003). "An alternatively spliced cyclin D1 isoform, cyclin D1b, is a nuclear oncogene." Cancer Res **63**(21): 7056-7061.
- Lukin, K., S. Fields, J. Hartley and J. Hagman (2008). "Early B cell factor: Regulator of B lineage specification and commitment." Semin Immunol **20**(4): 221-227.
- Lundberg, A. S. and R. A. Weinberg (1998). "Functional inactivation of the retinoblastoma protein requires sequential modification by at least two distinct cyclin-cdk complexes." Mol Cell Biol **18**(2): 753-761.
- MacLachlan, T. K., N. Sang and A. Giordano (1995). "Cyclins, cyclin-dependent kinases and cdk inhibitors: implications in cell cycle control and cancer." Crit Rev Eukaryot Gene Expr **5**(2): 127-156.
- Maier, H., R. Ostraat, H. Gao, S. Fields, S. A. Shinton, K. L. Medina, T. Ikawa, C. Murre, H. Singh, R. R. Hardy and J. Hagman (2004). "Early B cell factor cooperates with Runx1 and mediates epigenetic changes associated with mb-1 transcription." Nat Immunol **5**(10): 1069-1077.
- Malumbres, M. and M. Barbacid (2005). "Mammalian cyclin-dependent kinases." Trends Biochem Sci **30**(11): 630-641.
- Mansson, R., E. Welinder, J. Ahsberg, Y. C. Lin, C. Benner, C. K. Glass, J. S. Lucas, M. Sigvardsson and C. Murre (2012). "Positive intergenic feedback circuitry, involving EBF1 and FOXO1, orchestrates B-cell fate." Proc Natl Acad Sci U S A **109**(51): 21028-21033.
- Martelli, A. M., R. Bareggi, R. Bortul, V. Grill, P. Narducci and M. Zwyer (1997). "The nuclear matrix and apoptosis." Histochem Cell Biol **108**(1): 1-10.
- Martelli, A. M., E. Falcieri, M. Zwyer, R. Bortul, G. Tabellini, A. Cappellini, L. Cocco and L. Manzoli (2002). "The controversial nuclear matrix: a balanced point of view." Histol Histopathol **17**(4): 1193-1205.
- Matsuoka, S., M. Yamaguchi and A. Matsukage (1994). "D-type cyclin-binding regions of proliferating cell nuclear antigen." J Biol Chem **269**(15): 11030-11036.
- Matsushime, H., M. F. Roussel, R. A. Ashmun and C. J. Sherr (1991). "Colony-stimulating factor 1 regulates novel cyclins during the G1 phase of the cell cycle." Cell **65**(4): 701-713.

- McCormack, W. T., L. W. Tjoelker and C. B. Thompson (1991). "Avian B-cell development: generation of an immunoglobulin repertoire by gene conversion." Annu Rev Immunol **9**: 219-241.
- McHeyzer-Williams, M. G. and R. Ahmed (1999). "B cell memory and the long-lived plasma cell." Curr Opin Immunol **11**(2): 172-179.
- McKercher, S. R., B. E. Torbett, K. L. Anderson, G. W. Henkel, D. J. Vestal, H. Baribault, M. Klemsz, A. J. Feeney, G. E. Wu, C. J. Paige and R. A. Maki (1996). "Targeted disruption of the PU.1 gene results in multiple hematopoietic abnormalities." EMBO J **15**(20): 5647-5658.
- Medina, K. L., J. M. Pongubala, K. L. Reddy, D. W. Lancki, R. Dekoter, M. Kieslinger, R. Grosschedl and H. Singh (2004). "Assembling a gene regulatory network for specification of the B cell fate." Dev Cell **7**(4): 607-617.
- Miernyk, J. A. and J. J. Thelen (2008). "Biochemical approaches for discovering protein-protein interactions." Plant J **53**(4): 597-609.
- Mika, S. and B. Rost (2005). "NMPdb: Database of Nuclear Matrix Proteins." Nucleic Acids Res **33**(Database issue): D160-163.
- Milatovich, A., R. G. Qiu, R. Grosschedl and U. Francke (1994). "Gene for a tissue-specific transcriptional activator (EBF or Olf-1), expressed in early B lymphocytes, adipocytes, and olfactory neurons, is located on human chromosome 5, band q34, and proximal mouse chromosome 11." Mamm Genome **5**(4): 211-215.
- Milon, B. C., H. Cheng, M. V. Tselebrovsky, S. A. Lavrov, V. V. Nenasheva, E. A. Mikhaleva, Y. Y. Shevelyov and D. I. Nurminsky (2012). "Role of histone deacetylases in gene regulation at nuclear lamina." PLoS One **7**(11): e49692.
- Naderi, S., K. B. Gutzkow, H. U. Lahne, S. Lefdal, W. J. Ryves, A. J. Harwood and H. K. Blomhoff (2004). "cAMP-induced degradation of cyclin D3 through association with GSK-3beta." J Cell Sci **117**(Pt 17): 3769-3783.
- Nakase, H., Y. Takahama and Y. Akamatsu (2003). "Effect of CpG methylation on RAG1/RAG2 reactivity: implications of direct and indirect mechanisms for controlling V(D)J cleavage." EMBO Rep **4**(8): 774-780.
- Narayan, K. S., W. J. Steele, K. Smetana and H. Busch (1967). "Ultrastructural aspects of the ribonucleo-protein network in nuclei of Walker tumor and rat liver." Exp Cell Res **46**(1): 65-77.
- Neisch, A. L. and R. G. Fehon (2011). "Ezrin, Radixin and Moesin: key regulators of membrane-cortex interactions and signaling." Curr Opin Cell Biol **23**(4): 377-382.
- Neuman, E., M. H. Ladha, N. Lin, T. M. Upton, S. J. Miller, J. DiRenzo, R. G. Pestell, P. W. Hinds, S. F. Dowdy, M. Brown and M. E. Ewen (1997). "Cyclin D1 stimulation of estrogen receptor transcriptional activity independent of cdk4." Mol Cell Biol **17**(9): 5338-5347.

- Nichogiannopoulou, A., M. Trevisan, S. Neben, C. Friedrich and K. Georgopoulos (1999). "Defects in hemopoietic stem cell activity in Ikaros mutant mice." J Exp Med **190**(9): 1201-1214.
- Nickerson, J. (2001). "Experimental observations of a nuclear matrix." J Cell Sci **114**(Pt 3): 463-474.
- Nilsen, T. W. (2013). "Preparation of Nuclear Extracts from HeLa cells." Cold Spring Harb Protoc **2013**(6): 579-583.
- Nutt, S. L., B. Heavey, A. G. Rolink and M. Busslinger (1999). "Commitment to the B-lymphoid lineage depends on the transcription factor Pax5." Nature **401**(6753): 556-562.
- Nutt, S. L. and B. L. Kee (2007). "The transcriptional regulation of B cell lineage commitment." Immunity **26**(6): 715-725.
- Nutt, S. L., P. Urbanek, A. Rolink and M. Busslinger (1997). "Essential functions of Pax5 (BSAP) in pro-B cell development: difference between fetal and adult B lymphopoiesis and reduced V-to-DJ recombination at the IgH locus." Genes Dev **11**(4): 476-491.
- Okosun, J., C. Bodor, J. Wang, S. Araf, C. Y. Yang, C. Pan, S. Boller, D. Cittaro, M. Bozek, S. Iqbal, J. Matthews, D. Wrench, J. Marzec, K. Tawana, N. Popov, C. O'Riain, D. O'Shea, E. Carlotti, A. Davies, C. H. Lawrie, A. Matolcsy, M. Calaminici, A. Norton, R. J. Byers, C. Mein, E. Stupka, T. A. Lister, G. Lenz, S. Montoto, J. G. Gribben, Y. Fan, R. Grosschedl, C. Chelala and J. Fitzgibbon (2014). "Integrated genomic analysis identifies recurrent mutations and evolution patterns driving the initiation and progression of follicular lymphoma." Nat Genet **46**(2): 176-181.
- Parkhouse, R. M. (1990). "Three B-cell surface molecules associating with membrane immunoglobulin." Immunology **69**(2): 298-302.
- Passegue, E., A. J. Wagers, S. Giuriato, W. C. Anderson and I. L. Weissman (2005). "Global analysis of proliferation and cell cycle gene expression in the regulation of hematopoietic stem and progenitor cell fates." J Exp Med **202**(11): 1599-1611.
- Pauklin, S., P. Madrigal, A. Bertero and L. Vallier (2016). "Initiation of stem cell differentiation involves cell cycle-dependent regulation of developmental genes by Cyclin D." Genes Dev **30**(4): 421-433.
- Pederson, T. (2000). "Half a century of "the nuclear matrix"." Mol Biol Cell **11**(3): 799-805.
- Pei, J., B. H. Kim and N. V. Grishin (2008). "PROMALS3D: a tool for multiple protein sequence and structure alignments." Nucleic Acids Res **36**(7): 2295-2300.
- Peled, J. U., J. J. Yu, J. Venkatesh, E. Bi, B. B. Ding, M. Krupski-Downs, R. Shaknovich, P. Sicinski, B. Diamond, M. D. Scharff and B. H. Ye (2010). "Requirement for cyclin D3 in germinal center formation and function." Cell Res **20**(6): 631-646.

- Penman, S. (1995). "Rethinking cell structure." Proc Natl Acad Sci U S A **92**(12): 5251-5257.
- Perez-Vera, P., A. Reyes-Leon and E. M. Fuentes-Panana (2011). "Signaling proteins and transcription factors in normal and malignant early B cell development." Bone Marrow Res **2011**: 502751.
- Politz, J. C., E. S. Browne, D. E. Wolf and T. Pederson (1998). "Intranuclear diffusion and hybridization state of oligonucleotides measured by fluorescence correlation spectroscopy in living cells." Proc Natl Acad Sci U S A **95**(11): 6043-6048.
- Powers, S. E., M. Mandal, S. Matsuda, A. V. Miletic, M. H. Cato, A. Tanaka, R. C. Rickert, S. Koyasu and M. R. Clark (2012). "Subnuclear cyclin D3 compartments and the coordinated regulation of proliferation and immunoglobulin variable gene repression." J Exp Med **209**(12): 2199-2213.
- Prasad, M. A. J., J. Ungerback, J. Ahsberg, R. Somasundaram, T. Strid, M. Larsson, R. Mansson, D. A. Paepe, H. Lilljebjorn, T. Fioretos, J. Hagman and M. Sigvardsson (2015). "Ebf1 heterozygosity results in increased DNA damage in pro-B cells and their synergistic transformation by Pax5 haploinsufficiency." Blood **125**(26): 4052-4059.
- Pucci, B., M. Kasten and A. Giordano (2000). "Cell cycle and apoptosis." Neoplasia **2**(4): 291-299.
- Radulovich, N., N. A. Pham, D. Strumpf, L. Leung, W. Xie, I. Jurisica and M. S. Tsao (2010). "Differential roles of cyclin D1 and D3 in pancreatic ductal adenocarcinoma." Mol Cancer **9**: 24.
- Ramirez-Komo, J. A., M. A. Delaney, D. Strain, K. Lukin, M. Tsang, B. M. Iritani and J. Hagman (2017). "Spontaneous loss of B lineage transcription factors leads to pre-B leukemia in Ebf1(+/-)Bcl-xL(Tg) mice." Oncogenesis **6**(7): e355.
- Rao, S. S., C. Chu and D. S. Kohtz (1994). "Ectopic expression of cyclin D1 prevents activation of gene transcription by myogenic basic helix-loop-helix regulators." Mol Cell Biol **14**(8): 5259-5267.
- Richter, K., M. Nessling and P. Lichter (2007). "Experimental evidence for the influence of molecular crowding on nuclear architecture." J Cell Sci **120**(Pt 9): 1673-1680.
- Rober, R. A., H. Sauter, K. Weber and M. Osborn (1990). "Cells of the cellular immune and hemopoietic system of the mouse lack lamins A/C: distinction versus other somatic cells." J Cell Sci **95 (Pt 4)**: 587-598.
- Roessler, S., I. Gyory, S. Imhof, M. Spivakov, R. R. Williams, M. Busslinger, A. G. Fisher and R. Grosschedl (2007). "Distinct promoters mediate the regulation of Ebf1 gene expression by interleukin-7 and Pax5." Mol Cell Biol **27**(2): 579-594.
- Rothenberg, E. V. (2014). "Transcriptional control of early T and B cell developmental choices." Annu Rev Immunol **32**: 283-321.

Roti Roti, J. L. and W. D. Wright (1987). "Visualization of DNA loops in nucleoids from HeLa cells: assays for DNA damage and repair." Cytometry **8**(5): 461-467.

Rowat, A. C., J. Lammerding, H. Herrmann and U. Aebi (2008). "Towards an integrated understanding of the structure and mechanics of the cell nucleus." Bioessays **30**(3): 226-236.

Sage, J., G. J. Mulligan, L. D. Attardi, A. Miller, S. Chen, B. Williams, E. Theodorou and T. Jacks (2000). "Targeted disruption of the three Rb-related genes leads to loss of G(1) control and immortalization." Genes Dev **14**(23): 3037-3050.

Sawasdichai, A., H. T. Chen, N. Abdul Hamid, P. S. Jayaraman and K. Gaston (2010). "In situ subcellular fractionation of adherent and non-adherent mammalian cells." J Vis Exp(41).

Schmitt, H. M., H. R. Pelzel, C. L. Schlamp and R. W. Nickells (2014). "Histone deacetylase 3 (HDAC3) plays an important role in retinal ganglion cell death after acute optic nerve injury." Mol Neurodegener **9**: 39.

Seet, C. S., R. L. Brumbaugh and B. L. Kee (2004). "Early B cell factor promotes B lymphopoiesis with reduced interleukin 7 responsiveness in the absence of E2A." J Exp Med **199**(12): 1689-1700.

Sekine, R., T. Kitamura, T. Tsuji and A. Tojo (2008). "Efficient retroviral transduction of human B-lymphoid and myeloid progenitors: marked inhibition of their growth by the Pax5 transgene." Int J Hematol **87**(4): 351-362.

Selvaraj, U. M., K. Poinatte, V. Torres, S. B. Ortega and A. M. Stowe (2016). "Heterogeneity of B Cell Functions in Stroke-Related Risk, Prevention, Injury, and Repair." Neurotherapeutics **13**(4): 729-747.

Seo, W., T. Ikawa, H. Kawamoto and I. Taniuchi (2012). "Runx1-Cbfbeta facilitates early B lymphocyte development by regulating expression of Ebf1." J Exp Med **209**(7): 1255-1262.

Shen, X., Y. Yang, W. Liu, M. Sun, J. Jiang, H. Zong and J. Gu (2004). "Identification of the p28 subunit of eukaryotic initiation factor 3(eIF3k) as a new interaction partner of cyclin D3." FEBS Lett **573**(1-3): 139-146.

Sicinska, E., I. Aifantis, L. Le Cam, W. Swat, C. Borowski, Q. Yu, A. A. Ferrando, S. D. Levin, Y. Geng, H. von Boehmer and P. Sicinski (2003). "Requirement for cyclin D3 in lymphocyte development and T cell leukemias." Cancer Cell **4**(6): 451-461.

Sicinski, P., J. L. Donaher, Y. Geng, S. B. Parker, H. Gardner, M. Y. Park, R. L. Robker, J. S. Richards, L. K. McGinnis, J. D. Biggers, J. J. Eppig, R. T. Bronson, S. J. Elledge and R. A. Weinberg (1996). "Cyclin D2 is an FSH-responsive gene involved in gonadal cell proliferation and oncogenesis." Nature **384**(6608): 470-474.

- Sicinski, P., J. L. Donaher, S. B. Parker, T. Li, A. Fazeli, H. Gardner, S. Z. Haslam, R. T. Bronson, S. J. Elledge and R. A. Weinberg (1995). "Cyclin D1 provides a link between development and oncogenesis in the retina and breast." Cell **82**(4): 621-630.
- Simard, R., V. Bibor-Hardy, A. Dagenais, M. Bernard and M. F. Pinard (1986). "Role of the nuclear matrix during viral replication." Methods Achiev Exp Pathol **12**: 172-199.
- Smetana, K. and F. Hermansky (1963). "A Contribution to the Knowledge of the Ultrastructure of Leukaemic Lymphocytes." Neoplasma **10**: 405-411.
- Song, S., J. Cooperman, D. L. Letting, G. A. Blobel and J. K. Choi (2004). "Identification of cyclin D3 as a direct target of E2A using DamID." Mol Cell Biol **24**(19): 8790-8802.
- Spector, D. L. (1993). "Nuclear organization of pre-mRNA processing." Curr Opin Cell Biol **5**(3): 442-447.
- Spooner, C. J., J. X. Cheng, E. Pujadas, P. Laslo and H. Singh (2009). "A recurrent network involving the transcription factors PU.1 and Gfi1 orchestrates innate and adaptive immune cell fates." Immunity **31**(4): 576-586.
- Stelzer G, R. R., Plaschkes I, Zimmerman S, Twik M, Fishilevich S, Iny Stein T, Nudel R, Lieder I, Mazor Y, Kaplan S, Dahary D, Warshawsky D, Guan - Golan Y, Kohn A, Rappaport N, Safran M, and Lancet D. (2016). The GeneCards Suite: From Gene Data Mining to Disease Genome Sequence Analysis.
- Stengel, K. R., K. R. Barnett, J. Wang, Q. Liu, E. Hodges, S. W. Hiebert and S. Bhaskara (2017). "Deacetylase activity of histone deacetylase 3 is required for productive VDJ recombination and B-cell development." Proc Natl Acad Sci U S A **114**(32): 8608-8613.
- Stuurman, N., R. Van Driel, L. De Jong, A. M. Meijne and J. Van Renswoude (1989). "The protein composition of the nuclear matrix of murine P19 embryonal carcinoma cells is differentiation-stage dependent." Exp Cell Res **180**(2): 460-466.
- Taimen, P., K. Pflughaar, T. Shimi, D. Moller, K. Ben-Harush, M. R. Erdos, S. A. Adam, H. Herrmann, O. Medalia, F. S. Collins, A. E. Goldman and R. D. Goldman (2009). "A progeria mutation reveals functions for lamin A in nuclear assembly, architecture, and chromosome organization." Proc Natl Acad Sci U S A **106**(49): 20788-20793.
- Takahashi, A., E. S. Alnemri, Y. A. Lazebnik, T. Fernandes-Alnemri, G. Litwack, R. D. Moir, R. D. Goldman, G. G. Poirier, S. H. Kaufmann and W. C. Earnshaw (1996). "Cleavage of lamin A by Mch2 alpha but not CPP32: multiple interleukin 1 beta-converting enzyme-related proteases with distinct substrate recognition properties are active in apoptosis." Proc Natl Acad Sci U S A **93**(16): 8395-8400.
- Takaki, T., A. Echaliier, N. R. Brown, T. Hunt, J. A. Endicott and M. E. Noble (2009). "The structure of CDK4/cyclin D3 has implications for models of CDK activation." Proc Natl Acad Sci U S A **106**(11): 4171-4176.

- Tan, Y. J. and A. E. Ting (2000). "Non-ionic detergent affects the conformation of a functionally active mutant of Bcl-X(L)." Protein Eng **13**(12): 887-892.
- Tangye, S. G., D. T. Avery and P. D. Hodgkin (2003). "A division-linked mechanism for the rapid generation of Ig-secreting cells from human memory B cells." J Immunol **170**(1): 261-269.
- Thul, P. J., L. Akesson, M. Wiking, D. Mahdessian, A. Geladaki, H. Ait Blal, T. Alm, A. Asplund, L. Bjork, L. M. Breckels, A. Backstrom, F. Danielsson, L. Fagerberg, J. Fall, L. Gatto, C. Gnann, S. Hober, M. Hjelmare, F. Johansson, S. Lee, C. Lindskog and J. Mulder (2017). "A subcellular map of the human proteome." **356**(6340).
- Till, J. E. and C. E. Mc (1961). "A direct measurement of the radiation sensitivity of normal mouse bone marrow cells." Radiat Res **14**: 213-222.
- Tomasovic, S. P., G. N. Turner and W. C. Dewey (1978). "Effect of hyperthermia on nonhistone proteins isolated with DNA." Radiat Res **73**(3): 535-552.
- Treiber, N., T. Treiber, G. Zocher and R. Grosschedl (2010). "Structure of an Ebf1:DNA complex reveals unusual DNA recognition and structural homology with Rel proteins." Genes Dev **24**(20): 2270-2275.
- Treiber, T., E. M. Mandel, S. Pott, I. Gyory, S. Firner, E. T. Liu and R. Grosschedl (2010). "Early B cell factor 1 regulates B cell gene networks by activation, repression, and transcription-independent poisoning of chromatin." Immunity **32**(5): 714-725.
- Uhlen, M., L. Fagerberg, B. M. Hallstrom, C. Lindskog, P. Oksvold, A. Mardinoglu, A. Sivertsson, C. Kampf, E. Sjostedt, A. Asplund, I. Olsson, K. Edlund, E. Lundberg, S. Navani, C. A. Szigartyo, J. Odeberg, D. Djureinovic, J. O. Takanen, S. Hober, T. Alm, P. H. Edqvist, H. Berling, H. Tegel, J. Mulder, J. Rockberg, P. Nilsson, J. M. Schwenk, M. Hamsten, K. von Feilitzen, M. Forsberg, L. Persson, F. Johansson, M. Zwahlen, G. von Heijne, J. Nielsen and F. Ponten (2015). "Proteomics. Tissue-based map of the human proteome." Science **347**(6220): 1260419.
- UniProt Consortium, T. (2018). "UniProt: the universal protein knowledgebase." Nucleic Acids Res **46**(5): 2699.
- Vagenende, V., M. G. Yap and B. L. Trout (2009). "Mechanisms of protein stabilization and prevention of protein aggregation by glycerol." Biochemistry **48**(46): 11084-11096.
- van Zelm, M. C., M. van der Burg, D. de Ridder, B. H. Barendregt, E. F. de Haas, M. J. Reinders, A. C. Lankester, T. Revesz, F. J. Staal and J. J. van Dongen (2005). "Ig gene rearrangement steps are initiated in early human precursor B cell subsets and correlate with specific transcription factor expression." J Immunol **175**(9): 5912-5922.
- Vandenberg, C. J., P. Waring, A. Strasser and S. Cory (2014). "Plasmacytomagenesis in Emu-v-abl transgenic mice is accelerated when apoptosis is restrained." Blood **124**(7): 1099-1109.

- Varjosalo, M., S. Keskitalo, A. Van Droogen, H. Nurkkala, A. Vichalkovski, R. Aebersold and M. Gstaiger (2013). "The protein interaction landscape of the human CMGC kinase group." Cell Rep **3**(4): 1306-1320.
- Vemuri, M. C., N. N. Raju and S. K. Malhotra (1993). "Recent advances in nuclear matrix function." Cytobios **76**(305): 117-128.
- Vergnes, L., M. Peterfy, M. O. Bergo, S. G. Young and K. Reue (2004). "Lamin B1 is required for mouse development and nuclear integrity." Proc Natl Acad Sci U S A **101**(28): 10428-10433.
- Verheijen, R., W. van Venrooij and F. Ramaekers (1988). "The nuclear matrix: structure and composition." J Cell Sci **90 (Pt 1)**: 11-36.
- Vilagos, B., M. Hoffmann, A. Souabni, Q. Sun, B. Werner, J. Medvedovic, I. Bilic, M. Minnich, E. Axelsson, M. Jaritz and M. Busslinger (2012). "Essential role of EBF1 in the generation and function of distinct mature B cell types." The Journal of Experimental Medicine **209**(4): 775-792.
- Voss, T. C. and G. L. Hager (2014). "Dynamic regulation of transcriptional states by chromatin and transcription factors." Nat Rev Genet **15**(2): 69-81.
- Wan, K. M., J. A. Nickerson, G. Krockmalnic and S. Penman (1999). "The nuclear matrix prepared by amine modification." Proc Natl Acad Sci U S A **96**(3): 933-938.
- Wang, H., B. N. Nicolay, J. M. Chick, X. Gao, Y. Geng, H. Ren, H. Gao, G. Yang, J. A. Williams, J. M. Suski, M. A. Keibler, E. Sicinska, U. Gerdemann, W. N. Haining, T. M. Roberts, K. Polyak, S. P. Gygi, N. J. Dyson and P. Sicinski (2017). "The metabolic function of cyclin D3-CDK6 kinase in cancer cell survival." Nature **546**(7658): 426-430.
- Welinder, E., R. Mansson, E. M. Mercer, D. Bryder, M. Sigvardsson and C. Murre (2011). "The transcription factors E2A and HEB act in concert to induce the expression of FOXO1 in the common lymphoid progenitor." Proc Natl Acad Sci U S A **108**(42): 17402-17407.
- Widlak, P., O. Palyvoda, S. Kumala and W. T. Garrard (2002). "Modeling apoptotic chromatin condensation in normal cell nuclei. Requirement for intranuclear mobility and actin involvement." J Biol Chem **277**(24): 21683-21690.
- Winkler, T. H. and I. L. Martensson (2018). "The Role of the Pre-B Cell Receptor in B Cell Development, Repertoire Selection, and Tolerance." Front Immunol **9**: 2423.
- Wood, T. E., S. Dalili, C. D. Simpson, M. A. Sukhai, R. Hurren, K. Anyiwe, X. Mao, F. Suarez Saiz, M. Gronda, Y. Eberhard, N. MacLean, T. Ketela, J. C. Reed, J. Moffat, M. D. Minden, R. A. Batey and A. D. Schimmer (2010). "Selective inhibition of histone deacetylases sensitizes malignant cells to death receptor ligands." Mol Cancer Ther **9**(1): 246-256.
- Worman, H. J. and E. C. Schirmer (2015). "Nuclear membrane diversity: underlying tissue-specific pathologies in disease?" Curr Opin Cell Biol **34**: 101-112.

- Yang, C. Y., S. Ramamoorthy, S. Boller, M. Rosenbaum, A. Rodriguez Gil, G. Mittler, Y. Imai, K. Kuba and R. Grosschedl (2016). "Interaction of CCR4-NOT with EBF1 regulates gene-specific transcription and mRNA stability in B lymphopoiesis." Genes Dev **30**(20): 2310-2324.
- Yang, V. W. (2018). The Cell CYcle. Control of the Cell Cycle: 197-219.
- Yoshida, T., S. Y. Ng, J. C. Zuniga-Pflucker and K. Georgopoulos (2006). "Early hematopoietic lineage restrictions directed by Ikaros." Nat Immunol **7**(4): 382-391.
- Zal, T., A. Volkman and B. Stockinger (1994). "Mechanisms of tolerance induction in major histocompatibility complex class II-restricted T cells specific for a blood-borne self-antigen." J Exp Med **180**(6): 2089-2099.
- Zarnegar, M. A. and E. V. Rothenberg (2012). "Ikaros represses and activates PU.1 cell-type-specifically through the multifunctional Sfp1 URE and a myeloid specific enhancer." Oncogene **31**(43): 4647-4654.
- Zeitlin, S., A. Parent, S. Silverstein and A. Efstratiadis (1987). "Pre-mRNA splicing and the nuclear matrix." Mol Cell Biol **7**(1): 111-120.
- Zhai, Z. H., J. A. Nickerson, G. Krochmalnic and S. Penman (1987). "Alterations in nuclear matrix structure after adenovirus infection." J Virol **61**(4): 1007-1018.
- Zhang, Z., C. V. Cotta, R. P. Stephan, C. G. deGuzman and C. A. Klug (2003). "Enforced expression of EBF in hematopoietic stem cells restricts lymphopoiesis to the B cell lineage." EMBO J **22**(18): 4759-4769.
- Zhao, F., A. Vilardi, R. J. Neely and J. K. Choi (2001). "Promotion of cell cycle progression by basic helix-loop-helix E2A." Mol Cell Biol **21**(18): 6346-6357.
- Zhuang, Y., P. Soriano and H. Weintraub (1994). "The helix-loop-helix gene E2A is required for B cell formation." Cell **79**(5): 875-884.
- Zullo, J. M., I. A. Demarco, R. Pique-Regi, D. J. Gaffney, C. B. Epstein, C. J. Spooner, T. R. Luperchio, B. E. Bernstein, J. K. Pritchard, K. L. Reddy and H. Singh (2012). "DNA sequence-dependent compartmentalization and silencing of chromatin at the nuclear lamina." Cell **149**(7): 1474-1487.
- Zwijssen, R. M., E. Wientjens, R. Klomp maker, J. van der Sman, R. Bernards and R. J. Michalides (1997). "CDK-independent activation of estrogen receptor by cyclin D1." Cell **88**(3): 405-415.

Chapter 10 Appendix

Figure 10-1 *Ebf1* qRT-PCR forward and reverse primer aligned on the *Mus musculus Ebf1* transcript variant X1, where in green is shown *Ebf1* gene coding sequence, in grey is forward primer annealing site and in yellow is shown reverse primer annealing site, (NCBI Reference Sequence O30245520.1) (Benson, Cavanaugh et al. 2017).

```

1  ttgggggggaa gggctagggg caactgtcct atactgtttc catccccatg agcacagggg
61  tgggagtggt tggtagtgag agtgaattgg gtaactaggc tagaagcgaa agtgtgtgtg
121 tgtgtgtgtg tgtgtgtgtg tgtgtgtgtg tgtgtgtgtg ttgtccgata gtgtccggca
181 gtttgggctg tcattgtggg gccccggggc atcctattct ccagtcccc  gcggatcttc
241 tcagccaaga agccttggcc ctttgggttt ctggaatgtg tgaggaggat ttctcagaat
301 ggcaaaactt tggcaagaca ggtcttttat ttaaaaaaaaa aattaaccaa acaacaacag
361 tcacttacia cagtaaaaaca agacgcccc  gttctctttc ccatggcgat cgatcatttc
421 taatagccgc gagtccaat cagggaccct tctccgcttg cttgccgttt gtgtagaaaa
481 ttagcgtgct gaggtcgggt accatcagct ggccgaggct agggagtttc ctggagggtg
541 gctgaggcag cgaacaacct agcatgcctt catgcatttc cacctgcccc cttacttgcg
601 agatttgag  gcgtagtcgg agcctattcc cacgccctgg ccttcgaagt agtaaattgc
661 gcactttctc ttttaacccg tctcatttca ccacgggtca cgtttcctct ccacgcagcg
721 cgtttcaagt ggagtaaaga ttgtagcgtt tcatctcaca cccaaaacc  aaacaaaact
781 tccacacctc tgagtctga  tgaccgcgtg tctctggaag gggaggacag ggacatgagt
841 ggcatttgtc cggttcgtca gccgctcttg agctcctgat gggcatgga  aggagcccag
901 gggatgtttt gggagcagag aagcgggggtg ggtctggccc gggctcactt tgagaagcag
961 ccgcttcta  acctgcggaa atccaacttc ttccacttct tctggccct  ctacgacaga
1021 cagggccagc ccgtggagat tgagaggacg gcctttgtgg ggttcgtgga gaaggaaaa
1081 gaagccaaca gcgaaaagac caataatggg atccactacc ggtccagct  cctctacagc
1141 aatgggatac ggacagaaca ggatttctat gtgcgcctca tcgactccat gacaaaacaa
1201 gccatagtgt atgaaggcca agacaagaac cctgaaatgt gccgagtatt gctcacacac
1261 gagatcatgt gcagccgctg ttgtgacaag aaaagctgtg gcaaccgaaa tgagactccc
1321 tcagatccag tgataattga caggttcttc ctgaagtttt tcttaaatg  caaccaaaat
1381 tgcctaaaga atgcaggaaa cccacgtgac atgcccagat tccaggtcgt ggtgtctacc
1441 acagtcaacg tggatggcca tgtcctggca gtctctgata acatgtttgt ccacaataac
1501 tccaagcacg ggccggaggc tcggaggctt gaccctcgg  aaggtaocgc ctcttatctg
1561 gaacatgcta ctccctgtat caaagccatc agcccagtg  aaggatggac gacgggaggc
1621 gcgactgtga tcatcatagg ggacaatttc tttgatgggt tacaggatc  attcggtagc
1681 atgctggctc ggagtgagtt gataactcct catgccatcc  gaggttcagc acctcctcgg
1741 cacatccctg gtgtggtgga agtcacactg tcgtacaagt ccaagcagtt ctgcaaaggg
1801 acaccaggca gattcatcta cacagcactg aatgaacca  ccatcgacta cggcttccag
1861 aggttacaga aggtcattcc tcggcatcct ggtgaccag  agcgttggc  aaaggaagtg
1921 atccttaaaa gagctgcaga tctggttgaa gccctgtatg ggatgcccc  caacaaccag
1981 gagattatcc tgaagagagc tgccgacatt gcagaggctc tgtacagtgt ccctcggaac
2041 cacaaccagc tcccagccct tgctaacact tcggtccatg cagggatgat ggggtgtaac
2101 tccttcagtg gacaactggc tgtgaatgtc tcggaggcat cacaagccac caatcaaggt
2161 ttcaccgca  actcaagcag cgtgtcacca catggctatg tgccgagcac caccacacag
2221 caaaccaact ataactcagt caccacaagc atgaatggct acggctcagc cgccatgtcc
2281 aatttggcg  gctccccaac ctctctcaat ggctcagctg ccaactcacc ctatgccatt
2341 gtgccatcca gcccaccat  ggcctcatct acaagcctcc cctccaactg cagtagctcc
2401 tctggcatct tctccttctc accagccaac atggtctcag cagtgaacaa gaagagtgtc
2461 ttgcaccag  ttgtcagacc ccagacgtcc cctcctccca cctgcaaccag caccaacggg
2521 aacagcctgc aagcgatata tggcatgatt gtccctccca tgtgaaagaa ttgccttgaa
2581 gaattttatt aatgaagagg ttggattctg ctacgaaagt tatctgacat gagtcccaga
2641 gtggaacttt taactcaggc ctttttaaga ggaatcacac aataactgca gatttttaaa
2701 caaatcacc  gaccttgcaa atactgaaat  tggaaagggg gtctgccaga gcagggtgtt

```

Continued...

Continued...

2761 ggtaaagtt gtaacccccg agtatctggg ggatatatatt attctgtatt gataaaaagc
2821 aagcccacat tttctttttc tttcttttctt ttcttaagct taactctgca accatttgtc
2881 ttttataaac cattaagcta cacacaaggg ccactataaa caagactcca tgttttaatt
2941 tatgttttta aagctatgga aggggagaat gaagtgggga tatttacaaa aaaaaaaaaat
3001 ctaaaaggag aaaaaaaaaa gaaaaaacagg gaaaaataaa tttaaaaaaa gagctcgtat
3061 ggacagaata ggaatgccag ttagatTTTT tagtgaacta agggtcggct tctgcgcctt
3121 aaagcttatt agtggtagtt agctcagaca gtgcattttc aatatctaac ttaacacgcc
3181 accccttagc agtgcaagct tcgttctctc ttttगतगग ttgtcttaag taactgtgta
3241 aataagtgta gcctggaaag ttaccaagcg acatacatga tcacgtttgc ccttgctactc
3301 gaaaagccag tgctctaga cagattgttt aaaaacaaac aaaaacaaaa caaaacaaaa
3361 caaaacaaca tgcattctta aaccgatctt tattctttta cttaacatca acttctcccg
3421 aagccagcgg cctctgagag tggagcaaca catgttccga gcgagaatct ccttcaagac
3481 ttacaggac aggtccagg cacagaattc catatatgcc ctccagttta ccaagccaaa
3541 atctcgctcg cactccaccg tcaagagatc caagcttact caagctggaa tcctagatat
3601 taactctaga tctgggctca aaaacccaaa taaagcaaac ccacaaaggc aagtaggtgt
3661 gctgttccgg gctcccaaat cacacgggtc tatacccgca agactccgca aggtcccaaa
3721 tcacacaggg gtctgtatcc gcaagactcc gcaaggttgg aaagttctat attcagtcaa
3781 caggtaaagt gctttggagt tcagtgtgaa aggaaactgg gagagaggaa gggagggttg
3841 aggtctcaaa ctcagctttc tatgggaaat tttgctttca actgggaagt gttcttaag
3901 aatccatagc aaagattcag ccagcaagcg cctgaggggg cgtgttctctg ctgacctctg
3961 ccctctggtt tctgtatgta gttataaata ctgtagattt cttttgtgat ttttttttg
4021 ccaaagtgtt tttatttata cattttaatg tcttaagatt ttcgatctca cacacgcaaa
4081 gaattatact gcatattttg caaagaaata aaaagcgcac taccttttagc ttgcacatac
4141 ttgcaaagtt aattcaaagg ctttctgttt gtttgtttta atggggattt tgtaaaatat
4201 ccatataaat aatgtattta tctttggaat ttgtacattg cttttctctc ctctctccca
4261 tccccaccct ctagtattat ttgtgtgtgt gtttctttg tgaacagtgc gcaagtatag
4321 tttggctact tatagttgta tttagctgttt caatgtgatt tttaaacaat tcatttatag
4381 gtatttttag tattgtttta aaccatgctt cattttttta tttccacca aaagccattg
4441 tctatttttg tattatttgt aagttaagaa gttttttcca atatatggca aaaaaatagt
4501 agcatattat tctttagta tttagttctg tagattttaa aataatgtac cctttgcttt
4561 ggaagcatac aaaaacgctg ttttactcta gtaatatgca tggaaatctc ccctttggag
4621 tgacgcattt tgtgcattaa atttgggggga gaaacttcat agagatcaat gaacatactt
4681 tctttcttaa gtctgcttgt atattctctg tctttcacat aaatataaac cagcagattg
4741 gatgccttaa caatgcaaat catatccatt tcacctgtac attgtactgt gcaccccccc
4801 caactgtcag ccatcactaa cattctaaga aaaaaaaaaa agaaaaagaa gaaaaaaaaa
4861 gagagaaatc gaaaagcaca aaagaactgt tttgttactt taagacaatg ttactttttc
4921 tagtagagca agagaacatt acaaaagctg cgactgtgca tgcccggatg gatttcaacg
4981 gttttcacta gactgtcaga gtgcggattt ttatgggttg gggaggggag gggaggggag
5041 ttgggggggt tggtagggga ggggagggag gaaagctgat tttcatggt gagaaataat
5101 aataatgaca actgatgata ataataataa taataaaaaat aaaaagaaac tggaaaaaaa
5161 tataagcaag gtttagcatt gcttctccgt actcagaaag gttgtctgaa ttcgtgtggt
5221 aagcgtggc ctcaagatgt ctaacgtcta aagccatatt ttgtctggtg agccagacaa
5281 ctgtctgcaa aggaacgagc agcaagccgg tgagggtgcc ggctcagacc ctgacaaaag
5341 acgccaccaa tctgttagcc acgtgctgtg acgtgatgag aactttactg gaaagcccaa
5401 agagccttta aaaagaaaat gtgtatcaat tgtgttttgt tacttctggt tgattagccg
5461 atggagaagt agtttggtt taggaaccac tttcttctac acaaaatctt gtttttaagt
5521 ccctttaaga tatagcccc taaatacaga atatggcttt taaaagaag atggagttaga
5581 gaattcaatt cagatttccg ttttggggga agagccctgc ctctggatga ctggatatgt
5641 ccacgccatg cccggcctca caatgtagga tgcagctcca tgaactcatt ctgcaaatct
5701 ttacacttct tttcaaactg tttcaataga cacacactgt acaatccaat tgttagagca
5761 ctcaactact gtagagattg ttatatttca ttctttttta tttctttctt tcttttcttt
5821 tcttctcctt tttttttttc aaaaattcaa actgtaaaaa acttttcaac gttcacgata
5881 ttttaattaa gttacttctt gtctgtgata gca

Figure 10-2 *Ccnd3* qRT-PCR forward and reverse primer aligned on the *Mus musculus* *Ccnd3* transcript variant 1, where in green is shown *Ccnd3* gene coding sequence, in grey is forward primer annealing site and in yellow is shown reverse primer annealing site, (NCBI Reference NM_007632.2) (Matsushime, Roussel et al. 1991, Benson, Cavanaugh et al. 2017)

```

1  atcgtcgcga ggggcggggc gctgtcagg gaagcgggtg gcgcggggtg cgggcgggct
61  ggggcttctc cgcacagtgc cagcgcagc gccagaccg cccgcacccc gcgctctccc
121 tcacgcgctg cgcttctcct aggactcgtc aaccgcact cttgctctca cccgtgagcc
181 atcgcaggat ggagctgctg tgttgcgagg gcacccggca cgcgccccgg gccgggcccc
241 acccgcggct gcttggggac cagcgtgtcc tgcagagttt actccgcctg gaggagcgct
301 acgtgccgag agcctcctac ttccagtgcg tgcaaaagga gatcaagccg cacatgcgga
361 agatgctggc aactggtgat ctggagggtg gtgaggagca gcgctgcgag gaggatgtct
421 tcctctggc tatgaactac ctggatcgcct acctgtcctg cgtccccacc cgaagggcgc
481 aattgcagct tctaggtacc gtctgcctgt tgctggcctc caagctgcgc gaaaccacgc
541 ccctgactat tgagaagctt tgcactata cggaccaggc tgtggctcca tggcagttgc
601 gggagtggga ggtgctggtc ctggggaagc tcaagtggga cctggctgcc gtgattgcgc
661 acgactcctt ggcttgatt ctgcaccgcc tgcctctgcc cagtgaaccg caggctttgg
721 tcaaaaagca tgcccagacc tttttggccc tctgtgctac agattacacc tttgcgatgt
781 atcctccatc catgatcgcc acaggcagca ttggggcagc cgtgctagcc ctaggcgcct
841 gctctatgtc tgcggatgag ctacagagt tgctggccgg gatcacagcc actgaagtgg
901 actgctgcg agcctgccag gaacagatcg aagctgcctt cagggagagc ctcaggggag
961 ctgctcagac agccccagc ccagtgccca aagccccccg gggctctagc agccaggggc
1021 ccagtccagc cagcaactcc acagatgtca cagccattca cctgtagctt gagacaggcc
1081 ctctcaggcc accaagcaga ggagggggcc ctgccacccc ctccctgctt ctagaacaat
1141 ccatgctata tctgaagccc gaggggggct ctccctcccc ctcaaaagc ccaaggggcc
1201 aggtcctgcc tatccccaca gtgtgacta aggggttgca tggatcatgag gggcgtcttc
1261 atggccagtc agctcctctt ccttcccact caaccagctt ggctgtcctg ggccatgatg
1321 gtcagagaaa tacaacagc taaaatccac acaccagcat ttcttttgag tccctcttct
1381 gtcgggggct ccaaccttct cagttgccaa aacgccccag taccttccaa aggtggtggc
1441 ccttgaggc tccttcgggc atcccgatag aagcttatga ggagctgcc tagatggcct
1501 ctgtgtaatc cgtactccag ctgctcttag agggaacagc ctaggctttg gccagagcaa
1561 gaaccatac actggtgctt tgcttgctgc ttagcttctg tgattgtggg gtcttaaggg
1621 tgccgtggc attttaattt attgctttga atacaactgt aagagggtag agtgaggcct
1681 gtaccacaca agtgggtgta accctggcgg ttgctctttc cctcccttct tcccctctgc
1741 tactgctttg tggcccagga gctgctacag cctgggatgg gggtcacgcc ttcctctctt
1801 caccctcca ctcactctc atcagagcag ggtagggtg ggatggatcg atgccgtgga
1861 ggtgacagag ctatctggag agagggcaag ccctagggtc acaggtcttt cctcgggcca
1921 caaggtttg gctggtggcc catttctatc atgctgcctt aataaagatt tcggaataaa
1981 aaaaaaaaaa aa

```

Figure 10-3 *Hprt* qRT-PCR forward and reverse primer aligned on the *Mus musculus Hprt*, where in green is shown *Hprt* gene coding sequence, in grey is forward primer annealing site and in yellow is shown reverse primer annealing site, (NCBI Reference NM_013556.2) (Chapman and Shows 1976, Benson, Cavanaugh et al. 2017)

```

1 ggagcctggc cggcagcgtt tctgagccat tgctgaggcg gcgagggaga gcggtgggct
61 tacctcactg ctttccggag cggtagcacc tcctccgccg gcttcctcct cagaccgctt
121 ttgcccga gccgaccggt cccgtcatgc cgaccgcag tcccagcgtc gtgattagcg
181 atgatgaacc aggttatgac ctagatttgt tttgtatacc taatcattat gccgaggatt
241 tggaaa aagt gtttattcct catggactga ttatggacag gactgaaaga cttgctcgag
301 atgtcatgaa ggagatggga ggccatcaca ttgtggccct ctgtgtgctc aaggggggct
361 ataagttcct tgctgacctg ctggattaca ttaaagcact gaatagaaat agtgatagat
421 ccattcctat gactgtagat tttatcagac tgaagagcta ctgtaatgat cagtcaacgg
481 gggacataaa agttattggt ggagatgac tctcaacttt aactggaaaag aatgtcctga
541 ttgttgaaga tataattgac actggtaaaa caatgcaaac tttgctttcc ctggttaagc
601 agtacagccc caaaatggtt aaggttgcaa gcttgctggt gaaaaggacc tctcgaagtg
661 ttggatacag gccagacttt gttggatttg aaattccaga caagtttggt gttggatatg
721 cccttgacta taatgagtac ttcagggatt tgaatcacgt ttgtgtcatt agtgaaaactg
781 gaaaagccaa atacaaagcc taagatgagc gcaagttgaa tctgcaaata cgaggagtcc
841 tgttgatggt gccagtaaaa ttagcagggtg ttctagtcct gtggccatct gcctagtaaa
901 gctttttgca tgaaccttct atgaatgtta ctgttttatt tttagaaatg tcagttgctg
961 cgtccccaga cttttgattt gcactatgag cctataggcc agcctaccct ctggtagatt
1021 gtcgcttatc ttgtaagaaa aacaaatctc ttaaattacc actttttaaata aataatactg
1081 agattgtatc tgtaagaagg atttaaagag aagctatatt agttttttaa ttggatattt
1141 aatttttata tattcaggag agaaagatgt gattgatatt gttaatttag acgagctctga
1201 agctctcgat ttcctatcag taacagcatc taagagggtt tgctcagtggt aataaacatg
1261 tttcagcagt gttggctgta ttttcccact ttcagtaaat cgttgtcaac agttcctttt
1321 aatgcaaat aaataaatc taaaaatc

```

Figure 10-4 Potential binding partners of CCND3

Cell lines	Total	Proteins
1_1	31	ARPC5 CNPY2 ESYT1 RAC1 FAU NUCKS1 G3BP1 PDCD6 DSP PARK7 PSMB2 ILF2 KRT8 ATP5O GRPEL1 GM5039 IPO5 PSAT1 KCTD12 ANXA7 PGAM2 HPRT1 NHP2L1 SNRPB CALM1 APRT EIF3H BAX COPS3 HIST2H2BE ADSL PSMD5 RAB11B
1_4	122	UCHL3 TARS SRSF2 MCM3 RPS2 LCN1 SNRPE PDCD6 MTHFD1 VPS35 G3BP1 CST4 KPNA4 CALML5 UMPS PPP2R4 CBX3 GANAB YARS PKP1 DLD EIF3B AMY1A PSMC4 ANP32E BPIFA2 DES FASN DARS ELAVL1 BLMH NASP MCM6 GM10036 CLTA SNRPA1 EIF2S3X TUBB4B RANBP1 RBM39 H3F3C EIF3A SNRPB PPID ST13 GBP2 TNPO1 RPS15A RRS1 USP14 DDX39B ADSS C3 SDF2L1 RPS28 PTGR1 GIMAP4 TXNL1 SMR3B TAF15 RPL39 CMPK1 PPIB RBM3 CSE1L SEP7 ARF4 PSMD3 IARS TF GART LARS CAMK2D SND1 PDIA4 IPO7 NAA15 RFC4 IGHA1 TXNRD1 SNRPA CA6 PIGR SARS PRR4 DDX3X RPS24 STIP1 HNRNPL CA2 ZG16B ACADL PAFAH1B2 FERMT3 ASNS SRSF3 EIF3C CST1 MCM2 MYBBP1A SERPINA1 TCEA1 AARS PDCD10 RCC2 PPP1R7 STMN1 SEP11 PAK2 BZW2 FKBP4 SF3A3 GARS NSFL1C GM17190 PSMC6 PRPH PPP2CA ACO2 BIN1 DNAJB11 HIST1H2AB
MPI-2	30	RPS11 CDKN2D RPL10A ANXA1 JUP CNDP2 RPL13A TUBA1A LGALS3BP S100A4 PABPC1 CAPG KPNA2 IGKC CAPNS1 REEP5 RPN2 LGALS3 EIF3I ESD LMNA RAB14 ANXA4 RPL38 FLNA LYZ2 H1FO S100A10 RAB7A RPL13
1_1, and 1_4	84	ECHS1 PRKCSH ETFA ANXA6 DNAJC9 PRDX3 OTUB1 HNRNPD GOT1 CDK5 CDKN1A MSN GM6793 ERP29 UBA1 PRDX6 PCNA NOLC1 PSMA3 EPRS STK26 CAND1 CDKN2C EIF4H API5 ACAT1 ALDH1B1 HADHA SARNP EIF3K NAP1L4 MDH1 PCBP2 SOD1 RARS SAE1 CTH PDCD6IP SRI EIF3E ANP32A HDGF PSMB1 HIST1H3B DBI YWHAQ COPS4 XPO1 PRDX5 PSME3 TOMM34 PCK2 PSMB8 COPS8 AK2 MTAP ATIC FTL1 STK4 ERO1L CS RPLP2 AKR1B1 HINT1 EZR PSMB4 PRDX4 SLC3A2 HSPE1 ERAP1 PEBP1 VARS SHMT1 KHSRP GSTP1 HMGB2 AHCY ANXA11 FUBP1 FAM49B IDH3A RPS21 UBE2N HSPH1

Continued...

Continued..

Cell lines	Total	Proteins
1_1 and MPI-2	7	PCBP1 PSMD6 VAT1 VHL RAB5C AHNAK HNRNPC
1_4 and MPI-2	4	RPS6 MYH9 SRSF1 VCP
1_1, 1_4 and MPI-2	76	PSMA2 PSMA4 P4HA1 EIF6 TPT1 PSMD1 FTH1 TLN1 EEF2 VASP PGAM1 SOD2 PDIA6 DPYSL2 TCEB2 HIST1H2AA CALR PSMD13 ARHGDIA LCP1 PSMA1 PDIA3 KXD1 ARF3 TALDO1 CAP1 PSMD7 TAGLN2 ATP6V1A PFN1 EIF4A1 LGALS1 PCMT1 PSMD12 ALDH2 ACLY PSMB3 NACA CDK4 CDKN1B MZB1 IQGAP1 PSMA6 HYOU1 CFL1 PREP STRAP TCEB1 EIF3F PPIA RPS12 PPP2R1A PSMD11 PSME2 GNB2L1 H2AFZ MAPRE1 PSMA7 ANP32B PGD HSP90B1 FDPS HSPA4 CLIC1 PSMA5 CCT6A CLTC ANXA5 EIF3L PSME1 GDI2 RPS8 ACTR2 YWHAB PGK1 ARHGDIB